Lactate-based chain elongation

Production and separation of medium-chain carboxylates from complex organic residues

Carlos A. Contreras Dávila

Propositions

1. The upcycling of food waste to medium-chain carboxylates should be done using endogenous electron donors.
   (This thesis)
2. Application-compatible solvents enriched with medium-chain carboxylates are more attractive products than pure medium-chain carboxylates derived via conventional downstream processing.
   (This thesis)
3. In science, knowledge is the base, imagination leads the way.
4. The assumption that science inherently leads to progress cannot be justified without ideology.
5. Scientific information is currently considered an economic commodity with excessive publishing costs.
6. A culture emphasizing that humankind is part of nature will help reduce future environmental damage.

Propositions belonging to the thesis, entitled

Lactate-based chain elongation
Production and separation of medium-chain carboxylates from complex organic residues

Carlos A. Contreras Dávila

Wageningen, September 3rd, 2021.

Lactate-based chain elongation

Production and separation of medium-chain carboxylates from complex organic residues

Carlos A. Contreras Dávila

Thesis committee

Promotor
Prof. Dr C.J.N. Buisman
Professor of Biological Recovery & Reuse Technology
Wageningen University & Research

Co-promotor
Dr D.P.B.T.B. Strik
Associate professor, Environmental Technology
Wageningen University & Research

Other members
Prof. Dr JH Bitter, Wageningen University & Research
Prof. Dr MH Studer, Bern University of Applied Sciences, Switzerland
Dr KJJ Steinbusch, DAB, Delft
Dr M Roghair, DMT Environmental Technology, Joure

This research was conducted under the auspices of the Graduate School for Socio-Economic and Natural Sciences of the Environment (SENSE).

Lactate-based chain elongation

Production and separation of medium-chain carboxylates from complex organic residues

Carlos A. Contreras Dávila

Thesis

submitted in fulfilment of the requirements for the degree of doctor
at Wageningen University
by the authority of the Rector Magnificus,
Prof. Dr A.P.J. Mol,
in the presence of the
Thesis Committee appointed by the Academic Board
to be defended in public
on Friday 3 September 2021
at 1:30 p.m. in the Aula

Carlos A. Contreras Dávila

Lactate-based chain elongation
Production and separation of medium-chain carboxylates from complex organic residues
208 pages

PhD thesis, Wageningen University, Wageningen, the Netherlands (2021)
With references, with summary in English

ISBN: 978-94-6395-848-6
DOI: 10.18174/548132

To my family

"La esperanza le pertenece a la vida, es la vida misma defendiéndose"
"Hope belongs to life, it's life itself defending itself"

Julio Cortázar

Table of Contents

Chapter 1

General introduction

1.1 Circular bioeconomy – obtaining biobased materials from renewable sources

The degradation of the environment and resource scarcity related with human activities and population increase have, beyond raising concerns about the sustainability of the current economy scheme, encouraged global efforts to transition toward a more sustainable economy. It is expected that implementing circular approaches will help to reduce the current dependency on petroleum, mitigate climate change and promote local economies (Velenturf and Purnell, 2017; Kardung et al., 2021). Recent efforts in the European Union for moving to a more circular economy have resulted in increased cycling of materials, jobs and new business models (European Comission, 2019). However, resource-efficiency and economic growth goals must incorporate social equality and well-being (Velenturf and Purnell, 2017), and be implemented within consensual planetary boundaries in order to sustain a resilient Earth system (Steffen et al., 2015). Within the circular (bio)economy umbrella concept, the processing of natural resources and residual materials to obtain biobased products contributes to the overall goals of circularity: replacing non-renewables with biological resources, resource efficiency through waste minimization, and preservation of economic value (Kardung et al., 2021). Nowadays, renewable and residual biological resources are underutilized (The Circularity gap report, 2021) and, through effective processing, they may represent a sustainable source of valuable biobased materials (Cherubini, 2010).

1.2 Role of carboxylates in resource recovery from organic residual materials

Resource recovery bioprocesses are designed to allow the upcycling of carbon, nutrients, minerals and energy contained in residual materials into useful biobased products. Organic residual materials from the agri-food industry such as lignocellulosic biomass, industrial wastewater, manure or food waste are feedstocks with high potential for obtaining biobased fuels and chemicals. Food waste, for instance, amounts to about 88 million tons per year in Europe (Stenmarck et al., 2016) and 1.3 billion tons per year worldwide (FAO, 2011). While preventing waste generation is the first step in waste management, resource recovery from existing and future residual streams is essential to cycle materials, energy and value within the circular bioeconomy. The biorefining of residual organic feedstocks allow effective resource recovery to obtain a spectrum of chemicals, materials and fuels through a combination of (bio)processes. For instance, combinations of (thermo)chemical and biological hydrolysis, followed by fermentation and gasification have been proposed for lignocellulose conversion to ethanol with variations presented as the sugars, syngas and carboxylate biorefinery platforms (Holtzapple and Granda, 2009). The carboxylate platform is emerging as an important platform to biologically convert complex organic residues that are currently digested to methane into carboxylates as the central intermediates (Agler et al., 2011). The obtained carboxylates can be further processed through biological, thermochemical or electrochemical steps to yield substitutes for petrochemicals such as esters, alkanes, alcohols, among others (Agler et al., 2011; Kleerebezem et al., 2015). New bioprocesses are under development to expand the range of carboxylates attained and beyond to alcohols and other valuable chemicals.

1.3 Microbial chain elongation – turning anaerobic digesters into chain-elongating bioreactors

Resource recovery bioprocesses naturally rely on reactor microbiomes (open cultures) for effective bioconversion of non-sterile complex feedstock. One of the most common microbiome-based

bioprocesses is anaerobic digestion, which allows the treatment of residual materials and energy recovery through methane production. However, the economic value of methane is relatively low which makes the production of carboxylates a more attractive alternative (Kleerebezem et al., 2015). The potential for application of chain elongation is hardly exploited. Estimates show that worldwide, 20,000 industrial-scale anaerobic digesters are in operation (WBA, 2019) that could be used to produce more valuable and more versatile compounds. Under methane-inhibiting conditions, anaerobic microbiomes ferment proteins and carbohydrates present in organic residues into short-chain carboxylates (Kleerebezem et al., 2015) (SCC, 1-5 carbon units), including the monocarboxylates acetate, propionate, n-butyrate and n-valerate. Through microbial chain elongation, SCC are elongated into medium-chain carboxylates (MCC, 6-12 carbon units) in presence of reduced compounds used as electron donors (Angenent et al., 2016). Compared to SCC, the increased hydrophobicity and energy content of MCC facilitates their separation and expands their industrial applications. MCC find direct applications as plant growth promoters (Scalschi et al., 2013) and feed additives (Jackman et al., 2020) or as platform chemicals for the production of e.g. lubricants, bioplastics and biofuels (Sun et al., 2007; Angenent et al., 2016; Urban et al., 2017). MCC are conventionally sourced from palm and coconut oils. However, these oils naturally contain very low amounts of MCC (<2% in weight) (Turpeinen and Merimaa, 2011) and the growth of dedicated crops threatens biodiversity due to deforestation and habitat degradation (Cazzolla Gatti and Velichevskaya, 2020). Since residual feedstocks are generated worldwide, chain elongation represents a geographically unbound biotechnology to produce MCC and expand their availability as platform biochemicals.

Chain elongation to MCC was observed in earlier works supplying ethanol to environmental microbiomes derived from canal mud (Barker, 1947), from which *Clostridium kluyveri* was isolated (Barker and Taha, 1941). *Clostridium kluyveri* was found to use ethanol as electron donor to elongate acetate and n-butyrate to n-caproate (Barker et al., 1945). In recent years, chain elongation was developed as a microbiome-based resource recovery bioprocess to upgrade diluted ethanol and SCC from organic residues to MCC such as n-caproate and n-caprylate (Steinbusch et al., 2011). The technical and commercial feasibility of this bioprocess is currently being demonstrated by ChainCraft B.V. in Amsterdam, the Netherlands (www.chaincraft.nl). External electron donors such as ethanol, methanol or hydrogen, are typically supplied to promote chain elongation of SCC (Angenent et al., 2016). Depending on the way ethanol is produced, it may have a substantial impact in the environmental footprint of chain elongation (Chen et al., 2017). Alternatives to improve the environmental footprint include improving ethanol-use efficiency in chain elongation (Roghair et al., 2018c, 2018a). Nevertheless, the organic feedstock itself may be a source of electron donors.

1.4 Using complex residues to produce lactate as alternative electron donor for chain elongation

Substituting ethanol with electron donors that are accessible from the same feedstock would allow to produce MCC independently of external electron donors availability. Lactate, being an α-hydroxycarboxylate, is also an intermediate in the carboxylate platform that can serve as electron donor in chain elongation (Zhu et al., 2015). Lactate may be produced as one or a mixture of the two

enantiomeric forms (D-lactate or L-lactate) during primary fermentation of several feedstocks such as food-processing sidestreams, plant residues, municipal and food wastes (López-Gómez et al., 2020). Complex residues provide lactic acid bacteria (LAB) with fermentable carbohydrates and the necessary nutrients to grow and produce lactate (Hofvendahl and Hahn-Hägerdal, 2000; López-Gómez et al., 2020) with specific fermentation conditions supporting LAB dominance (Kim et al., 2016b). Steering primary fermentation toward lactate accumulation, thus, provides an endogenous electron donor to promote subsequent lactate-based chain elongation.

1.5 Lactate-based chain elongation – competing pathways and potential products

In pure-culture studies, *Megasphaera elsdenii* converts lactate into a mixture of straight C2-C6 carboxylates (Elsden et al., 1956) while recently isolated *Ruminococcaceae*-related bacteria produce high concentrations of n-caproate (Zhu et al., 2017). The metabolic pathway for MCC production from lactate was suggested to be similar to the reverse β-oxidation (RBO) pathway used by *Clostridium kluyveri* (Seedorf et al., 2008) but with lactate being the energy and carbon source (Zhu et al., 2015). Under anaerobic conditions, lactate is oxidized to pyruvate by confurcating lactate dehydrogenase which transfer electrons from lactate and reduced ferredoxin (Fd_{red}) to reduce NAD (Weghoff et al., 2015; Buckel and Thauer, 2018). Then, pyruvate is further converted to acetyl-CoA, carbon dioxide (CO_2) and Fd_{red} through pyruvate:ferredoxin oxidoreductase (PFOR) (Hino and Kuroda, 1993; Weimer and Moen, 2013). The produced Fd_{red} is oxidized to maintain the cytoplasmic redox balance through the production of hydrogen (H_2) or NADH (Liu et al., 2020). This two-step lactate oxidation yielding electrons and acetyl-CoA was recently confirmed to be coupled with the RBO pathway in lactate-elongating bacteria (Liu et al., 2020). In the cyclic RBO pathway, carboxylates are elongated with two carbons from acetyl-CoA to get elongated carboxylates such as n-butyrate (nC4) and n-caproate (nC6) (Figure 1.1) (Angenent et al., 2016). Alternatively, lactate may be converted to propionate through the intermediates oxaloacetate or acryloyl-CoA by propionic acid bacteria (PAB) (Gonzalez-Garcia et al., 2017). Propionate was suggested to be produced from the L-lactate enantiomer by *M. elsdenii* (Hino and Kuroda, 1993; Kucek et al., 2016a) while other PAB may use either or both lactate isomers . Lactate conversion through either of these processes in open-culture fermentation can be steered by using ecological engineering principles (Lawson et al., 2019) whereby selection pressures (e.g. substrate type, pH) typically determine the dominant function.

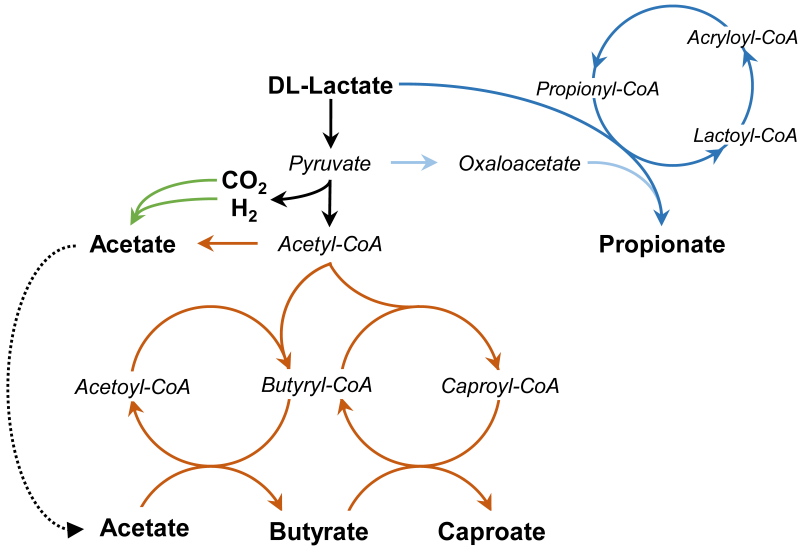

Figure 1.1 Simplified combination of metabolic pathways potentially occurring in anaerobic lactate conversion. The chain elongation pathway includes lactate oxidation to acetate followed by reverse β-oxidation (orange). H_2 and CO_2 may be converted to acetate through the Wood-Ljungdahl pathway (green). Lactate can be converted to propionate through the acrylate pathway (dark blue) or through the Wood-Werkman and the succinate pathways with oxaloacetate as intermediate (light blue) [see Gonzalez-Garcia (Gonzalez-Garcia et al., 2017) for reviewed propionate-producing pathways]. Figure adapted from (Hoelzle et al., 2014; Angenent et al., 2016; Liu et al., 2020).

Earlier works between 2015 and 2016 used reactor microbiomes to convert lactate to n-caproate (Zhu et al., 2015; Kucek et al., 2016a). These studies identified that lactate was chain-elongated up to n-caproate in microbiomes dominated by uncultured bacteria growing at either mildly acidic (Kucek et al., 2016a) or near-neutral (Zhu et al., 2015) pH conditions. At mildly acidic conditions, it was shown that controlling pH at 5.0 improved n-caproate production over n-butyrate (Kucek et al., 2016a). However, thus far the MCC product spectrum has been limited to n-caproate with relatively low chain elongation rates (~3 g n-caproate·L^{-1}·d^{-1}) compared to ethanol-based chain elongation (5.5-52 g n-caproate·L^{-1}·d^{-1}) (Grootscholten et al., 2013b; Roghair et al., 2018c).

Controlling competing and complementary processes lactate-elongating microbiomes may help improve MCC production. Propionate production, for instance, has been identified as a competing process capable of outcompeting chain elongation (Kucek et al., 2016a). A complementary process is acetate formation from H_2 and CO_2, side-products of lactate oxidation, by homoacetogenic bacteria. The adequate control of these parallel processes could improve carbon and energy recovery and augment the product spectrum of lactate-based chain elongation to include odd-chain MCC. Acetate from homoacetogenesis could be activated to acetyl-CoA and enter the RBO pathway as an additional electron acceptor for MCC formation. Analogously, propionate could be activated to propionyl-CoA and elongated to odd-chain carboxylates such as n-valerate (nC5) and n-heptylate (nC7) in a similar fashion as in elongation of ethanol and propionate (Grootscholten et al., 2013c). Therefore, part of this research aimed at steering lactate metabolism to broaden the product spectrum and increasing conversion rates of lactate-based chain elongation.

1.6 Carboxylates separation – the need for alternative methods

The commercial application of carboxylates generally requires downstream processing (DSP) for product separation and purification. The development of effective DSP faces several challenges. First, they should selectively separate the target chemical while keeping fermentation substrates in the bioreactor. Reduced DSP complexity and efficient chemical/energy use are looked-for since DSP contributes importantly to the environmental footprint and economics of biochemicals production (Straathof, 2011; Saboe et al., 2018). Thus, the development of alternative separation methods is subject of ongoing research. Several separation methods are available such as distillation, precipitation, liquid-liquid extraction, ion exchange and electrodialysis (López-Garzón and Straathof, 2014). These methods can be applied during (*in situ*) or after fermentation. *In situ* separation may be preferred since it can decrease end-product inhibition, improve fermentation performance and reduce the environmental footprint of bioprocesses (López-Garzón and Straathof, 2014; Saboe et al., 2018).

At lab-scale, *in situ* MCC separation from ethanol-based chain elongation bioprocesses has been performed through liquid-liquid extraction (Ge et al., 2015; Kucek et al., 2016b) and ion exchange (Yu et al., 2019) while only liquid-liquid extraction has been used in lactate-based chain elongation (Kucek et al., 2016a). Carboxylates are weak acids. Therefore, the method applied depends on the fermentation pH in relation with the pK_a of the target carboxylate. At pH values the pK_a of MCC (nC6-nC8, pK_a 4.88-4.89), high fractions of undissociated carboxylic acids are present, which are more hydrophobic. A typically used method under these pH conditions is liquid-liquid extraction. In chain elongation at mildly acidic conditions (e.g. pH 5.5), this method is shown to selectively separate MCC (Kucek et al., 2016b) due to their increased hydrophobicity. At pH close to neutrality, MCC are mainly dissociated and may be separated with ion exchange resins or electrodialysis (López-Garzón and Straathof, 2014). After separation, further steps to regenerate the solvent/adsorbent and to purify MCC are usually needed. Solvent regeneration is frequently done with strong inorganic bases, which results in increased costs and generates waste inorganic salts (López-Garzón and Straathof, 2014). At industrial scale, DSP trains including several separation and purification steps may be applied. For instance, the company ChainCraft proposed a six-steps DSP to convert food waste and ethanol to MCC salts for animal nutrition applications. The proposed DSP consists of a train of physical separation methods using ultrafiltration, reverse osmosis and nanofiltration followed by evaporation and drying to obtain powder MCC salts (EFSA (European Food Safety Authority), 2018). Other companies may use liquid-liquid extraction to recover MCC salts (Capro-X, US) (Angenent and Agler, 2014) or liquid-liquid extraction (using MCC as biocompatible solvents) coupled with two distillation steps to recover neat carboxylic acids (AFYREN, France) (Nouaille and Pessiot, 2017).

1.7 Thesis objective and outline

This thesis explores strategies to steer open-culture fermentation to produce a range of MCC from organic residues and intermediates (i.e. lactate) as well as alternatives for MCC separation. First, food waste was selected to study the feasibility of producing MCC without addition of external electron donor (e.g. ethanol). After identifying lactate as a central intermediate and endogenous electron donor for chain elongation, further research focused on two technological challenges: I)

steering lactate metabolism to carboxylates (C3-C8) (Chapters 3-5), and II) the recovery of MCC through alternative *in situ* extraction and adsorption processes (Chapters 5 and 6).

Proof that MCC can be produced from complex food waste without adding any exogenous electron donor was obtained in **Chapter 2**. It was hypothesized that repeated-batch fermentation of food waste at mildly acidic conditions would allow both lactate production and consumption, which would in turn reduce chemicals input due to self-regulated pH and no need of external ethanol. This was achieved in mesophilic reactors through lactate cross-feeding between homofermentative *Lactobacillus* and uncultured *Caproiciproducens* species, where repeated food waste addition allowed accumulation of SCC for further elongation with lactate to increase MCC selectivities.

To get more insights on lactate features and explore the possibility to influence DL-lactate metabolism, in **Chapter 3**, zero-valent iron nanoparticles (nZVI) were added to batch fermentation experiments to evaluate its potential to promote odd-chain MCC formation. nZVI did not promote the formation of odd-chain MCC but affected n-caproate and propionate formation in a dose-dependent manner, mainly through abiotic reactions (e.g. hydrolysis of lactate oligomers and increased pH). By following the lactate enantiomers distribution and by feeding enantiopure or racemic lactate, it was observed that lactate was racemized and converted to even-chain carboxylates during chain elongation.

Continuous lactate-based chain elongation was studied in **Chapter 4** where nitrogen gas was supplied at different regimes to evaluate its effect on L-lactate conversion and biomass growth at mildly acidic conditions (pH 5.5). Mixing through nitrogen gas supply was anticipated to influence the thermodynamics of chain elongation and to potentially promote granulation. High superficial gas velocities washed out *Caproiciproducens* species and enriched *Clostridium tyrobutyricum* strains, changing lactate metabolism from MCC production (nC6-nC8) to co-production of propionate and n-butyrate. Propionate supply did not inhibit chain elongation but increased lactate conversion rates toward odd-chain carboxylates (n-valerate and n-heptylate). Nitrogen gas supply was proposed as a strategy for increasing lactate conversion rates and producing odd-chain MCC in two-stage systems.

In **Chapter 5**, the effect of conductive materials on lactate fermentation and the feasibility of carboxylates separation through adsorption were evaluated. The addition of conductive materials (granular activated carbon [GAC], nickel foam and stainless steel) was expected to promote direct interspecies electron transfer in favor of new chain elongation products. The screening of conductive materials had two outcomes: I) all conductive materials decreased propionate production and II) some materials (GAC and nickel foam) steered chain elongation toward isobutyrate formation. The former effect may be an alternative strategy to control propionate formation while the latter adds branched-chain carboxylates as new products of open culture lactate-based chain elongation. In continuous chain elongation, GAC adsorbed MCC. After discovering the high MCC affinity and adsorption capacities of GAC from reactor broths and effluents, a design for selective *in situ* MCC adsorption-recovery to obtain neat medium-chain carboxylic acids was proposed.

Lastly, an alternative bioprocess to produce potential novel product formulations (e.g. MCC-rich feed additives) using application-compatible solvents was studied in **Chapter 6**. In Chapter 2, part of the

MCC produced seemed to be extracted into the food-waste oil which suggested that vegetable and food-waste derived oil may be suitable solvents to accumulate MCC. In this last experimental chapter, sunflower oil was enriched with MCC through extractive lactate-based chain elongation and the obtained MCC-enriched oil proposed as a potential functionalized feed additive for direct application with no further DSP. Sunflower oil, which had a similar biocompatibility with chain-elongating microbiomes as oleyl alcohol, selectively extracted MCC and improved chain elongation performance in continuous reactor microbiomes dominated by uncultured *Caproiciproducens* species. Potential applications of MCC-enriched solvents were discussed.

To conclude, the insights obtained through this research and their biotechnological implications for MCC production and separation are discussed in Chapter 7. Potential feedstocks and processing schemes are also suggested. Lactate-based chain elongation offers the potential to obtain a diverse product portfolio from the upcycle of complex organic residues.

Chapter 2

Consecutive lactate formation and chain elongation from food waste

A modified version of this chapter was published as:
Carlos A. Contreras-Dávila, Víctor J. Carrión, Vincent R. Vonk, Cees J.N. Buisman and David P.B.T.B. Strik (2020). Consecutive lactate formation and chain elongation to reduce exogenous chemicals input in repeated-batch food waste fermentation. Water Res. 169, 115215.

Abstract

The production of biochemicals from renewables through biorefinery processes is important to reduce the anthropogenic impact on the environment. Chain elongation processes based on microbiomes have been successfully developed to produce medium-chain carboxylates (MCC) from organic waste streams. Yet, the sustainability of chain elongation can still be improved by reducing the use of electron donors and additional chemicals. This work aimed to couple lactate production and subsequent chain elongation to decrease chemicals input such as electron donors and hydroxide for pH control in repeated-batch food waste fermentation. Food waste with adjusted pH was used as substrate and fermentation proceeded without pH control. During fermentation, lactate was first formed through the homolactic pathway and then converted to carboxylates, mainly n-butyrate and n-caproate. The highest n-caproate carbon selectivities (mmol C·mmol $C_{carboxylates}^{-1}$) and production rates were 38% and 4.2 g $COD \cdot L^{-1} \cdot d^{-1}$, respectively. Hydroxide input was reduced over time to a minimum of 0.47 mol $OH^- \cdot mol\ MCC^{-1}$ or 0.79 mol $OH^- \cdot kg\ COD_{carboxylate}^{-1}$. Lactate was a key electron donor for chain elongation and its conversion was observed at pH as low as 4.3. The microbiome enriched in this work was dominated by *Lactobacillus* spp. and *Caproiciproducens* spp.. The high abundance of *Caproiciproducens* spp. and their co-occurrence with *Lactobacillus* spp. suggest *Caproiciproducens* spp. used lactate as electron donor for chain elongation. This work shows the production of n-caproate from food waste with decreased use of hydroxide and no use of exogenous electron donors.

2.1. Introduction

Sustainable production of biochemicals is a key factor to reduce anthropogenic contributions to climate change and to develop a biobased economy (Cherubini, 2010). The biobased economy is grounded in biorefinery processes that allow effective conversion of renewable materials into a broad spectrum of chemicals, materials and fuels. Numerous microbial chain elongation processes exist that are able to elongate single- or short-chain molecules into longer-chain molecules. One recently developed microbial chain elongation process makes use of anaerobic microbiomes to convert organic wastes into medium-chain carboxylates (MCC, i.e., carboxylates with 6-12 carbons), such as n-caproate (Steinbusch et al., 2011). MCC are preferred products over short-chain carboxylates (SCC, i.e., carboxylates with <6 carbons) due to their higher energy content and their increased hydrophobicity makes MCC easier to separate from the fermentation broth. MCC are versatile compounds with different applications e.g., feed additives, bioplastics, lubricants, aviation fuels. Although chain elongation is a promising technology, the sustainability of the process can be improved considerably by reducing the use of electron donors and additional chemicals for pH control (Chen et al., 2017). Thus, electron donors with a more sustainable nature are needed to improve the environmental performance of the chain elongation technology.

Chain elongating bacteria can use a variety of electron donors as energy and carbon sources. In ethanol-based chain elongation, ethanol is metabolized by *Clostridium kluyveri* into acetyl-CoA and NADH. Electrons in NADH are used to drive the reverse β-oxidation (RBO) pathway elongating available acetate (C2) to n-butyrate (nC4) by the condensation of two acetyl-CoA (Angenent et al., 2016). When enough ethanol is available, n-butyrate is condensed with another acetyl-CoA in a second round and elongated to n-caproate (nC6) (Angenent et al., 2016). In lactate-based chain elongation, pyruvate and NADH are products of lactate oxidation. Pyruvate is further oxidized to acetyl-CoA and CO_2 with electrons released in form of reduced ferredoxin (Spirito et al., 2014). The derived acetyl-CoA are used for n-butyrate and n-caproate formation through RBO (Zhu et al., 2017). In this paper, we denote n-caproate as undissociated n-caproic acid and dissociated n-caproate together, and we refer to each specific form when appropriate. Bacteria possessing the RBO pathway have been enriched in MCC-producing microbiomes fed with ethanol, lactate and sugars (with ethanol as intermediary) (Ding et al., 2010; Steinbusch et al., 2011; Kucek et al., 2016a). Recently, a few processes have been developed to produce n-caproate from organic waste streams which either contain electron donors for chain elongation (Kucek et al., 2016b) or were acidified to produce electron donors such as lactate (Nzeteu et al.; Xu et al., 2018).

Lactate is produced by lactic acid bacteria (LAB) mainly from carbohydrates (Gänzle and Follador, 2012). During lactate production, the release of protons (eq. 1) causes acidification of the medium and eventually stops microbial activity due to metabolism disruption or toxicity of undissociated acids (Kashket, 1987). In contrast, a net proton consumption occurs in lactate-based chain elongation due to a decrease in the total acids molar concentration (equations 2 and 3). Therefore, the proton consuming behavior of lactate-based chain elongation could be used to compensate for the protons released during lactate production in the acidification phase. Besides, propionate production from lactate, an important competing pathway in lactate-based chain elongation (Kucek et al., 2016a), could be restricted when coupling these two processes since LAB and lactate

elongators are able to grow at pH ≤5.0 (Kashket, 1987; Weimer and Moen, 2013) which can limit the occurrence of propionate producing bacteria (Hettinga and Reinbold, 1972; Janssen, 1991).

$$C_6H_{12}O_6 \rightarrow 2\ C_3H_5O_3^- + 2\ H^+ \quad (1)$$

$$2\ C_3H_5O_3^- + H^+ \rightarrow C_4H_7O_2^- + 2\ H_2 + 2\ CO_2 \quad (2)$$

$$3\ C_3H_5O_3^- + 2\ H^+ \rightarrow C_6H_{11}O_2^- + 2\ H_2 + 2\ H_2O + 3\ CO_2 \quad (3)$$

Therefore, the aim of this study was to evaluate the effectivity of producing n-caproate from food waste through chain elongation with *in situ* produced lactate via repeated-batch operation which would result in 1) no need of exogenous electron donor addition and 2) reduction of chemicals addition for pH control. With repeated-batch operation, a concentrated food waste was consecutively added over 3 cycles which enabled to increase the n-caproate concentration over time. Food waste fermentation was performed without pH control. Changes in the microbiome composition were evaluated using 16S rRNA gene-based metagenomic data.

2.2. Materials and methods

2.2.1. Experimental set-up and procedure

Food waste was used as the only substrate in this study and consisted of outdated food remainders. Food waste was obtained from a recycling company (Rotie, the Netherlands) and preserved at -20°C for long-term storage. This was the same original food waste used in an earlier study in which microbially acidified waste was used to develop an effective ethanol-based chain elongation process (Roghair et al., 2018c). Prior to use, the waste was thawed in a 4°C room and kept at this temperature during the experimental work. The waste had a total solids content (TS) of 200.2±2.2 g TS·L^{-1}, volatile solids content (VS) of 179.4±1.1 g VS·L^{-1} and total acidity of 15036±152 mg $CaCO_3$·L^{-1} (Table S1). Chemical oxygen demand (COD) for the total (COD_T) and soluble (COD_S) fractions of food waste were 276.6±52.5 g COD_T·L^{-1} and 125.2±0.6 g COD_S·L^{-1}. Total carbohydrates were estimated to be 83.53±4.19 g·L^{-1} (in glucose equivalents). Some organic acids and alcohols were present in the waste e.g., lactate (18.64±1.34 g·L^{-1}), ethanol (4.41±0.04 g·L^{-1}), acetate (4.87±0.43 g·L^{-1}), propionate (1.92±1.45 g·L^{-1}), n-butyrate (0.36±0.06 g·L^{-1}) and valerate (0.20±0.02 g·L^{-1}).

Fermentation was carried out in a stirred tank reactor (1L-RBF) with working volume of 1 litre which was inoculated with a microbiome obtained from previous food waste fermentation. This was the same reactor used in earlier chain elongation studies (Roghair et al., 2016). For the start-up, the 1L-RBF reactor was fed with a mixture of mineral medium, vitamins and food waste to reach a food waste concentration of 10% v/v. The pH of the mixture was adjusted to an initial value of 6.0. Mineral medium and vitamins were added only at the beginning of the experiment with concentrations as reported by Roghair et al. (2016), except that $(NH_4)H_2PO_4$ was reduced to 1.8 g·L^{-1}. During 1L-RBF operation, concentrated food waste was adjusted to pH 6.0 with 4 M KOH before addition to the reactor to have comparable pH in the waste fed and fermentation was allowed to proceed without pH control. Food waste was added on days 0 and 15 at concentrations of 10% v/v and on day 32 at 15% v/v. Nitrogen gas was bubbled for 15 min after each substrate addition to ensure anaerobic

conditions. The reactor was connected to a gas flow meter (μFlow, Bioprocess Control) to quantify gas production and temperature was 35°C.

Duplicate experiments were performed using 500 mL Schott bottles with working volume of 300 mL to systematically assess repeated-batch fermentation (0.3L-RBF). Procedure in 0.3L-RBF experiments was the same as in 1L-RBF except that food waste was added at constant concentration of 10% v/v once lactate was depleted (every 7-8 days). In the same way, mineral medium and vitamins, were added only at the beginning of the experiment together with yeast extract (1 $g \cdot L^{-1}$). For the 0.3L-RBF experiment, inoculum was taken from the 1-L reactor on day 19 and added at 3% v/v. The same procedure as in 0.3L-RBF was followed in duplicate single-batch experiments except that food waste was added only once. Single-batch experiments were performed to evaluate the products distribution of long-term hydrolysis and acidification of food waste. The 0.3L-RBF and single-batch experiments were placed in a shaker at 120 rpm and 35°C. To evaluate the effect of higher temperature on hydrolysis/lactate formation, duplicate experiments were operated likewise to 0.3L-RBF but at a temperature of 50°C until day 17. The same mesophilic inoculum was mixed with thermophilic anaerobic sludge from a recycling company (Heerenveen, the Netherlands) and added (3% v/v) as inoculum for the thermophilic experiments. On day 17, temperature was switched to 35°C for subsequent chain elongation. A modified cap was used for the Schott bottles to allow liquid sampling and gas was collected via connected gas bags.

Liquid and gas samples were taken regularly to measure metabolites, pH and gas composition. The following parameters were used to evaluate the performance of the process and for comparison with literature: substrate hydrolysis, estimated as the increase in measured COD_S between the beginning and end of each cycle divided by the TS in the added food waste (g $COD_S \cdot kg\ TS_{added}^{-1}$); conversion efficiency, regarded as the amount of COD in a given product with respect to either COD_T or COD_S measured at the end of the cycle (g $COD_{product} \cdot g\ COD^{-1}$); carbon specificity, equivalent to the product/carboxylates ratio, in mmol $C \cdot L^{-1}$; hydroxide input, calculated based on the production of both MCC (mol $OH^- \cdot mol\ MCC^{-1}$) and total fatty acids (FA) (mol $OH^- \cdot kg\ COD_{FA}^{-1}$).

2.2.2. Analytical methods

Gas headspace composition, carboxylates and alcohols were determined by gas chromatography methods (Roghair et al., 2018c). Carboxylates and alcohols measured in the soluble fraction of samples were: straight-chain carboxylates (C2-C8), isobutyrate, b-valerate (both 2- and 3-methylbutanoic acid together), isocaproate (4-methyl-pentanoic acid) and straight-chain alcohols (C1-C6). L-lactate, succinate and formate were measured in the soluble fraction of samples by HPLC (Thermo Scientific Dionex UltiMate 3000, Thermo Fischer) equipped with a refractive index detector (Shodex RI-71, Separations) and an Alltech OA-1000 column (length 300 mm; ID 6.5 mm). The column oven was maintained at 60°C and 1.25 mM sulphuric acid was used as mobile phase at a continuous flow of 0.6 $mL \cdot min^{-1}$. The injection volume was 20 μL. Chromatography data were analysed with Chromeleon software (version 6.80 SR13). COD_S measurements were performed at the end of each cycle with LCK514 kits (HACH GmbH, Germany) after sample centrifugation (10000 rpm, 10 min) and dilution of the supernatant. Raw experimental data is available in the DANS-EASY database (https://doi.org/10.17026/dans-z44-2z4d).

2.2.3. Microbiome composition analysis

Samples for microbiome composition analysis were taken (Figure S1) from the fermentation broth, centrifuged at 10000 rpm for 10 min and stored at -20°C for DNA extraction and sequencing. DNA was extracted from the pellets applying a PowerSoil DNA isolation kit, according to the manufacturer's instructions. The isolated DNA was used as template for amplifying the V3-V4 region of 16S rRNA via Illumina sequencing using the primer sets described by Takahashi et al. (2014). This allowed simultaneous amplification of bacterial and archaean 16S rRNA. The sequences were deposited in the ENA database under accession number PRJEB33791. DNA sequences were processed with the DADA2 pipeline to identify ASVs (amplicon sequence variants) (Callahan et al., 2016). ASVs are alleged to be independent of reference databases, reproducible in future data sets and reusable across studies (Callahan et al., 2017). The sequences were submitted to the SILVA database for taxonomic identification (Quast et al., 2013). The entire ASV table was normalized using the cumulative-sum scaling (CSS) method which helps to avoid biases generated with current sequencing technologies due to uneven sequencing depth (Paulson et al., 2013). A Bray–Curtis dissimilarity matrix was calculated and used to build Principal Coordinate Analyses and Constrained Principal Coordinate Analysis, both retrieved from Phyloseq and Vegan packages (McMurdie and Holmes, 2013; Oksanen et al., 2019). To compare the differences in taxonomic composition and to assess whether some bacterial taxa were differentially abundant, we conducted a statistical analysis in which we assessed separately the read counts at ASV level using the metagenomeSeq package (Paulson et al., 2013). With the coefficients from the model, we applied moderated t-tests between accessions and the differences in the abundance of taxa between accessions were considered significant when adjusted P-values were lower than 0.05.

2.2.4. Co-occurrence and identity networks

Network analyses were performed to assess the dynamics of the interactions in the microbiomes. Non-random co-occurrence analyses were performed using SparCC, a tool capable of estimating correlation values from compositional data (Friedman and Alm, 2012). Using Python, we calculated SparCC correlations between microbial taxa at ASV level based on the 16S rRNA extracted from the reads. Correlations with a magnitude > 0.8 or < -0.8 and statistical significance ($P<0.01$) were included in the network analyses. For the identity network, a multiple alignment sequences of approximately 400 bp was performed using Muscle v3.7 (Edgar, 2004) and used to calculate a pairwise distance with Clustal Omega - 1.2.3 (Sievers et al., 2011) for all detected 16S rRNA sequences and thresholds were settled at 0.9 and 0.95 for the clustering. Networks visualizations were constructed using Cytoscape (v. 3.7.1) (Shannon et al., 2003). More information on the DNA analysis and networks construction can be found in the Supplementary Data.

2.3. Results

2.3.1. Microbiome can be steered to produce n-caproate as the dominant product

Fermentation of complex substrates (e.g. food waste) may result in a mixture of products (carboxylates, alcohols, diols, methane) when using microbiomes. In this study, the main products were carboxylates with increasing overall length over time. The operation of the 1L-RBF was divided in three cycles. Hydrolysis, acidification and chain elongation were expected to occur in each cycle.

No methane was observed during 1L-RBF operation (Figure S2). During the first cycle, we could not detect any lactate formation from food waste. Instead, the lactate present in food waste was consumed within two days for SCC production. Mainly acetate (C2) and n-butyrate (nC4) accumulated (~2 $g \cdot L^{-1}$ by day 15) and pH decreased from 6.0 to 4.7 (Figure 2.1). Other carboxylates such as propionate (C3), n-valerate (nC5) and n-caproate (nC6) were detected at concentrations below 500 $mg \cdot L^{-1}$. After a second addition of food waste in cycle 2, lactate was again consumed within three days and a further increase of n-butyrate and n-caproate was observed. n-butyrate and n-caproate concentrations increased ~1.7 and ~3-times, respectively, whereas acetate and propionate concentrations were stable (Figure 2.1) as well as pH which remained between 4.9-5.0.

In contrast to the first two cycles, lactate production was observed when increasing food waste concentration to 15% v/v in cycle 3. Lactate was detected at a maximum concentration of 4.5 $g \cdot L^{-1}$ and was subsequently consumed within 5 days (Figure 2.1). n-caproate was the main product during lactate consumption with n-caproate concentrations displaying a ~5-fold increase from 1.2±0.03 (days 29 and 32) to 5.4±0.01 $g \cdot L^{-1}$ (days 39 and 41); which equals to 11.9 g $COD_{nC6} \cdot L^{-1}$. The concentrations of SCC increased to a lesser extent, ~1.3 times for acetate and ~1.6-times for n-butyrate. In cycle 3, n-heptanoate (nC7) and n-caprylate (nC8) were detected at a maximum concentration of 89 and 142 mg/L, respectively. During the period of lactate production, pH went down from 5.1 to 4.7 and increased back to ~5.3 when lactate was consumed. Overall, changes in pH and metabolites profile indicate that two separate phases occurred: an acidification phase towards lactate as the main product followed by a chain elongation phase where n-caproate production was favored the most (Figure S3). The synthesis of n-caproate in cycle 3 seemed to be linked to lactate as electron donor. Hydrolysis was estimated to be 20, 265 and 96.7 g $COD_S \cdot kg\ TS_{added}^{-1}$ for cycles 1, 2 and 3, respectively. These values are comparable to those obtained by Bolaji and Dionisi (2017) who observed a maximum substrate degradation of ~283 g $COD_S \cdot kg\ TS_{added}^{-1}$ when vegetables waste was fermented to a mixture of SCC and MCC. The highest n-caproate production rate of 1.89 $g \cdot L^{-1} \cdot d^{-1}$ (4.2 g $COD_{nC6} \cdot L^{-1} \cdot d^{-1}$) (days 34-36) was measured in cycle 3 while the overall n-caproate production rate in this cycle (including hydrolysis, acidification and chain elongation; days 32-39) was 0.61 $g \cdot L^{-1} \cdot d^{-1}$ (1.35 g $COD_{nC6} \cdot L^{-1} \cdot d^{-1}$) (Table S2).

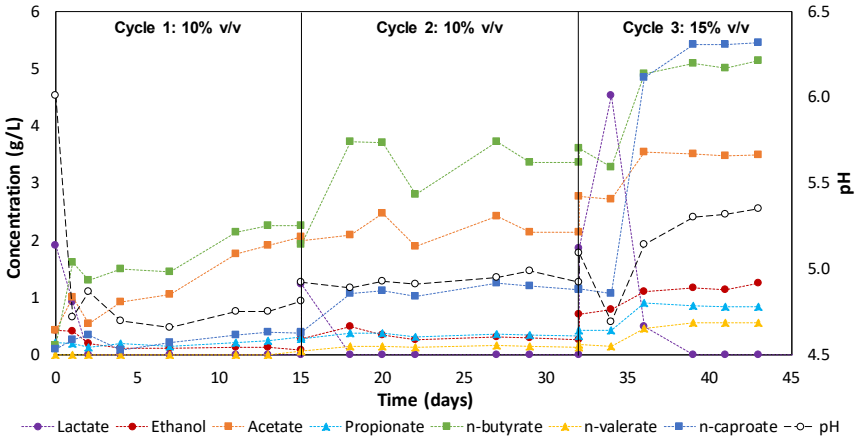

Figure 2.1 Profile of metabolites and pH during 1L-RBF operation. Potential electron donors (circles); even-chain carboxylates (squares); odd-chain carboxylates (triangles). Solid vertical lines show the days of substrate addition.

Process efficiency was evaluated in terms of COD and carbon conversion. In 1L-RBF, between 25-34% of the COD_T added as food waste was identified in the measured metabolites (Figure S4) which equals to 50-80% of COD_S. Conversion efficiency of COD_S into n-caproate ($COD_{nC6}{\cdot}COD_S^{-1}$) was 29.7±0.5% (days 39-41) in cycle 3, equivalent to a 5-fold increase during the experiment (Figure S5). The same increasing trend was observed for n-valerate (~6.8-fold increase) although it remained at low proportions. The highest COD_T conversion efficiency towards n-caproate ($COD_{nC6}{\cdot}COD_T^{-1}$) was 12.4% in cycle 3. Carbon specificity (product/carboxylates ratio) for n-caproate reached a maximum of 38.2±0.1% in cycle 3 (Table S2). In a comparable continuous one-stage reactor, Xu et al. (2018) obtained an n-caproate carbon specificity of 23% using solely yogurt-waste as substrate. These authors also observed equivalent carbon specificities for propionate, which has been reported as a product of the competitive acrylate pathway in lactate-based chain elongation with in-line extraction (Kucek et al., 2016a). Here nevertheless, propionate was always a minor metabolite and propionate carbon specificities remained at 4-5% probably due to the low pH levels which can limit the growth of propionate producing bacteria (Hettinga and Reinbold, 1972).

Fermentation proceeded without pH control but food waste pH was adjusted before being added to the reactor. Hydroxide used for pH adjustment equals to 0.77-4.35 mol OH^-·mol MCC^{-1} and hydroxide input showed a decreasing trend after every cycle (Table S2). These values are 0.8- to 2.3-times the amount of hydroxide used by Roghair et al. (2018) in a chain elongation reactor fed with the same original food waste (previously acidified at pH 5.5) and ethanol.

2.3.2. Subsequent acidification and chain elongation regulate pH dynamics while repeated food waste addition enhances n-caproate selectivity

Results of 1L-RBF suggest that lactate was an important electron donor for carboxylates chain elongation. Therefore, food waste fermentation to lactate and carboxylates was systematically studied in the duplicate 0.3L-RBF experiments. In these experiments, lactate was produced within 1-2 days causing the pH to drop and was subsequently consumed for FA formation (Figure 2.2a). The corresponding increase in pH was observed during lactate consumption. This same behavior in

lactate and pH profiles was observed after each addition of food waste. In cycle 2 and 3, n-butyrate, n-valerate and n-caproate were the main carboxylates formed during lactate consumption, all being products of the RBO pathway. Thus, reproducible acidification and chain elongation phases could be distinguished. In batch and repeated-batch food waste fermentation, initial environments rich in nutrients and easily fermentable substrate would promote lactate formation as a readily produced ATP-yielding electron sink. After lactate production, the medium is acidified and only a few specialists (e.g., *M. elsdenii*) can take up lactate at low pH levels to produce FA (Counotte and Prins, 1981). Hydrolysis was estimated to be 212.5±30 g COD_S·kg TS_{added}^{-1} in cycle 1 but high deviations were observed in the following cycles and it is, therefore, not clear whether hydrolysis occurred in cycles 2 and 3 (data not shown). During the 0.3L-RBF experiments, n-caproate concentrations increased after every cycle and n-caproate was the second main metabolite produced after n-butyrate. Methane was not detected in any of the cycles in 0.3L-RBF (Figure S6). The highest n-caproate concentrations and production rates in 0.3L-RBF were observed in cycle 3 (Figure 2.2a, Table S2), being 3.4±0.20 g·L^{-1} and 0.3±0.11 g·L^{-1}·d^{-1}, respectively.

Similarly to the 0.3L-RBF experiments, lactate was also produced in the single-batch fermentation and was further converted to SCC with the respective changes in pH (Figure 2.2b). Metabolites profile and final pH at the moment of lactate depletion (day 8) were similar in 0.3L-RBF and single-batch experiments. After lactate depletion, however, the single-batch experiment showed a fairly stable pH (~4.9) and product spectrum. n-caproate concentration remained <1 g·L^{-1} after more than 40 days of reaction time with acetate and n-butyrate produced at similar concentrations. Thus, chain elongation is promoted by both the addition of substrate and the availability of electron acceptors. Addition of substrate results in more lactate which in the presence of electron acceptors (i.e., C2, nC4) can be more efficiently used for MCC production. Experiments with pure cultures have shown that the lactate needed to produce one molecule of n-caproate was reduced in 11% when acetate was supplemented or in 37% when n-butyrate was added to the medium (Zhu et al., 2017). In our experiments, electron acceptors were always available and they might have substantially contributed to n-caproate formation. Whether one-time addition of 30% v/v food waste (the total amount added after 3 cycles) would allow the occurrence or enhancement of acidification and chain elongation was not assessed. In cycle 3 of the 0.3L-RBF, acidification and chain elongation occurred simultaneously and lactate, SCC and n-caproate were produced during the acidification phase (Figure S3). Also, part of the products formed during chain elongation in cycle 3 could not be accounted for since probably they sorbed onto the organic phase (i.e., solids or oily phase of food waste).

Thermophilic conditions did not improve lactate production after two additions of food waste compared to 0.3L-RBF experiments (Figure S7). The lactate produced accumulated over time (~8.5 g·L^{-1}) and was not metabolized to carboxylates at 50°C. However, lactate conversion to n-butyrate and traces of n-caproate was observed (after ~24 days) when temperature was switched to 35°C suggesting a similar behavior as in 0.3L-RBF experiments.

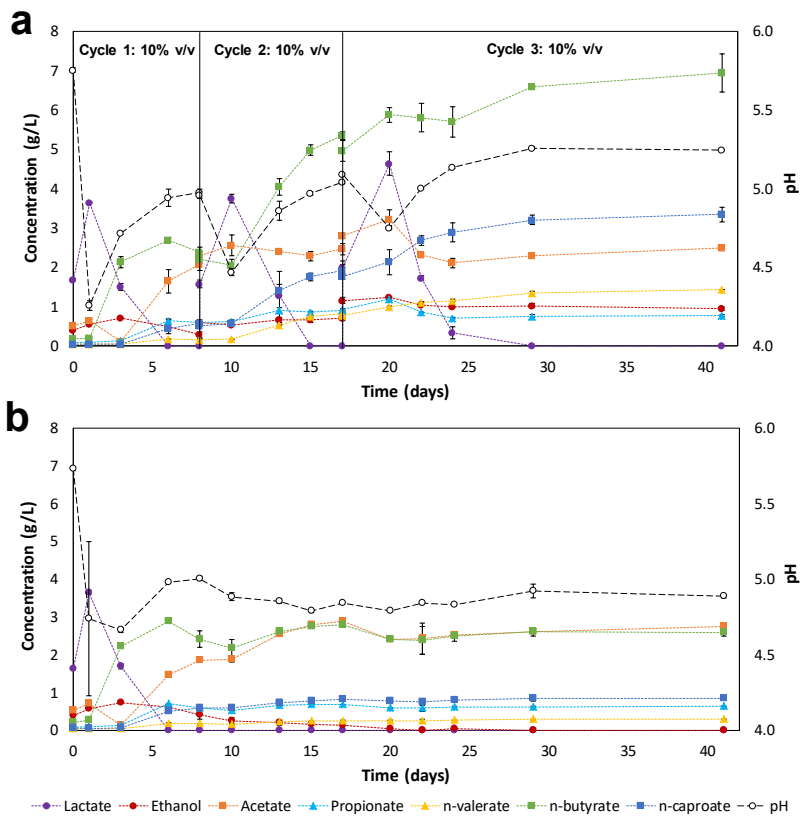

Figure 2.2 Metabolites produced during food waste fermentation in (**a**) 0.3L-RBF and (**b**) single-batch experiments. Potential electron donors (circles); even-chain carboxylates (squares); odd-chain carboxylates (triangles). Duplicates values were averaged and error bars depict actual values with respect to the mean.

Regarding process efficiency, similar tendencies to previous experiments were observed. Measured metabolites in 0.3L-RBF comprised 36-42% of COD_T (Figure S4). COD_S conversion efficiency and carbon specificity showed and increasing trend for n-caproate with values between 8-18% and 9-22%, respectively (Figure S8). The branched-chain SCC isobutyrate (iC4) and isovalerate (bC5) were detected at maximum concentrations of 350 and 500 mg/L, respectively, together with other minor metabolites i.e., succinate, formate, butanol, propanol, hexanol, methanol, n-heptanoate and pentanol (Figure S9). Among them, succinate (up to 500 mg/L) and formate (up to 1.1 $g \cdot L^{-1}$) were the most dominant and were metabolized during fermentation. However, all minor metabolites together never reached concentrations higher than 2.5 g $COD \cdot L^{-1}$. In the case of 0.3L-RBF, the hydroxide input ranged from 0.47 to 1.47 mol $OH^- \cdot$mol MCC^{-1} (Table S2). The decreasing trend in hydroxide input together with the increasing trend in pH after every cycle suggest that besides hydroxide being used more efficiently after every cycle due to higher MCC selectivity, buffer capacity also accumulated and contributed to neutralize acids.

2.3.3. *Lactobacillus* and *Caproiciproducens* dominated the microbiome composition

Despite the complex composition of the food waste, only a few microorganisms were enriched during fermentation experiments in both 1L-RBF and 0.3L-RBF. Two genera were persistently dominant in all the samples: *Caproiciproducens* and *Lactobacillus* which together showed a relative abundance of 57-93% (Figure 2.3). *Caproiciproducens* spp. were most dominant (32-72% relative abundance) followed by *Lactobacillus* spp. (12-56% relative abundance). *Clostridium* spp. were also persistent during the experiments although at lower relative abundances (≤15%). In total, 22 ASVs belonging to *Caproiciproducens*, 12 ASVs belonging to *Lactobacillus* and 13 ASVs belonging to *Clostridium* were identified (Figure S10). *Lactobacillus* sp. ASV1 was the most abundant *Lactobacillus* (≤95%) (Figure 2.4) and was closely related to *L. johnsonii* (100% identity), *L. gasseri* (99.5% identity) and *L. taiwanensis* (99.5% identity). These *Lactobacillus* species are obligately homolactic LAB (Vandamme et al., 1996) and their high abundance support that lactate formation occurred through homolactic fermentation. It is worth mentioning that even though obligately heterolactic LAB were the most abundant (~95% of *Lactobacillus* spp.) in the food waste (ASV18; 100% identity to *L. sanfransiscensis*), homolactic bacteria (present in the inoculum) were enriched in the experiments. This could be a result of the specific conditions of the experiments or due to inactivation of indigenous LAB during food waste storage. Since LAB are abundant in food waste (Wu et al., 2018), heterolactic and homolactic metabolisms might compete when fresh food waste is used as substrate.

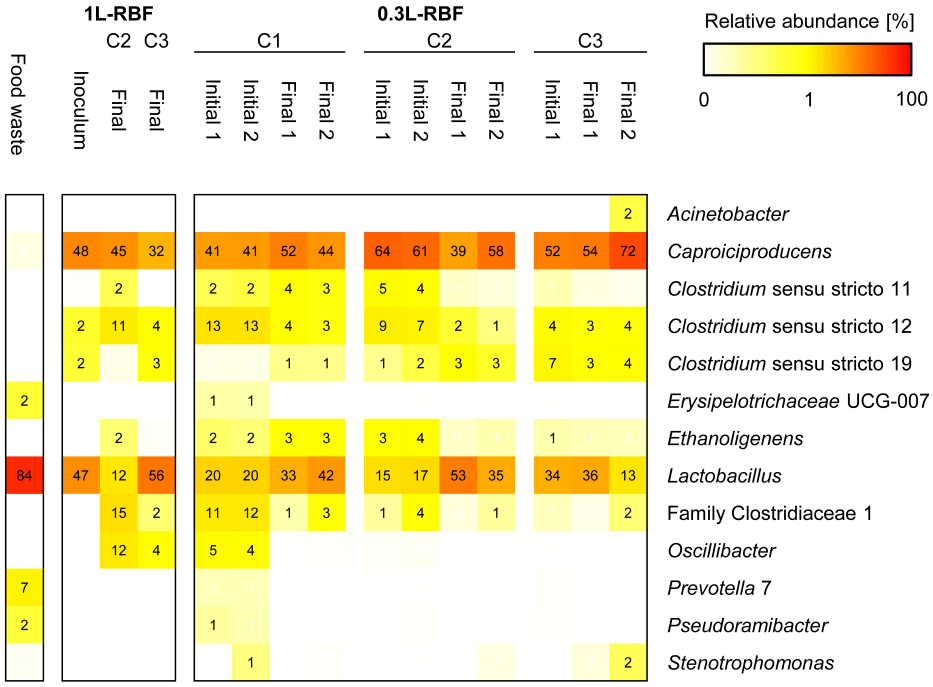

Figure 2.3 Heat map with relative abundance for effective ASVs (after CSS normalization) at genus level unless specified otherwise. 0.3L-RBF duplicate reactors are designated with numbers 1 and 2. Samples were taken at the beginning (Initial) and end (Final) of cycles 1 (C1), 2 (C2) and 3 (C3). No DNA could be extracted from the beginning of cycle 3 in 0.3L-RBF reactor 2.

2.3.4. Enriched *Caproiciproducens* spp. co-occurred with *Lactobacillus* spp.

The microbiomes developed in this study tended to be more alike as fermentation proceeded. Similarities between 1L-RBF and 0.3L-RBF microbiomes, shown by a reduced beta-diversity, increased at the end compared to the beginning of the experiments (Figure S11a). Preliminary analysis of the 0.3L-RBF experiments showed major changes in the microbiomes during fermentation. The microbiomes clustered into two groups (Figure S11b) referred to as: SCC-producing microbiomes (end of cycle 1/beginning of cycle 2; group 1) and MCC-producing microbiomes (from end of cycle 2 onwards; group 2). Differential abundance analysis revealed that many *Caproiciproducens* spp. including *Caproiciproducens* spp. ASV4 and ASV7 were enriched in MCC-producing microbiomes whereas *Clostridium* spp. and *Ethanoligenens* spp. were enriched in SCC-producing microbiomes (Figure S12). This suggests that chain elongating microorganisms require longer time or specific conditions (e.g., higher pH or electron acceptors concentration) to grow. Furthermore, co-occurrence network analysis (Figure S13) showed a positive interaction between ASV1, belonging to *Lactobacillus* spp., and ASVs 2, 3, 4 and 5, which were the most abundant ASVs belonging to *Caproiciproducens* spp. (Figure 2.4).

Lactobacillus sp. ASV1 was a key LAB in the microbiome closely related to microorganisms capable of using starch, oligosaccharides, disaccharides and monosaccharides as substrate for lactate production (Gänzle and Follador, 2012). The produced lactate would then be utilized by lactate elongators to produce MCC. However, microorganisms commonly reported to use lactate for MCC formation such as *Ruminococcaceae* bacterium CPB6 or species belonging to the *Megasphaera* genus were not found in this study. Instead, species of the genus *Caproiciproducens* are likely responsible of MCC production in our experiments. ASVs belonging to the *Caproiciproducens* genus showed 91-95% similarity to *Caproiciproducens galactitolivorans*. *Caproiciproducens* is a recently defined genus with *Caproiciproducens galactitolivorans* strain BS-1 as the only species described so far. *Caproiciproducens galactitolivorans* is reported to utilize hexoses, pentoses, disaccharides and glycerol to produce acetate, n-butyrate, n-caproate and hydrogen (Kim et al., 2015). Therefore, sugars were most likely used for MCC production. However, the remarkable dominance of *Caproiciproducens* in our experiments suggests that organisms belonging to this genus used lactate to produce n-caproate. At the moment of this research, there was no report on the capability of *Caproiciproducens* spp. to use lactate for MCC production. The low similarity between *Caproiciproducens galactitolivorans* and the *Caproiciproducens*-related ASVs found here suggests that new species of *Caproiciproducens* were enriched in our experiments. The capability of *Caproiciproducens* organisms to metabolize both lactate and sugars could be foreseen, similarly to lactate elongators being capable of metabolizing sugars (Weimer and Moen, 2013; Wang et al., 2018). Hence, it is reasonable to hypothesize that *Caproiciproducens* spp. found in this study used lactate and sugars for chain elongation (Figure S14).

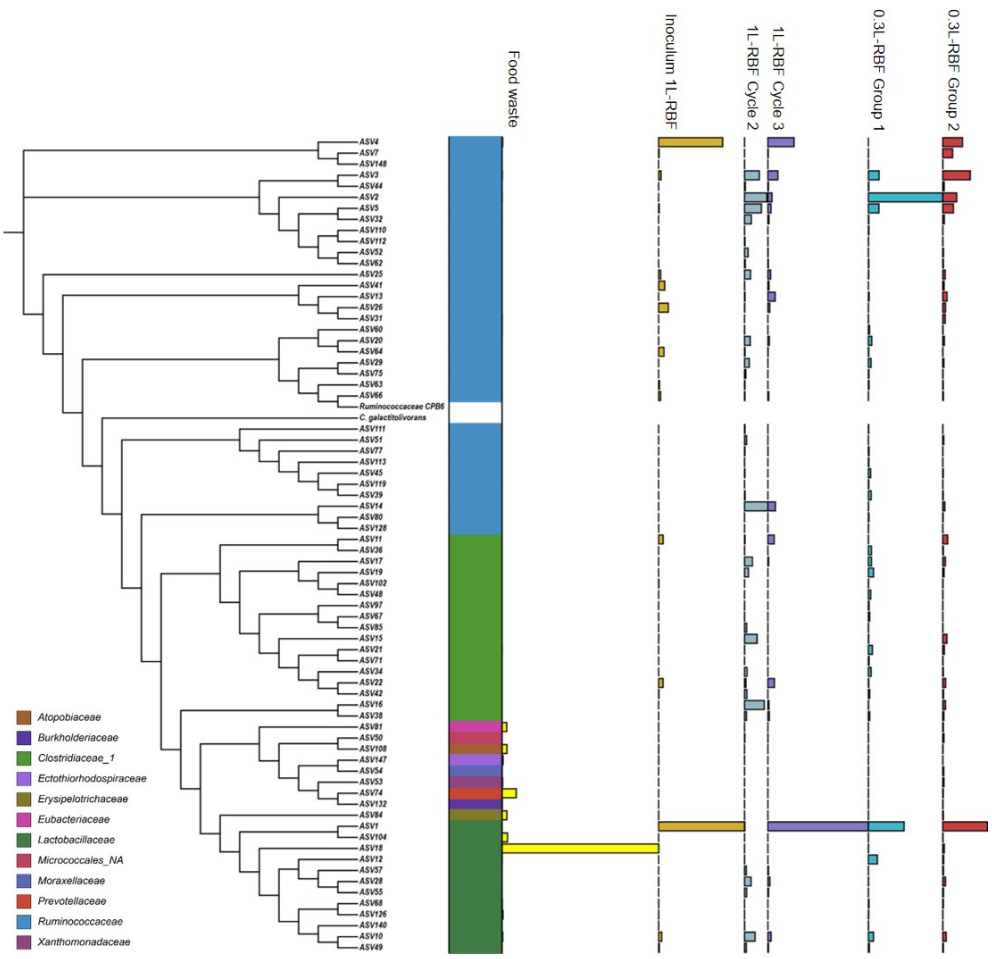

Figure 2.4 Phylogenetic tree and relative abundance of bacterial taxa at ASV level for food waste, 1L-RBF and 0.3L-RBF microbiomes.

2.4. Discussion

2.4.1. n-caproate production performance

In this study, n-caproate production was linked to lactate as electron donor, which is revealed by the increase in n-caproate concentrations and the increase in pH during lactate consumption. Lactate was produced through the homolactic pathway which is an efficient way to improve the production of MCC (Scarborough et al., 2018a). During acidification, lactate was the main product formed (>79% of acidification products, in COD) (Figure S3) and negligible CO_2 release was accordingly observed (Figure S2 and Figure S6). Since various electron donors and electron acceptors could have been produced/consumed to different extents, it is difficult to quantify the effectivity of lactate conversion through the RBO pathway. Relatively small amounts of ethanol were detected that may also contribute as electron donor together with sugars, amino acids, D-galacticol, propanol and electron acceptors, such as succinate, that could be present in the system (Angenent et al., 2016). Hydrogen was present in the reactors and glycerol could be present in the food waste, both of which can act as

indirect electron donors in chain elongation (Zhang et al., 2013; Leng et al., 2017). Besides, degradation of lipids and proteins present in the food waste could also result in MCC formation. Apart from lactate, other compounds (electron donors/acceptors) contributed to n-butyrate and n-caproate formation (Figure S3).

Coupling acidification and chain elongation helped to reduce hydroxide input for pH control. However, buffer capacity (Figure S15) also played an important role in determining the degree of acidification of the medium. Actual pH measured in 0.3L-RBF was higher than the levels expected by the total acids concentration, making evident that the alkalinity of the system was important to keep the pH levels high enough to prevent microbial inhibition (Figure S16). The initial buffer capacity helped to avoid extreme acidic conditions but also carboxylates and probably other buffer agents (NH_4^+, HS^-) were formed during fermentation. It is also evident from Figure S16 that the stoichiometry of lactate production and consumption partially describes the downward/upward pH trends caused by protons production/consumption and that the fluctuations in pH were attenuated by the buffer capacity of the system. Although hydroxide was added to the reactors with the neutralized food waste, the main changes in pH seemed to be due to acids production or destruction rather than substrate addition. However, buffer capacity accumulated in the reactor due to substrate addition and FA formation which explains the increasing trend in pH by the end of the experiments. Even though the eventual accumulation of buffer capacity might be detrimental for the long-term operation, this effect could be reduced by tuning operational parameters such as substrate concentration and volume replacement in sequencing-batch or fed-batch reactors. A trade-off between buffer capacity accumulation, conversion efficiencies and rates could then be achieved.

Even though optimization was out of the scope of this study, our results are comparable to other chain elongation processes using carbon-rich wastes (Table 2.1). Overall, the n-caproate production rates observed in our study (0.3 to 4.2 g $COD \cdot L^{-1} \cdot d^{-1}$) are in agreement with other works that used solely organic waste streams. The highest n-caproate production rate in this study is 2.7- to 6.4-times higher than other studies working with solid organic wastes (Grootscholten et al., 2013a; Reddy et al., 2018) and similar to the maximum obtained by Xu et al. (2018). Comparable n-caproate carbon specificities to this work (23-38%) have been reported from fresh food waste fermentation in batch leach-bed reactors (38%) (Nzeteu et al., 2018). Promising results have been obtained from liquid waste streams as well such as 45% n-caproate conversion efficiencies from yogurt-processing wastewater (Xu et al., 2018) and 79% n-caproate carbon specificities from acid whey (Duber et al., 2018). In a one-stage reactor equipped with in-line extraction, Xu et al. (2018) observed a lower n-caproate carbon specificity compared to our work (23% vs 38%). To improve the carbon specificity, the authors implemented a thermophilic acidification stage to produce lactate prior to the lactate-based chain elongation stage. The implementation of this two-stage system resulted in a doubled carbon specificity (48%) towards n-caproate and reached 66% for MCC. Unfortunately, data on the amount of chemicals used to control pH in the two separate reactors are not available.

A previous work from our group focused on the efficient use of ethanol and hydroxide in a continuous chain elongation reactor fed with acidified food waste and ethanol. The efficient use of ethanol resulted in a higher MCC conversion efficiency, MCC carbon specificity and a reduced hydroxide input for pH control (0.92 mol $OH^- \cdot$mol MCC^{-1} in the chain elongation stage and 5.5 mol $OH^- \cdot$kg $COD\text{-}FA^{-1}$

for the overall process) (Roghair et al., 2018c). Under these conditions, around 24% of the n-caproate produced was derived from the acidified food waste (COD from acetate and n-butyrate consumed). In the present study, n-caproate came entirely from food waste and hydroxide addition was lowered by a 2-times (0.47 mol OH^-·mol MCC^{-1}) and 7-times (0.79 mol OH^-·kg $COD_{carboxylates}^{-1}$) factor (Table 2.1). These benefits were attained by changing from a two-stage ethanol-based chain elongation to a one-stage lactate-based chain elongation process. However, n-caproate concentrations and productivities were much lower in the present study. Improved n-caproate productivities from food waste could be achieved by using a fed-batch reactor with higher substrate concentration and shorter cycles. In this case, residual amounts of electron acceptors should be maintained to promote higher MCC selectivities. Substrate conversion was limited by hydrolysis which can be improved by using leach-bed reactors (Nzeteu et al., 2018) or *in situ* extraction (Grootscholten et al., 2013a).

Table 2.1 n-caproate production and hydroxide input in chain elongation processes from waste streams.

Substrate	Process	pH control	nC6 concentration	Maximum nC6 production rate	nC6 conversion efficiency*	nC6 carbon specificity	Hydroxide input		Reference
			[g·L^{-1}]	[g COD·L^{-1}·d^{-1}]	[%]	[%]	[mol OH$^-$·mol MCC]	[mol OH$^-$ ·kg COD$_{carbox}$]	
Food waste	Repeated-batch[a]	Substrate pH adjusted	3.21	0.62	18	23	0.47	0.79	**This study**
Food waste	Repeated-batch[b]	Substrate pH adjusted	5.52	4.20	30	38	0.77	0.99	**This study**
OFMSW and ethanol	Batch	No	2.70	1.55	N.A.	N.A.	N.A.	N.A.	(Grootscholten et al., 2013a)
Food waste	Batch	Initial medium adjustment	10	6.61	N.A.	38[c]	N.A.	N.A.	(Nzeteu et al., 2018)
Vegetable and salad waste	Fed-batch	No	1.80	N.A.	N.A.	22[c]	N.A.	N.A.	(Bolaji and Dionisi, 2017)
	Batch	Buffer addition	3.08	N.A.	N.A.	23[c]	N.A.	N.A.	
Wine lees	Continuous	Yes	<0.5[d]	4.30	N.A.	36	N.A.	N.A.	(Kucek et al., 2016c)
Acidified food waste and ethanol	Continuous	Yes	23.40	12.16	59	76	0.92	5.50	(Roghair et al., 2018c)
	Continuous	Yes	7.10	12.38	13	46	1.93	N.A.	
Yogurt industry waste stream	Continuous single-stage	Yes	<0.5[d]	N.A.	N.A.	23	N.A.	N.A.	(Xu et al., 2018)
	Continuous two-stage	Yes	<0.5[d]	3.71	45	48	N.A.	N.A.	
Food waste	Batch	No	8.10	0.66	N.A.	N.A.	N.A.	N.A.	(Reddy et al., 2018)
Acid whey wastewater	Continuous	Yes	10.45	7.07	N.A.	79	N.A.	N.A.	(Duber et al., 2018)
Thin stillage	Continuous	Yes	6.80	27.20	33	44	N.A.	N.A.	(Carvajal-Arroyo et al., 2019)

*Based on COD$_S$; N.A.= not available; [a]Data from 0.3L-RBF , cycle 3; [b]Data from 1L-RBF, cycle 3; [c]COD$_{n\text{-}C6}$/COD in products; [d]in-line extraction was applied.

2.4.2. Outlook and process boundaries

2.4.2.1. Relevance of pH for balanced acidification and chain elongation

When no pH control is intended, the balance between substrate supplementation, alkalinity, reactor operation and the microbiome resilience will determine the conditions to avoid bioprocess instability due to outranged pH.

Although, LAB show hydrolytic activity at pH as low as 4.0, glycolysis is not functional under these conditions and lactate production would be inhibited (Kashket, 1987; Ohkouchi and Inoue, 2006). Hence, pH>4.0 is essential to allow lactate formation. However, such acidic conditions are inhibitory for lactate utilizers. Growth of *M. elsdenii* has been shown to be substantially affected at pH 4.65 (Weimer and Moen, 2013) and a recent work showed that lactate elongation to n-butyrate occurred only at pH≥4.5 (Sträuber et al., 2018). In the present study, lactate utilization for n-butyrate production occurred at a lower pH (4.0-4.3) (0.3L-RBF, day 1; thermophilic experiment, day 41). Moreover, the highest n-caproate production rate in our study was detected at an initial pH 4.7 (1L-RBF, day 34) even though pH<5.0 was reported to completely inhibit n-caproate production in a similar process (Nzeteu et al., 2018). It is worth mentioning that the undissociated n-caproic acid concentration (0.65 $g \cdot L^{-1}$) at this day was below the toxic limit (0.87 $g \cdot L^{-1}$) proposed to inhibit n-caproate production in ethanol-based chain elongation (Ge et al., 2015). Nevertheless, undissociated n-caproic acid concentration on day 36, when n-caproate formation was still observed, reached 1.72 $g \cdot L^{-1}$. These observations show that the microbiome developed in our experiments could function at more acidic environments than previous reports and in the presence of higher concentrations of the toxic undissociated n-caproic acid. The low pH and the presence of undissociated n-butyric (≤35 mM) and n-caproic (≤20 mM) acids could have prevented the acrylate pathway from being dominant despite the temporary high lactate concentrations. Propionate could still be formed at low pH levels when in-line extraction is applied and lactate accumulation is observed (Kucek et al., 2016a). Although it seems that lactate elongators can stand higher undissociated n-caproic acid concentrations than ethanol elongators or propionate producers, more research is needed to systematically determine the toxic limit of undissociated n-caproic acid for these three microbiomes.

2.4.2.2. Maximum hydroxide use for n-caproate production from carbohydrates

Reduced chemical use for pH control can help to increase the life cycle performance of the technology (Chen et al., 2017). At present, however, few studies report on either base or acid needed in their processes. In our study, homolactic fermentation (eq. 1) and lactate-based chain elongation (eq. 2, eq. 3) were the main identified processes. Considering glucose conversion to lactate through homolactic fermentation and lactate-based chain elongation to n-caproate, a maximum of 2/3 of the protons released can be self-neutralized by coupling these two processes. To keep a constant pH, base addition or intrinsic alkalinity from the substrate would still be needed. This equals to a maximum hydroxide need of 1 mol $OH^- \cdot$mol $nC6^{-1}$ or 3.9 mol $OH^- \cdot$kg $COD\text{-}C6^{-1}$. In this study, n-caproate was almost the only MCC produced and the values for hydroxide addition were always below the theoretical maximum (except for 1L-RBF cycles 1 and 2 were lactate was not produced, Table S2) even though SCC were always produced together with n-caproate. Hydroxide input was improved as pH started to increase over cycles due to increased n-caproate selectivity and

accumulation of buffer capacity. Clearly, the production of SCC increases the base need and the opposite is true for longer MCC production (e.g., n-caprylate).

2.5. Conclusions

Repeated-batch food waste fermentation without exogenous electron donor was steered to n-caproate as the dominant product. Lactate production and subsequent chain elongation from food waste regulated pH dynamics and buffer capacity of the substrate helped to avoid inhibitory acidic conditions and large pH fluctuations. These phenomena together lead to reduced hydroxide input for n-caproate production. Lactate was attributed as key electron donor for chain elongation and its uptake for n-caproate formation was observed at conditions suggested as inhibitory in the literature. *Lactobacillus* spp. and *Caproiciproducens* spp. dominated and co-occurred in the microbiome which shows the involvement of *Caproiciproducens* spp. in the use of lactate as electron donor.

Chapter 3

Effects of nZVI and lactate enantiomers on batch fermentation of lactate and acetate

This chapter was published as:
Carlos A. Contreras-Dávila, Johan Esveld, Cees J.N. Buisman and David P.B.T.B. Strik (2021). nZVI impacts substrate conversion and microbiome composition in chain elongation from D- and L-lactate substrates. Front Bioeng Biotechnol. 9, 666582.

Abstract

Medium-chain carboxylates (MCC) derived from biomass biorefining are attractive biochemicals to uncouple the production of a wide array of products from the use of non-renewable sources. Biological conversion of biomass-derived lactate during secondary fermentation can be steered to produce a variety of MCC through chain elongation. We explored the effects of zero-valent iron nanoparticles (nZVI) and lactate enantiomers on substrate consumption, product formation and microbiome composition in batch lactate-based chain elongation. In abiotic tests, nZVI supported chemical hydrolysis of lactate oligomers present in concentrated lactic acid. In fermentation experiments, nZVI created favorable conditions for either chain-elongating or propionate-producing microbiomes in a dose-dependent manner. Improved lactate conversion rates and n-caproate production were promoted at 0.5-2 g nZVI·L^{-1} while propionate formation became relevant at ≥3.5 g nZVI·L^{-1}. Even-chain carboxylates (n-butyrate) were produced when using enantiopure and racemic lactate with lactate conversion rates increased in nZVI presence (1 g·L^{-1}). Consumption of hydrogen and carbon dioxide was observed late in the incubations and correlated with acetate formation or substrate conversion to elongated products in the presence of nZVI. Lactate racemization was observed during chain elongation while isomerization to D-lactate was detected during propionate formation. *Clostridium luticellarii*, *Caproiciproducens* and *Ruminococcaceae* related species were associated with n-valerate and n-caproate production while propionate was likely produced through the acrylate pathway by *Clostridium novyi*. The enrichment of different potential n-butyrate producers (*Clostridium tyrobutyricum*, *Lachnospiraceae*, *Oscillibacter*, *Sedimentibacter*) was affected by nZVI presence and concentrations. Possible theories and mechanisms underlying the effects of nZVI on substrate conversion and microbiome composition are discussed. An outlook is provided to integrate (bio)electrochemical systems to recycle (n)ZVI and provide an alternative reducing power agent as durable control method.

3.1. Introduction

Production of biochemicals from renewables is of outmost importance to reduce anthropogenic impact on the environment. Carboxylates are platform chemicals that are produced by chemical or biological means. Short-chain carboxylates (SCC, up to 5 carbons) and methane are commonly observed in biological conversion of organics during anaerobic fermentation whereas medium-chain carboxylates (MCC, 6 to 12 carbons) are produced by specialized chain-elongating bacteria in the presence of reduced compounds in the so-called chain elongation process (Angenent et al., 2016). The metabolic energy to drive the chain elongation process is supplied by a variety of electron donors (e. g. alcohols, lactate, sugars) that can be obtained from waste biomass materials (Zhu et al., 2015; Angenent et al., 2016; Contreras-Dávila et al., 2020). Lactate is produced as one or a mixture of the two enantiomeric forms (D-lactate or L-lactate) depending on the culture conditions (Hofvendahl and Hahn-Hägerdal, 2000). Numerous (bio)process reactions can occur within lactate-based chain elongation microbiomes (Table 3.1). Lactate may be interconverted between the two enantiomeric forms by lactate racemase (Lar) (eq. 1). Under anaerobic conditions, lactate is first oxidized to pyruvate by confurcating lactate dehydrogenase which transfer electrons from lactate and reduced ferredoxin (Fd_{red}) to reduce NAD (Buckel and Thauer, 2018). Then, pyruvate is further converted to acetyl-CoA and carbon dioxide (CO_2) through pyruvate:ferredoxin oxidoreductase (PFOR) (Liu et al., 2020). This two-step lactate oxidation to acetate (eq. 2) yields electrons and carbon for the reverse-β-oxidation (RBO) pathway (Liu et al., 2020). In the RBO pathway, acetate is elongated with two carbons from acetyl-CoA to even-chain carboxylates such as n-butyrate (nC4) and n-caproate (nC6). Additionally, odd-chain carboxylates such as n-valerate (nC5) may be produced from propionate elongation (eq. 4-8). Propionate can be produced from lactate (eq. 9) by organisms such as *Megasphaera elsdenii* (Hino and Kuroda, 1993) or propionic acid bacteria (PAB) (Seeliger et al., 2002; Gonzalez-Garcia et al., 2017).

Several operational conditions such as pH, electron donor-to-acceptor ratio and hydrogen partial pressure can be used to steer chain elongation microbiomes (Angenent et al., 2016). The use of additional electron donors that do not act as carbon sources (e.g. hydrogen, cathodes, transition metals) can result in lower oxidation-reduction potential (ORP) and unbalanced fermentation in e.g. carboxylates and alcohol producing processes (Moscoviz et al., 2016; Wang et al., 2020). In this study, nano zero-valent iron (nZVI) was tested for steering product formation in chain elongation. Anaerobic corrosion of zero-valent iron (eq. 10-11) may decrease ORP by increasing pH or reducing anions such as NO_3^- and SO_4^{2-} present in the medium (Tratnyek et al., 2003). Together with Fe^{2+} released, reduced ORP stimulate the interconversion between the two lactate enantiomers by lactate racemase (Katagiri et al., 1961). L-lactate isomerization to D-lactate has been induced with zero-valent iron addition during lactate production in open-culture organic waste fermentation (Li et al., 2017). Lactate enantiomers interconversion could in turn impact lactate-based chain elongation product spectrum since organisms like *M. elsdenii* have been suggested to produce even-chain carboxylates from D-lactate and odd-chain carboxylates from L-lactate (Hino and Kuroda, 1993). nZVI may also donate electrons to bacteria through direct or H_2-mediated electron transfer (Tang et al., 2019; Gong et al., 2020), potentially influencing metabolic processes such as lactate oxidation to pyruvate (Fd_{red}-dependent lactate dehydrogenase (Weghoff et al., 2015)), pyruvate decarboxylation (PFOR) (Meng et

al., 2013), hydrogen formation and energy conservation (Angenent et al., 2016). These effects would in turn affect conversion rates and elongation of carboxylates. The electron donor hydrogen, for instance, improves MCC formation from lactate and food waste (Nzeteu et al., 2018; Wu et al., 2019).

Pyruvate decarboxylation by PFOR is a carbon-diverging step in lactate-based chain elongation as it results in carbon lost as CO_2. Although lactate-elongating bacteria do not seem to metabolize CO_2 to carboxylates (Tao et al., 2017), this could be done by other organisms in anaerobic microbiomes to increase carbon recovery. Homoacetogenic bacteria may use electrons or H_2 to reduce CO_2 to acetate (eq. 13-14). Acetate can then be used by chain-elongating bacteria to produce MCC. However, CO_2 recapture would be limited to 33-50% since homoacetogenic bacteria requires four H_2 molecules to reduce two CO_2 to acetate (H_2/CO_2 ratio = 2) while the stoichiometric H_2/CO_2 ratio produced from lactate is 1 or 2/3 when n-butyrate or n-caproate are produced, respectively (Contreras-Dávila et al., 2020). To achieve higher carbon recoveries, additional electron donors such as hydrogen (Wu et al., 2019) or nZVI (eq. 11) could be used. nZVI addition is reported to promote homoacetogenic activity in anaerobic digestion microbiomes (Meng et al., 2013). Lastly, nZVI may also increase substrate conversion when lactate (poly)esters are present e.g. poly-lactic acid (PLA) bioplastics or concentrated lactate solutions (Vu et al., 2005). Thus, appropriate nZVI doses should be added to adequately steer the microbiome. Recent reports on ethanol-elongating microbiomes showed improved substrate conversion to MCC with nZVI supplementation (Fu et al., 2020; Wang et al., 2020). However, nZVI effects on lactate-based chain elongation have not been studied. The aim of this work was to evaluate the effect of nZVI addition on batch lactate-based chain elongation. We hypothesized that nZVI could promote 1) lactate conversion to MCC by donating extra electrons; 2) lactate isomerization to produce even/odd carbon chains; and 3) carbon dioxide capture through acetate formation (Table 3.1). Abiotic tests with nZVI were done to evaluate chemical hydrolysis of lactate oligomers present in concentrated lactic acid (experiment I). Chain elongation incubations were carried out at different nZVI (experiment II) and H_2 (experiment III) concentrations. Finally, chain elongation of enantiopure lactate (D-lactate and L-lactate separately) or a racemic mixture of both enantiomers was studied with and without nZVI (experiment IV).

3.2. Materials and Methods

3.2.1. Mineral medium and inoculum

Salts and vitamins were added to the experiments as in Roghair et al. (Roghair et al., 2016). The trace elements solution contained: nitrilotriacetic acid, 2.0 $g{\cdot}L^{-1}$; $MnSO_4{\cdot}H_2O$, 1.0 $g{\cdot}L^{-1}$; $Fe(SO_4)_2(NH_4)_2{\cdot}6H_2O$, 0.8 $g{\cdot}L^{-1}$; $CoCl_2{\cdot}6H_2O$ 0.2 $g{\cdot}L^{-1}$; $ZnSO_4{\cdot}7H_2O$ 0.2 $mg{\cdot}L^{-1}$; $CuCl_2{\cdot}2H_2O$ 20.0 $mg{\cdot}L^{-1}$; $NiCl_2{\cdot}6H_2O$ 20.0 $mg{\cdot}L^{-1}$; $Na_2MoO_4{\cdot}2H_2O$ 20.0 $mg{\cdot}L^{-1}$; Na_2SeO_4 , 20.0 $mg{\cdot}L^{-1}$; Na_2WO_4, 20.0 $mg{\cdot}L^{-1}$, and was added at 1 $mL{\cdot}L^{-1}_{medium}$ according to Zhu et al. (Zhu et al., 2015). Yeast extract was added at 1 $g{\cdot}L^{-1}$. Biomass from a lab-scale chain elongation bioreactor converting lactate and acetate to n-caproate was used as inoculum (Contreras-Dávila et al., 2020). The lab-scale reactor contained granular activated carbon as carrier material. Inoculum samples were taken during (experiments II-III) and after (experiment IV) continuous operation (section 3.2.3). Inoculum was added at 5% v/v after centrifugation at 10000 rpm for 10 min and resuspension of the pellet in N_2-bubbled demi water.

Table 3.1 Thermodynamics of (bio)process reactions potentially involved in lactate-based chain elongation microbiomes and nZVI conversion.

No.	Equation	e⁻ mol transferred	ΔG°' (kJ·reaction^{-1})	ΔG' (kJ·reaction^{-1})	ΔG' (kJ·e⁻ mol^{-1})
	Lactate (inter)conversion				
1	L-lactic acid ↔ D-lactic acid	-	-0.4	-0.4	-
2	lactate$^-$ + H_2O → acetate$^-$ + 2 H_2 + CO_2	4	-9.5	-9.5	-2.38
3	lactate$^-$ + Fe^{2+} + H_2O → acetate$^-$ + 2 Fe^0 + CO_2 + 4H^+	4	-169.2	-135.0	-33.75
	Lactate-based chain elongation				
4	1.4 lactate$^-$ + 0.6 acetate$^-$ + H^+ → n-butyrate$^-$ + 0.8 H_2 + 1.4 CO_2 + 0.6 H_2O [a]	5.6	-61.7	-70.2	-12.54
5	lactate$^-$ + acetate$^-$ + H^+ → n-butyrate$^-$ + CO_2 + H_2O [b]	4	-57.9	-66.4	-16.61
6	lactate$^-$ + propionate$^-$ + H^+ → n-valerate$^-$ + CO_2 + H_2O [b]	4	-57.8	-66.3	-16.58
7	lactate$^-$ + n-butyrate$^-$ + H^+ → n-caproate$^-$ + CO_2 + H_2O [b]	4	-57.9	-66.4	-16.61
8	2 lactate$^-$ + acetate$^-$ + 2 H^+ → n-caproate$^-$ + 2 CO_2 + 2 H_2O [c]	8	-115.7	-132.8	-16.61
	Propionate formation				
9	3 lactate$^-$ → 2 propionate$^-$ + acetate$^-$ + CO_2 + H_2O [d]	12	-172.0	-172.0	-14.33
	Chemical reactions involving nZVI				
10	Fe^0 + 2 H^+→ Fe^{2+} + H_2	2	-10.6	-27.7	-13.87
11	Fe^0 + 2 H_2O → Fe^{2+} + 2 OH^- + H_2	2	-10.6	-27.7	-13.87
12	Lactyl lactate$^-$ + OH^- → 2 lactate$^-$ [e]	-	-112.1	-103.6	-
	Homoacetogenesis with nZVI or hydrogen				
13	4 Fe^0 + 2 CO_2 + 7 H^+ → 4 Fe^{2+} + acetate$^-$ + 2 H_2O	8	-137.6	-197.5	-24.68
14	4 H_2 + 2 CO_2 → acetate$^-$ + 2 H_2O + H^+	8	-95.7	-87.2	-10.90
	Chain elongation with nZVI or hydrogen				
15	2 Fe^0 + 2 acetate$^-$ + 5 H^+ → 2 Fe^{2+} + n-butyrate$^-$ + 2 H_2O	4	-69.7	-112.5	-28.13
16	2 Fe^0 + acetate$^-$ + n-butyrate$^-$ + 5 H^+ → 2 Fe^{2+} + n-caproate$^-$ + 2 H_2O	4	-69.7	-112.5	-28.13
17	2 H_2 + 2 acetate$^-$ + H^+ → n-butyrate$^-$ + 2 H_2O	4	-48.4	-56.9	-14.23
18	2 H_2 + acetate$^-$ + n-butyrate$^-$ + H^+ → n-caproate$^-$ + 2 H_2O	4	-48.4	-56.9	-14.23

Free energies of formation used for calculations are shown in Table S1.

All free energies of reaction are calculated considering reactants and products concentrations of 1 M or 1 atm (H_2, CO_2).

$\Delta G^{o'}$ values are corrected for pH 7; $\Delta G'$ for pH 5.5 according to $\Delta G' = \Delta G^o + RT \cdot Y_{H^+} \cdot \ln[H^+]$ where Y_{H^+} is the reaction proton yield/consumption. $Y_{H^+} = -Y_{OH^-}$ in equations 2 and 3.

[a] Based on results from this study and similar to *C. acetobutylicum* (Diez-Gonzalez et al., 1995).

[b] Proposed for a reactor microbiome dominated by *Ruminococcaceae* bacterium CPB6 (Zhu et al., 2015).

[c] Equations 5 + 7.

[d] (Seeliger et al., 2002).

[e] (Ivanova et al., 2000).

3.2.2. Substrates and nZVI material

Lactate used as electron donor in the experiments were: concentrated lactic acid (≥90%) (VWR, the Netherlands), sodium-D-lactate ≥99.0% (Sigma-Aldrich, the Netherlands) and sodium-L-lactate ≥99.0% (Sigma-Aldrich, the Netherlands). The concentrated lactic acid was a mixture of lactate monomers and oligomers (Vu et al., 2005) containing mainly L-lactic acid (≥97%, as reported by VWR); D-lactic acid was not detected in these chemicals by our lab analysis. Acetic acid 99-100% (Merck KGaA, Germany) was added as electron acceptor. The nZVI particles (Nanofer Star, Nano Iron, Czech Republic) used in this study had an average particle size of 60±1.3 nm and contained 74% Fe^0, along with 8% FeO and 18% Fe_3O_4 with an oxides layer thickness of 4.3±0.53 nm (as reported by Nano Iron). Before application, 1 g of nZVI powder was suspended in 4 mL of N_2-bubbled demi water. The suspension was mixed for 10 minutes using a high shear mixer (Ultra-Turrax T25, IKA, Germany). After this, the bottle containing the slurry was loosely closed to avoid overpressure due to hydrogen gas release and left to rest at room temperature for ~48 hours before adding it to the experiments. This procedure followed the instructions of the supplier and served to erode the protective oxides layer present on the nZVI particles.

3.2.3. Experimental set-up

Incubations were carried out in 125 mL serum bottles using a liquid volume of 40 mL. An overview of the initial conditions in the different experiments can be found in Table 3.2. First, chemical hydrolysis of lactate oligomers by nZVI particles was evaluated under abiotic conditions in experiment I. Since concentrated lactic acid solutions contain lactate oligomers (Vu et al., 2005), nZVI was added at 1 and 5 $g \cdot L^{-1}$ to a 27 $g \cdot L^{-1}$ total lactate (monomers + oligomers) solution prepared with concentrated lactic acid. Hydrolysis was followed by measuring the increase in monomeric lactate concentrations. A control experiment with no nZVI was included. Experiments were done in triplicate at an initial pH of 5.5. Vitamins, yeast extract, $(NH_4)H_2PO_4$ and trace elements were left out to prevent microbial growth.

In experiment II, the effect of different nZVI concentrations (0.5, 1, 2, 3.5 and 5 $g \cdot L^{-1}$) on lactate-based chain elongation was tested in duplicate batch incubations using 30 $g \cdot L^{-1}$ total lactate and 6 $g \cdot L^{-1}$ acetic acid. This resulted in monomeric L-lactate concentrations of 19.3±0.6 $g \cdot L^{-1}$ (64% of total lactate added) as expected from 90% concentrated lactic acid solutions (Vu et al., 2005). The control experiment was carried out without nZVI. The experiment with 3.5 g nZVI·L^{-1} was done using a 30 mL liquid volume. Since hydrogen release from nZVI corrosion could be an additional electron donor, the effect of H_2 on lactate-based chain elongation was studied in experiment III by adding H_2 at initial partial pressures (P_{H2}) of 0.45 and 1.2 atm. Acetate (5.7 $g \cdot L^{-1}$) and n-butyrate (9.3 $g \cdot L^{-1}$) elongation with H_2 as sole electron donor (0.75 atm) was also tested in the same experiment. Lastly, to test the effect of the lactate enantiomer fed and the presence of nZVI on lactate conversion and product spectrum, fermentation of D-lactate and L-lactate with and without nZVI (1 $g \cdot L^{-1}$) was studied in triplicates in experiment IV. Enantiopure or a racemic mixture (1:1) of D- and L-lactate sodium salts were added to reach a lactate concentration of 18 $g \cdot L^{-1}$. This concentration is comparable to the monomeric lactate concentrations measured in the experiments supplied with concentrated lactic acid. Acetate was added as electron acceptor at 5 $g \cdot L^{-1}$. All the experiments were incubated in a shaker at 120 rpm and 30°C. Initial pH was adjusted to 5.5 by adding 4 M KOH and/or 1 M HCl.

Headspace gas was exchanged by vacuum/filling cycles (5 times) with N_2 in experiment I and N_2:CO_2 (80:20) in experiments II-IV to a final overpressure of 0.5 atm. N_2 was partly replaced with H_2 to reach designated P_{H2} for experiment III. When pressure raised above 2.5 atm during experiments II and III, gas was manually released to bring headspace pressure down to 1.2-1.5 atm and the released gas volume was measured. Gas bags were used in experiment IV to avoid overpressure. Process performance in the incubations was evaluated based on substrate conversion (total lactate + acetate); lactate enantiomeric distribution; and electron and carbon selectivities (see Supplementary Material).

Table 3.2 Overview of experimental design.

Experiment	Substrate	Lactate monomers concentration [g·L^{-1}]	Lactate oligomers concentration[a] [g·L^{-1}]	Electron acceptor concentration [g·L^{1}]	nZVI concentration [g·L^{-1}]	Hydrogen [atm]
I) Chemical hydrolysis	Concentrated lactic acid	19.3	10.7	0	0 (Control)	0
	Concentrated lactic acid	19.3	10.7	0	1	0
	Concentrated lactic acid	19.3	10.7	0	5	0
II) nZVI concentrations	Concentrated lactic acid	19.3	10.7	6	0 (Control)	0
	Concentrated lactic acid	19.3	10.7	6	0.5	0
	Concentrated lactic acid	19.3	10.7	6	1	0
	Concentrated lactic acid	19.3	10.7	6	2	0
	Concentrated lactic acid	19.3	10.7	6	3.5	0
	Concentrated lactic acid	19.3	10.7	6	5	0
III) Hydrogen effect	Concentrated lactic acid	17.2	9.5	6	0	0 (Control)
	Concentrated lactic acid	17.2	9.5	6	0	0.45
	Concentrated lactic acid	17.2	9.5	6	0	1.2
	acetate + n-butyrate	0	0	6 + 9	0	0.75
IV) Lactate enantiomers	Sodium D-lactate	18	0	5	0	0
	Sodium D-lactate	18	0	5	1	0
	Sodium L-lactate	18	0	5	0	0
	Sodium L-lactate	18	0	5	1	0
	Racemic sodium lactate	18	0	5	0	0
	Racemic sodium lactate	18	0	5	1	0

[a] Difference between total lactate added and measured lactate monomers.

3.2.4. Analytical methods

Liquid samples were taken regularly to measure pH and soluble metabolites. Samples were centrifuged (15000 rpm, 10 min) and stored at -20°C before metabolites analyses. Lactate (both D- and L-lactate monomers together), succinate and formate were measured by HPLC (Contreras-Dávila et al., 2020). Lactate enantiomers (D-lactate and L-lactate) were separated and quantified *via* isocratic HPLC using a chiral column. Fatty acids, alcohols and gas headspace composition (O_2, N_2, CO_2, CH_4, H_2) were quantified by gas chromatography. For methods description see Supplementary Material. The gas production/consumption and partial pressures were estimated using headspace

composition, manually measured pressure and gas released during pressure adjustments. Raw experimental data are available in the 4TU.ResearchData repository (https://doi.org/10.4121/14236922).

3.2.5. Microbiome analysis

Samples were centrifuged at 10,000 rpm for 10 min and stored at -20°C for DNA extraction and sequencing. DNA was extracted from the pellets (PowerSoil DNA isolation kit) and used as template for amplifying the V3-V4 region of 16S rRNA via Illumina sequencing using the primer sets described by Klindworth et al. (Klindworth et al., 2013) for simultaneous amplification of bacterial and archaean 16S rRNA. The sequences were deposited in the European Nucleotide Archive (https://www.ebi.ac.uk/ena) under accession number PRJEB41368. DNA sequences were processed as described previously (Contreras-Dávila et al., 2020): the DADA2 pipeline (Callahan et al., 2016) was used and the identified ASVs were submitted to the SILVA database for taxonomy assignment. Forward and reverse reads were trimmed at cycles 240 and 220, respectively, based on the quality profiles obtained. Species assignment is based on exact sequence matching. Selected sequences with non-exact match were submitted to NCBI BLAST query (megablast 16S rRNA bacterial and archaean sequences) and the percentage of identity is reported. ASVs with ≥0.05% of total counts were used for analyses. Distance-based redundancy analysis (dbRDA) was done using Bray-Curtis dissimilarity with the capscale function from the vegan package (Oksanen et al., 2019) and visualized with ggord and ggplot2 (Wickham, 2008; Beck and Mikryukov, 2020). Correlations between nZVI addition, chemical parameters and relative abundance of microbial taxa were investigated using Spearman's rank correlation coefficient with the PerformanceAnalytics package (cor.test function-based) (Peterson et al., 2020).

3.3. Results

3.3.1. Experiment I - Chemical hydrolysis of lactate oligomers with nZVI

Addition of nZVI to a solution of concentrated lactic acid and nitrogen-free medium resulted in an increase of lactic acid monomers concentration. Lactate concentrations increased from 17.4±0.9 to 20.0±1.0 g·L^{-1} when 1 g·L^{-1} of nZVI was added and from 16.5±1.0 to 24.5±0.3 g·L^{-1} with 5 g nZVI·L^{-1}, showing that nZVI is capable to support hydrolysis of lactate oligomers present in concentrated lactic acid solutions (Figure 3.1). Lactic acid oligomerization is known to occur as acid concentrations increase. The hydroxyl and carboxyl groups in lactic acid interact with other lactate molecules resulting in intermolecular self-esterification forming lactyl lactic acid (dimer), lactyl-lactylactic acid (trimer) and so on (Vu et al., 2005). Here, addition of nZVI resulted in chemical hydrolysis of lactate oligomers as evidenced by an increase in lactate monomers concentration. The final pH at 1 and 5 g·L^{-1} of nZVI·L^{-1} was 5.8±0.2 and 6.7±0.1, respectively, compared to 5.4 in the control experiment. We estimated that 29±19 and 88±22% of lactate oligomers were hydrolyzed at 1 and 5 g nZVI·L^{-1}, respectively. These value was 8±1% for the control without nZVI.

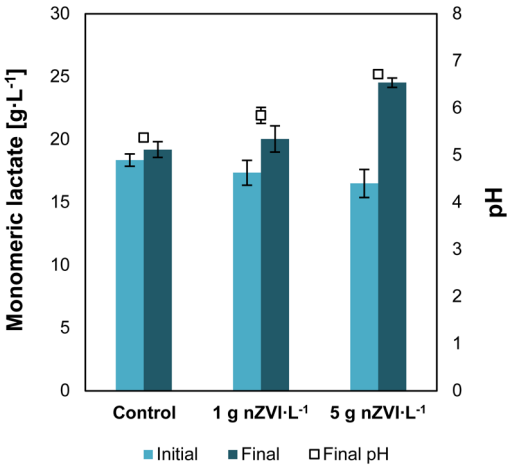

Figure 3.1 Experiment I - Increase in monomeric lactate concentrations and pH due to nZVI addition. Data shows the initial and final results after 18 days of reaction. Error bars depict ±one standard deviation.

3.3.2. Experiment II & III - nZVI addition to a mixture of lactate monomers and oligomers steers to microbial n-caproate formation

Adding nZVI at concentrations ranging from 0.5 to 5 g·L^{-1} showed no evident inhibition on chain elongation activity. Lactate was completely consumed within 5-9 days in all cases. A lag phase of two days was observed in the control without nZVI which was shortened in the presence of nZVI. After adaptation, a lactate-based chain elongation phase was observed where lactate and acetate were converted to mainly n-butyrate accompanied by an increase in pH and hydrogen release (days 0-7) (Figure 3.2C, Figure S1). The highest lactate conversion rate was detected at 1 g nZVI·L^{-1} (6.87±0.53 g·L^{-1}·d^{-1}; days 0-2), slightly higher than at 0.5 and 2 g nZVI·L^{-1} (6.08±0.05 and 6.17±0.21 g·L^{-1}·d^{-1}, respectively; days 0-2). Conversion rates were much lower at higher nZVI doses of 3.5 and 5 g·L^{-1} (3.28±0.41 and 2.62±1.61 g·L^{-1}·d^{-1}, respectively; days 0-2).

n-butyrate concentrations reached 14±0.8 g·L^{-1} in the control experiment and were consistently lower in the presence of nZVI. With nZVI concentrations between 0.5-2 g·L^{-1}, n-caproate production was promoted, reaching n-caproate concentrations of 4.3±0.3 g·L^{-1} at 1 g nZVI·L^{-1} (Figure 3.2F). Despite apparent lactate depletion, n-caproate formation did not reach a plateau (Figure 3.2F) with a similar trend for n-valerate (Figure S2). This suggests that lactate oligomers or other electron donors were used for chain elongation. A similar behavior in hydrogen partial pressure (P_{H2}) was observed in all tested conditions for experiment II giving no obvious relation between P_{H2} and n-caproate formation (Figure S1A). Substituting nZVI with hydrogen at 0.45 atm (amount expected from dissolution of 1 g nZVI·L^{-1}) or 1.2 atm in experiment III did not result in n-caproate formation. Additionally, neither acetate nor n-butyrate were elongated with hydrogen as sole electron donor (Figure S3). Further chain elongation to n-caproate was apparently limited by lactate availability. L-lactate was racemized to near-equilibrium concentrations of both D-lactate and L-lactate with 0-2 g nZVI·L^{-1} (Figure S4). At 5 g nZVI·L^{-1} propionate formation instead of n-caproate was favored. n-butyrate formation was primarily observed in the first two days. pH increased to a value of 7.5 (Figure 3.2C) and propionate started being produced from the leftover lactate to reach 6.5±1.2 g·L^{-1} of propionate with no clear

acetate consumption thereafter. Moreover, D-lactate reached an enantiomeric excess of 71±21% when substantial propionate formation was observed (Figure S4) suggesting that propionate was formed through the acrylate pathway in which D-lactate is selectively reduced (Akedo et al., 1983; Schweiger and Buckel, 1984; Kuchta and Abeles, 1985). Fermentation with 3.5 g nZVI·L^{-1} exhibited a transitional behavior between chain elongation and propionate production, with similar n-valerate but less n-caproate formation compared to incubations with lower nZVI doses (Figure S2, Figure 3.2). In all conditions tested, a hydrogen consumption phase (days 7-12) was observed (Figure S1). During this phase different processes such as chain elongation, acetate and propionate formation continued to occur which may have contributed to hydrogen consumption. H_2 conversion through homoacetogenesis was estimated to contribute in minor proportions to acetate formation as the expected acetate production from the H_2 consumed was lower than the measured increase in acetate concentrations (Figure S5). However, homoacetogenesis could have been underestimated due to continuous H_2 release from nZVI, acetate uptake for chain elongation and/or direct electron transfer during both chain elongation and hydrogen consumption phases.

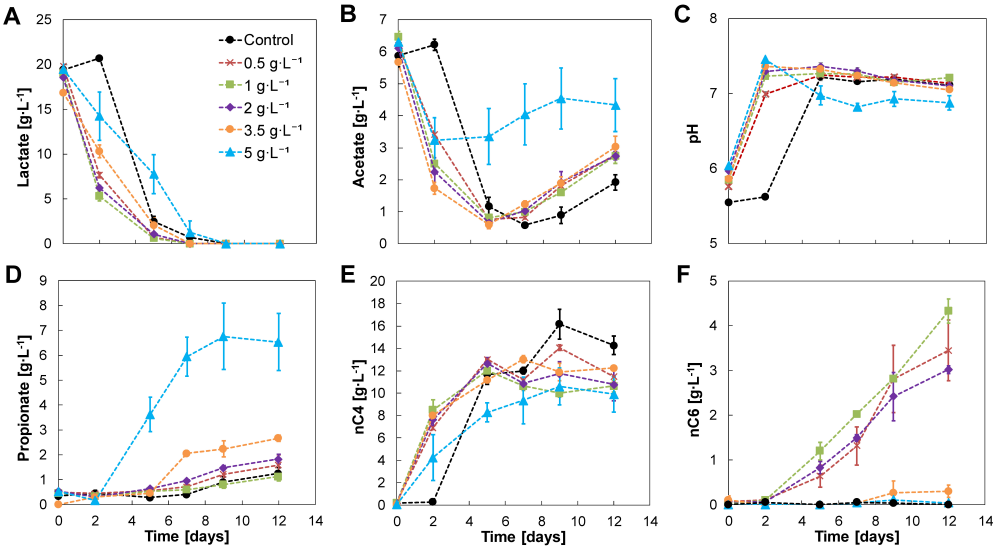

Figure 3.2 Experiment II - Substrates (**A**, **B**), pH (**C**) and metabolites (**D**-**F**) profile of lactate-based chain elongation with different nZVI concentrations. Error bars show duplicates absolute deviation from the average.

The electron balance shows that part of the lactate oligomers were used for fermentation to carboxylates (Figure 3.3). Lactate monomers and acetate in the substrate comprised about 70% of the total electrons added (total lactate and acetate). Substrate conversion was 75±4% in the control experiment suggesting slight hydrolysis in the absence of nZVI. However, substrate conversion was 87-88% under conditions of n-caproate production where hydrolysis of lactate oligomers was estimated to be >2-times higher than without nZVI (Table S2). When hydrogen was initially added (experiment III), substrate conversion was similar to without nZVI (≤81%) (Figure S3, Table S3).

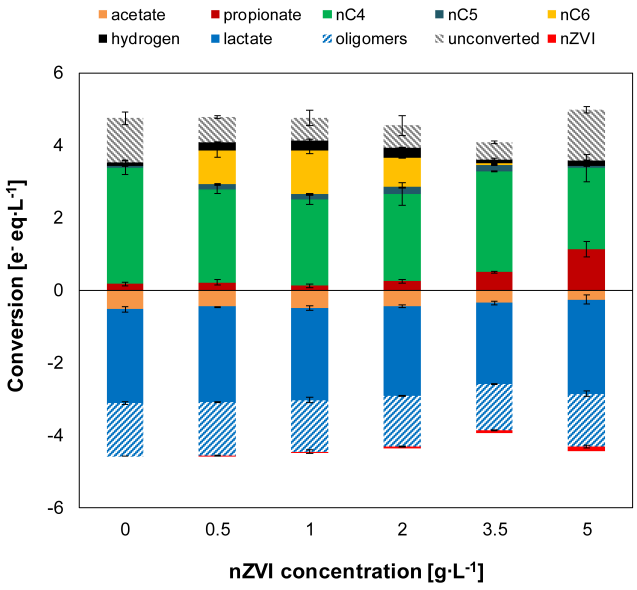

Figure 3.3 Experiment II - Net conversion by the end of the experiments at different nZVI concentrations. Oligomers were estimated as a fraction (0.36) of total lactate. The unconverted fraction shows missing electrons (from nZVI and oligomers) between metabolic products and substrates added (acetate, total lactate and Fe^0). Error bars show duplicates absolute deviation from average.

The microbiome produced n-butyrate efficiently with an electron selectivity of 91±1% in the control experiment. At 1 g nZVI·L^{-1}, n-caproate electron selectivity peaked to 28±1% while n-butyrate selectivity was reduced to 57±1%. Propionate reached a maximum electron selectivity of 32±7% at 5 g nZVI·L^{-1}. Carbon selectivity for n-butyrate reached 54±6% in the control experiment and 15±1% for n-caproate at 1 g nZVI·L^{-1} while n-valerate was produced at much lower proportions (3±1% at 3.5 g nZVI·L^{-1}). Carbon was diverged towards propionate at low selectivities (2-4% at 0-2 g nZVI·L^{-1}) although it raised up to 10±1% and 21±6% when adding 3.5 and 5 g nZVI·L^{-1}, respectively. Carbon selectivity for CO_2 ranged between 37-52% by the end of the chain elongation phase (days 0-7) and showed a decreasing trend during the hydrogen consumption phase (Figure S2). Evident decrease in CO_2 carbon selectivity (8-15% lower) was observed in incubations displaying n-valerate and n-caproate formation.

3.3.3. Experiment IV - Lactate enantiomers conversion to n-butyrate at different rates boosted by nZVI

To evaluate the effect of the two different lactate enantiomers on microbial chain elongation, separate experiments (experiment IV) with either D-lactate, L-lactate or a racemic mixture were carried out with (1 g·L^{-1}) and without nZVI. Both enantiomers were converted into n-butyrate (Figure 3.4) at high electron selectivities (96-100%) (Figure S6). The efficient conversion of lactate into n-butyrate probably resulted in a shortage of electron donor for further elongation to n-caproate. Addition of nZVI did not affect the product spectrum of fermentation but resulted in lactate depletion within 3 days irrespectively of the enantiomer supplied. No odd-chain carboxylates (propionate, n-valerate, n-heptanoate) were produced.

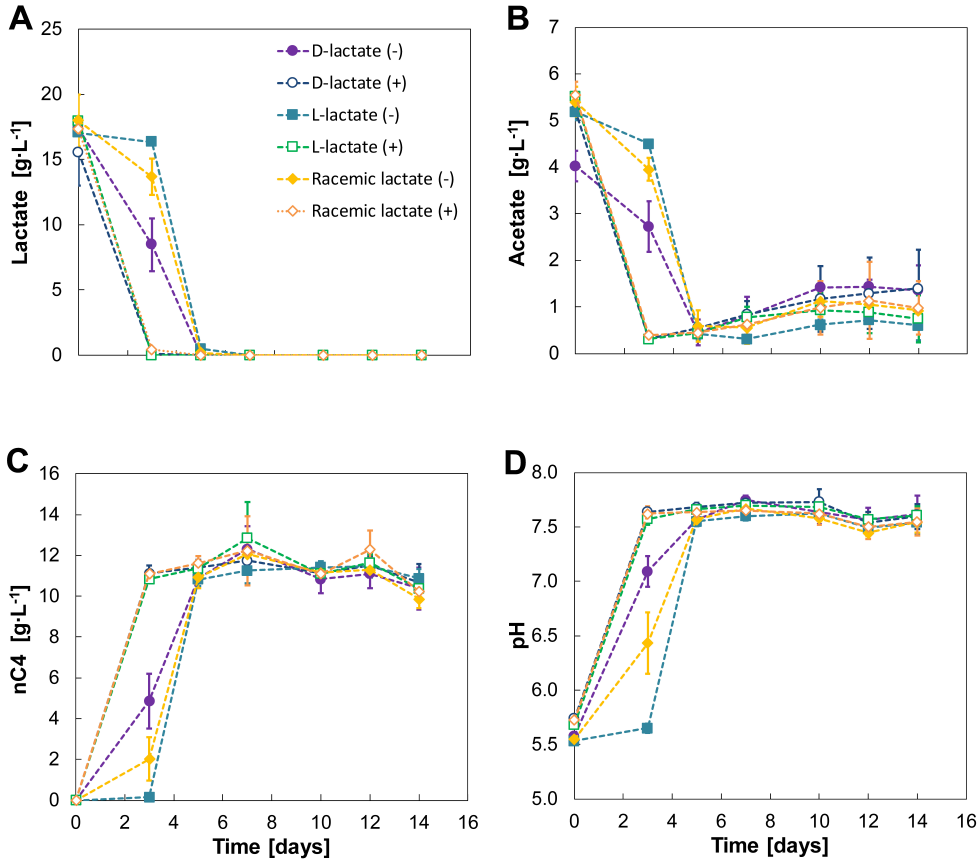

Figure 3.4 Experiment IV - Substrate (**A**, **B**), n-butyrate (**C**) and pH (**D**) profiles for D-lactate, L-lactate and racemic lactate conversion. A positive or negative sign between braces indicate absence (-) or presence (+) of nZVI (added at 1 g·L^{-1}). Error bars indicate ±one standard deviation.

Although lactate was converted to n-butyrate in all cases, different lag phases were evident for the two enantiomers. D-lactate was converted earlier than L-lactate with the latter being barely consumed during the first three days. Racemic lactate showed a reduced the lag phase compared to fermentation of L-lactate alone. During this first three days, D-lactate and the racemic mixture showed conversion rates of 2.13±0.8 and 1.2±1.1 g·L^{-1}·d^{-1}, respectively. After the lag phase, however, L-lactate conversion was observed at 8.59±0.1 g·L^{-1}·d^{-1} and was almost depleted within two days (days 3 to 5). Conversion rates on days 3-5 were 4.6±1.2 g·L^{-1}·d^{-1} for D-lactate and 7.1±0.7 g·L^{-1}·d^{-1} for racemic lactate. n-butyrate production rates for days 0-3 were 0.67±0.35 and 1.62±0.45 for the racemic mixture and D-lactate, respectively. From days 3 to 5, n-butyrate productivities from L-lactate, D-lactate and the racemic mixture were, respectively, 5.34±0.15, 3.0±0.56 and 4.46±0.49 g·L^{-1}·d^{-1}. The enantiomeric excess for L-lactate was still high (88±7%) on day 3 and D-lactate was measured to be 1.07±0.64 g·L^{-1} (6±3% of total lactate). In general, enantiopure lactate (either D- or L-lactate) was racemized during fermentation while racemic equilibrium was maintained when feeding racemic lactate (Figure S7). Chain elongation was followed by a hydrogen consumption phase with concomitant CO_2 consumption and acetate formation (Figure S8, Figure 3.4B). H_2 and CO_2

consumption resulted in decreased CO_2 carbon selectivity from 34±1% by the end of the chain elongation phase to 29±2% by the end of the experiment.

3.3.4. nZVI shapes microbiome composition

Composition of microbiomes from experiment II was affected by nZVI presence and concentration (Figure S9A). nZVI presence was negatively related to the occurrence of *Anaerotignum* (only member *Anaerotignum propionicum* sp. ASV23; 100% identity, formerly *Clostridium propionicum*) and *Eubacterium* species (Figure 3.5A). Several taxa were enriched at different nZVI concentrations. *Clostridium* sensu stricto 12 species were enriched (32-47% relative abundance) in n-caproate producing conditions compared to incubations without nZVI (12-16%). This genus was predominantly represented (65-86% of counts) by *Clostridium tyrobutyricum* sequences (ASV1) which showed relative abundances of 21-32% (samples 0.5-1 g nZVI·L^{-1}). *Clostridium luticellarii* (ASV29) from the same genus was also enriched to relative abundances 3-7% when n-caproate was produced while it remained <1% in the other conditions. Three sequences were classified as *Caproiciproducens* species of which *Caproiciproducens* sp. ASV37 was identified only in n-caproate producing incubations (3-4% relative abundance) and showed low similarity to *C. galactitolivorans* BS-1 (90% identity). *Caproiciproducens* sp. ASV37 ($p<0.01$), *Clostridium tyrobutyricum* sp. ASV1 ($p<0.001$) and *Clostridium luticellarii* sp. ASV29 ($p<0.001$) were positively correlated with n-caproate concentrations. The genus *Ruminococcaceae* was correlated with both n-valerate ($p<0.01$) and n-caproate ($p<0.001$). At ≥3.5 g nZVI·L^{-1}, relative abundance for *Clostridium* sensu stricto 12 was reduced (8-18% relative abundance) while *Clostridium novyi* sp. ASV7, only member of the genus *Clostridium* sensu stricto 7, was enriched to relative abundances of 14-24% (Figure 3.5A). At 5 g nZVI·L^{-1}, *Oscillibacter* sp. ASV22 (98.5% identity *Oscillibacter valericigenes*) and *Sedimentibacter* sp. ASV10 (97% identity *Sedimentibacter saalensis*) reached 17 and 7% relative abundance, respectively. *Clostridium* sensu stricto 7, *Oscillibacter*, *Oscillospiraceae* and *Sedimentibacter* species were among the highly abundant genera related with high nZVI and propionate production.

In experiment IV, feeding enantiopure or racemic sodium lactate did not influence the microbial community composition whereas nZVI presence and acetate formation during the hydrogen consumption did (Figure S9B). Species of *Clostridium* sensu stricto 12, *Haloimpatiens*, unclassified *Lachnospiraceae* and *Oscillibacter* were negatively related with nZVI (Figure 3.5B). Notably, *Clostridium* sensu stricto 12 species (being >77% *C. tyrobutyricum* sp. ASV1) showed decreased relative abundances from up to 75 to <1% with nZVI addition. On the other hand, *Sedimentibacter* species along with the less abundant genus *Caproiciproducens*, unclassified *Microbacteraceae* and unclassified *Oscillospiraceae* showed a positive correlation with nZVI. Other highly abundant genera such as *Proteiniborus* and *Corynebacterium,* with *Corynebacterium provencense* sp. ASV4 as the only member, showed no significant correlation with nZVI (Figure 3.5B). Identified genera correlating with acetate formation were *Eubacterium* ($p<0.001$), *Lachnospiraceae* UCG-010 ($p<0.001$), *Lutispora* ($p<0.01$) and *Methanoculleus* ($p<0.0005$). *Corynebacterium provencense* was negatively correlated with acetate formation ($p<0.0005$). *Methanoculleus* sequences (*Methanoculleus palmolei* sp. ASV6; 100% identity) were highly abundant in the inoculum sample and were also detected in the incubations. However, methane was not detected in our experiments and *M. palmolei* is reported to not grow on lactate (Zellner et al., 1998). Since the reactor used as inoculum source was unattended

for some time when the inoculum aliquot for experiment IV was taken, it is possible that leftover sequences from inactive *M. palmolei* were amplified from the incubations.

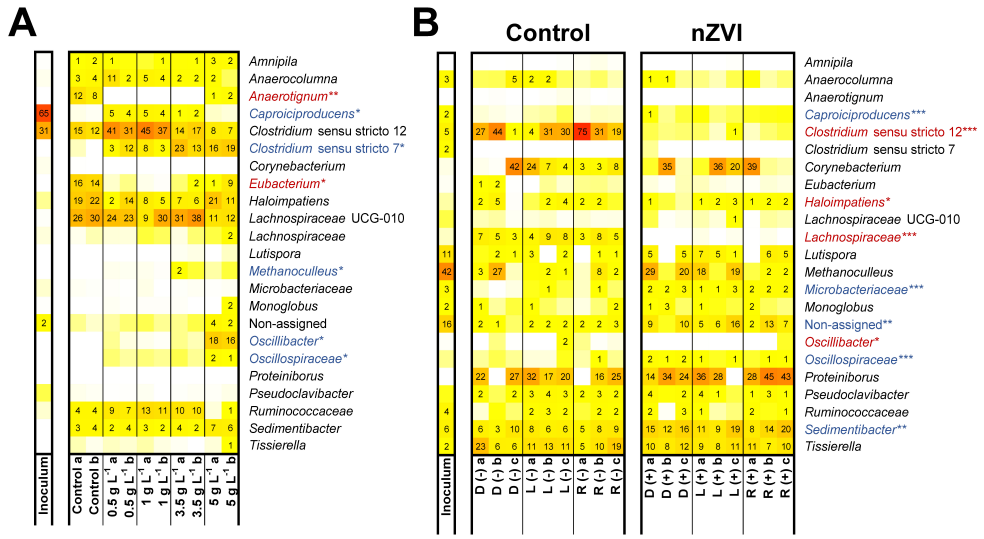

Figure 3.5 Microbiome composition in experiment II (**A**) and experiment IV (**B**). Experiment IV used D-lactate (D), L-lactate (L) or racemic lactate (R) in the absence (-) or presence (+) of nZVI (1 g·L^{-1}) (**B**). Blue and red shaded taxa indicate whether relative abundance was found positively or negatively correlated with nZVI presence (*** indicates p-values <0.0005; ** indicates p-values <0.001; * indicates p-values <0.01).

3.4. Discussion

3.4.1. Alkaline hydrolysis of lactate esters with nZVI may improve chain elongation

Dosing nZVI resulted in higher substrate availability due to chemical hydrolysis of lactate oligomers which translated into higher substrate conversion to carboxylates. Here we report that hydrolysis of lactate esters can occur purely chemically due to the high reactivity of nZVI. During iron corrosion, pH close to metallic surfaces can be up to 2 units higher than the bulk pH depending on reaction rates and mixing conditions (Kahyarian et al., 2017). This ΔpH is expected to be higher in highly reactive ZVI nanoparticles (eq. 10-11), likely promoting alkaline de-esterification of lactate oligomers (eq. 12). At alkaline conditions, OH^- ions cleave the ester bonds of lactate oligomers unzipping them to yield lactate as the final hydrolytic product (Ivanova et al., 2000). This observed effect of nZVI could be used to promote hydrolysis of PLA-based bioplastics (Ivanova et al., 2000). Chemical hydrolysis was probably limited by nZVI reacting only partially and by being used for side reactions other than oligomers hydrolysis e.g. hydrogen formation (eq. 10). Assuming that OH^- ions from anaerobic corrosion of nZVI (eq. 11) react with lactyl lactate (2 mol lactyl lactate$^-$·mol $Fe^{0\,-1}$) to produce lactate (eq. 12), 1 g nZVI·L^{-1} could hydrolyze 50% of the lactate oligomers. Instead, hydrolysis was observed at about 30%. nZVI was added in excess at 5 g nZVI·L^{-1} with incomplete hydrolysis obtained despite nZVI corrosion was still feasible at the near-neutral pH observed (eq. 11 at pH 7; ΔG' = -10.6 kJ·reaction^{-1}). Hydrolysis of lactate oligomers was enhanced with nZVI under fermentation conditions probably by a combination of chemical and biological hydrolysis (Li et al., 2017) as well as continuous lactate consumption. Since microbial chain elongation is shown to be dependent on

lactate availability (Kucek et al., 2016a), continuous, gradual hydrolysis of lactate oligomers could have enhanced chain elongation.

3.4.2. nZVI affects fermentation conditions shaping microbiome composition and lactate metabolism

Addition of nZVI created specific fermentation conditions that influenced microbiomes composition, lactate conversion rates and final product spectrum. In experiment II, the presence of nZVI was negatively correlated with n-butyrate concentrations ($p<0.01$) while n-caproate showed a positive correlation ($p<0.01$) (Figure S10). Moreover, dose-dependent effects were observed on substrate conversion rates. Initial lactate conversion occurred at higher rates with nZVI doses of 0.5-2 $g \cdot L^{-1}$ compared to ≥3.5 $g \cdot L^{-1}$ (days 0-2). Overall, lactate was depleted within 7-9 days. Under anaerobic conditions, nZVI corrosion occurs rapidly in the first ~24 h to gradually level out reaching almost full depletion in 2-7 days depending on the system conditions (Fan et al., 2016; Qin et al., 2018). The associated decrease in ORP (Wang et al., 2020) and increased pH due to the rapid initial nZVI corrosion probably shortened the lag phase compared to fermentation without nZVI. Adding 0.5-2 g $nZVI \cdot L^{-1}$ improved substrate conversion and chain elongation to n-valerate and n-caproate. Although elongation of acetate and n-butyrate is thermodynamically more favorable with nZVI as the electron donor (eq. 15-16) compared to lactate (eq. 4-8) or hydrogen (eq. 17-18), lactate was available at higher amounts with nZVI being a secondary electron source. Considering that bacteria may derive electrons from the conversion of lactate to acetate (4 $e^- \cdot mol \cdot lactate^{-1}$; eq. 2) to drive the RBO pathway, Fe^0 in added nZVI (2 $e^- \cdot mol \cdot Fe^{0-1}$; eq. 10-11) could have contributed to 1-10% (0.5-5 g $nZVI \cdot L^{-1}$) of electrons in total lactate. Both n-valerate and n-caproate production correlated ($p<0.01$) with increased substrate conversion (Figure S10) indicating that chain elongation was related to increased use of lactate as electron donor. Hydrolyzed lactate seemed to be rapidly used for chain elongation since chain elongation products showed sustained production over time despite lactate monomers were depleted (Figure 3.2). Several bacteria harboring genes involved in lactate oxidation (lactate dehydrogenases, Ldh) and the RBO pathway such as *C. tyrobutyricum* (Wu et al., 2017), *C. luticellarii* (Poehlein et al., 2018) and members of the family *Ruminococcaceae* (Tao et al., 2017) including *Caproiciproducens* species (e.g. (Bengelsdorf et al., 2019)) were enriched in these conditions. *C. tyrobutyricum* is known as an efficient n-butyrate producer (Wu et al., 2017) but is not reported to produce longer carboxylates. The capability of *C. luticellarii* (Petrognani et al., 2020), *Ruminococcaceae* (Yang et al., 2020) and *Caproiciproducens* (Bengelsdorf et al., 2019) organisms to produce carboxylates with >4 carbons and their high correlation with n-valerate and n-caproate formation suggest their involvement in chain elongation.

At high nZVI concentrations (5 $g \cdot L^{-1}$), other potential n-butyrate producers such as *Oscillibacter*, unclassified *Oscillospiraceae* and *Sedimentibacter* species were enriched. These taxa have also been enriched in bioelectrochemical systems (Breitenstein et al., 2002; Lin et al., 2018; Dessì et al., 2021) and *Oscillibacter* species in ethanol-based chain elongation with nZVI (Fu et al., 2020; Wang et al., 2020). However, nZVI caused higher pH conditions and directed the conversion of residual lactate towards propionate formation. Known propionic acid bacteria (PAB) grow optimally at pH values close to neutrality (Hettinga and Reinbold, 1972; Seeliger et al., 2002). *Clostridium novyi* was markedly enriched in this conditions, an organism reported to use the acrylate pathway for propionate

formation (Reichardt et al., 2014). *C. novyi* strains also possess key genes for H_2/CO_2 uptake (Ryan et al., 2008) which might have facilitated its growth in the presence of nZVI over *Anaerotignum propionicum*, a well-known PAB using the acrylate pathway (Akedo et al., 1983; Kuchta and Abeles, 1985). Propionate concentrations correlated with increasing nZVI concentrations ($p<0.001$) (Figure S10). Here, n-valerate formation was not promoted despite the high propionate concentrations. Hydrogen partial pressure (P_{H2}) did not seem to influence lactate chain elongation or propionate formation since similar P_{H2} values and behavior were observed with and without nZVI addition in experiment II. Other reports show improved lactate conversion to MCC with hydrogen addition (Nzeteu et al., 2018; Wu et al., 2019). This was not the case in our study even when P_{H2} up to 2.6 atm (experiment II) were observed. H_2 addition in experiment III did not alter product spectrum from lactate and H_2 did not elongate acetate or n-butyrate in the absence of lactate. Although not tested in this study, acetate and n-butyrate elongation with nZVI (eq. 15-16) may be more feasible than with H_2 as the electron donor (eq. 17-18). Figure 3.6A summarizes the observed effects of nZVI on the overall conversion process.

Isomerization of L-lactate to D-lactate has been suggested to be a required rate-limiting step prior chain elongation (Kucek et al., 2016a). Therefore, an enrichment of D-lactate induced with nZVI addition (Li et al., 2017) would be expected to improve chain elongation rates. This was probably based on the fact that *M. elsdenii* is reported to produce even-chains from D-lactate and propionate/odd-chains from L-lactate (Hino and Kuroda, 1993). In contrast, D-lactate is the substrate for the acrylate pathway in PAB (Akedo et al., 1983; Schweiger and Buckel, 1984). Despite the enantiomer fed, however, racemase activity in *M. elsdenii* resulted in similar carboxylates proportions (Hino and Kuroda, 1993). This is in line with our observations that both D-lactate and L-lactate are racemized in chain-elongating microbiomes regardless of nZVI addition (Figure 3.6B). Thus, improved chain elongation rates in the presence of nZVI are not related with an excess of D-lactate. Instead, D-lactate excess was associated to the dominance of propionate formation most likely through the acrylate pathway (Figure 3.6C).

nZVI has been shown to decrease ORP creating favorable conditions for ethanol-based chain elongation (Wang et al., 2020). The same authors showed that nZVI increase conductivity which was suggested to facilitate direct electron transfer and MCC formation. In the present work, n-valerate and n-caproate production may have been partly promoted by nZVI donating electrons to bacteria. Electron uptake may support a high intracellular Fd_{red} pool facilitating anaerobic lactate oxidation. Anaerobic lactate oxidation is an energetically unfavored reaction that requires bacteria to use confurcating Ldh (Ldh and electron transfering flavoprotein [EtfAB] complex) to drive the endergonic reduction of NAD ($E°'_{NAD/NADH}$ = -320 mV (Thauer et al., 1977)) with lactate ($E°'_{pyruvate/lactate}$ = -190 mV) by simultaneously oxidizing Fd_{red} (Weghoff et al., 2015; Buckel and Thauer, 2018). Under anaerobic conditions, nZVI ($E°'Fe^{2+}/Fe^0$ = -469 mV (Rickard and Iii, 2007)) could transfer electrons directly to ferredoxins ($E°'Fd_{ox}/Fd_{red}$ = -500 - -398 mV (Thauer et al., 1977; Li and Elliott, 2016)) when ferredoxins are present extracellularly (Marshall et al., 2017). Alternatively, ferredoxin can be reduced through membrane-bound or cytoplasmic reversible electron-bifurcating systems (Buckel and Thauer, 2018) *via* direct or H_2-mediated electron transfer. For instance, direct electron transfer may involve the membrane-bound Rnf complex using electrochemically-driven Na^+/H^+ gradients and NADH for Fd_{ox}

reduction (Gong et al., 2020). H_2-mediated ferredoxin reduction could occur through the cytoplasmic Hyd complex oxidizing H_2 to provide Fd_{red} and NADH for microbial metabolism (Buckel and Thauer, 2013). Reverse electron transport by the membrane-bound Ech complex uses H_2 and Na^+/H^+ gradients to form Fd_{red} (Hedderich and Forzi, 2005) being therefore influenced by both direct and H_2-mediated electron transfer. Genes encoding for Rnf and Ech are reported to be present in several chain-elongating bacteria with Rnf being more widespread than Ech (Liu et al., 2020). As mentioned earlier, nZVI could have contributed to 1-10% (0.5-5 g nZVI·L^{-1}) of electrons in total lactate. However, when considering the confurcating lactate oxidation to pyruvate step (lactate + 2 Fd_{red} + 2 NAD → pyruvate + 2 Fd_{ox} + 2 NADH; 2 e^- eq·$lactate^{-1}$ and 2 e^- eq·Fd_{red}^{-1}), nZVI contributions through Fd_{red} would be doubled. Therefore, small amounts of nZVI could significantly influence lactate-to-pyruvate flux and the formation of elongated products. nZVI could also influence energy conservation and butyryl-CoA dehydrogenase in the RBO pathway (Angenent et al., 2016). Extracellular Fe^{2+} reduction may also be coupled to lactate oxidation in a more energetically favorable reaction (eq. 3).

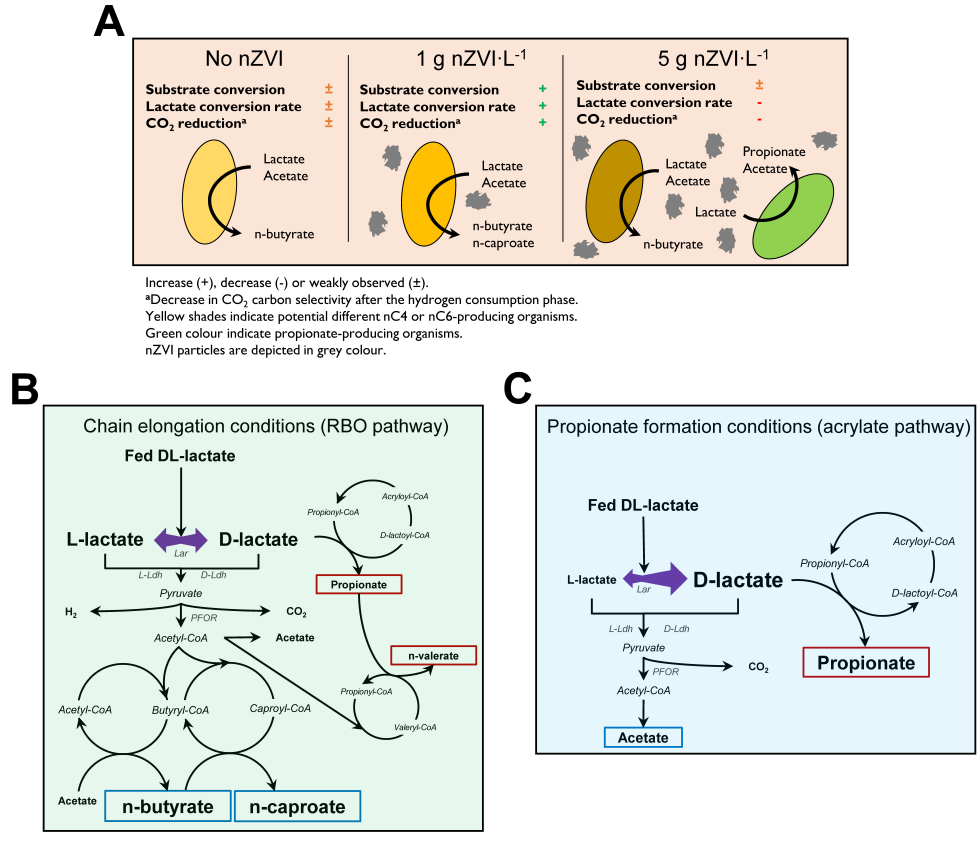

Figure 3.6 Proposed effects of nZVI on lactate-based chain elongation (**A**), enantiomeric proportions during lactate conversion to elongated carboxylates (**B**) and to propionate through the acrylate pathway (**C**). Blue and red boxes depict even- and odd-chained carboxylates, respectively. Abbreviations: Lar, lactate racemase; D-Ldh, D-lactate dehydrogenase; L-Ldh, L-lactate dehydrogenase; PFOR, pyruvate:ferredoxin oxidoreductase. Figures B and C adapted from (Schweiger and Buckel, 1984; Kuchta and Abeles, 1985; Hino and Kuroda, 1993; Angenent et al., 2016).

The addition of nZVI to fermentation of both enantiopure and racemic lactate substrates resulted in faster lactate conversion to n-butyrate. Notably, the microbiome composition was drastically

changed by nZVI addition with *Clostridium* (*C. tyrobutyricum*) and unclassified *Lachnospiraceae* being outcompeted by other potential n-butyrate producing bacteria. *Sedimentibacter* isolates are reported to use pyruvate and amino acids, but not lactate, with production of SCC, mainly acetate and n-butyrate without H_2 formation (Zhang et al., 1994; Breitenstein et al., 2002; Imachi et al., 2016). Some strains, however, possess putative proteins involved in lactate metabolism (section 3.4.4). *Sedimentibacter* species have been suggested to be electroactive as they were enriched in bioelectrochemical systems (Vilajeliu-Pons et al., 2016) and graphene-amended anaerobic digestion (Lin et al., 2018). Additionally, some species are involved in extracellular electron transfer for Fe^{3+} reduction (Burkhardt et al., 2011). Therefore, *Sedimentibacter* capability to interact with external electron donors/sinks and iron availability might have been advantageous to thrive in the presence of nZVI. This may be the case also for other taxa enriched with nZVI addition. Other highly abundant species from the genera *Corynebacterium* and *Proteiniborus* are able to metabolize lactate to n-butyrate but showed low or no correlation with nZVI addition. *Corynebacterium provencense* genome harbors genes that encode a predicted lactate utilization protein with a ferredoxin-type domain (NCBI Reference Sequence WP_110482617.1). Genes involved in the RBO pathway are also present in *C. provencense* and other *Corynebacterium* species (Takeno et al., 2013; Kittl et al., 2018). A *Proteiniborus* isolate from anaerobic digestion was predicted to harbor lactate dehydrogenases and produce acetate (including Wood-Ljungdahl pathway), propionate (acrylate pathway) and n-butyrate (butyrate kinase pathway) (Maus et al., 2017). Differences in inoculum composition and/or Na^+ levels between experiment IV using sodium lactate (~4.8 g $Na^+ \cdot L^{-1}$) and experiment II using concentrated lactic acid (~0.13 g $Na^+ \cdot L^{-1}$) (section 3.3.2) may have contributed to relatively different microbiomes developed in the two experiments.

Although nZVI may inactivate gram-negative more severely than gram-positive bacteria (Diao and Yao, 2009), taxa enriched with nZVI addition include species showing both positive and negative gram stains. Therefore, selective inhibition based on cell wall composition was not clearly observed. Instead, the enriched taxa may have thrived probably due to changed pH, ORP and iron availability conditions and by being involved in extracellular electron transfer as discussed in this section.

3.4.3. Improved carbon recovery through chain elongation and carbon dioxide recapture

Carbon dioxide could be reduce to acetate with electrons from nZVI (eq. 13) or H_2 (eq. 14). Hydrogen consumption was observed in the last days of incubation in experiments II (days 7-12) and IV (days 3-12 and days 5-12 with and without nZVI, respectively). However, different substrate conversions observed in experiment II affected apparent H_2 and CO_2 formation/consumption during this phase. No significant correlation was found between H_2 consumption and CO_2 or acetate formation during the hydrogen consumption phase but acetate formed during this phase was positively related with substrate conversion, n-valerate and n-caproate concentrations (all with $p<0.01$) (Figure S10). This suggests that part of this acetate was formed as a side product of chain elongation. In days 7-12, CO_2 was produced at similar amounts in all conditions. Assuming that lactate was the electron donor used for elongation to nC5/nC6, higher amounts of CO_2 due to lactate decarboxylation are expected when chain elongation activity was observed (0.5-2 g nZVI$\cdot L^{-1}$). This indicates that CO_2 may have been recovered with nZVI or H_2. Decreases in CO_2 carbon selectivity during the hydrogen consumption phase were related with higher substrate conversions ($p<0.001$) (towards chain

elongation) and less CO_2 release ($p<0.01$) (Figure S10). CO_2 could be incorporated into acetate, n-valerate and/or n-caproate thereby improving carbon recovery in the chain elongation process. Increased relative abundance in chain-elongating conditions (0.5-2 g nZVI·L^{-1}) was observed for *C. luticellarii* which may use the Wood-Ljungdahl pathway to take up electrons, H_2 and/or CO_2 coupled to chain elongation (Poehlein et al., 2018; Petrognani et al., 2020). *Caproiciproducens* and *Ruminococcaceae* species were also enriched under these same conditions but their capability to utilize CO_2/H_2/electrons for chain elongation remains to be studied. In contrast, homoacetogenic activity was more clearly observed in experiment IV where acetate formation correlated with H_2 ($p<0.01$) and CO_2 ($p<0.05$) consumption during the hydrogen consumption phase (Figure S11). Of the CO_2 formed from lactate conversion, 24±5% in absence and 20±10% in presence of nZVI was consumed. Hence, nZVI presence showed no significant correlation with H_2/CO_2 consumption nor with acetate production (Figure S11). Overall, several genera comprising homoacetogenesis-related genes such as *Clostridium*, *Eubacterium*, *Lachnospiraceae*, *Proteiniborus* and *Corynebacterium* (Singh et al., 2019) were identified in the incubations. Further studies using omics or pure cultures could be done to clarify the role of aforementioned organisms in H_2/CO_2 utilization and chain elongation.

Soluble iron concentrations by the end of the experiments were below 3 mg·L^{-1} (<0.5% of iron added) in all the incubations with nZVI. Thus, we could not quantify the extent of nZVI reaction based on soluble iron. The formation of insoluble iron species may account for such low soluble iron concentrations.

3.4.4. Lactate metabolism and racemization

Even though lactate-to-acetate ratios tested here could in principle yield n-caproate (Table 3.1, eq. 8), n-butyrate was the main product with stoichiometry shown in equation 4 (average of L(-), D(-) and R(-) log-phase). Comparable n-butyrate yields were observed in experiment II in the absence of nZVI. A similar reaction stoichiometry was reported for *Clostridium acetobutylicum* converting lactate and acetate to n-butyrate (Diez-Gonzalez et al., 1995). This experimental reaction stoichiometry was slightly more thermodynamically feasible during the incubations compared to the proposed reaction in equation 5 but was still less favorable compared to n-caproate formation (Figure S12). n-butyrate over n-caproate formation may be a common outcome of batch lactate chain elongation with reactor microbiomes. Although n-caproate formation is more energetically favorable than n-butyrate (Table 3.1), it requires one extra RBO cycle with the concomitant higher ATP yield (Angenent et al., 2016). Based on the microbial ecology theory on so called r- and K-selection, conditions of excess substrate (high food-to-microorganism ratio) select for r-strategists displaying high-flux metabolism (q_s^{max}, μ^{max}) while K-strategists exhibiting high-yield metabolism ($Y_{X,ATP}$, K_S) thrive under substrate-limiting conditions (Andrews and Harris, 1986). Following this principle, fast-growing n-butyrate producers may dominate in batch microbiomes while more efficient n-caproate producers would thrive under substrate limitation. This principle is evidenced here by the late n-caproate production in our experiments (day 5 onwards) and *C. tyrobutyricum* outcompeting *Caproiciproducens*-related species that were highly abundant in the inoculum derived from a continuous chain elongation reactor (section 3.3.4). Presence of n-butyrate favors n-caproate producers in (repeated) batch reactors fermenting food waste (Nzeteu et al., 2018; Contreras-Dávila et al., 2020) which is also in line with the aforementioned theory (Andrews and Harris, 1986). Despite that the pH-independent propionate

production reaction (eq. 9) was thermodynamically favored during the incubations (Figure S12), growth of PAB was constrained by the initial acidic pH conditions applied (Hettinga and Reinbold, 1972; Stinson and Naftulin, 1991) and high propionate concentrations observed at 5 g nZVI·L^{-1} were related to high pH and residual lactate (section 3.4.2).

Lactate oxidation is catalyzed by stereospecific Ldh. Prompt utilization of D-lactate is usually observed since D-Ldh is a constitutive enzyme in many microorganisms while L-Ldh is inducible by the presence of L-lactate (Kato et al., 2010). When only one of the two stereospecific Ldh is present, utilization of both enantiomers may still proceed by lactate isomerization through lactate racemase (Lar). In the acrylate pathway, D-lactate is selectively converted through lactoyl-CoA and acryloyl-CoA to propionate (Akedo et al., 1983; Schweiger and Buckel, 1984; Kuchta and Abeles, 1985). This requirement of D-lactate may explain the isomerization of L-lactate to a large D-lactate excess when propionate was formed, most likely through the acrylate pathway present in *C. novyi*. In rumen fermentation, where the acrylate pathway is dominant, an excess of D-lactate was also associated with higher propionate formation (Counotte and Prins, 1981). The role of lactate racemization in other lactate-consuming bacteria is not quite clear. Lactate racemization was first observed in butyrate-producing bacteria in early reports (Tatum et al., 1936; Christensen et al., 1939). Lar was determined to be an excretable enzyme acting on the dissociated lactate form with optimal pH 5 (Christensen et al., 1939; Dennis and Kaplan, 1965). Although lactate isomerization itself does not give bacteria any energetic advantage ($\Delta G° = -0.4$ kJ·mol^{-1}; eq. 1), a racemic mixture of lactate might result in higher chain-elongating rates in the case that both enantiomers are metabolized simultaneously. However, we observed higher conversion rates with enantiopure substrates (D-lactate [days 0-3] and L-lactate [days 3-5], section 3.3.3). Whether D- or L-lactate was the required substrate for chain elongation is not clear from our experiments due to the observed lactate racemization. The n-caproate producer *Rumminococcaceae* bacterium CPB6 possess both L-Ldh and D-Ldh and the expression of L-ldh in recombinant *E. coli* was shown to enhance lactate conversion by 17-fold (Yang et al., 2020). However, properties of the D-Ldh were not studied. High L-lactate conversion rates observed in the present study could be related to lower pyruvate inhibition of L-Ldh compared to D-Ldh similarly to PAB *P. freudenreichii* (Crow, 1986). Alternatively, a higher concentration of Lar induced at high L/D lactate ratios (Goffin et al., 2005) may increase lactate racemization and, consequently, chain elongation rates. Genes encoding Lar are present in several bacteria including chain-elongating organisms such as *M. elsdenii* and *E. limosum* (Desguin et al., 2014). A Pfam query (El-Gebali et al., 2019) for Lar (N-terminal domain, PF09861.10) showed that most of the genera detected in this study include organisms with putative Lar such as *Caproiciproducens*, *Clostridium* (including *C. tyrobutyricum*, *C. luticellarii*), *Corynebacterium*, *Eubacterium*, *Haloimpatiens*, *Lachnoclostridium*, *Lachnospiraceae*, *Oscillibacter*, *Rumminococcaceae* (including *Rumminococcaceae* bacterium CPB6) and *Sedimentibacter*. Other genera include the PAB *Propionibacterium* and *Veillonella* (Supplementary Material). An hypothetical role of Lar in energy conservation *via* transmembrane proton gradient formation has been suggested (Desguin et al., 2017). Pure culture studies using lactate-elongating organisms and mutants lacking Lar genes could be useful to elucidate the relevance of lactate racemization and enantiomers metabolism under different operational conditions.

3.4.5. Outlook

Reaction rates and MCC selectivity observed here could be improved by testing nZVI in pH-controlled experiments. Mildly acidic conditions not only favor both iron corrosion and chain elongation but may decrease the likelihood of iron precipitates formation (Kahyarian et al., 2017) and allow complete nZVI utilization. Spent nZVI precipitates could be collected and recycled to Fe^0 and, when $FeCO_3$ is present, to reduced one-carbon compounds (CO, CH_4) through reductive calcination (Lux et al., 2019). Soluble Fe^{2+} can also be electrochemically recovered as goethite (FeOOH) (Nguyen and Ahn, 2018) and may be recycled together with the other precipitates. Carbon monoxide (CO) could be looped back into the chain elongation process as additional electron and carbon source. Although nZVI may be a costly additive, its use in chain elongation may be feasible when dealing with complex substrates. nZVI addition to waste activated sludge supplied with ethanol increased substrate conversion and n-caproate selectivity (Wang et al., 2020). Importantly, some of the effects triggered with nZVI can be replicated with (bio)electrochemistry. Production of OH^- ions to hydrolyze lactate oligomers or PLA bioplastics could be achieved by applying cathodic current, avoiding the need of Fe^0 or external caustic input. Biological chain elongation is also susceptible to external control under so-called electro-fermentation conditions (Moscoviz et al., 2016) where relatively small proportions of electrons (compared to electrons in fermentable substrate) supplied or subtracted through electrodes affect microbial metabolism. Although fermentable substrates (lactate and acetate) were the main source of electrons in our experiments, small contributions to this electron pool coming from nZVI (0.3-3% total substrate; 1-20% electrons transferred) could have influenced specific oxidation-reduction reactions significantly e.g. Fd_{red}-dependent lactate oxidation, pyruvate decarboxylation and energy conservation (section 3.4.2). Therefore, cathodic electrons could be continuously supplied under controlled pH conditions to steer propionate formation and chain elongation of even or odd carboxylates.

3.5. Conclusions

Lactate-based chain elongation microbiomes, lactate conversion rates and production spectrum were affected at different nZVI doses. The effects of nZVI on chain elongation were related to hydrolysis of lactate oligomers, changes in pH and possibly by acting as additional electron donor. The metabolism arising under specific conditions (e.g. pH, lactate and nZVI concentrations) determined both lactate enantiomeric proportions and product spectrum. Lactate was racemized in chain-elongating microbiomes while D-lactate excess was observed during propionate production through the acrylate pathway. Our results suggest that feeding D-lactate to continuous reactors would not necessarily translate into higher chain elongation rates due to lactate racemization. Carbon recovery into carboxylates was increased after hydrogen consumption which was presumably coupled with carbon dioxide recapture into acetate and elongated carboxylates. Fermentation conditions imposed by the presence and concentration of nZVI could be replicated with bioelectrochemical systems to control carboxylates production under continuous operation.

Chapter 4

Continuous lactate-based chain elongation with nitrogen gas supply to n-caproate and n-heptylate

This chapter was published as:
Carlos A. Contreras-Dávila, Arielle Ali, Cees N.J. Buisman and David P.B.T.B. Strik (2021). Lactate metabolism and microbiome composition are affected by nitrogen gas supply in continuous lactate-based chain elongation. Fermentation. 7, 41, 7010041.

Abstract

Chain elongation reactor microbiomes produce valuable medium-chain carboxylates (MCC) from non-sterile residual substrates where lactate is a relevant intermediate. Gas supply has been shown to impact chain elongation performance. In the present study, the effect of nitrogen gas (N_2) supply on lactate metabolism, conversion rates, biomass growth and microbiome composition was evaluated in a lactate-fed upflow anaerobic reactor with continuous or intermittent N_2 gas supply. Successful MCC production was achieved with continuous N_2 gas supply at low superficial gas velocities (SGV) of 0.22 $m \cdot h^{-1}$. Supplying N_2 at high SGV (>2 $m \cdot h^{-1}$) either continuously (2.2 $m \cdot h^{-1}$) or intermittently (3.6 $m \cdot h^{-1}$) disrupted chain elongation resulting in production of short-chain carboxylates (SCC) i.e. acetate, propionate and n-butyrate. *Caproiciproducens*-dominated chain-elongating microbiomes enriched at low SGV were washed out at high SGV where *Clostridium tyrobutyricum*-dominated microbiomes thrived by displaying higher lactate consumption rates. Suspended growth seemed to be dominant regardless SGV and gas supply regime applied with no measurable sludge bed formed. The highest MCC production from lactate of 10 g $COD \cdot L^{-1} \cdot d^{-1}$ with electron selectivities of 72±5%was obtained without N_2 gas supply at an hydraulic retention time (HRT) of 1 day. Addition of 5 $g \cdot L^{-1}$ propionate did not inhibit chain elongation but rather boosted lactate conversion rates towards MCC with n-heptylate reaching 1.8 g $COD \cdot L^{-1} \cdot d^{-1}$. N_2 gas supply can be used for mixing purposes and to steer lactate metabolism to MCC or SCC production.

4.1. Introduction

Chain elongation reactor microbiomes produce valuable medium-chain carboxylates (MCC) from non-sterile residual substrates. MCC are saturated monocarboxylic acids with 6 to 12 carbon atoms that find applications in lubricants, bioplastics, antimicrobials, feed additives and biofuels production (Angenent et al., 2016). For bioplastics, MCC can be used in a second bioprocess to accumulate medium-chain length polyhydroxyalkanoates in bacteria such as *Pseudomonas putida* (Sun et al., 2007). Chain-elongating microbiomes utilize energy-rich substrates e.g. ethanol, lactate, glucose as electron donors to elongate short-chain carboxylates (SCC, 1-5 carbon units) to MCC through a series of biochemical condensation and reduction reactions in the reverse-β-oxidation (RBO) pathway (Angenent et al., 2016). Electron donors are oxidized to provide electrons (e.g. NADH) and acetyl-CoA for the RBO pathway where two acetyl-CoA are elongated to even-chain carboxylates e.g. n-butyrate (nC4), n-caproate (nC6) or n-caprylate (nC8). Lactate is an interesting electron donor that can be easily obtained from residual biomass materials (Kim et al., 2016b; Contreras-Dávila et al., 2020; Costa et al., 2021) and has been successfully converted to n-caproate (Zhu et al., 2015; Kucek et al., 2016a; Candry et al., 2020a; Contreras-Dávila et al., 2020). Alternatively, reactor microbiomes may convert lactate to propionate and acetate (Seeliger et al., 2002). Propionate can be activated to propionyl-CoA and enter the RBO pathway (Grootscholten et al., 2013c) to be elongated with additional lactate to odd-chain elongated carboxylates such as n-valerate (nC5) and n-heptanoate (nC7).

There is an increasing interest in lactate-based chain elongation processes as lactate seems to be an important intermediate during the conversion of residual heterogenous materials into MCC (Carvajal-Arroyo et al., 2019; Contreras-Dávila et al., 2020). However, lactate conversion rates and selectivities towards MCC remain relatively low. Previous studies using lactate as model substrate showed n-caproate selectivities below 45% with production rates reaching 2.3 g $COD \cdot L^{-1} \cdot d^{-1}$ in a continuous stirred tank reactor (CSTR) (Candry et al., 2020a) and 6.9 g $COD \cdot L^{-1} \cdot d^{-1}$ in an anaerobic filter (Kucek et al., 2016a). Chain elongation performance may be improved through, for instance, gas supply. The CO_2 loading rate has been shown to control chain elongation rates and ethanol conversion efficiency in continuous ethanol-based chain elongation (Roghair et al., 2018a). Hydrogen addition increases MCC production in incubations with ethanol and acetate (Steinbusch et al., 2011) and lactate (Wu et al., 2019). However, high P_{H2} may slow down MCC production rates by affecting energy metabolism in chain-elongating bacteria such as *Clostridium kluyveri* as explained by Angenent et al. (2016). Thus, nitrogen gas (N_2) may be supplied to avoid inhibition by high P_{H2}. N_2 may also be supplied to improve mixing and, subsequently, fermentation in full-scale reactors (Noorman et al., 2018) as it is also done in full-scale ethanol-based chain elongation processes (EFSA (European Food Safety Authority), 2018). However, the effect of N_2 gas supply at different rates in chain elongation performance is not reported yet.

Additionally, gas supply may create hydrodynamic shear force and induce the formation of granular sludge or biofilm which would help to increase biomass concentrations. Hydrodynamic shear force applied through continuous gas supply increased granulation rates and sludge properties in anaerobic (Wu et al., 2009) and aerobic (Tay and Liu, 2001) granular sludge reactors. Granulation has been reported to occur in an ethanol-based chain elongation process (Roghair et al., 2016) and

granular sludge reactors converting complex waste streams such as thin stillage have achieved MCC production rates around 30 g COD·L^{-1}·d^{-1} (Carvajal-Arroyo et al., 2019; Wu et al., 2020). However, the presence of several other substrates and nutrients in the complex wastes may have contributed to granulation (Sudmalis et al., 2018; Gagliano et al., 2020) and MCC production.

Besides gas supply, the addition of SCC serving as electron acceptors is one other option to increase chain elongation rates as has been shown in pure culture incubations with lactate and sucrose (Wang et al., 2018). Reactor microbiomes also show sluggish ethanol-based chain elongation rates in the absence of acetate as electron acceptor (Spirito et al., 2018). The authors explained that ethanol conversion to MCC without an electron acceptor may be less energetically favorable and could also result in high hydrogen formation inhibiting conversion rates.

The present study aimed to evaluate the effects of N_2 gas supply on lactate metabolism and conversion rates during continuous lactate-based chain elongation. Different volumetric flows and superficial gas velocities were applied through continuous or intermittent gas supply in an upflow anaerobic reactor fed with lactate and operated at pH 5.5 and hydraulic retention time (HRT) of 1-2 days. Since MCC production rates remained moderate, propionate was added as electron acceptor as an alternative way to increase chain elongation rates. Lactate conversion rate, product spectrum, biomass concentration and microbiome composition were studied.

4.2. Materials and Methods

4.2.1. Substrate, mineral medium and inoculum

L-lactate (50% sodium-(S)-lactate, Merck) was used as electron donor at a constant concentration of 40 g·L^{-1}. Mineral medium and vitamins were added as described elsewhere (Roghair et al., 2016) and trace elements were prepared after Zhu et al. (2015). Additionally, 1 g·L^{-1} yeast extract (Merck, for microbiology) and 4 g·L^{-1} tryptone (Sigma-Aldrich, Microbiologically tested, N content 11-16%) were added. The feeding solution containing lactate, minerals and nutrients was adjusted to pH 5.5 with 6 M HCl. The inoculum was obtained from several sources including reactor microbiomes from ethanol-based chain elongation (Roghair et al., 2018c) and food waste fermentation (Contreras-Dávila et al., 2020). These reactor microbiomes were mixed with uncharacterized microbiomes from unfiltered Chinese liquor; rumen fluid; a full-scale lipid-degrading anaerobic digestor; and lab-scale acetate-oxidizing bioanode and biocathode producing n-butyrate. Equal volumes of each source culture were centrifuged separately at 4000 rpm and 20°C for 10 minutes. The supernatant was removed and the pellet resuspended in oxygen-free demi water. The resuspensions were then combined to get the inoculum. 20mL of the inoculum was injected into the reactor.

4.2.2. Reactor setup and operation

The reactor used was a double-walled glass upflow anaerobic reactor consisting of a vertical column (D_{in} = 6.5 cm; length = 62 cm), a settler (1.1 L), an inverted funnel for solid-gas-liquid separation and a recirculation line (Figure S1) for a total working volume of 3.2 L. The fermentation broth was recirculated from the top to the bottom of the reactor where it mixed with the feeding solution before flowing upwards into the reactor. Two two-neck glass tubes were connected in the recirculation line for pH control and redox measurements. A N_2 gas connection branched into the recirculation for gas

supply. Effluent overflowed at the top of the reactor and was collected in a reservoir. Headspace overpressure was controlled <0.1 bar with a pressure meter and a vacuum pump. When pressure reached 0.1 bar, gas was pumped from the headspace towards the gas flow meter (drum-type gas meter, Ritter). Temperature was controlled at 30°C using a water bath.

The reactor was filled with the feeding solution at pH 5.5, bubbled with N_2 gas for 15 min and inoculated. The reactor was first operated in batch mode with pH control switched off and a liquid recirculation rate of 9.96 $L \cdot h^{-1}$ equivalent to an upward liquid velocity (ULV) of 3 $m \cdot h^{-1}$. Continuous operation (Table 4.1) was started at an HRT of 2 days once gas production and pH increase were observed (7 days). Automatic addition of 2 M HCl was used to keep a pH of 5.5 throughout operation. Once n-caproate production became dominant, N_2 gas was supplied either continuously or intermittently. Continuous gas flow was supplied at 12 $mL \cdot min^{-1}$ in phase 1 resulting in a superficial gas velocity (SGV) of 0.22 $m \cdot h^{-1}$ from day 59.7. For phase 2, gas supply was increased to 120 $mL \cdot min^{-1}$ (SGV = 2.2 $m \cdot h^{-1}$) on day 85.7. Due to the loss of n-caproate production in this phase, gas supply was decreased to 11.3 $mL \cdot min^{-1}$ in phase 3 and changed to intermittent addition (days 104.8-149.9). Intermittent gas was supplied at 3.33 $mL \cdot s^{-1}$ for 20 seconds followed by 5 min of no gas addition equivalent to SGV of 3.6 $m \cdot h^{-1}$ during moments of gas supply. For phase 4 (days 154-188.8), gas was still added intermittently but HRT was shortened to 1 day. Gas supply was stopped in phase 5 (days 197.7-231.9) and recirculation rate was increased (day 195.7) to 29.9 $L \cdot h^{-1}$ (ULV = 9 $m \cdot h^{-1}$) maintaining these conditions for the rest of the operation time. Lastly, propionate was added in the feed 5 $g \cdot L^{-1}$ for phase 6 (days 232.7-237.7) to test whether it could decrease or improve chain elongation rates. Periods (I-V) with stabilized operation (pH, HRT) and conversion rates for ≥5 HRT are identified to compare chain elongation performance between phases.

Table 4.1 Conditions applied during operation.

Phase	Days	Supply	Flow rate [$mL \cdot min^{-1}$]	SGV [$m \cdot h^{-1}$]	HRT [d]	ULV [$m \cdot h^{-1}$]
1	62.7-85.7	Continuous gas	12	0.22	2	3
2	87.7-100.8	Continuous gas	120	2.2	2	3
3	104.8-149.9	Intermittent gas	11.3	3.6	2	3
4	154-188.8	Intermittent gas	11.3	3.6	1	3
5	190.7-231.9	No gas	0	0	1	9
6	232.7-237.7	Propionate, no gas	0	0	1	9

4.2.3. Calculations

Chain elongation performance was evaluated based on conversion rates (e^- $eq \cdot L^{-1} \cdot d^{-1}$; eq. 1) and selectivity (eq. 2).

$$\text{Conversion rate} = (n_{e,i}/V_r) \cdot (Q_{out} \cdot C_{out,i} - Q_{in} \cdot C_{in,i}) \quad (1)$$

where $n_{e,i}$ refers to the number of electrons in compound *i* (liquid and gas metabolites quantified as described in the analytical methods section); V_r the reactor working volume (L); Q_{in} the influent and Q_{out} the effluent flow rates ($L \cdot d^{-1}$); $C_{in,i}$ the concentration in the influent and $C_{out,i}$ the concentration in

the effluent of compound *i* (mmol·L^{-1}). The number of electrons are: lactate (12 e$^-$ eq·mol^{-1}), acetate (8 e- eq/mol), propionate (14 e$^-$ eq·mol^{-1}), n-butyrate (20 e$^-$ eq·mol^{-1}), n-valerate (26 e$^-$ eq·mol^{-1}), n-caproate (32 e$^-$ eq·mol^{-1}), n-heptylate (38 e$^-$ eq·mol^{-1}), n-caprylate (44 e$^-$ eq·mol^{-1}), hydrogen (2 e$^-$ eq·mol^{-1}) and methane (8 e$^-$ eq·mol^{-1}).

Electron selectivity was calculated with respect to liquid and gas metabolites production rates:

$$\text{Selectivity} = 100 \cdot [\text{rate}_i / (\sum \text{rate}_{liq} + \sum \text{rate}_{gas})] \quad (2)$$

where rate_i is calculated as in eq. 1 for product *i*; rate_{liq} is the production rate of liquid metabolites (propionate, isobutyrate, n-butyrate, isovalerate, n-valerate, isocaproate, n-caproate, n-heptanoate and n-caprylate) and rate_{gas} is the production rate of gaseous metabolites (hydrogen and methane).

The effect of hydrogen partial pressure (P_{H2}) on thermodynamics of lactate conversion was evaluated at pH 5.5 and 30°C. Reactions considered are lactate oxidation to acetate (eq.3), lactate conversion to n-butyrate (eq. 4), n-caproate (eq. 5) and propionate and acetate (eq. 6). Acetate formation through homoacetogenesis from hydrogen and carbon dioxide (eq. 7) and from lactate (eq. 8).

$$\text{lactate}^- + H_2O \rightarrow \text{acetate}^- + 2\ H_2 + CO_2 \quad (3)$$

$$2\ \text{lactate}^- + H^+ \rightarrow \text{n-butyrate}^- + 2\ H_2 + 2\ CO_2 \quad (4)$$

$$3\ \text{lactate}^- + 2\ H^+ \rightarrow \text{n-caproate}^- + 2\ H_2 + 3\ CO_2 + H_2O \quad (5)$$

$$3\ \text{lactate}^- \rightarrow 2\ \text{propionate}^- + \text{acetate}^- + CO_2 + H_2O \quad (6)$$

$$4\ H_2 + 2\ CO_2 \rightarrow \text{acetate}^- + 2\ H_2O + H^+ \quad (7)$$

$$4\ \text{lactate}^- \rightarrow 6\ \text{acetate}^- + 2\ H^+ \quad (8)$$

Standard Gibbs free energy change of reactions were calculated using Gibbs free energy of formation values from Kleerebezem and van Loosdrecht (2010) and adjusted for temperature, pH, P_{H2} and reactants concentration according to eq. 9.

$$\Delta G' = \Delta G° + R \cdot T \cdot \ln Q \quad (9)$$

4.2.4. DNA extraction and sequencing analysis

DNA samples were taken from the middle height sampling port of the reactor, centrifuged at 15,000 rpm for 10 min and stored at -20°C for DNA extraction and sequencing. DNA was extracted from the biomass pellets (PowerSoil DNA isolation kit) for amplification of the V3-V4 region of 16S rRNA following the Illumina library generation and sequencing method described by Takahashi et al. (2014) (Takahashi et al., 2014). The primer set used (full-length IUPAC nomenclature; forward: 5' TCGTCGGCAGCGTCAGATGTGTATAAGAGACAGCCTACGGGNGGCWGCAG; reverse: 5' GTCTCGTGGGCTCGGAGATGTGTATAAGAGACAGGACTACHVGGGTATCTAATCC) allowed simultaneous amplification of bacterial and archaean 16S rDNA (Klindworth et al., 2013). DNA sequences were processed as described previously (Contreras-Dávila et al., 2020). In short, the

DADA2 pipeline (v. 1.16) (Callahan et al., 2016) was used and the identified ASVs were submitted to the SILVA database (Quast et al., 2013) for taxonomic identification (SILVA 138 SSU Ref NR 99). Forward and reverse reads were trimmed at cycles 240 and 220, respectively, based on the quality profiles obtained. Sequences were deposited in the ENA database (https://www.ebi.ac.uk/ena) under the accession number PRJEB43372. Species assignment is based on exact sequence matching. Selected sequences with non-exact match were submitted to NCBI BLAST query (megablast 16S rRNA bacterial and archaean gene sequences) and the percentage of identity is reported. ASVs with ≥0.01% of total counts were used for further analyses. Statistical analyses were done using R Studio (v. 1.3.959). Shannon diversity index boxplots were obtained using the InteractiveDisplay package (v. 1.26.0) (Balcome and Carlson, 2020). Normalized counts using the Cumulative Sum Scaling (CSS) method (Paulson et al., 2013) were used for Distance-based Redundancy Analysis (dbRDA) and Canonical Correspondence Analysis (CCA). dbRDA was done using Bray-Curtis dissimilarity with the capscale function and CCA with the CCA function, both from the vegan package (v. 2.5.7) (Oksanen et al., 2019). Visualization was done using the ggord (v. 1.1.5) (Beck and Mikryukov, 2020) and ggplot2 (v. 3.3.3) (Wickham, 2008) packages.

4.2.5. Analytical methods

Aqueous samples were centrifuged at 10000 rpm for 10 min and stored at -4°C before analyses. Gas chromatography was used for carboxylates (C2-C8) and alcohols (C1-C6) quantification with an injection volume of 1 µL (Sudmalis et al., 2018). Lactate, succinate and formate were measured by injecting 20 µL of sample into an HPLC equipped with a refractive index detector (Contreras-Dávila et al., 2020). Lactate enantiomers (D-lactate and L-lactate) were separated and quantified with a chiral column Astec CLC-L (15 cm × 4.6 mm, 5 µm) (Supelco) using isocratic HPLC (Thermo Scientific Dionex UltiMate 3000 RS, Thermo Fischer) with UV-detection at 254 nm (Dionex UltiMate VWD-3400). The mobile phase was 5 mM cupric sulfate at 1 mL/min and injection volume of 30 µL. Temperature in the column oven was 25°C. Chromatography data were analyzed with Chromeleon software (v6.8).

Nitrogen, oxygen, methane and carbon dioxide were measured using GC (Shimadzu GC-2010, Japan) equipped with TCD detector and parallel column setup (gas split 1:1) of Agilent PoraBOND Q (50 m x 0.53 mm x 10 µm) and Molsieve 5A (25 m x 0.53 mm x 50 µm). Carrier gas was helium at 22.5 $mL \cdot min^{-1}$. The oven temperature was 80 °C and TCD 150 °C. Hydrogen was measured with an HP 5890 gas chromatograph by injecting 100 µl of gas-sample on a Molsieve 5A column (30 m × 0.53 mm × 25 µm) with thermal conductivity detection (TCD). The oven temperature was 40 °C and µ-TCD 150 °C. The carrier gas was argon with a flow rate of 20 $mL \cdot min^{-1}$. Solids samples were taken from the middle height of the column and after a gas pulse during phases of intermittent gas addition for mixed liquor suspended solids quantification. Total (TSS) and volatile (VSS) suspended solids were measured following Standard Methods [15]. Liquid samples were centrifuged at 10000 rpm for 20 minutes. The supernatant was filtered and the pellet was placed onto the filter paper using demi water. Samples were dried to at 105 °C for at least 12 hours before TSS weighing and then placed in an oven at 550 °C for 2-3 hours to quantify VSS. Raw chemical experimental data are available in the 4TU.ResearchData repository (https://doi.org/10.4121/14208530.v1).

4.3. Results

4.3.1. Lactate conversion performance and biomass growth

After an initial time period of fluctuating pH and HRT values, lactate conversion rates stabilized and n-caproate became dominant (Figure 4.1A, 4.1B). Then, continuous gas supply was started in phase 1 at 12 mL·min^{-1} (SGV = 0.22 m·h^{-1}). By the end of phase 1 (period I), about 40% of the fed lactate was converted (1.2±0.04 e$^-$ eq·L^{-1}·d^{-1}; 8.9±0.3 g·L^{-1}·d^{-1}) to mainly n-caproate (Figure S3). n-caproate was produced at concentrations of 5.4±0.2 g·L^{-1} with productivities and selectivities of 0.7±0.4 e$^-$ eq·L^{-1}·d^{-1} (2.6±0.1 g·L^{-1}·d^{-1}) and 60±6%, respectively (Figure 4.2). n-heptylate and n-caprylate were produced at selectivities of 5±2% and 2±1%, respectively. Mixed liquor biomass concentrations remained comparable during operation with and without gas addition (Figure 4.1C) and a thin biofilm was formed on the reactor walls with gas supply (Figure S2). To increase the gas mixing, gas supply was increased 10-fold (120 mL·min^{-1}; SGV = 2.2 m·h^{-1}) in phase 2 which resulted in degradation of chain elongation activity with n-butyrate and propionate increasing at the expense of n-caproate formation. Some of the biofilm detached due to the increased gas addition settling at the bottom of the column but not to a measurable sludge bed height (Figure S2). Gas supply was reduced back to similar volumetric flows to phase 1 but added intermittently thereafter (phases 3 and 4) to keep high gas mixing. Intermittent gas supply was done at 11.3 mL·min^{-1} with a resulting SGV of 3.6 m·h^{-1}. Initially, the gas bursts pressurized the recirculation line causing a wash out of biomass. Therefore, the reactor had to be re-inoculated (190 mL effluent) and put in batch on days 104.8-109. Continuous reactor operation with intermittent gas supply was resumed after the batch phase and once the recirculation line was reinforced. During period II, lactate was converted at 45% higher rates (1.71±0.41 e$^-$ eq·L^{-1}·d^{-1} (12.9±1.3 g·L^{-1}·d^{-1}) compared to period I towards propionate and n-butyrate which showed selectivities of 25±2% and 61±2%, respectively. Decreasing the HRT to 1 day in phase 4 resulted in a ~50% increase in lactate conversion rate to 2.5±0.41 e$^-$ eq·L^{-1}·d^{-1} (18.9±3.1 g·L^{-1}·d^{-1}) with n-butyrate and propionate production rates being 1.5-times and 2-times higher in period III compared to period II. Traces of n-valerate and n-caproate were observed in phases 3 and 4 but n-heptylate and n-caprylate were not produced. Similar mixed liquor biomass concentrations were observed during continuous (phases 1 and 2) and intermittent (phases 3 and 4) gas supply with no noticeable changes in biofilm growth. During intermittent gas supply, detached biofilm particles were being re-suspended with every gas pulse and took a more irregular shape (Figure S2) but they did not grow into a measurable sludge bed. Due to the change in lactate metabolism from MCC to SCC production, gas supply was stopped in phase 5 to recover chain elongation activity. Propionate and n-butyrate continued to be produced despite gas supply was stopped but chain elongation activity was recovered after increasing the liquid recirculation rate on day 195.7 (Figure 4.1A). Once chain elongation was recovered, lactate consumption decreased to comparable rates as in period I and similar product selectivities. The highest n-caprylate production was observed in this period at 0.04±0.01 e$^-$ eq·L^{-1}·d^{-1} (0.13±0.03 g·L^{-1}·d^{-1}) and selectivity of 2.3±0.4% (Figure 4.2).

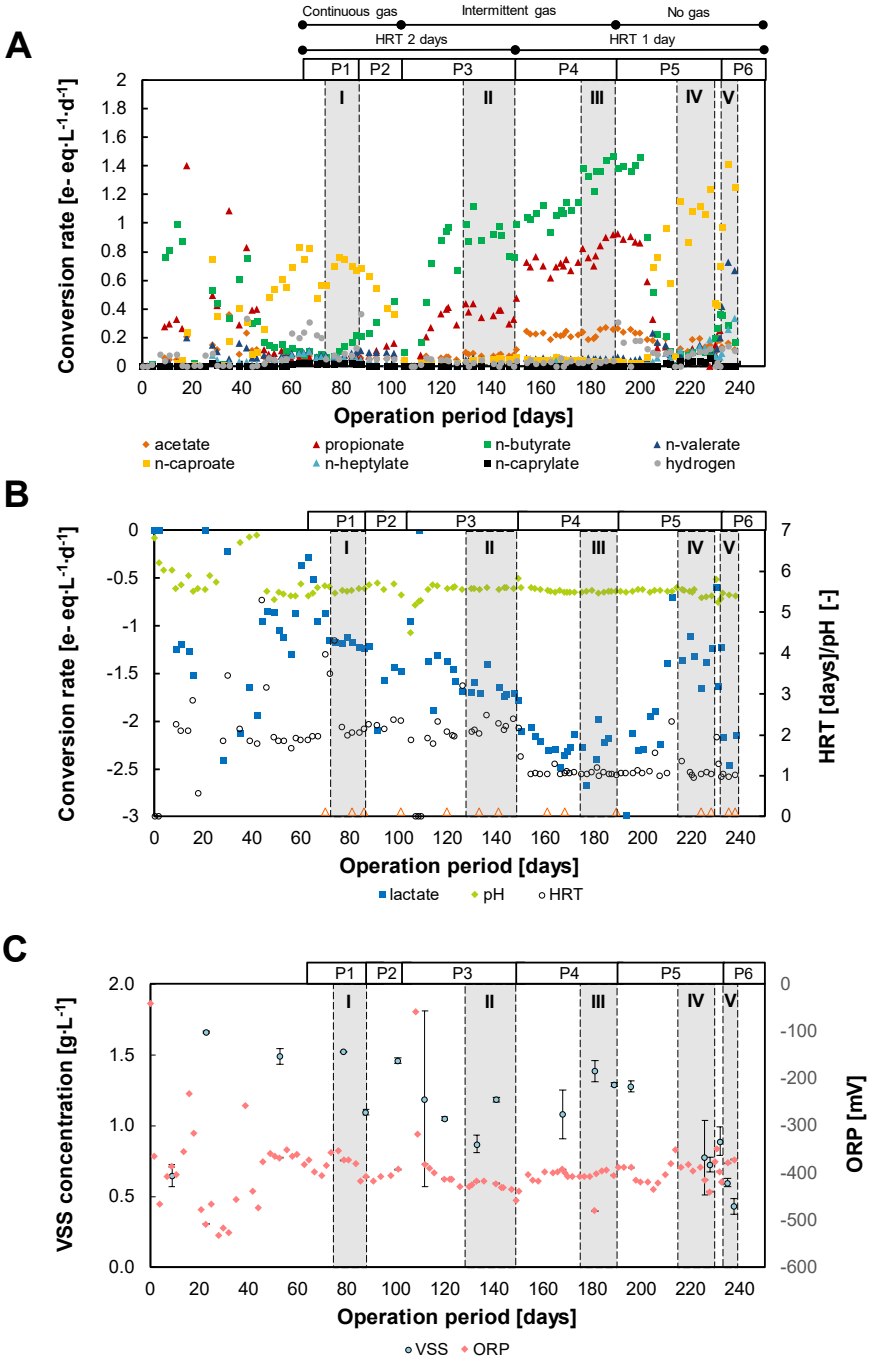

Figure 4.1 Reactor performance over operation time. (**A**) Metabolites production rates; (**B**) HRT, pH and lactate conversion rates; and (**C**) volatile suspended solids (VSS) concentrations and oxidation-reduction potential (ORP). Shaded areas indicate periods I-V. Orange triangles indicate DNA sampling days (**B**).

Propionate was added in the feed during phase 6 to test whether propionate was inhibiting chain elongation in phases 3-4 or it could be used as electron acceptor and instead improve chain elongation rates. Propionate addition at 5 g·L^{-1} (similar to phases 3 and 4) improved chain elongation rates with lactate conversion reaching a maximum of 2.26±0.15 e$^-$ eq·L^{-1}·d^{-1} (17±1.1 g·L^{-1}·d^{-1}). n-caproate and n-heptylate production rates increased by ~20 and ~90% reaching values of 1.22±0.18 e$^-$ eq·L^{-1}·d^{-1} (4.4±0.7 g·L^{-1}·d^{-1}) and 0.23±0.10 e$^-$ eq·L^{-1}·d^{-1} (0.9±0.3 g·L^{-1}·d^{-1}). However, lower mixed liquor biomass concentrations were measured with the addition of propionate compared to the previous phase (Figure 4.1C). Despite the faster lactate conversion, increased selectivities were obtained for SCC i.e. n-butyrate and n-valerate instead of MCC. A longer operation time could lead to microbiome adaptation and improved more stable lactate and propionate elongation to odd-chained MCC. This was not possible here due to a pH drop to 4.7-4.8 due to technical problems with pH control. At this low pH conditions, lactate and propionate conversion continued for <4 HRT with halved conversion rates and similar product selectivities (data not shown).

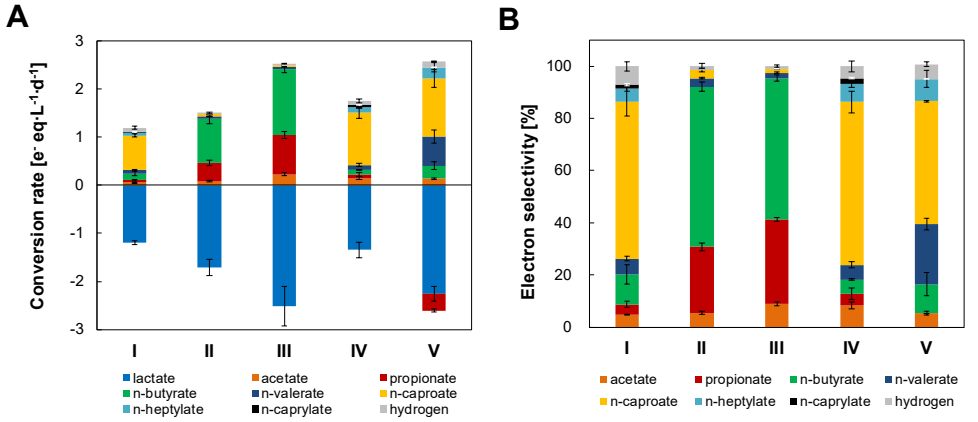

Figure 4.2 (**A**) Lactate and metabolites conversion rates and (**B**) product selectivity during the different stabilized operation periods.

Overall, lactate conversion rates were higher when the microbiome produced SCC compared to MCC production at both long (phase 1 vs phase 3) and short (phase 4 vs phase 5) HRT conditions (Figures 4.3A, 4.3B). Oxidation-reduction potential (ORP) remained stable between -378 and -401 mV in chain elongation conditions (periods I, IV and V) and between -412 and -430 mV in SCC-producing conditions (periods II and III) (Figure 4.1C). Residual lactate concentrations ranged between 6-17 g·L^{-1} during SCC production and between 15-25 g·L^{-1} during MCC production. The proportions of L-lactate enantiomer over D-lactate (enantiomeric excess = 100*[L-lactate - D-lactate]/[L-lactate + D-lactate]) showed a ~10% enantiomeric excess during SCC production in phase 4 and approached racemic equilibrium (~1% L-lactate excess) during chain elongation in phase 5 (Figure S3). Addition of propionate (phase 6) allowed lactate to be converted to longer carboxylates at rates similar to SCC-producing conditions (phase 4) (Figures 4.3A, 4.3B) with doubled apparent specific lactate consumption rates due to lower mixed liquor biomass concentrations (Figures 4.3C, 4.3D). Methane production was observed at low proportions (~0.01 e$^-$ eq·L^{-1}·d^{-1}; ≤1% selectivities) in phases 1, 2 and 5 and at ~0.05 e$^-$ eq·L^{-1}·d^{-1} (<2% selectivity) in phase 6.

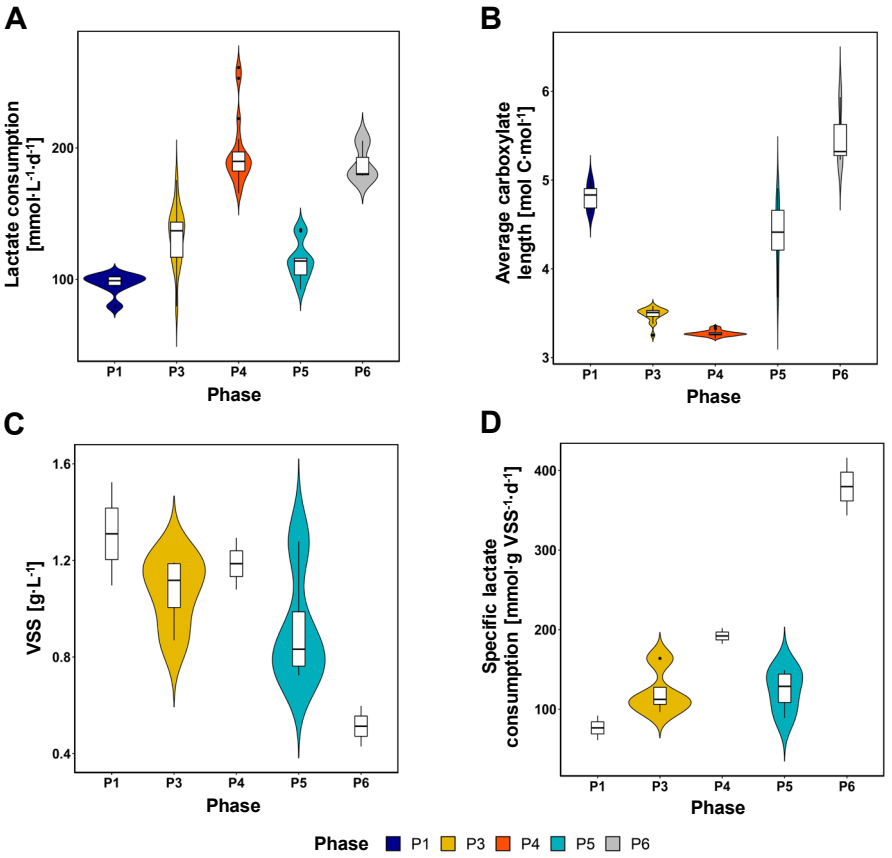

Figure 4.3 Violin plots showing lactate conversion and biomass concentrations for each operational phase. (**A**) Lactate consumption rate; (**B**) average carboxylate length produced; (**C**) mixed liquor biomass concentration; and (**D**) specific lactate conversion based on mixed liquor biomass concentrations. Violin shapes show the data kernel probability density with boxplots embedded. Boxplots show the interquartile range (IQR) in boxes divided by median values (horizontal lines) with whiskers depicting ±1.5 IQR and outliers as points. Plots include data from stable HRT and pH operational days. Phase 2 was excluded and data from days 209.8-231.9 (when chain elongation was recovered) were used for phase 5.

4.3.2. *Caproiciproducens* outcompeted by *Clostridium* at high superficial gas velocities

The reactor microbiomes developed into less diverse microbial communities compared to the initial inoculum (Figure S4) with chain-elongating microbiomes showing higher diversity than SCC-producing microbiomes from phases 3 and 4 (Figure 4.4A). Both N_2 gas flow rate (N_2) and SGV affected the microbiome composition (P<0.0005) and SCC-producing microbiomes clustered apart from chain-elongating communities (Figure 4B). MCC-producing microbiomes showed similar compositions in phases 5 and 6 but relatively distant from microbiomes from phase 1. This difference was related to the different HRT and gas flow applied as these two variables were linked to the variation captured by CAP2 (Figure 4.4B). High SGV applied in phases 2-4 resulted in decreased relative abundance for the genera *Caproiciproducens* and *Tuzzerella* while *Clostridium* sensu stricto 12 became dominant (Figure 4.4C). MCC production was linked to increased relative abundance of ASVs belonging to the genera *Caproiciproducens*, *Tuzzerella*, *Oscillibacter*, *Haloimpatiens* and *Clostridium* sensu stricto 15 (Figure 4.4D). *Caproiciproducens* spp. ASV1, ASV7 and ASV11,

Oscillibacter sp. ASV6 and *Tuzzerella* sp. ASV3 were among the most abundant ASVs in chain-elongating microbiomes from phases 1, 5 and 6 (Figure 4.5) and were strongly related to n-caproate production (except ASV7) (Figure 4.4D). *Haloimpatiens* sp. ASV5 (99.7% similar to *Haloimpatiens lingqiaonensis*) was linked to n-heptylate production. *Clostridium* cochlearum sp. ASV8 was also related with MCC-producing microbiomes. Microbiomes producing propionate and n-butyrate were related to high SGV and were composed by up to 74% of *Clostridium tyrobutyricum* spp. ASV2 and ASV4, except on day 140.8 where *Anaerotignum* sp. ASV18 was also abundant (Figure 4.5). *C. tyrobutyricum* spp. ASV2 and ASV4 were 99.7 and 99.4% similar to *C. tyrobutyricum* strain ATCC 25755, respectively.

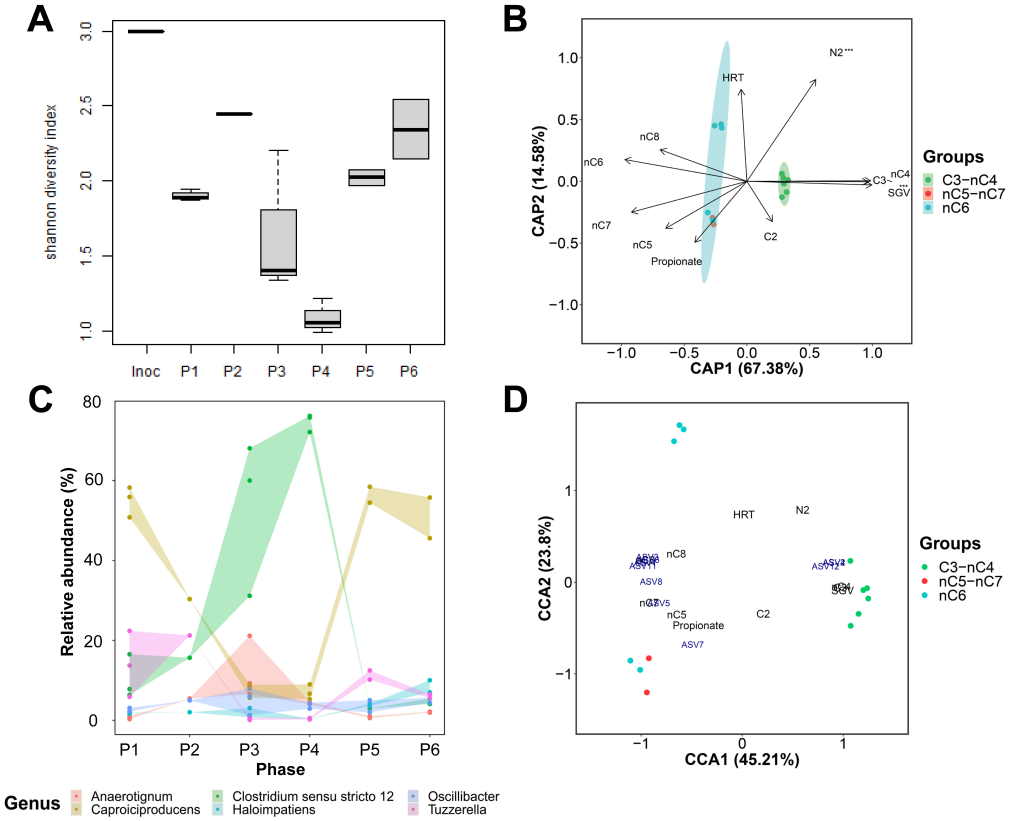

Figure 4.4 Reactor microbiome dynamics through the operational phases related to environmental conditions. (**A**) Shannon diversity index. Boxplots show the interquartile range (IQR) in boxes divided by median values (horizontal lines) with whiskers depicting ±1.5 IQR. (**B**) Distance-based Redundancy Analysis (dbRDA) using Bray-Curtis dissimilarity index; ASVs relative abundance as response variables; and environmental parameters as explanatory variables (constraints). Environmental parameters considered were: gas flow rate (N_2), SGV, HRT, propionate addition and metabolites electron selectivities on the DNA sampling days (acetate [C2], propionate [C3], nC4, nC5, nC6, nC7 and nC8). Concentration ellipses depict confidence intervals with α = 0.05. Significance code: '***' associated with a variable at P <0.0005. (**C**) Relative abundance of dominant genera for each operational phase. Shaded area cover the minimum and maximum relative abundance values. (**D**) Canonical Correspondence Analysis (CCA) using Hellinger transformation and same constraints as in dbRDA. CCA triplot shows top 10 ASVs best described by the model scaled proportionally to eigenvalues. Analyses were done using 16S rRNA gene sequencing data of ASVs with >0.01% of total counts. Counts were CSS-normalized for dbRDA and CCA analyses (**C**-**D**).

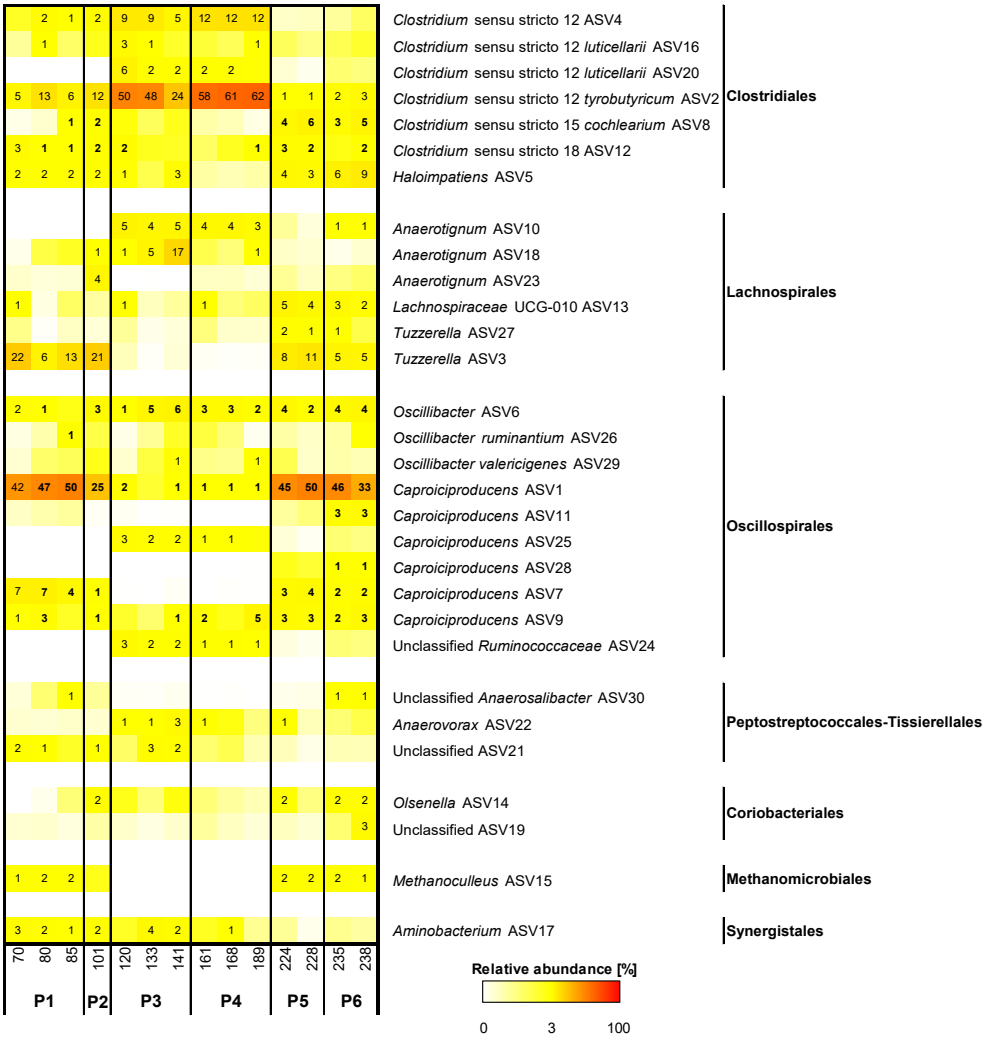

Figure 4.5 Reactor microbiomes composition at ASV level. Top 30 ASVs are shown and relative abundance values ≥1% are displayed. Sampling days and corresponding operational phases are shown below the heatmap. Taxonomy was assigned based on SILVA 138 SSU Ref NR 99 database.

4.4. Discussion

4.4.1. Lactate was efficiently converted into MCC at low gas velocities with conversion rates improved after electron acceptor supplementation

In the present study, it was shown that N_2 supply can be used for mixing chain elongation reactors with sustained MCC production at SGV ≤0.22 m·h^{-1}. Chain elongation was obtained when N_2 was either continuously supplied at 12 mL·min^{-1} with an equivalent SGV of 0.22 m·h^{-1} (phase 1) or when not supplied at all (phase 5). In both conditions, n-caproate electron selectivity was ~61% but n-caproate yields from consumed lactate were higher in phase 5 (period IV: 0.31±0.04 mol nC6·mol lactate^{-1}) compared to phase 1 (period I: 0.23±0.02 mol nC6·mol lactate^{-1}) indicating a more efficient

lactate conversion in phase 5. *Caproiciproducens*-related species dominated the suspended microbiome composition in both conditions. The obtained n-caproate yields are similar to yields reported for *Ruminococcaceae* bacterium CPB6-enriched microbiomes (0.3 mol nC6·mol lactate^{-1}) (Zhu et al., 2015) and pure cultures (0.23 mol nC6·mol lactate^{-1}) (Zhu et al., 2017). MCC production rates reached 1.25±0.15 e^- eq·L^{-1}·d^{-1} (10 g COD·L^{-1}·d^{-1}) with electron selectivities of 72±5% when HRT was kept at 1 day and gas was not supplied (phase 5) with MCC composed of 87% n-caproate (8.7 g COD·L^{-1}·d^{-1}), 9.5% n-heptylate (0.97 g COD·L^{-1}·d^{-1}) and 3% n-caprylate (0.32 g COD·L^{-1}·d^{-1}). In the present study, relatively higher n-caproate production rates (1.3- to 3.8-times) and selectivities (1.5- to 1.8-times) compared to previous reports were obtained. Kucek et al. (2016a) obtained a maximum n-caproate productivity of 6.9 g COD·L^{-1}·d^{-1} in an upflow anaerobic filter fed with L-lactate and n-butyrate using in-line extraction. In a lactate-fed CSTR, Candry et al. (2020a) obtained maximum n-caproate concentrations of 36 mM at pH 6 and HRT of 4 days equivalent to a maximum n-caproate production rate of 2.3 g COD·L^{-1}·d^{-1}. n-caproate selectivities reported in the mentioned studies reached maximum values of 34 and 41%, respectively.

Despite the consumed lactate was efficiently converted into MCC during phases 1 and 5, 46% and 70% of the fed lactate at HRT of 2 and 1 days, respectively, was not converted. Added propionate (phase 6) increased lactate consumption rates by 1.7-times (2.26±0.15 e^- eq·L^{-1}·d^{-1}; 18 g COD·L^{-1}·d^{-1}) by acting as electron acceptor and reducing the unconverted lactate fraction to 55% at 1 day HRT. As a result, n-caproate and n-heptylate production reached maximum values of 1.21±0.18 e^- eq·L^{-1}·d^{-1} (9.7 g COD·L^{-1}·d^{-1}) and 0.23±0.10 e^- eq·L^{-1}·d^{-1} (1.8 g COD·L^{-1}·d^{-1}), respectively, indicating that lactate-based chain elongation rates can be significantly improved with addition of an electron acceptor. The use of an electron acceptor may allow chain-elongating bacteria to harvest more ATP thereby increasing chain elongation rates (Scarborough et al., 2018a; Spirito et al., 2018). It is assumed that acetate and propionate compete for the same enzyme system with a preference for acetate in the RBO pathway (Roghair et al., 2018a). In the present study, acetate concentrations (7.1-18.3 mM) were 2-3 times higher than propionate (3.5-5.6 mM) during chain elongation without electron acceptor supply (periods I and IV) which may help explain the high even-chain (nC4, nC6 plus nC8, ~73% selectivity) over odd-chain (nC5 and nC7, ~12% selectivity) products. However, residual propionate concentrations (42 mM) were higher than acetate (24 mM) when adding propionate which may have compensated for a lower enzyme affinity increasing odd-chain products selectivity to 32% (58% for even-chain products). About 40% of the added propionate was consumed (~25 mmol·L^{-1}·d^{-1}) with a corresponding odd-chain carboxylates production (nC5 and nC7) of ~29 mmol·L^{-1}·d^{-1}. These values indicate stoichiometric conversion of consumed propionate to odd-chains. Alcohols (C1-C6) and branched-chain carboxylates were not detected in any operational phase. The extra 4 mmol·L^{-1}·d^{-1} of odd-chain products could originate from in situ produced propionate. In situ produced propionate seemed to be reduced by a factor of ~3 when external propionate was added (5 g·L^{-1}; 13 mM undissociated propionic acid) considering that odd-chains (propionate, nC5 and nC7) were produced at ~13 mmol·L^{-1}·d^{-1} in the previous period (period IV) when only lactate was fed. Although the propionate concentrations added did not inhibit chain elongation, relatively lower mixed liquor biomass concentrations were observed (phase 5 vs phase 6) resulting in apparent 3-times higher specific lactate consumption rates compared to lactate-elongation with no electron acceptor (~136 mmol lactate·g VSS^{-1}·d^{-1} vs ~380 mmol lactate·g VSS^{-1}·d^{-1}). Suspended biomass growth seemed to

dominate in the reactor although the contribution of biofilms and aggregates present in the reactor to the measured lactate conversion and chain elongation rates was not well characterized. However, biomass aggregation into sludge beds typically observed in high-rate granular reactors was not observed (Wu et al., 2009). Chain-elongating microbiomes with propionate supplementation were also dominated by *Caproiciproducens*-related species. Increased proportions of *Haloimpatiens* and *C. cochlearum* species was observed which have no reported role in MCC production. *Haloimpatiens* species have recently been enriched in chain elongation microbiomes fermenting a mixture of lactose, lactate, ethanol and acetate (Zagrodnik et al., 2020). MCC selectivities were reduced upon propionate addition due to a marked increase in n-valerate electron selectivity to 23±2% (4.8 g COD·L^{-1}·d^{-1}) while n-heptanoate selectivity was 9±3%. Future studies may focus on improving long-term n-heptylate production from lactate and propionate as has been done for the ethanol-based chain elongation process for which an n-heptylate production of 10.4 g COD·L^{-1}·d^{-1} and 23% selectivity has been achieved (Grootscholten et al., 2013c).

4.4.2. High gas velocities and dilution rates may favor fast lactate metabolism

Supply of N_2 at high rates had a marked effect on lactate conversion and microbiome composition. The SCC acetate, propionate and n-butyrate were the main fermentation products when gas was supplied at SGV >2 m·h^{-1}. Chain elongation showed a decreasing trend during continuous gas supply at SGV of 2.2 m·h^{-1} (phase 2) while SCC were persistently produced during intermittent gas supply at SGV of 3.6 m·h^{-1} (phases 3 and 4). Although biomass concentrations were only slightly lower during operation at high SGV (phases 2-4) compared to low SGV (phase 1), the microbiome composition was completely changed to a dominance of *Clostridium tyrobutyricum* species. *Clostridium tyrobutyricum* type strain ATCC 25755 is usually regarded as an efficient n-butyrate producer through the RBO pathway (Lee et al., 2016). The type strain ATCC 25755 and several other strains are also capable of producing propionate, isobutyrate and n-valerate (Ingham et al., 1998). Although the propionate production pathway for this species is not described. Likely, the strong change in microbiome composition and metabolites profile was caused by washout of MCC-producing chain-elongating bacteria due to high gas velocities. In high-rate reactors, hydrodynamic shear force created with gas supply is reported to favor biomass aggregation into granules. Hydrodynamic shear force effected with continuous N_2 supply at a SGV of 0.24 m·h^{-1} increased nucleation rates and granular sludge properties in an UASB anaerobic digester (Wu et al., 2009). Applying shear force *via* aeration at SGV >4 m·h^{-1} led to compact granules formation in sequential aerobic sludge blanket reactors (Tay and Liu, 2001). Despite similar SGV were applied in the present study (0.22-3.6 m·h^{-1}), measurable granular sludge was not obtained. Instead, chain-elongating bacteria were washed out and SCC-producing microbiomes with a faster lactate metabolism were enriched. This indicates that the first step of chain elongation (acetate to nC4) occurs at higher rates than the second step (nC4 to nC6) with the first step being selected at high gas velocities.

Moreover, increased production of propionate (period III: 0.82±0.07 e^- eq·L^{-1}·d^{-1}; 6.6 g COD·L^{-1}·d^{-1}) in detriment of n-butyrate allowed higher lactate consumption rates at similar biomass concentrations when HRT was reduced to 1 day (phase 3 vs phase 4). Although pH conditions below 6 units can effectively limit growth of known propionate-producing bacteria and promote lactate-based chain elongation (Candry et al., 2020a), propionate was produced at high rates in the present study. A

previous study also showed propionate production (5.5 g COD·L^{-1}·d^{-1}) over chain elongation at high lactate loading rates (~16 g COD·L^{-1}·d^{-1}), HRT 1.5 days and pH 5.0 in lactate-fed reactor microbiomes (Kucek et al., 2016a). The production of propionate might allow bacteria to cope with conditions of high lactate loading (up to 37 g COD·L^{-1}·d^{-1}) and dilution (high SGV and short HRT) rates as applied in phases 3 and 4. This is supported by observations with pure cultures where lactate conversion to propionate allows higher growth rates at pH ~7 (0.12-0.33 h^{-1}) (Seeliger et al., 2002) and pH ≥5.0 (0.66 h^{-1}) (Weimer and Moen, 2013) compared to n-butyrate from lactate and acetate at pH 6.2 (0.05 h^{-1}) (Diez-Gonzalez et al., 1995). These results open the opportunity of increasing the productivity and broaden the product spectrum of lactate-based chain elongation in, for instance, a two-stage system. Lactate conversion could be steered toward SCC (e.g. propionate or nC4) by supplying N_2 to a first reactor which can then be fed as electron acceptors in a second reactor for chain elongation to MCC (e.g. nC7 or nC8) potentially achieving high lactate conversion rates in both stages.

4.4.3. Shift from MCC to SCC production was unrelated to hydrogen partial pressure

N_2 supply at high levels decreased partial pressures of hydrogen (P_{H2}) and carbon dioxide (P_{CO2}) which could affect chain elongation. It is known that CO_2 is required for amino acid synthesis and growth in ethanol-elongating bacteria such as *Clostridium kluyveri* becoming limiting at concentrations below 3 mM (Tomlinson and Barker, 1954). In the present study, calculated dissolved inorganic carbon (~90% H_2CO_3 at pH 5.5) increased from 10 mM in phase 1 to 20 mM in phase 2 to then decrease to 3-4 mM in phases 3 and 4. Thus, although CO_2 availability might have limited chain elongation in phases 3 and 4, this was not the case for phase 2. Additionally, the CO_2 requirements of lactate-elongating bacteria remain to be studied. Dissolved inorganic carbon was 17-18 mM during chain elongation without gas supply (phases 5 and 6).

Decreased P_{H2} caused by N_2 supply did not seem to have caused the shift from n-caproate to n-butyrate production either. Observed P_{H2} during chain elongation with continuous gas supply at 12 mL·min^{-1} (SGV = 0.22 m·h^{-1}) (period I, 0.10±0.03 atm) was lower than P_{H2} reached at 120 mL·min^{-1} (SGV = 2.2 m·h^{-1}) (phase 2 ~0.23 atm) at which chain elongation first declined. The Gibbs free energy change (ΔG') calculated from concentrations measured in period I suggest that P_{H2} had a negligible effect on determining whether n-butyrate or n-caproate is dominant (Figure 4.6). The efficient conversion of lactate to n-caproate in this period resulted in low n-butyrate concentrations making n-butyrate formation (eq. 4) more thermodynamically favorable than n-caproate (eq. 5). Other parameters such as preferred pH (Diez-Gonzalez et al., 1995; Zhu et al., 2017), use of SCC as electron acceptors (Angenent et al., 2016) and energetics of chain-elongating bacteria (Scarborough et al., 2018a) may explain the dominance of n-caproate production over acetate and n-butyrate. Formation of propionate along with acetate (eq. 6) is independent of P_{H2} and was more thermodynamically favorable than n-butyrate and n-caproate. Thus, P_{H2} thermodynamics does not seem to explain the shift from n-caproate to propionate and n-butyrate production. This indicates that chain-elongating *Caproiciproducens* species were likely kinetically outcompeted by SCC-producing *Clostridium* species under high shear and loading stress as discussed before (section 4.4.2).

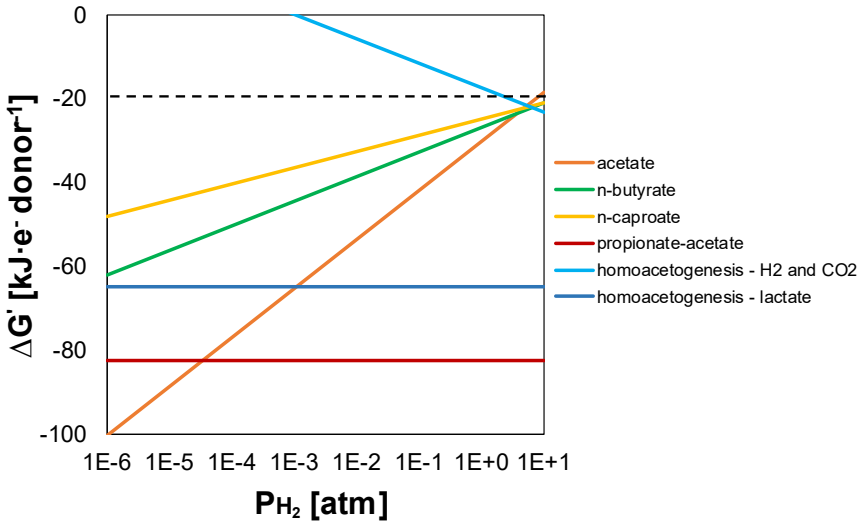

Figure 4.6 Actual Gibbs free energy change (ΔG') of lactate fermentation reactions and homoacetogenesis (section 4.2.3) as a function of hydrogen partial pressure (P_{H2}) with concentrations of period I, pH 5.5 and 30°C. A minimum free energy change of 20 kJ·e$^-$ donor^{-1} (dashed line) was assumed to be required for a reaction to be feasible (Schink, 1997).

Lactate conversion to MCC has been improved in incubations with external hydrogen addition (Wu et al., 2019). This improvement was shown to result from increased homoacetogenesis and acetate and propionate hydrogenation to their respective alcohols to then be used as electron donors/acceptors in chain elongation. Hydrogen supplementation also improved n-caproate formation from food waste fermentation leachate containing mainly lactate (Nzeteu et al., 2018). In the present study, no alcohols were detected throughout the operation time. Bacteria capable of performing homoacetogenesis such as *Oscillibacter* (Godwin et al., 2014) and *Clostridium luticellarii* (Poehlein et al., 2018) were present in chain-elongating microbiomes. However, homoacetogenesis from H_2 and CO_2 did not seem likely to occur (ΔG' <20 kJ·e$^-$ donor^{-1}) at the P_{H2} observed here (0.1 atm period I; ~0.3 atm periods IV-V). Alternatively, homoacetogens may produce acetate from lactate independent of P_{H2} and P_{CO2} (eq. 8) (Weghoff et al., 2015) which was a feasible reaction throughout the operation time (-65 to -57 kJ·e$^-$ donor^{-1}). However, H_2 and CO_2 yields during chain elongation periods indicate that lactate was primarily converted to n-caproate according to eq. 5. H_2 yields were 1.36±0.37 and 1.41±0.26 mol H_2·mol lactate^{-1} during chain elongation in periods I and IV, respectively. CO_2 yields averaged 0.73±0.25 mol CO_2·mol lactate^{-1} and 1.03±0.16 mol CO_2·mol lactate^{-1} in periods I and IV, respectively. These values are close to or higher than the H_2 and CO_2 yields expected from chain elongation according to eq. 5 (0.67 mol H_2·mol lactate^{-1}; 1 mol CO_2·mol lactate^{-1}). Thus, homoacetogenesis seemed to have little or no contribution in chain-elongating microbiomes with and without N_2 supply.

4.5. Conclusions

The supply of N_2 was observed to impact the microbiome composition and, subsequently, lactate conversion processes dependent on the superficial gas velocity (SGV) applied. Production of MCC through lactate-based chain elongation occurred when N_2 was supplied at SGV of 0.22 m·h^{-1} with

similar product selectivities to operation without N_2 supply. Chain elongation conditions enriched for organisms from the genera *Caproiciproducens*, *Tuzzerella*, *Oscillibacter* and *Haloimpatiens*. Higher SGV (2.2 and 3.6 $m \cdot h^{-1}$) washed out chain-elongating bacteria and enriched SCC-producing microbiomes dominated by *Clostridium tyrobutyricum* converting lactate into acetate, propionate and n-butyrate at higher rates. Lactate conversion into MCC occurred at similar rates as in SCC-producing conditions only when added propionate served as electron acceptor. Suspended biomass growth seemed to dominate and biomass aggregation typically observed in high-rate granular reactors was not observed at the SGV applied here (0.22-3.6 $m \cdot h^{-1}$). Based on the results of this study, N_2 supplementation at SGV ≤0.22 $m \cdot h^{-1}$ is suitable to provide mixing in lactate-based chain elongation bioprocesses while SGV >2 $m \cdot h^{-1}$ can severely affect microbiome composition and MCC production. N_2 supply may be useful to increase conversion rates and broaden the product spectrum of lactate-based chain elongation in two-stage systems.

Chapter 5

n-Caproate adsorption-recovery with granular activated carbon and isobutyrate formation with conductive materials

This manuscript was submitted as:
Carlos A. Contreras-Dávila, Natalia Nadal Alemany, Cris Garcia-Saravia Ortiz-de-Montellano, Zhipeng Bao, Cees J.N. Buisman and David P.B.T.B. Strik. Designing a selective n-caproate adsorption-recovery process with granular activated carbon and screening of conductive materials in chain elongation.

Abstract

Microbial chain elongation using biomass-derived lactate can be steered to produce a variety of MCC which need to be separated before application. In this study, we evaluated the effects of adding conductive and/or adsorbing materials to batch and continuous open-culture lactate-based chain elongation. Incubations with granular activated carbon (GAC), nickel foam (NF) and stainless steel mesh (SS) showed improved lactate use for chain elongation due to a 30-40% reduction in propionate formation, compared to the control (no material) and non-conductive polyurethane foam (PU). Isobutyrate production was stimulated in presence of GAC and NF (up to 1.2 $g \cdot L^{-1}$, 9% electron selectivity). Adding GAC to a continuous reactor led to *in situ* adsorption of n-caproate. GAC showed high affinity for n-caproate from real and artificial effluent as well as from mock blends containing C2-C8 carboxylates, adsorbing 60-80% of the initial n-caproate with recoveries up to 42% after desorption. Adsorption of n-caproate (184-243 $mg \cdot g\ GAC^{-1}$) increased with decreasing pH conditions. In conclusion, conductive materials decreased propionate and steered isobutyrate formation in batch open-culture chain elongation. Based on the promising adsorption properties of GAC, a first design of chain elongation with in-line adsorption-recovery is proposed as well as potential direct applications of MCC-loaded porous carbons.

5.1. Introduction

Resource recovery bioprocesses using chain elongation reactor microbiomes produce medium-chain carboxylates (MCC), which are saturated monocarboxylic acids with 6 to 12 carbon atoms that find applications in lubricants, biodegradable plastics, antimicrobials, feed additives and biofuels production (Angenent et al., 2016). Chain-elongating bacteria utilize energy-rich substrates e.g. ethanol, lactate, glucose as electron donors to elongate short-chain carboxylates (SCC, 1-5 carbon units) to MCC such as n-caproate (nC6) or n-caprylate (nC8) through a series of biochemical reactions in the reverse β-oxidation pathway (Angenent et al., 2016). Lactate is an interesting electron donor that can be easily obtained from residual biomass materials to produce n-caproate (Zhu et al., 2015; Contreras-Dávila et al., 2020). Alternatively, lactate may be converted to isobutyrate (Liu et al., 2020) or propionate (Seeliger et al., 2002). To steer microbiome-based bioprocesses toward effective production of a desired carboxylate, several operational conditions are applied such as gas supply (Contreras-Dávila et al., 2021), pH control or electron donor-to-acceptor ratio adjustment (Angenent et al., 2016). An alternative approach could be the use of conductive materials which may improve electron transfer in chain elongation. Conductive materials have been used to enhance anaerobic bioprocesses such as methanogenesis (Salvador et al., 2017) and SCC production (acetate and n-butyrate) from hydrogen (H_2) and carbon dioxide (CO_2) (Blanchet et al., 2018). Porous carbon materials such as granular activated carbon (GAC) have also been shown to enhance syntrophic methane production through direct interspecies electron transfer (DIET) due to its high conductivity (Liu et al., 2012). A similar effect has been observed with nickel foam (Guo et al., 2020). In chain elongation, biochar was suggested to facilitate electron transfer between ethanol oxidizers and chain-elongating bacteria with observed higher n-caproate and n-caprylate productions (Liu et al., 2017). However, the effect of conductive materials in lactate-based chain elongation has not been studied.

Additionally to their conductive properties, porous carbon materials may adsorb MCC reducing their toxicity to chain-elongating bacteria (Roghair et al., 2018b) and potentially facilitating MCC recovery. Since the produced MCC should be separated and recovered from the fermentation broth for further valorization, several methods have been applied in chain elongation, including liquid-liquid extraction (Kucek et al., 2016a) and ion exchange (Yu et al., 2019). Carboxylates recovery with GAC has only been studied for SCC such as lactate, acetate and n-butyrate from effluents of primary fermentation (Yousuf et al., 2016; Pradhan et al., 2017). Recently, GAC and biochar were observed to adsorb n-caproate in pure culture ethanol-based chain elongation incubations (Ghysels et al., 2021). However, the recovery of MCC from chain elongation systems through adsorption and desorption with GAC has not been assessed. Adsorption with GAC may have the advantages of easy handling along with reduced space and energy demands (López-Garzón and Straathof, 2014).

The aim of this work was to evaluate the effect of conductive materials on lactate-based chain elongation and the potential of GAC to recover chain elongation products with a focus on n-caproate. First, conductive (GAC, nickel foam and stainless steel) and non-conductive (polyurethane foam) materials were tested in incubations to understand whether the addition of conductive materials can affect fermentation performance. Since GAC promoted chain elongation and may facilitate MCC recovery, GAC was chosen for further tests in a continuous chain elongation reactor converting

lactate and acetate to n-caproate. Next, the feasibility of carboxylates adsorption and recovery with GAC was evaluated from real and artificial chain elongation effluents and from mock blends containing carboxylates with 2 to 8 carbons. Finally, adsorption isotherms were carried out to determine the effect of pH on n-caproate adsorption capacity.

5.2. Materials and methods

5.2.1. Materials used in batch chain elongation

Three conductive (granular activated carbon [GAC], nickel foam [NF] and stainless steel mesh [SS]) and one non-conductive (polyurethane [PU] foam) materials were tested. The GAC used (Norit PK 1-3, Cabot Norit Nederland B.V., the Netherlands) is produced from peat through steam activation, has an alkaline pH, particle size between 0.71-3.15 mm (85 wt%), a total surface area (B.E.T.) of 875 $m^2 \cdot g^{-1}$ and a methylene blue adsorption capacity of 110 $g \cdot kg^{-1}$ (as reported by Cabot Norit Nederland B.V.). The same material has been reported to have a pore volume of 0.55 $cm^3 \cdot g^{-1}$ and an average pore size of 2.7 nm (Schouten et al., 2007). The other materials were stainless steel T304 mesh 40 (Salomon's metalen B.V., the Netherlands); nickel foam (Salomon's Metalen B.V., the Netherlands); and PU foam (Recticel, Ltd., Brussels, Belgium) with a density of 30.4 $kg \cdot m^{-3}$ and a porosity of 20 pores per inch (PPI) (pore diameter of ~13 µm) (Sudirjo et al., 2020).

5.2.2. Screening of conductive materials in batch chain elongation

All the materials were added at 15 $g \cdot L^{-1}$ in triplicate batch chain elongation experiments. A duplicate control experiment with no added material was included. Lactate (≥90% concentrated lactic acid, VWR, the Netherlands) was added as electron donor and acetate (99-100% acetic acid, Merck KGaA, Germany) as electron acceptor. The concentrated lactic acid was a mixture of lactate monomers (~64%) and oligomers (Vu et al., 2005) containing mainly L-lactic acid (≥97%, as reported by VWR). Incubations were done in 500-mL Scotch bottles (300 mL liquid volume) with the headspace connected directly to a gas flow measuring device (AMPTS II, Bioprocess Control). The feeding medium contained lactate (20 $g \cdot L^{-1}$), acetate (1.5 $g \cdot L^{-1}$), yeast extract (1 $g \cdot L^{-1}$), BisTris buffer (100 mM) and was supplemented with mineral medium, trace elements and vitamins as described elsewhere (Roghair et al., 2016). The medium was bubbled for 5 minutes with N_2 gas and added to the bottles. The inoculum was derived from a food waste fermentation reactor (Contreras-Dávila et al., 2020) added at 4% v/v. Once the bottles were closed, the headspace was flushed for 12 min with a mixture of 80% N_2 and 20% CO_2 to ensure anaerobic conditions. The liquid was stirred intermittently (40 seconds on; 20 seconds off) at 70 rpm and temperature was controlled at 30°C in the water bath.

5.2.3. Continuous lactate-based chain elongation with GAC addition

From the conductive materials tested, GAC was selected for testing in continuous chain elongation. The reactor used was a double-walled glass upflow anaerobic reactor consisting of a vertical column (D_{in} = 5.7 cm; length = 90 cm), a settler, an inverted funnel for solid-gas-liquid separation and a recirculation line (Figure S1) with a liquid working volume of 2.2 L. The fermentation broth was recirculated from the top to the bottom of the reactor where it mixed with the feeding solution before flowing upwards into the reactor. A two-neck glass tube was connected in the recirculation line for pH control. Effluent overflowed at the top of the reactor and was collected in a reservoir. Temperature was controlled at 35°C using a water bath. The reactor was filled with feeding medium adjusted to

pH 5.0 containing lactate (30 g·L^{-1}), acetate (1.5 g·L^{-1}), yeast extract (2.5 g·L^{-1}), mineral medium and trace elements (Roghair et al., 2016) and vitamins (Zhu et al., 2015), bubbled with N_2 gas for 15 min and inoculated (4% v/v) with biomass derived from a food waste fermentation reactor (Contreras-Dávila et al., 2020). The reactor was operated in batch mode with pH control switched off until gas production and pH increase were observed (11 days). Then, continuous operation was started by feeding medium to an HRT of 2.2 days with automatic pH control at 5.1-5.2 with 1 M HCl. Chain elongation was first evaluated without GAC addition until stable conditions were observed (period I, days 55-77). Then, GAC was added at 20% v/v (~112 g) on day 77 with stable conditions observed in days 84-88 (period II). Before addition, GAC was sieved to remove fine particles (No. 18; 1 mm) and "pre-treated" by submerging it for 4 days in the same feeding medium fed to the reactor containing lactate, acetate and nutrients. To test whether lactate or acetate could still be adsorbed by the "pre-treated" GAC, 20% v/v GAC (4.1 g) was mixed with 80 mL of feeding medium and shaken at 30°C and 120 rpm for 2 days in duplicate serum bottles. The headspace in the bottles was exchanged with N_2 gas through vacuum and filling cycles to an overpressure of 0.2 atm.

5.2.4. Adsorption and desorption experiments with GAC

To evaluate the possibility of recovering fermentation products through adsorption with GAC, adsorption and desorption tests were conducted with four different media: real effluent, artificial effluent and mock C2-nC6 and C2-nC8 carboxylates blends (Table 5.1). The real effluent was derived from a lab-scale CSTR reactor producing n-caproate from lactate and acetate (Chapter 6) and centrifuged two times at 10,000 rpm for 20 min to remove biomass. The artificial effluent and the two mock carboxylates blends contained the same mineral medium as in the real effluent (Roghair et al., 2016) except that $(NH_4)HPO_4$ was replaced at equimolar phosphate concentrations with KH_2PO_4 (4.26 g·L^{-1}) to avoid microbial growth by elimination of a nitrogen source. Trace elements, vitamins and yeast extract were left out for the same purpose. Lactate was added as a sodium salt (50% sodium-(S)-lactate, Merck) while the rest were added as carboxylic acids (≥99% purity, Sigma Aldrich). Triplicate experiments were conducted in 125 mL serum bottles with 40 mL liquid volume and 40 g·L^{-1} (1.6 g) of washed and dried GAC. pH was adjusted to 5.0 by adding 1 M HCl. The serum bottles were closed and the headspace exchanged with N_2 gas through vacuum and filling cycles to an overpressure of 0.2 atm. The bottles were placed in a rotary shaker at 30°C and 120 rpm. The adsorption period lasted 9 days, after which the bottles were opened to remove the liquid with the help of a syringe, refilled with 40 mL of alkaline sodium borate buffer (0.5 M borate, pH ~9.4), headspace-exchanged and returned to the rotary shaker for desorption. Desorption lasted at least 5 days at 30°C and 120 rpm.

Table 5.1 Carboxylates concentrations used in the adsorption and desorption experiments.

Carboxylate	Concentrations [mM (g·L^{-1})]			
	Real effluent	Artificial effluent	C2-nC6 mixture	C2-nC8 mixture
lactate	200 (18)	200 (18)	-	-
acetate (C2)	42 (2.5)	49 (2.9)	57 (3.42)	57 (3.42)
propionate (C3)	3 (0.2)	-	57 (4.22)	57 (4.22)
n-butyrate (nC4)	22 (1.9)	2 (0.2)	57 (5.02)	57 (5.02)
n-valerate (nC5)	-	-	57 (5.85)	57 (5.85)
n-caproate (nC6)	57 (6.7)	60 (7.0)	57 (6.65)	57 (6.65)
n-heptylate (nC7)	-	-	-	3.8 (0.5)
n-caprylate (nC8)	-	-	-	3.5 (0.5)

5.2.5. Adsorption isotherms

Since n-caproate was the main chain elongation product in the continuous reactor, isotherm experiments with GAC were conducted to determine the n-caproate adsorption behavior at different pH. The GAC used was the same as in the previous experiments (Norit PK 1-3). Isotherms were determined at three different pH values (4.5, 5.0 and 5.5). Each pH was established with an acetate buffer with different proportions of sodium acetate and acetic acid. The acetic acid concentration remains similar between buffers (4.4-5 g·L^{-1}) with calculated sodium concentrations being 0.45, 0.95 and 1.63 g·L^{-1} at pH 4.5, 5.0, and 5.5, respectively. An additional isotherm at pH 5.0 was carried out in artificial effluent containing mineral medium (Roghair et al., 2016) and lactate (18 g·L^{-1}) (50% sodium-(S)-lactate, Merck). $(NH_4)HPO_4$ in the mineral medium was replaced with equimolar phosphate concentrations of KH_2PO_4 (4.26 g·L^{-1}) to avoid microbial growth.

Experiments were carried out in triplicates in 125 mL serum bottles containing 40 mL liquid, 10 g·L^{-1} (0.4 g) GAC and varying initial n-caproate concentrations (≥99% hexanoic acid, Sigma Aldrich). Before use, GAC was rinsed several times with demi-water (a total of ~83 mL demi-water·g GAC^{-1}) to remove fine particles and dried at 40°C for 24 h. Seven initial n-caproate concentrations were set (0.1, 0.2, 0.5, 1, 3, 6, and 8 g·L^{-1}) for experiments at pH 5.0 and 5.5. Due to decreased n-caproate solubility in the acetate buffer at pH 4.5, GAC was reduced to 5 g·L^{-1} (0.2 g) and n-caproate concentrations used were 0.05, 0.1, 0.25, 0.5, 1.5, 3 and 4 g·L^{-1} to ensure all the n-caproate was solubilized. After filling the bottles with GAC and the buffer containing n-caproate, pH was measured and adjusted to the initial value by adding a 1 M HCl or KOH when needed. The serum bottles were closed and the headspace exchanged with N_2 gas through vacuum and filling cycles to an overpressure of 0.2 atm. The bottles were placed in a rotary shaker at 30°C and 120 rpm. Equilibrium was measured at day 10, except for n-caproate concentrations of 0.5, 1.5, 3 and 4 g·L^{-1} at pH 4.5 for which samples were taken again on day 59. For the n-caproate concentrations of 3, 6 and 8 g·L^{-1} at pH 5.0 and 6 and 8 g·L^{-1} at pH 5.5, samples were taken again on day 72 to make sure equilibrium took place.

5.2.6. Calculations

Fermentation and adsorption results were evaluated for the as described in the Supplementary Material. Substrate conversion, productivities and selectivities of batch and continuous chain elongation were calculated based on electron equivalents. Adsorption, desorption and recovery performances were based on mass balances. Adsorption isotherms were fitted to the Freundlich model. Finally, the thermodynamics of fermentative and DIET-based bioprocesses was evaluated using Gibbs free energy change calculations. See Supplementary Material for details on the calculations.

5.2.7. Analytical methods

Liquid samples were centrifuged (15000 rpm, 10 min) and stored at -20°C before analyses. Lactate, succinate and formate were measured by HPLC (Contreras-Dávila et al., 2020). Gas chromatography was used to quantify monocarboxylates (straight-chain C2-C8 and branched-chain isobutyrate, isovalerate, isocaproate) and alcohols (C2-C6) (Sudmalis et al., 2018) as well as gas headspace composition (O_2, N_2, CO_2, CH_4, H_2) (Contreras-Dávila et al., 2021). Raw experimental data are available in the 4TU.ResearchData repository (https://doi.org/10.4121/14445576).

5.3. Results

5.3.1. Conductive materials reduce propionate production and promote isobutyrate and n-valerate formation

In the incubations, n-butyrate (nC4) was the main chain elongation product with no clear effect of the added materials on its production (60-70% electron selectivities) (Figure 5.1). However, propionate was produced at lower amounts and selectivities in the presence of conductive materials. Propionate production was the lowest with NF (0.36±0.01 e^- eq·L^{-1}; 14±1%), followed by SS (0.41±0.07 e^- eq·L^{-1}; 15±2%) and GAC (0.43±0.03 e^- eq·L^{-1}; 17±2%) whereas propionate was produced at 0.64±0.09 e^- eq·L^{-1} (25±3%) in the control and 0.64±0.20 e^- eq·L^{-1} (21±6%) in the PU experiments. This equals to a 33-44% reduction in propionate production with respect to the control. Chain elongation with GAC and NF yielded considerably high amounts of isobutyrate. Isobutyrate (iC4) was produced at 0.20±0.03 e^- eq·L^{-1} (0.9±0.14 g·L^{-1}) and a selectivity of 7±1% with addition of GAC while NF showed increased formation of both isobutyrate (0.27±0.11 e^- eq·L^{-1}; 1.2±0.57 g·L^{-1}) and n-valerate (0.22±0.04 e^- eq·L^{-1}; 0.8±0.16 g·L^{-1}) with respective selectivities of 9±4% and 8±1%. n-Valerate (nC5) selectivities remained low (3-4%) in the other conditions tested. With addition of SS, n-caproate (nC6) was observed at high concentrations (2.5 g·L^{-1}) in one (SS1) but was <0.3 g·L^{-1} in the other two replicates. Although gas measurements showed high variations between replicates (probably due to gas leaks in the set-up), gas production was observed earlier (Figure S2) in experiments with GAC and NF (on days 2-3) accompanied with n-butyrate production (Figure S3), compared to the control and PU experiments (4-6 days). Part of the substrates or produced n-butyrate seemed to be adsorbed on GAC in the initial days since n-butyrate concentrations were lower than the expected from lactate and acetate consumption. Additionally, the hydrogen partial pressure (P_{H2}) at the end of the incubations was lower in experiments with GAC ($5{\cdot}10^{-4}$±$1{\cdot}10^{-4}$ atm) and NF ($4{\cdot}10^{-3}$±$3{\cdot}10^{-3}$ atm) compared to the control (0.19±0.02 atm), SS (0.12±0.13 atm) and PU (0.14±0.09 atm) experiments (Figure S2). Acetate formation seemed to occur before lactate was depleted in experiments with GAC (0.27±0.05 e^- eq·L^{-}

^{1}; 2.03±0.38 g·L^{-1}) and NF (0.18±0.09 e^{-} eq·L^{-1}; 1.35±0.67 g·L^{-1}) while acetate was formed after lactate depletion in the control experiment (0.14±0.09 e^{-} eq·L^{-1}; 1.05±0.67 g·L^{-1}). Net acetate production was not clear with SS and PU (<0.06 e^{-} eq·L^{-1}) (Figure S3).

The electron balance showed that part of the lactate oligomers present in the concentrated lactic acid solution were used for fermentation (Figure 5.1A). Lactate monomers and acetate comprised about 68% of the electrons in added substrate (total lactate and acetate). Substrate conversion was 82±3% in the control experiment increasing to 88-92% with conductive materials and reaching a maximum of 95±4% in the PU experiment. Considering a composition of $CH_{1.7}O_{0.5}N_{0.2}$ (Chen et al., 2016a), yeast extract amounted to <5% (34.5 mM carbon) of the substrates (total lactate + acetate) and was, therefore, not considered in the electron balances.

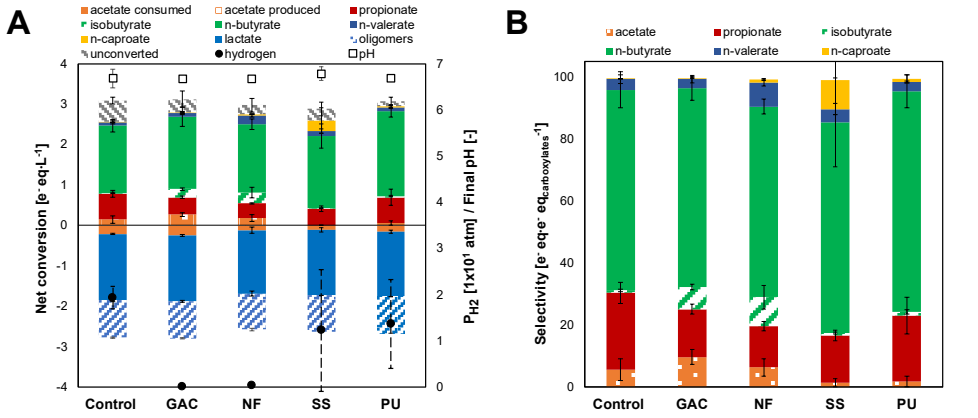

Figure 5.1 (**A**) Net substrate conversion by the end of the experiments with different conductive materials (granular activated carbon [GAC], nickel foam [NF], stainless steel mesh [SS]) and non-conductive polyurethane (PU) foam cubes. Oligomers were estimated as a fraction (0.36) of total lactate. The unconverted fraction shows missing electrons (from lactate oligomers) between metabolic products and substrates added (acetate and total lactate). (**B**) Electron selectivity of chain elongation products. Error bars indicate ±one standard deviation except for the control experiment where error bars indicate duplicates absolute deviation from the average.

5.3.2. GAC increases conversion rates in continuous chain elongation

From the conductive materials, GAC was further studied for its effect on continuous chain elongation. GAC was added (20% v/v) to an upflow anaerobic reactor that was converting lactate and acetate into mainly n-caproate (Figure 5.2). Before GAC addition (period I), the reactor produced n-caproate at 0.61±0.07 e^{-} eq·L^{-1}·d^{-1} (2.3±0.4 g·L^{-1}·d^{-1}) at 2 days HRT with a selectivity of 80±3%. Other carboxylates were produced at lower selectivities such as propionate (2±1%), n-butyrate (9±4%) and n-caprylate (3±1%). n-caproate and lactate concentrations were 1.35±0.16 e^{-} eq·L^{-1} (4.9±0.6 g·L^{-1}) and 0.42±0.21 e^{-} eq·L^{-1} (3.2±1.5 g·L^{-1}), respectively (Table S1). Electron recovery in the fermentation products was 96±15%. When GAC was added, n-caproate concentrations dropped to ~0.8 g·L^{-1} after two days of continuous operation (day 79) to slowly increase afterwards and stabilize after 7 days of continuous operation (day 84 onwards). Despite the drop in n-caproate from day 77 to 84, lactate and acetate were still consumed resulting in electron recoveries of 34% on day 79 and 60% on day 81. These observations suggest that a major fraction of fermentation products was adsorbed. Adsorption of substrates was most likely low since before being added to the reactor, GAC was

soaked in feed medium containing nutrients and substrates. Furthermore, "pre-treated" GAC did not adsorb lactate or acetate in adsorption tests (Figure S4). This indicates that the lower electron recovery observed from day 79 onwards in the reactor was related with adsorption of fermentation products rather than substrates. Once productivities stabilized in period II, lactate was consumed at higher rates although MCC production rates were comparable to period I (Table S1). Additionally, the electron recovery was 79±11% and n-caprylate was not detected in the effluent suggesting that adsorption of carboxylates still occurred. Isobutyrate formation was, in contrast to the batch screening of conductive materials (section 5.3.1), not observed with GAC addition to the continuous reactor.

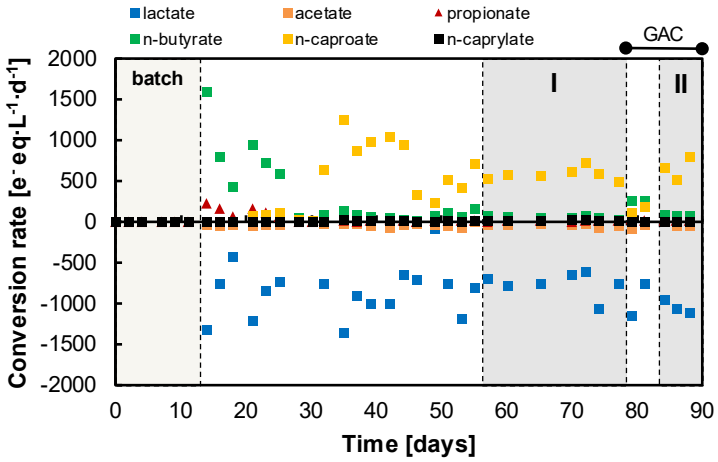

Figure 5.2 Conversion rates in continuous lactate-based chain elongation with GAC addition. Shaded areas show the start-up of the reactor (batch); stable operation before GAC addition (period I) and stable operation with GAC (period II). GAC was added on day 77.

5.3.3. MCC are preferentially adsorbed and recovered with GAC

Tests with real and artificial chain elongation effluents showed low adsorption of SCC while n-caproate was readily adsorbed within 2 days (Figure 5.3). Microbial activity was observed when using real effluent with net production of propionate and n-butyrate. n-caproate concentrations also increased in the last days of the adsorption phase. After 1.7 days, 0.86±0.02 mmol·g GAC^{-1} (~100 mg·g GAC^{-1}) of n-caproate was adsorbed, equivalent to 60±2% of the initial concentrations. These values were 0.9±0.07 mmol·g GAC^{-1} (~105 mg·g GAC^{-1}; 63±5% adsorbed) on day 3.8 before substantial amounts of n-butyrate and n-caproate were produced (Table 5.2). Microbial activity was not apparent in the artificial effluent where n-caproate adsorption on day 1.7 was 1.1±0.03 mmol·g GAC^{-1} (~128 mg·g GAC^{-1}; 73±2% adsorbed) reaching 1.22±0.01 mmol·g GAC^{-1} (~142 mg·g GAC^{-1}; 81±1% adsorbed) by the end of the adsorption phase (Table 5.2). From the high lactate concentrations in the artificial effluent, 16±3% was adsorbed (0.78±0.014 mmol·g GAC^{-1}; ~70 mg·g GAC^{-1}). Adsorption of SCC could not be quantified in the real effluent but 8±5% of acetate and 12±5% of n-butyrate was adsorbed from the artificial effluent by the end of the adsorption phase.

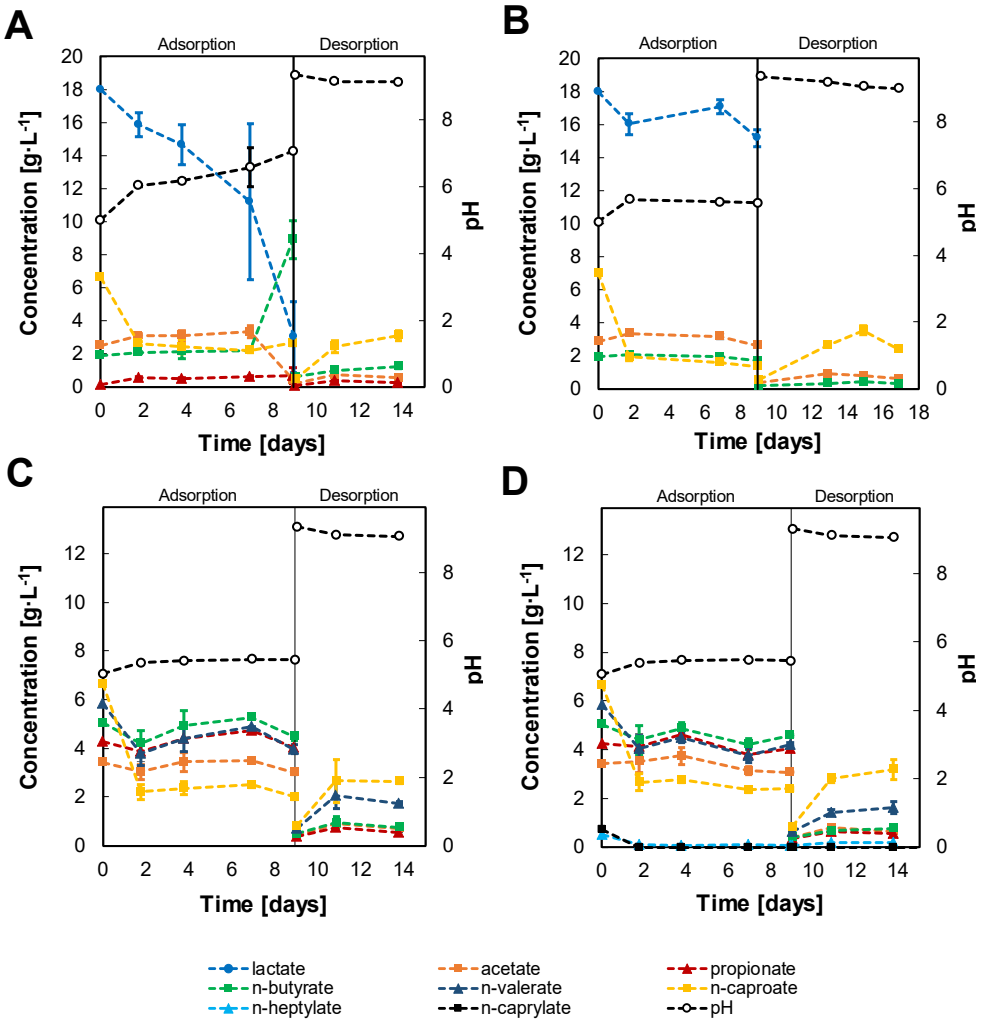

Figure 5.3 Adsorption and desorption of carboxylates over time from (**A**) real effluent; (**B**) artificial effluent; (**C**) C2-nC6 blend; and (**D**) C2-nC8 blend.

From the adsorbed n-caproate, 64±10% and 53±4% was desorbed from real and artificial effluents, respectively, resulting in similar n-caproate recoveries (40-42%) with respect to the n-caproate initially present in the experiments (Table 5.2). About 2.6-times more n-butyrate was desorbed from the real effluent experiment (0.18 mmol·g GAC^{-1}) compared to the artificial effluent (0.07 mmol·g GAC^{-1}) showing that n-butyrate was produced *in situ* and partly adsorbed onto GAC. Recovery of acetate and n-butyrate from the artificial effluent was ≤15% (Table 5.2).

Table 5.2 Adsorption and desorption performance from effluents and mock blends.

Parameter	Carboxylate	Effluent		Mock blend	
		Real[a]	Artificial[b]	C2-nC6	C2-nC8
q_{ads} [mmol·g GAC^{-1}]	lactate	-	0.78±0.14	-	-
	acetate (C2)	-	0.1±0.06	0.17±0.03	0.15±0.01
	propionate (C3)	-	-	0.08±0.04	0.07±0.04
	n-butyrate (nC4)	-	0.07±0.03	0.16±0.04	0.13±0.01
	n-valerate (nC5)	-	-	0.46±0.03	0.4±0.01
	n-caproate (nC6)	0.9±0.07	1.22±0.01	1±0.02	0.92±0.01
	n-heptylate (nC7)	-	-	-	0.09±0
	n-caprylate (nC8)	-	-	-	0.09±0
Adsorption [%]	lactate	-	16±3	-	-
	acetate (C2)	-	8±5	12±2	10±1
	propionate (C3)	-	-	6±2	5±2
	n-butyrate (nC4)	-	12±5	11±3	9±1
	n-valerate (nC5)	-	-	32±2	28±1
	n-caproate (nC6)	63±5	81±1	70±1	64±1
	n-heptylate (nC7)	-	-	-	91±1
	n-caprylate (nC8)	-	-	-	100±0
Desorption [%]	lactate	-	-	-	-
	acetate (C2)	-	99±1	75±16	68±13
	propionate (C3)	-	-	86±24	79±16
	n-butyrate (nC4)	-	92±6	51±12	76±12
	n-valerate (nC5)	-	-	55±5	60±11
	n-caproate (nC6)	64±10	53±4	39±2	55±7
	n-heptylate (nC7)	-	-	-	37±22
	n-caprylate (nC8)	-	-	-	0±0
Recovery [%]	lactate	-	-	-	-
	acetate (C2)	-	15±1	8±1	7±2
	propionate (C3)	-	-	4±1	5±1
	n-butyrate (nC4)	-	13±2	5±1	7±2
	n-valerate (nC5)	-	-	17±1	17±4
	n-caproate (nC6)	40±4	42±3	27±1	35±5
	n-heptylate (nC7)	-	-	-	34±20
	n-caprylate (nC8)	-	-	-	0±0

Values ±one standard deviation

[a] Adsorption on days 0-3.8; desorption and recovery on day 13.8.

[b] Adsorption on days 0-8.9; desorption and recovery on day 14.9. Lactate desorption was not measured.

Acetate, propionate and n-butyrate showed low adsorption and recovery from the mock blends, compared to carboxylates with ≥5 carbons (nC5-nC8) (Figure 5.3, Table 5.2). For carboxylates with ≥5 carbons, higher fractions were adsorbed as the carbon chain length increased (Figure 5.4) with >90% of n-heptylate and n-caprylate adsorbed. n-caproate adsorption was ~2.2-times higher than n-valerate, ~6-times higher than acetate and n-butyrate and more than 12-times higher than propionate (Figure 5.4, Table 5.2). Less than 13% of acetate, propionate and n-butyrate was adsorbed in both C2-nC6 and C2-nC8 mock blends. Notably, the presence of n-heptylate and n-caprylate in the C2-nC8 mock blend seemed to decrease the adsorption of other carboxylates, especially n-valerate and n-caproate (about 13 and 8% lower, respectively), compared to the C2-nC6 mock blend.

The desorbed fraction negatively correlated with carboxylates chain length (Figure 5.4). Only a fraction of the adsorbed n-valerate (55-60%), n-caproate (39-55%) and n-heptylate (37%) was desorbed while n-caprylate did not seem to desorb into the alkaline solution. Despite adsorption of n-valerate and n-caproate was slightly reduced in the C2-nC8 blend, similar amounts of n-valerate were desorbed from both mock blends, whereas n-caproate desorption in the C2-nC8 blend was higher (55±7%) than in the C2-nC6 blend (39±2%). n-caproate recovery was also higher in the C2-nC8 blend (35±5%) at similar levels to n-heptylate. n-caprylate was not recovered.

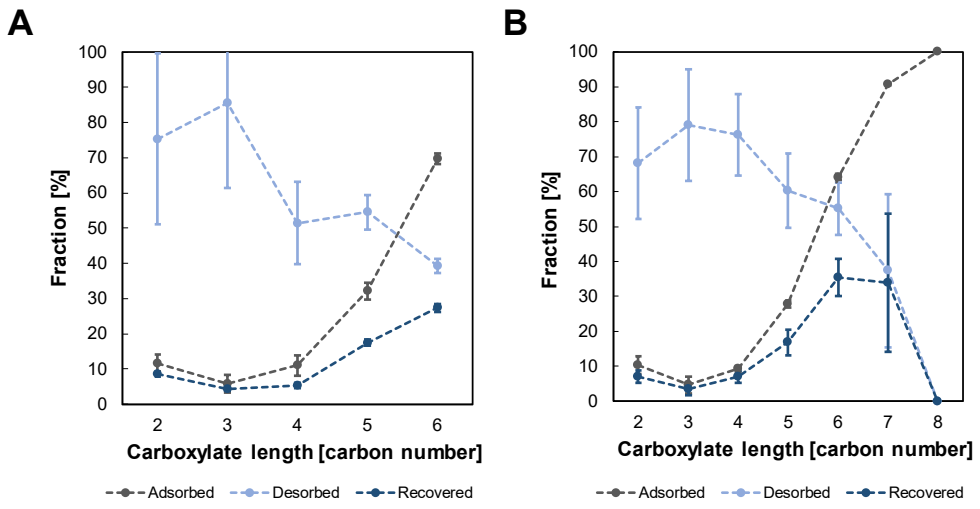

Figure 5.4 Adsorption, desorption and recovery of carboxylates with GAC in (**A**) C2-nC6 and (**B**) C2-nC8 mock blends. Carboxylates with 2-6 carbons were added at 57 mM; carboxylates with 7 and 8 carbons were added at 3.8 and 3.5 mM, respectively (Table 5.1). Initial pH was 5.0. Adsorption shows the fraction of initial carboxylates being adsorbed onto GAC; desorption shows the fraction of adsorbed carboxylates that was desorbed into the alkaline solution; and recovery shows the fraction of initial carboxylates recovered after desorption. Error bars depict ±one standard deviation.

5.3.4. Increased n-caproate adsorption capacity at decreasing pH

Adsorption isotherms with GAC and n-caproate in acetate buffer showed that n-caproate adsorption increased as pH decreased (Figure 5.5). The data from adsorption isotherms could be described by the Freundlich model (R^2 ≥0.997) with increasing K_F and decreasing n values as pH decreased (Table S2). The maximum adsorption capacity at pH 4.5 (2.1±0.01 mmol·g GAC^{-1}; 243±2 mg·g GAC^{-1}) was followed closely by pH 5.0 (2.06±0.01 mmol·g GAC^{-1}; 239±15 mg·g GAC^{-1}). At pH 5.5, n-caproate adsorption capacity decreased considerably to 1.58±0.08 mmol·g GAC^{-1} (184±7 mg·g GAC^{-1}) and similar values were observed with artificial effluent (containing mineral medium and lactate) at pH 5.0 (1.77±0.11 mmol·g GAC^{-1}; 205±13 mg·g GAC^{-1}). The lower buffer capacity of the artificial effluent compared to the pH 5.0 acetate buffer resulted in higher final pH values (Figure S5) which may explain the lower adsorption with the artificial effluent.

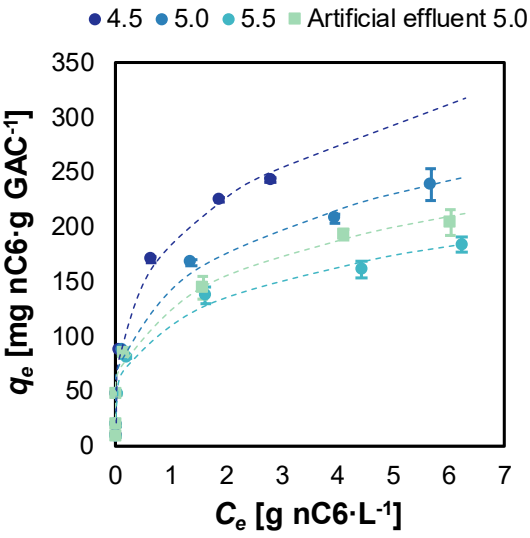

Figure 5.5 Effect of pH on n-caproate adsorption with GAC. Adsorption isotherms show the equilibrium n-caproate concentrations in the liquid (C_e) and n-caproate loads on GAC (q_e). Isotherms were carried out using acetate buffers to keep pH values close to 4.5, 5.0 and 5.5; and artificial effluent at initial pH 5.0.

5.4. Discussion

5.4.1. Chain elongation is favored with conductive materials

The presence of conductive materials has been shown to improve anaerobic microbial conversion processes. Carbon nanotubes, for instance, decreased the lag phase in pure cultures and improved methane production in both pure and co-cultures (Salvador et al., 2017). Stainless steel increased acetate and n-butyrate production in microbiomes converting H_2 and CO_2 (Blanchet et al., 2018). Nickel foam was recently shown to improve methane production by enriching organisms potentially involved in direct interspecies electron transfer (DIET) (Guo et al., 2020). In the present work, granular activated carbon (GAC), nickel foam (NF) and stainless steel (SS) decreased the lag phase and changed the product spectrum of batch lactate-based chain elongation. The lag phase was decreased to roughly >1 day with conductive materials compared to experiments without (>4 days). Propionate production was consistently lower when any of the conductive materials was present resulting in higher selectivities for chain elongation products (n-butyrate, isobutyrate, n-valerate or n-caproate). This effect was not observed when a non-conductive carrier material was present (polyurethane foam cubes [PU]), indicating that improved chain elongation was likely associated to a higher conductivity rather than to the provision of a carrier material that can support biofilm formation. The lowest production of propionate was observed for NF which may be partially explained by a higher fraction of propionate being elongated to n-valerate. Propionate production in open-culture chain elongation is a competing process that is typically controlled by adjusting the pH conditions. The growth of propionate-producing bacteria is known to be inhibited at low pH (Hettinga and Reinbold, 1972; Stinson and Naftulin, 1991) at which chain-elongating bacteria thrive (Candry et al., 2020a). However, propionate is also produced at mild acidic pH under high dilution and loading rates, which may constrain high-rate MCC production from lactate (Contreras-Dávila et al., 2021).

DIET-based chain elongation to iso/n-butyrate in the presence of conductive materials, however, may more favorable than propionate production.

Conductive materials such as GAC are known to promote DIET between ethanol-oxidizing bacteria and methanogens (Liu et al., 2012). In open-culture chain elongation, conductive materials may promote lactate oxidation to acetate, electrons and protons (eq. 1), which may be coupled to acetate and electrons uptake by specialized chain-elongating bacteria to produce iso/n-butyrate (eq. 2) or propionate and acetate to n-valerate (Jourdin et al., 2018; Raes et al., 2020). An analogous scheme has been proposed for ethanol-based chain elongation where biochar was suggested to promote electron transfer between ethanol-oxidizers and chain-elongators with improved production of MCC (Liu et al., 2017). The feasibility of coupling the oxidation and reduction reactions is, in principle, determined by the redox potential of the two reactions. Under standardized conditions (1 M, 1 atm, pH 7.0), the reduction potential of electrons released from lactate oxidation (eq. 1, $E^{\circ\prime}$ = -0.44 V) is low enough to drive the elongation of two acetate to iso/n-butyrate (eq. 2, $E^{\circ\prime}$ = -0.29 V). Figure 5.6A shows that, when lactate is not depleted, the coupled reaction (eq. 3) could occur in the incubations with conductive materials, considering the measured bulk substrates and products concentrations. The reduction potentials of the two reactions between -0.5 and -0.1 V suggest that they could be coupled through a combination of redox mediators covering this potential window such as ferredoxins (-0.5 to -0.4 V), c-type cytochromes (-0.42 to -0.21 V) and other redox mediators (Kracke et al., 2015). The thermodynamic feasibility of this syntrophic DIET-based chain elongation process seems, however, only initially and somewhat more favorable than propionate production (eq. 4) (Figure 5.6B). Although factors like local pH, substrate adsorption on the materials surface and variations in energy conservation mechanisms influence the energetics of DIET (Nagarajan et al., 2013; Cheng and Call, 2016; Salvador et al., 2017), these calculations suggest that other factors rather than thermodynamics may be involved in the decreased propionate production.

$$\text{lactate}^- + H_2O \rightarrow \text{acetate}^- + 4\ e^- + 4\ H^+ + CO_2 \quad (1)$$

$$2\ \text{acetate}^- + 4\ e^- + 5\ H^+ \rightarrow \text{iso/n-butyrate}^- + 2\ H_2O \quad (2)$$

$$\text{lactate}^- + \text{acetate}^- + H^+ \rightarrow \text{iso/n-butyrate}^- + CO_2 + H_2O \quad (3)$$

$$3\ \text{lactate}^- \rightarrow \text{acetate}^- + 2\ \text{propionate}^- + H_2O + CO_2 \quad (4)$$

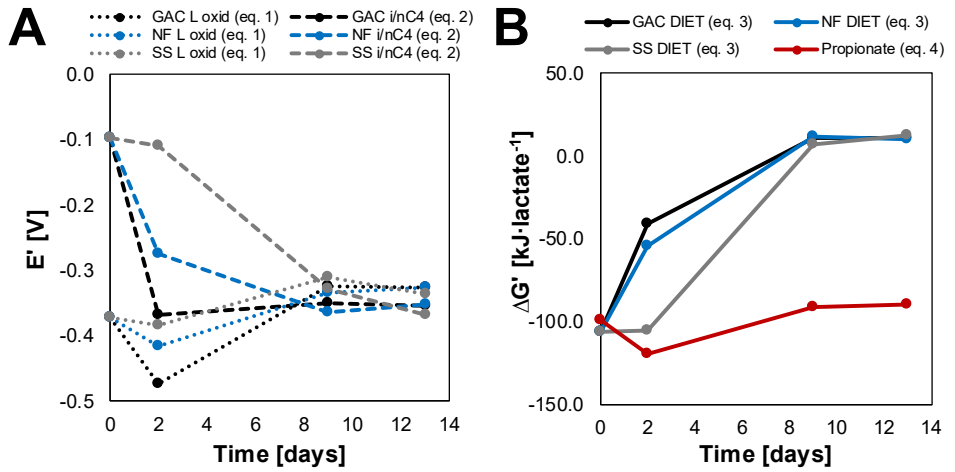

Figure 5.6 Thermodynamic calculations of DIET-based chain elongation and propionate production. (**A**) Estimated reduction potential of lactate oxidation (L ox, eq. 1) and acetate elongation to iso/n-butyrate (i/nC4, eq. 2) reactions during the incubations with granular activated carbon (GAC), nickel foam (NF) and stainless steel mesh (SS). Bulk concentrations, averaged from triplicates, were used for each conductive material. (**B**) Gibbs free energy change of the coupled DIET half reactions (eq. 3) and of propionate formation (eq. 4). Products and lactate concentrations close to zero at the beginning and end (days 9-13) of the incubations, respectively, were approximated to 10^{-10} M for all reactions, and the sum of both isobutyrate and n-butyrate concentrations was used for reactions producing i/nC4 (assuming same Gibbs energy of formation for isobutyrate as n-butyrate) (**A**, **B**).

One possible explanation is that specialized electroactive syntrophic bacteria carry out DIET-based chain elongation at higher rates compared to conventional single-species fermentation (e.g. propionate formation), directing a larger fraction of lactate towards chain elongation in the incubations with conductive materials. Division of labor between two organisms performing the oxidation and reduction reactions separately would require shorter metabolic pathways for each partner which may result in increased overall conversion rates, similarly to nitrifying bioprocesses and some synthetic consortia (Tsoi et al., 2018). Additionally, highly conductive materials allow faster electron transfer rates through DIET, accelerating syntrophic processes (Viggi et al., 2014). Thus, selecting for DIET-based chain elongation could be an alternative to control competing fermentative pathways such as propionate production and potentially achieve higher conversion rates compared to single-species chain elongation.

5.4.2. Potential isobutyrate formation mechanisms with addition of NF and GAC

Notably, isobutyrate production was also promoted with addition of GAC and NF, reaching concentrations of 1.2±0.57 g·L^{-1} with NF. Thus far, isobutyrate production from lactate has only been reported for pure cultures of *Clostridium* species recently isolated from a reactor producing n-caproate (but not isobutyrate) from corn silage (Liu et al., 2020). These new *Clostridium* species produced acetate, n-butyrate, isobutyrate, n-valerate and n-caproate, but not propionate in batch fermentation of lactate at similar pH conditions (pH 5.5) to the present study (pH 5.0). It is possible that bacteria with a similar metabolism were enriched in our experiments with conductive materials, explaining the increased isobutyrate, n-valerate and n-caproate formation. Isobutyrate could also be formed from H_2 and CO_2 by e.g. *Clostridium luticellarii* (Petrognani et al., 2020) probably through acetate formation and subsequent elongation. A similar mechanism involving H_2 or electrons may

occur in a bioelectrochemical system producing isobutyrate where conductive carbon (graphite) was used as cathode (Vassilev et al., 2018). In the present study, the P_{H2} by the end of the incubations was much lower with addition of GAC and NF (4-5·10^{-4} atm) than in the other conditions (0.12-0.2 atm). Acetate formation was also the highest with these two materials, which could be produced from homoacetogenesis and then promote isobutyrate formation with H_2 or electrons. Reactor microbiomes producing isobutyrate at high selectivities (~65%) have been developed with methanol as electron donor (Chen et al., 2016a; de Leeuw et al., 2020) where *Clostridium luticellarii* was presumed responsible for isobutyrate production (de Leeuw et al., 2020). This was confirmed for a wild-type strain of *Clostridium luticellarii* shown to produce isobutyrate from methanol and H_2/CO_2 but not from lactate (Petrognani et al., 2020). Possibly, syntrophic DIET processes may have enriched electroactive isobutyrate producers using electrons produced from lactate oxidation (section 5.4.1). However, further research is needed to clarify the mechanisms of isobutyrate production from lactate in the presence of conductive materials.

5.4.3. n-Caproate adsorption with GAC at high selectivities and loadings

Isobutyrate formation was not promoted when GAC was added to continuous chain elongation where n-caproate continued to be produced at high selectivities (~80%). Lactate consumption continued at apparent higher conversion rates (~40% higher) probably due to *in situ* adsorption of potentially toxic n-caproate (Roghair et al., 2018b) and/or biomass retention on GAC. Assuming that the missing electrons during extensive adsorption (days 77-82) correspond to adsorbed n-caproate, about 116 mg nC6·g GAC^{-1} (5.9 g nC6·L^{-1}) were adsorbed from days 77-79 and 160 mg nC6·g GAC^{-1} (8.1 g nC6·L^{-1}) from days 77-82 at an average rate of 58 and 40 mg·g GAC^{-1}·d^{-1}, respectively. Moreover, n-caproate adsorption seemed to continue during period II where ~79% electron recovery was observed (compared to ~96% in period I). Assuming again that the missing electrons ended up in n-caproate, productivities in period II would be ~0.9 e^- eq nC6·L^{-1}·d^{-1} (3.3 g nC6·L^{-1}·d^{-1}), ~54% higher than without *in situ* adsorption (period I). The estimated n-caproate selectivity would also be increased to 85%. Then, a maximum of 274 mg·g GAC^{-1} (13.9 g·L^{-1}) of n-caproate was adsorbed from the time when GAC was added to the reactor. This estimated amount is comparable to the adsorption capacity of GAC determined at pH 5.0 (239 mg·g GAC^{-1}) supporting the idea that n-caproate adsorption continued in period II. The GAC loaded with n-caproate could then be regenerated for n-caproate recovery or collected for other applications (section 5.4.4). Additionally, n-caproate can also be recovered after fermentation. Within two days of adsorption, similar amounts of n-caproate were adsorbed from real (100 mg·g GAC^{-1}; 57 mg·g GAC^{-1}·d^{-1}) and artificial (130 mg·g GAC^{-1}; 74 mg·g GAC^{-1}·d^{-1}) effluents. Differences in performance may be related to initial n-caproate concentrations in the artificial (7 g nC6·L^{-1}) and real (6.7 g nC6·L^{-1}) effluents or potential bacterial cell adsorption on GAC, which may reduce the area available for carboxylates adsorption.

GAC showed increasing affinity for longer carboxylates with ≥5 carbon atoms. Particularly, n-caproate adsorption was two-times higher than for n-valerate. Shorter carboxylates such as acetate, propionate and n-butyrate were poorly adsorbed (<13%). The MCC n-heptylate and n-caprylate were effectively adsorbed (>90%), although they were present at ~10-times lower concentrations. Better adsorption for longer carboxylates is expected due to increased hydrophobic interactions with GAC (Traube's rule) as reported in literature (Giusti et al., 1974). More acidic conditions increase the

fraction of the hydrophobic undissociated n-caproic acid, which may explain the improved adsorption as pH was decreased. The pH values (4.5-5.5) tested here are at comparable levels used in chain elongation processes from food waste (Contreras-Dávila et al., 2020), lactate (Kucek et al., 2016a; Candry et al., 2020a; Contreras-Dávila et al., 2021) and ethanol with in-line extraction (Ge et al., 2015).

The adsorption capacities observed in the present study are within the high range of previously reported values for GAC (Table 5.3). Earlier works reported n-caproate adsorption on GAC at 194 $mg \cdot g^{-1}$ (Giusti et al., 1974). In adsorption tests (10 g $nC6 \cdot L^{-1}$; pH 6.7) and batch pure culture ethanol-based chain elongation (final pH ~7) with 30 g $GAC \cdot L^{-1}$, GAC adsorbed ~140 mg $nC6 \cdot g\ GAC^{-1}$ (Ghysels et al., 2021), similar to our results with real and artificial effluents (105-142 $mg \cdot g\ GAC^{-1}$). More n-caproate was adsorbed in single-acid than in multi-acid systems (Table 5.3). In general, GAC shows higher adsorption capacities for n-caproate compared to biochar and anion exchange resins. Compared to GAC, anion exchange resins show higher affinity for lactate than for acetate or n-butyrate (Yousuf et al., 2016). Anion exchange resins also show lower n-caproate loads (6.2 wt%) from artificial chain elongation effluent (Yu et al., 2019) compared to the results obtained here (15.4 wt%). However, they are easily regenerated and can be reused several times (Yu et al., 2019) whereas only a fraction of the adsorbed carboxylates could be desorbed from GAC in the present study (<60% for nC5-nC8). This may decrease GAC adsorption capacity and reusability over time. However, desorption can be improved with thermal (Xue et al., 2016) or solvent (Zhang et al., 2014) regeneration.

Table 5.3 Adsorption capacity and total acids load for different systems.

Material	System	pH	Adsorption capacity [mg·g^{-1}]								Acids load	Reference
			lactate	acetate	propionate	nC4	nC5	nC6	nC7	nC8	wt%	
GAC	continuous reactor[b]	5	-	-	-	-	-	274	-	-	27.4	This study
	real effluent	5	-	-	-	-	-	105	-	-	10.5	
	artificial effluent	5	70.3	6	-	6.2	-	142	-	-	22.4	
	multi-acid	5	-	10	5.9	14.1	47	116	-	-	19.3	
	multi-acid	5	-	9	5.2	11.5	40.9	107	11.7	13.0	19.8	
	single-acid	4.5	-	-	-	-	-	243	-	-	24.3	
	single-acid	5	-	-	-	-	-	239	-	-	23.9	
	single-acid	5.5	-	-	-	-	-	184	-	-	18.4	
	single-acid	-	-	48	65	119	159	194	-	-	19.4[c]	(Giusti et al., 1974)
	batch fermentation[b]	6.95	-	-	-	-	-	142	-	-	14.2	(Ghysels et al., 2021)
	DSM 52 medium	6.7	-	-	-	-	-	141	-	-	14.1	
	single-acid	2	121	-	-	-	-	-	-	-	12.1	(Pradhan et al., 2017)
	single-acid	2	48.3	31.6	-	44.8	-	-	-	-	12.5	(Yousuf et al., 2016)
	multi-acid	2	18.6	13.8	-	42.7	-	-	-	-	7.5	
Biochar	DSM 52 medium	6.7	-	-	-	-	-	18.7	-	-	1.9	(Ghysels et al., 2021)
AER[a]	artificial effluent	7	-	<5	-	<5	-	62	-	-	6.2[c]	(Yu et al., 2019)
	single-acid	2	60	-	-	-	-	-	-	-	6.0	(Pradhan et al., 2017)
	single-acid	5	48	-	-	-	-	-	-	-	4.8	
	single-acid	2	60.1	20.8	-	52.5	-	-	-	-	13.3	(Yousuf et al., 2016)
	multi-acid	2	84	20.5	-	50.7	-	-	-	-	15.5	

[a] Anion exchange resin.

[b] Estimated from electron balances.

[c] For n-caproate only.

5.4.4. Adsorptive chain elongation and potential uses of MCC-loaded GAC

Based on the adsorption properties observed for GAC, in-line MCC separation with "adsorptive" chain elongation processes can be designed. The fermentation broth of chain elongation reactors can be recirculated to external packed columns filled with GAC to adsorb MCC while maintaining low concentrations in the effluent. Suspended biomass may be filtered out to avoid adsorption and operational problems related to GAC fouling. Assuming a maximum adsorption capacity of 243 mg nC6·g GAC^{-1}, an apparent GAC density of 290 kg·m^{-3} (Norit PK1-3, Cabot Norit Nederland B.V.) and an n-caproate productivity of 4 g·L^{-1}·d^{-1} as reported for an efficient lactate-fed chain elongation reactor (Contreras-Dávila et al., 2021), a reactor-to-adsorbent volumetric ratio of ~18:1 is estimated to adsorb the n-caproate produced during one day of operation. The volume of the adsorbent could be divided in at least two packed columns alternating adsorption and desorption to achieve in-line product separation. Thermal desorption may be ideal to obtain MCC-oils after spontaneous phase separation of the desorbed undissociated medium-chain carboxylic acids (Figure 5.7). A similar bioprocess with *in situ* adsorption has been proven effective in butanol fermentation where thermal regeneration of GAC produced concentrated butanol after phase separation (Xue et al., 2016). In the aforementioned study, the authors estimated an energy input for butanol desorption of 14.1 kJ·g $butanol^{-1}$ of which ~90% was required to evaporate the adsorbed water. Assuming similar values for water adsorption (~1.2 g·g GAC^{-1}) and heat capacity of GAC (0.84 J·g^{-1}·K^{-1}), the minimum energy input estimated to recover n-caproate is 13.8 kJ·g $nC6^{-1}$ (at boiling point of nC6 [205°C]), equal to 3.8 kWh·kg $nC6^{-1}$ (Table S3). However, further research is needed to evaluate MCC recovery efficiency, actual energy requirements and overall feasibility of in-line adsorption in chain elongation processes. MCC recovery can be optimized by modifying GAC size and surface properties to increase MCC loadings, facilitate desorption and reduce water adsorption.

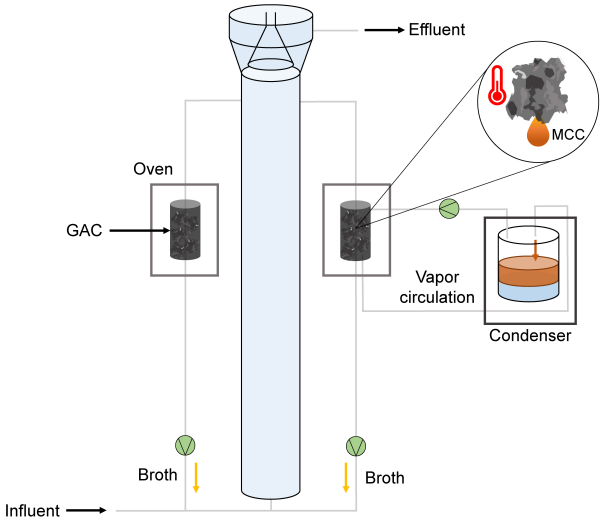

Figure 5.7 Proposed continuous chain elongation process with in-line adsorption and thermal regeneration to obtain undissociated medium-chain carboxylic acids. The fermentation broth is recirculated to external packed columns filled with adsorbent, alternating adsorption and desorption cycles between columns. After thermal desorption, spontaneous phase separation of undissociated medium-chain carboxylic acids yields MCC-oils.

GAC was experimentally determined to hold n-caproate mass contents up to 24.3 wt% which are much higher values than reported for ion exchange resins (6.2 wt%) (Table 5.3). Such high loadings make GAC an attractive transport matrix when MCC production and upcycling processes are done at two different geographic locations. Furthermore, direct use of MCC-loaded GAC may be preferred over conventional desorption and GAC regeneration steps in some cases or when GAC regeneration is not efficient anymore. For instance, activated carbon or biochar loaded with MCC may be used as feed additive for prolonged delivery of MCC in the animal gut. Both biochar and MCC have beneficial effects on animal welfare and methane emissions mitigation (Machmüller, 2006; Schmidt et al., 2019; Jackman et al., 2020). MCC-loaded porous carbon could also be used as slow-release soil conditioners. MCC may desorb or be taken up by microorganisms. Bacteria have been shown to degrade adsorbed organic molecules and regenerate GAC (Piai et al., 2021) and a similar mechanism may occur in soils. Biochar amendments provide beneficial effects on soil properties and crop production (Woolf et al., 2010) while MCC promote plant growth (Scalschi et al., 2013). The addition of biochar with adsorbed plant growth promoters (nitrate) improved plant biomass yield compared to biochar alone (Kammann et al., 2015). In polluted soils, slowly released MCC may sustain biodegradation of micropollutants by inhibiting methanogenesis and providing electron equivalents for reductive biodegradation (Robles, 2019).

5.5. Conclusions

Conductive materials such as GAC, NF and SS are compatible with microbiomes and promote chain elongation. In batch chain elongation, lactate conversion to propionate was reduced (30-40% lower) probably by facilitated syntrophic DIET processes, which may display higher conversion rates than single-species fermentation. Batch open-culture chain elongation was steered to isobutyrate formation with addition of GAC and NF, reaching 1.2 $g \cdot L^{-1}$ and 9% electron selectivity with NF. These materials could be used to enrich and further study isobutyrate production with reactor microbiomes.

MCC recovery with GAC shows promising features such as high n-caproate affinities (>2-times and ≥6-times higher than nC5 and C2-nC4, respectively) and loadings (184-243 mg nC6·g GAC^{-1}) at pH conditions used in chain elongation bioprocesses (pH 4.5-5.5). Furthermore, thermal regeneration may yield MCC-oils after phase separation of undissociated medium-chain carboxylic acids. The hereby presented isobutyrate formation with conductive materials, the adsorptive chain elongation design as well as the potential direct applications of MCC-loaded porous carbons may develop into innovative chain elongation processes.

Chapter 6

Reactor microbiome enriches vegetable oil with n-caproate and n-caprylate via extractive chain elongation

This chapter was submitted as:
Carlos A. Contreras-Dávila, Norwin Zuidema, Cees J.N. Buisman and David P.B.T.B. Strik (under review). Reactor microbiome enriches vegetable oil with n-caproate and n-caprylate for functionalized feed additive production via extractive lactate-based chain elongation.

Abstract

Biotechnological processes for efficient resource recovery from residual materials rely on complex conversions carried out by reactor microbiomes. Chain elongation reactor microbiomes allow the production of valuable medium-chain carboxylates (MCC) that can be used as biobased starting materials in the chemical, agriculture and food industry. In this study, sunflower oil is used as an application-compatible solvent to accumulate microbially produced MCC during extractive lactate-based chain elongation. The MCC-enriched solvent is harvested as a potential novel product for direct application without further MCC separation or purification e.g. direct use for animal nutrition applications. Sunflower oil biocompatibility, *in situ* extraction performance and effects on chain elongation were evaluated in batch and continuous reactor microbiome experiments. Reactor microbiome composition of continuous experiments was analyzed based on 16S rRNA gene sequencing data. Sunflower oil showed high MCC extraction specificity and similar biocompatibility to oleyl alcohol in batch extractive fermentation of lactate and food waste. The MCC n-caproate (nC6) together with considerable amounts of n-caprylate (nC8) were produced from L-lactate and acetate in continuous lactate-based chain elongation reactors at pH 5.0. Extractive chain elongation with sunflower oil relieved apparent toxicity of MCC with production rates and selectivities reaching values of 5.16±0.41 g nC6·L^{-1}·d^{-1} (MCC: 11.5 g COD·L^{-1}·d^{-1}) and 84% (e^- eq MCC *per* e^- eq products), respectively. MCC were selectively enriched in sunflower oil to concentrations up to 72 g nC6·L^{-1} and 3 g nC8·L^{-1}, equivalent to 8.3 wt% in MCC-enriched sunflower oil. Extractive fermentation at pH 7.0 produced propionate and n-butyrate instead of MCC. Sunflower oil showed stable linoleic and oleic acids composition during extractive chain elongation regardless pH conditions. Reactor microbiomes showed reduced diversity at pH 5.0 with MCC production linked to *Caproiciproducens* co-occurring with *Clostridium tyrobutyricum*, *Clostridium luticellarii* and *Lactobacillus* species. Abundant taxa at pH 7.0 were *Anaerotignum*, *Lachnospiraceae* and *Sporoanaerobacter*. Sunflower oil is a suitable biobased solvent to selectively concentrate MCC. Extractive reactor microbiomes produced MCC with improved selectivity and production rate while downstream processing complexity was reduced. Potential applications of MCC-enriched solvents are discussed including feed & food purposes, along with future research directions.

6.1. Introduction

Many biotechnological processes for resource recovery from residual materials are being developed based on reactor microbiomes. Reactor microbiomes are capable of carrying out complex conversions as compared to pure cultures to produce valuable products such as methane, carboxylic acids or polyhydroxyalkanoates from non-sterile residual substrates (Oleskowicz-Popiel, 2018). Selection pressures (e.g. temperature, pH, solids or liquid retention times) applied to adapted environments (reactors) are central for steering bioprocesses (Angenent et al., 2016) and engineering reactor microbiomes (Lawson et al., 2019). Understanding the factors governing reactor microbiomes assembly and functioning will help harness the full potential of microbiomes (Oleskowicz-Popiel, 2018; Lawson et al., 2019). Novel resource recovery bioprocesses using chain elongation reactor microbiomes produce medium-chain carboxylates (MCC), saturated monocarboxylic acids with 6 to 12 carbon atoms that find applications in lubricants, biodegradable plastics, antimicrobials, feed additives and biofuels production (Angenent et al., 2016). Chain-elongating bacteria utilize energy-rich substrates e.g. ethanol, lactate, sugars as electron donors to elongate short-chain carboxylates (SCC, 1-5 carbon units) to MCC such as n-caproate (nC6) or n-caprylate (nC8) through a series of biochemical condensation and reduction reactions in the reverse β-oxidation pathway (Angenent et al., 2016). These electron donors can be obtained from low-cost organic waste materials to achieve MCC production directly from the waste materials (Carvajal-Arroyo et al., 2019; Contreras-Dávila et al., 2020) or with externally added electron donors (Roghair et al., 2018c; Chwialkowska et al., 2019).

The produced MCC should be separated from the fermentation broth for their valorization. A six-steps down stream processing (DSP) was proposed by ChainCraft B.V. to convert food waste and ethanol to MCC salts for animal nutrition applications (EFSA (European Food Safety Authority), 2018). Several alternative methods for carboxylates (referred here as the sum of their undissociated and dissociated forms) separation are emerging including extractive fermentation (López-Garzón and Straathof, 2014). Extractive fermentation is the process where the broth (aqueous phase) is contacted with a solvent (organic phase) during fermentation, resulting in simultaneous production and *in situ* recovery of fermentation products. Adequate extractive fermentation may decrease product inhibition, chemicals input for pH control and increase bioprocess effectivity (López-Garzón and Straathof, 2014). Solvent biocompatibility is one first prerequisite to attain successful extractive fermentation, with biocompatibility meaning that the solvent must not hamper the pertinent bioprocess (Raes et al., 2018). Other important criteria are: high selectivity towards the product, low solubility in broth, high carboxylates recovery at low concentrations, low-cost and suitable physical properties for phase separation (Weilnhammer and Blass, 1994; López-Garzón and Straathof, 2014). Oleyl alcohol is a commonly used solvent shown to be biocompatible with different bioprocesses (Weilnhammer and Blass, 1994; Tong et al., 1998) including chain-elongating bacteria (Choi et al., 2013; Jeon et al., 2013). Alternatively, vegetable oils containing triglycerides of long-chain carboxylates (LCC) may be used as biobased, biocompatible solvents (Offeman et al., 2006). In a previous study, MCC seemed to be partly extracted by the oil contained in food waste during chain elongation (Contreras-Dávila et al., 2020). However, the MCC extraction performance and

biocompatibility with chain-elongating microbiomes of vegetable oils have not been reported. In this work, the terms extractive fermentation and extractive chain elongation are used interchangeably.

Vegetable oils are envisioned here as promising matrixes to accumulate MCC during extractive chain elongation for the direct application of MCC-enriched oils after being harvested or skimmed off the reactor. Extractive fermentation with application-compatible solvents can lead to novel products from microbial chain elongation while impacting the process positively by, for instance, increasing fermentation efficiency, reducing process complexity as well as production costs. Typically, further steps are needed for solvent regeneration and MCC purification after MCC are concentrated in the solvent. Solvent regeneration is usually done through back-extraction with strong inorganic bases which requires additional chemicals and generates waste inorganic salts (López-Garzón and Straathof, 2014). Purification may be done by energy-demanding processes such as distillation (Saboe et al., 2018) or electrodialysis (Xu et al., 2015). Application-compatible solvents to avoid product-solvent separation has been deemed attractive also for advanced biofuels fermentation processes (Brennan et al., 2012) with benefits including reduced production costs and environmental footprint (Pedraza-de la Cuesta et al., 2019). One potential application is the use of MCC-enriched vegetable oils as novel food or feed additives with diverse functionalities. MCC display differential effects on human health compared to unsaturated LCC (Marten et al., 2006). Vegetable oils and the LCC contained in them are shown to have positive effects in livestock growth (Hess et al., 2008; Li et al., 2019) while MCC can be used in low doses to inactivate pathogens in feed and improve swine health and performance (Jackman et al., 2020). Both LCC and MCC can be used as natural alternatives to antibiotics (Li et al., 2019; Jackman et al., 2020) and for methane mitigation in cattle (Dohme et al., 2001; Machmüller, 2006; Poteko et al., 2020).

Thus, this work aims to assess the feasibility of producing MCC-enriched vegetable oil *via* lactate-based chain elongation microbiomes. Extraction capability and biocompatibility of sunflower oil, a widely available vegetable oil, is compared against oleyl alcohol in batch extractive fermentation using lactate and food waste as substrates. Then, continuous bioreactor experiments were performed to evaluate extractive chain elongation of L-lactate and acetate and MCC accumulation in sunflower oil. Changes in microbiome composition and taxa differential abundance were studied using 16S rRNA gene sequencing data. Lastly, MCC extraction with sunflower oil was compared using synthetic effluent in abiotic continuous reactors.

6.2. Materials and methods

6.2.1. Extractive batch fermentation with sunflower oil and oleyl alcohol

Carboxylates extraction with sunflower oil was compared against oleyl alcohol in extractive batch experiments. Experiments were carried out in 125 mL serum bottles containing either lactate (3 $g \cdot L^{-1}$; ≥90% L-lactic acid, VWR) or food waste (Contreras-Dávila et al., 2020) (10% v/v; 3.46 e^{-} $eq \cdot L^{-1}$) as fermentation substrates. Mineral medium, yeast extract and vitamins were added as described elsewhere (Roghair et al., 2016). Trace elements were prepared after Zhu *et al.*, (2015). BisTris buffer (~pH 9.8) was added at 100 mM concentration to reduce pH changes due to biological substrate conversion. The same mineral medium and nutrients were used for both substrates. Initial pH was

then adjusted using either 1 M KOH or HCl. An initial pH value of 5.0 was used for lactate experiments to select for n-caproate producers (Kucek et al., 2016a) while pH was set to 6.0 in bottles fed with food waste to allow acidification to lactate and subsequent chain elongation (Contreras-Dávila et al., 2020). The batch bottles were sealed with a rubber septum and aluminium crimp cap. The headspace was exchanged by filling and vacuum cycles (five times) with 100% N_2. Inoculum was derived from a completely stirred tank reactor (CSTR) fermenting food waste to MCC (Contreras-Dávila et al., 2020), centrifuged, resuspended in oxygen-free demi water and injected (2 mL) into the bottles. Fermentation medium volume was 40 mL. Finally, sunflower oil (AH Biologisch Zonnebloemolie, Albert Heijn, the Netherlands) and oleyl alcohol (technical grade, 85% purity, Sigma Aldrich) were injected into the respective bottles to form an organic phase layer on top of the fermentation medium with a solvent-to-medium volume ratio of 20%. Sunflower oil had a room temperature density of 0.902 $kg{\cdot}L^{-1}$ with main components measured to be (g *per* 100 g carboxylic acids): linoleic acid (C18:2 cis9, 12), 53; oleic acid (C18:1 cis9), 35; octadecanoic acid (C18:0), 3; and palmitic acid (C16:0), 6. Both solvents were tested separately in duplicate experiments. For each substrate, singletons without solvent were done to serve as blank experiments. The bottles were incubated in an orbital shaker at 30°C and 100 rpm. Gas and liquid samples were taken regularly. Carboxylates were quantified in both aqueous and solvent (after back-extraction) samples. Extraction performance was evaluated with reference to the carboxylates distribution ratio (K_D), partition coefficient (P), recovery and specificity in each solvent by the end of the incubations. Details on these calculations can be found in Supplementary Information.

6.2.2. Continuous lactate-based chain elongation and extraction with sunflower oil

Continuous experiments were carried out using L-lactate (50% sodium-(S)-lactate, Merck) and acetate (acetic acid >99%, Sigma Aldrich) as substrates for microbial chain elongation. Experiments were done in two independent 2-liters CSTR (R1 and R2) each with a diameter of 10.5 cm and working volume of 1.2 liters (Applikon, Schiedam, the Netherlands). Polyurethane foam was used as carrier material (two sheets of 9 cm x 9 cm x 1 cm) positioned at baffles level (FigureS1). The reactors were adapted for feed and acid dosing below the overlaid organic phase and for solvent and fermentation broth sampling (Figure S1). The medium composition (minerals, trace elements, yeast extract and vitamins) was the same as described in section 6.2.1. L-lactate was added as electron donor at 40 $g{\cdot}L^{-1}$, acetate at 5 $g{\cdot}L^{-1}$ as electron acceptor and pH was adjusted to 5.0 with 4 M KOH. Fermentation broth was bubbled with N_2 to ensure anaerobic conditions. The inoculum (30 mL) derived from a chain elongation reactor (Contreras-Dávila et al., 2020) was the same as for extractive batch experiments. Operational conditions for each period are shown in Table S1. Temperature (30°C), HRT (2 days) and stirring speed (80 rpm) were kept constant throughout the experiments. pH was controlled by automatic addition of 1 M HCl. Non-extractive chain elongation was evaluated at pH 5.0 (without solvent addition). Then, sunflower oil was added to evaluate extractive chain elongation keeping the same pH and HRT conditions. Sunflower oil was added through the solvent sampling port on day 99 in R1 and day 100 in R2 to an oil-to-medium volume ratio of 20% v/v. Sunflower oil was laid as a static layer over the fermentation broth whilst the fermentation medium was continuously stirred and replenished. After ~15 days, the oil was collected out of the reactors. After adjusting pH in the fermentation broth to 7.0, sunflower oil was added for the second occasion on

day 116 to R1 and day 117 to R2. Gas, aqueous and oil phases were sampled every other day. Long-chain carboxylates in sunflower oil (saturated and unsaturated LCC) were monitored during extractive fermentation. Calculations on chain elongation performance can be found in the Supplementary Material.

6.2.3. Abiotic sunflower oil saturation in continuous experiments

The same CSTR set-up was used to test extraction of carboxylates into sunflower oil in continuous abiotic experiments. For this, R1 and R2, hereafter referred to as R3 and R4, respectively, were used after the biological continuous experiments (section 6.2.2). Synthetic effluent was prepared resembling carboxylates concentrations from non-extractive CSTR fermentation effluents. The synthetic effluent was fed to keep an HRT of 2 days, temperature and pH in the reactors were respectively controlled at 30°C and 5.0 (with 1 M HCl). The synthetic effluent contained ($g \cdot L^{-1}$): lactate, 11; acetate, 2.6; n-butyrate, 1.3 and n-caproate, 6.1. Carboxylates (except L-lactate which was added as sodium lactate, section 6.2.2) were added in their acid form. Mineral medium and trace elements were added as in the fermentation experiments. The nitrogen source was removed from the medium to avoid microbial growth. Therefore phosphate in $NH_4H_2PO_4$ was replaced with K_2HPO_4 and yeast extract was left out. Synthetic effluent pH was adjusted to 5.0 with 4 M KOH. Carboxylates concentration in aqueous and oil samples was measured regularly.

6.2.4. Analytical methods

Aqueous and solvent samples were centrifuged at 10000 rpm for 10 min and stored at -4°C before analyses. Solvent samples were mixed with an alkaline solution (0.5 M sodium borate, pH ~9.4) to back-extract any carboxylates contained in the solvent. 500 µL of oil sample were placed into a 10 mL serum bottle containing 2 mL of sodium borate solution (1:4 solvent-to-alkali). The mixture was shaken vigorously for 1 min and left 30 min to phase separate. The aqueous phase was then collected for carboxylates quantification. Gas chromatography (GC) was used for headspace gas composition as well as for carboxylates (C2-C8) and alcohols (C1-C6) quantification. Lactate, succinate and formate were measured by means of HPLC (Contreras-Dávila et al., 2020). Methods description can be found in Supplementary Material.

Total carboxylic acids composition of sunflower oil, including SCC (nC4 and nC5), MCC (nC6-nC12, C10:1 and C12:1) and LCC (saturated, unsaturated and isomeric C13-C24), was analyzed according to the ISO 15885 standard. The analyses were done externally at the Dutch Milk Controlling Laboratory (Qlip B.V., Zutphen, the Netherlands) using gas chromatography (Trace GC Ultra, Thermo Fischer) with FID detection. Results are expressed as grams *per* 100 g of total carboxylic acids. Raw chemical experimental data are available in the 4TU.ResearchData repository (htpps://doi.org/10.4121/c.5265740).

6.2.5. Microbiome composition

Samples were centrifuged at 15,000 rpm for 10 min and stored at -20°C for DNA extraction and sequencing. DNA was extracted from the pellets (PowerSoil DNA isolation kit) for amplification of the V3-V4 region of 16S rRNA via Illumina sequencing. The primer set used allowed simultaneous

amplification of bacterial and archaean 16S rRNA as described elsewhere (Klindworth et al., 2013). DNA sequences were processed as described previously (Contreras-Dávila et al., 2020). In short, the DADA2 pipeline was used and the identified ASVs were submitted to the SILVA database (SILVA 138 SSU Ref NR 99) for taxonomic identification. Forward and reverse reads were trimmed at cycles 240 and 220, respectively, based on the quality profiles obtained. Sequences were deposited in the ENA database (https://www.ebi.ac.uk/ena) under the accession number PRJEB42300. Species assignment is based on exact sequence matching. Selected sequences with non-exact match were submitted to NCBI BLAST query (megablast 16S rRNA bacterial and archaean gene sequences) and the percentage of identity is reported. ASVs with ≥0.01% of total counts were used for further analyses. ASVs counts and taxonomy can be found in (htpps://doi.org/10.4121/c.5265740).

Shannon diversity index boxplots were obtained using the InteractiveDisplay package (Balcome and Carlson, 2020). Distance-based Redundancy Analysis (dbRDA) was carried out using Bray-Curtis dissimilarity with the capscale function from the vegan package (Oksanen et al., 2019) and visualized with ggord and ggplot2 (Wickham, 2008; Beck and Mikryukov, 2020). Differential abundance analysis was done at ASV level using CSS normalization and the metagenomeSeq package (Paulson et al., 2013) as described elsewhere (Contreras-Dávila et al., 2020). In brief, a Zero-Inflated Gaussian Distribution Mixture Model was applied and obtained P-values from moderated t-tests between accessions were adjusted using the Benjamini–Hochberg correction method. Differences in taxa abundance between accessions with adjusted P-values<0.05 were considered significant. Non-random co-occurrence networks were created using SparCC correlations between microbial taxa at ASV level. For each network, SparCC correlations were calculated for 100 random selections of the ASV counts table with 100 internal iterations using the sparcc function from the SpiecEasi package (). This procedure was repeated 20 times and the resulting sparCC covariance matrixes were averaged. The average covariance matrixes were used to create co-occurrence networks using the qgraph package (Epskamp et al., 2012). Correlations with P-values<0.05 were used to build the co-occurrence analyses and correlations with absolute strength values >0.6 are shown in the networks. Nodes depict ASVs sized according to their betweenness centrality (BC) scores to identify hub bacterial species. Networks properties such as number of edges (correlations), nodes (ASVs), average path length (APL) and transitivity were obtained using the igraph package (Dickey et al., 2019).

6.3. Results

6.3.1. Sunflower oil and oleyl alcohol biocompatibility and carboxylates extraction efficiency in batch extractive chain elongation

Addition of sunflower oil and oleyl alcohol to achieve extractive fermentation resulted in similar amounts of carboxylates produced compared to the blank experiments without solvent (Figure 6.1A). A short delay in the exponential phase was observed for both solvents only in the lactate experiments although this was not the case with food waste as substrate (Figure S2). These observations show the biocompatibility of both solvents with chain-elongating microbiomes since the process occurred at similar carboxylates yield despite direct contact with the solvents. However, solvent choice affected product distribution (Figure 6.1). Although n-butyrate (nC4) was the main fermentation

product, extraction with sunflower oil favored the formation of n-caproate (nC6) from both substrates (lactate: 98±12 e^- meq·L^{-1}; food waste: 196±11 e^- meq·L^{-1}) when compared to oleyl alcohol (lactate: 44±25 e^- meq·L^{-1}; food waste: 140±33 e^- meq·L^{-1}). n-caproate production selectivities were higher with sunflower oil than with oleyl alcohol (sunflower oil with lactate [14±2%] and food waste [12±1%] *vs* oleyl alcohol with lactate [7±4%] and food waste [9±1%]). Additionally, sunflower oil addition to lactate-fed experiments showed higher acetate, propionate and n-valerate (nC5) formation with n-valerate reaching 49±12 e^- meq·L^{-1} (selectivity 7±2%) (Figure 6.1B). n-caprylate (nC8) production occurred in low amounts (<0.4% selectivity) showing no improvement with extraction. Sunflower oil extracted n-caproate preferably over n-butyrate whereas the opposite trend was observed for oleyl alcohol (Figure S3). Extraction efficiency under fermentation conditions is compared for both solvents in Table 6.1. Oleyl alcohol displayed overall higher K_D (1-6 times) and recovery (1.5-3.8 times) for both n-butyrate and n-caproate compared to sunflower oil. On the other hand, sunflower oil specificity for n-caproate was similar or higher than that of oleyl alcohol with nC6 extraction specificity being 1.8-2.3 higher than that for nC4 for sunflower oil *vs* 0.7-1.3 for oleyl alcohol.

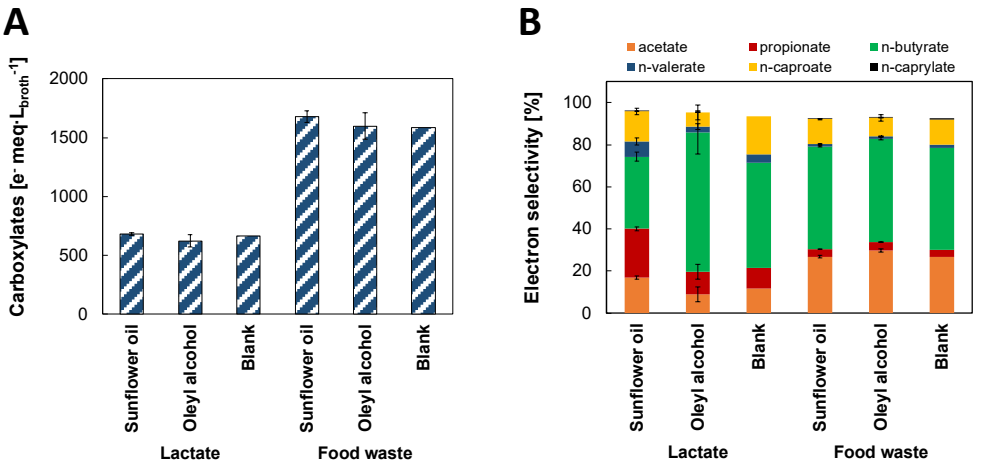

Figure 6.1 (**A**) Total carboxylates produced from substrates and (**B**) products selectivity of lactate and food waste (non-)extractive fermentation. Carboxylates partitioned in the organic and aqueous phases were added up and normalized to the initial aqueous (fermentation broth) volume. Error bars depict duplicates absolute deviation from the average.

6.3.2. Continuous lactate-based chain elongation with(out) sunflower oil

Continuous chain elongation experiments were carried out in two independent CSTR fed with lactate and acetate. Fermentation performance was first evaluated in the absence of sunflower oil at constant pH 5.0 and 2 d HRT. Under these conditions, n-caproate was the dominant product with both reactors showing similar performance throughout the operation. The overview of both reactors performance can be found in Figure S4, Table S2 and Table S3. After ~20 days of adaptation, n-caproate was steadily produced at rates of 943.5±36 e^- meq·L^{-1}·d^{-1} (3.43±0.13 g·L^{-1}·d^{-1}) in R1 and 894±46 e^- meq·L^{-1}·d^{-1} (3.24±0.17 g·L^{-1}·d^{-1}) in R2 during the period I-a (Figure 6.2). Production of MCC (nC6-nC8) was 969±63 e^- meq·L^{-1}·d^{-1} and 921±36 e^- meq·L^{-1}·d^{-1} in R1 and R2, respectively. n-caproate was the main product of chain elongation with electron selectivities of 74±2% (76±1% MCC) in R1

and 77±2% (80±2% MCC) in R2. n-butyrate and hydrogen were the main side-products (~10% electron selectivity each) and selectivity for the MCC n-heptanoate and n-caprylate was ~1% for each (Table S2, Table S3). n-caproate concentrations were ~6.5 g·L^{-1} and about half of the lactate fed (47-64%) remained unconsumed. After period I-a, technical complications caused pH to temporarily reach near-neutral values (pH 7.0-7.4) with higher lactate consumption and n-caproate concentrations (8.2-14.5 g·L^{-1}) observed (Figure S5). Manual acidification of the medium back to pH 5.0 resulted in biomass wash out (R1 day 45.8; R2 day 46.8). The reactors were operated in batch mode with no pH control to allow biomass regrowth. Once biomass growth was observed and pH stabilized at ~7.3 (~5 days), continuous operation was reinitiated and pH was readjusted in a stepwise manner by automatic acid addition (0.5 units every 0.5-1 HRT). The acid input in period I-a was 67-76 mmol H^{+}·L^{-1}·d^{-1} and 2.4-2.5 mol H^{+}·mol MCC^{-1} (Table S2, Table S3). Both CSTR recovered n-caproate production after these perturbations. However, R2 showed high variability in n-caproate production rates thereafter (Figure S4B) expressed by unstable oxidation-reduction potential (ORP). ORP increased from -405±8 mV in period I-a to -367±19 mV in period I-b and varied around -400±45 in period I-c (Table S3). In contrast, ORP remained constantly lower in R1, between -475±8 and -496±1 mV during non-extractive chain elongation (Table S2). Methane was only sporadically produced (<5 mmol·L^{-1}·d^{-1}) during R2 batch recovery from biomass wash out.

Table 6.1 Average sunflower oil and oleyl alcohol extraction efficiency during extractive fermentation.

Parameter	Carboxylate	Sunflower oil		Oleyl alcohol	
		Lactate	Food waste	Lactate	Food waste
Final pH		5.97	4.84	6.52	4.94
K_D	nC4	0.1	0.2	0.1	1.0
	nC5	0.2	0.6	0.3	2.9
	nC6	0.5	2.5	1.7	15.0
	nC8	n.a.	1.1	n.a.	1.1
P	nC4	1.1	0.4	4.4	2.2
	nC5	2.8	1.2	16.1	6.8
	nC6	7.1	4.8	73.3	32.1
	nC8	n.a.	2.1	n.a.	2.2
Recovery in solvent [%]	nC4	2	6	3	23
	nC5	6	15	9	48
	nC6	15	44	34	83
	nC8	n.a.	26	n.a.	25
Specificity in solvent [%]	nC4	18	30	36	50
	nC5	8	2	5	3
	nC6	42	55	46	33
	nC8	n.a.	1	n.a.	0.3

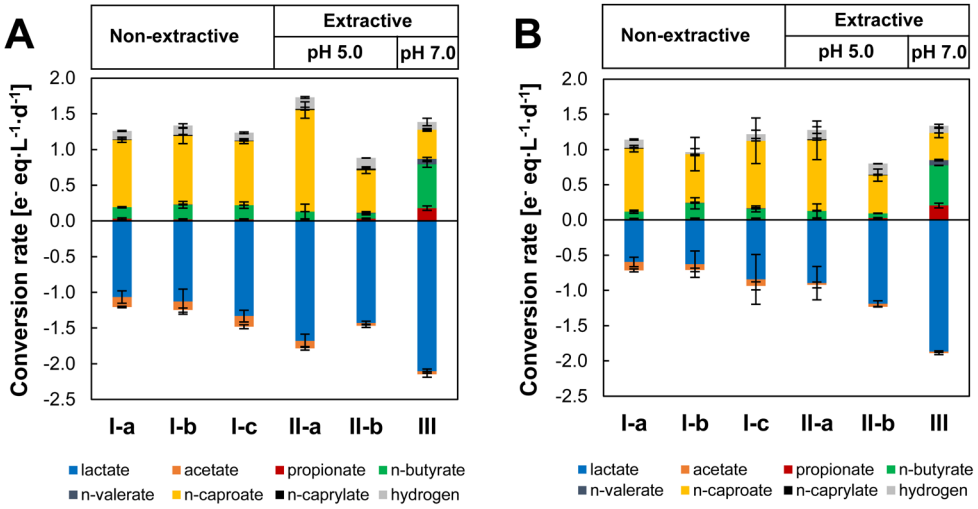

Figure 6.2 Conversion rates in non-extractive and extractive lactate-based chain-elongating reactors: (**A**) R1 and (**B**) R2. Conversion rates include carboxylates in aqueous and organic phases normalized to reactors working volume. Error bars show ±one standard deviation except for periods II-a and III for which absolute deviation is shown.

In extractive chain elongation, sunflower oil was present on top of the fermentation broth. The solvent phase was above the stirring propeller level resulting in only slight mixing due to stirring turbulence and biogas bubbling up to the headspace. During extractive fermentation, aqueous phase HRT and stirring speed operational conditions were kept constant. Lactate conversion rates increased after addition of sunflower oil with no apparent adaptation phase. n-caproate production rates were enhanced with sunflower oil addition in both reactors but this effect was only maintained in R1 for over 5 HRTs (period II-a) at 1421±114 e^- meq·L^{-1}·d^{-1} (5.16±0.41 g·L^{-1}·d^{-1}) (Table S2). After this period, a drop in n-caproate production (542±86 e^- meq·L^{-1}·d^{-1}; 1.97±0.32 g·L^{-1}·d^{-1}) and extraction rates was observed (period II-b). R2 performance remained unstable during period II-a with no clear improvement in n-caproate production rates and a similar decrease in n-caproate production was observed in period II-b (Figure 6.2). n-caproate and n-caprylate accumulated in the sunflower oil to concentrations of 72 and 3 g·L^{-1}, respectively, by the end of period II-a in R1. These concentrations were 59 g·L^{-1} for n-caproate and 1.3 g·L^{-1} for n-caprylate in R2 (Figure 6.3). The highest measured extraction rates were 1.9 g nC6·L_{broth}^{-1}·d^{-1} in R1 (260.7 g nC6·m^{-2}·d^{-1}) and 3.7 g nC6·L_{broth}^{-1}·d^{-1} (507.6 g nC6·m^{-2}·d^{-1}) in R2 (Figure 6.3). Under these conditions, n-caproate and n-caprylate were selectively extracted with no other SCC or MCC detected in sunflower oil. This was confirmed in abiotic continuous experiments where n-caproate from synthetic effluent was the only carboxylate extracted into sunflower oil while lactate, acetate and n-butyrate remained in the effluent (Figure S6). Maximum extraction rates in the abiotic experiment were around half those observed during extractive chain elongation (1.1-1.7 g nC6·L_{broth}^{-1}·d^{-1}; 149-236 g nC6·m^{-2}·d^{-1}).

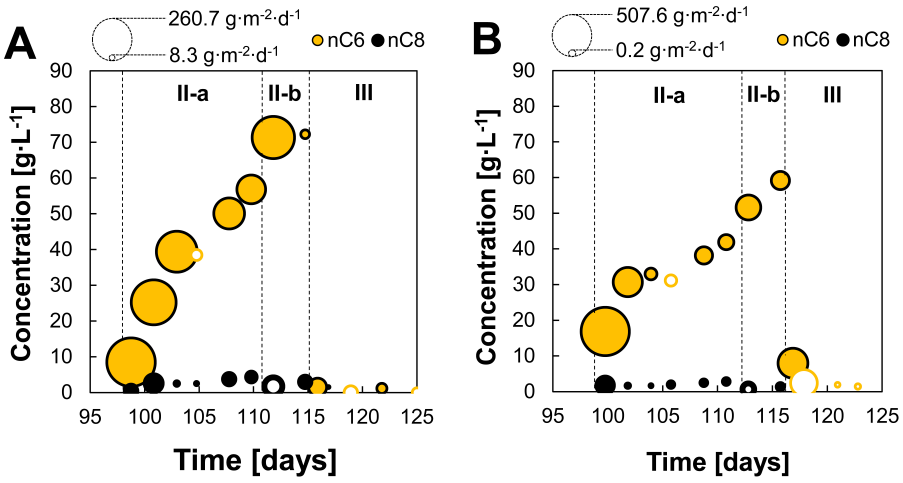

Figure 6.3 Medium-chain carboxylates concentrations in sunflower oil as measured from back-extracted samples from chain elongation reactors: (**A**) R1 and (**B**) R2. Bubble size shows extraction flux into the solvent based on cumulative carboxylates concentrations between two contiguous sampling points. Empty bubbles show negative flux values (apparent re-solubilization into the aqueous phase).

Extractive chain elongation also improved n-caproate electron selectivity in R1 from 71±3% during non-extractive chain elongation (average periods I-a to I-c) to 83±6% (period II-a). Likewise, n-caproate carbon selectivity increased from 50±3% to 58±3%. Carbon conversion efficiency towards n-caproate improved from period I-c (35±2%) to period II-a (45±3%) but was not different from the average of non-extractive chain elongation periods (I-a to I-c; 40±4%) (Table S2). For the case of R2, improvement in the aforementioned parameters was not clear due to reactor instability e g. n-caproate electron selectivity was 76±6% during non-extractive chain elongation (periods I-a to I-c) compared to 80±8% during period II-a (Table S3). About 15-18% of the n-caproate flux was recovered in sunflower oil while the totality of n-caprylate was partitioned to the organic phase (Figure S7).

Before period III, sunflower oil was collected from the reactors, fermentation broth pH adjusted to 7.0 and new sunflower oil added. The highest substrate conversion rates were observed under this neutral pH conditions for both reactors (Figure 6.2). Nevertheless, n-caproate production declined over time and increasing n-butyrate, propionate and n-valerate were observed (Figure S4). Electron selectivity in R1 decreased to 28±3% for n-caproate while it reached 44±2% for n-butyrate, 13±2% for propionate and 6±2% for n-valerate. Similar metabolites profile and selectivities were observed in R2. n-caproate was still extracted into sunflower oil at pH 7.0 but it was re-solubilized into the aqueous phase as n-caproate production declined over time (Figure 6.3, Figure S7).

6.3.3. MCC-enriched sunflower oil composition

About 80% of the added sunflower oil was recovered from the reactors after extractive fermentation and the respective carboxylic acids compositions before and after extractive fermentation are shown

in Table 6.2. From the back-extracted samples measured in our lab, MCC were estimated to make up 6-8.6% of the total carboxylic acids in MCC-enriched sunflower oil with nC8-to-nC6 carbon ratios of 2-4% (this ratio was ~1% in the effluent). Linoleic and oleic acids remained at similar proportions in sunflower oil after extractive fermentation. The proportions of unsaturated carboxylic acids (UCA) decreased due to accumulation of MCC. Monounsaturated carboxylic acids (MUCA) proportions showed minor declines at pH 5.0 related with decrease in oleic acid content (Figure S8). The actual proportions of LCC and UCA may be lower in MCC-enriched oil since the ISO 15885 analysis seemed to underestimate MCC concentrations. Underestimation of SCC (nC4) and MCC (nC6 and nC8) is reported to be a limitation of the ISO 15885 standard (Contarini et al., 2013). n-caproic and n-caprylic acid presence as free carboxylic acids instead of esterified forms may have also influenced their correct quantification.

Table 6.2 Carboxylic acids composition of sunflower oil before and after extractive chain elongation at different pH conditions.

Compound	Initial sunflower oil	R1		R2	
		pH 5.0 (period II-b)	pH 7.0 (period III)	pH 5.0 (period II-b)	pH 7.0 (period III)
Back-extraction estimations					
% n-caproic acid (C6:0)[a]	0	8.20±0.05	0.07±0.07	6.33±0.43	0.08±0.08
% n-caprylic acid (C8:0)[a]	0	0.27±0.07	0	0.11±0.04	0
wt% MCC		8.22±0.12	0.06±0.06	6.48±0.23	0.08±0.08
nC8-to-nC6 [% mol C]	N.A.	3.5±0.1	N.A.	1.9±0.5	N.A.
ISO 15885 standard					
% n-caproic acid (C6:0)	0	0.84±0.11	0	0.40±0.03	0
% n-caprylic acid (C8:0)	0	0	0	0	0
% oleic acid (C18:1, cis 9)	34.85±0.03	34.29±0.1	35.08±0.01	34.58±0.21	35.07±0.11
% linoleic acid (C18:2, cis 9, 12)	52.92±0.06	52.78±0.22	53.14±0.05	52.95±0.18	53.06±0.08
% saturated carboxylic acids (SCA)	10.64±0.02	11.34±0.11	10.19±0.02	10.95±0.01	10.28±0.21
% unsaturated carboxylic acids (UCA)	89.36±0.02	88.66±0.11	89.81±0.02	89.05±0.01	89.72±0.21
% conjugated linoleic acids (CLA)	0	0	0	0	0
% Ω-3 carboxylic acids	0.14±0.01	0.13±0.01	0.14±0.01	0.13±0.01	0.13±0.01
% Ω-6 carboxylic acids	52.92±0.07	52.78±0.22	53.14±0.05	52.95±0.18	53.06±0.08
% monounsaturated carboxylic acids (MUCA)	35.74±0.02	35.16±0.10	35.95±0.02	35.43±0.20	35.95±0.12
% polyunsaturated carboxylic acids (PUCA)	53.06±0.6	52.91±0.21	53.28±0.04	53.08±0.19	53.19±0.08
% unnamed carboxylic acids	0.56±0.03	0.59±0.01	0.58±0.01	0.54±0.01	0.58±0.01

[a]Assuming carboxylic acids make 97 wt% of sunflower oil.

Values from last two samples of each operational period are averaged.

Error represents average absolute deviation from actual values (n=2).

6.3.4. *Caproiciproducens* species dominate MCC-producing chain elongation microbiomes

Reactor microbiomes composition analysis based on 70 ASVs accounting for >98.8% of microbiomes counts showed that bacteria species from the orders *Clostridiales*, *Lachnospirales* and *Oscillospirales* accounted for 88-99% of reactors microbiomes with shifted proportions as pH was increased (Figure 6.4). Both reactors showed similar Shannon diversity indexes throughout operation with microbiomes developed at pH 7.0 showing higher diversity compared to those developed at pH 5.0 (Figure 6.5A-B). Biofilm microbiomes resembled suspended microbiomes composition in most of the cases although biofilms were more diverse at pH 7.0 compared to the corresponding

suspended microbiomes. Reactor microbiomes composition was significantly affected by pH conditions (P<0.0005) with weak influence of sunflower oil addition (P<0.05) (Figure 6.5C). *Caproiciproducens*-related ASVs were associated with MCC production and low pH conditions (Figure 6.5D) and were differentially abundant at pH 5.0 (Figure 6.5E). At this pH, *Caproiciproducens* was the most abundant genus under both non-extractive and extractive chain elongation conditions (48-82% relative abundance) followed by *Clostridium* sensu stricto 12 (12-42% relative abundance). *Caproiciproducens* spp. ASV1 and ASV2 showed low similarity with the type strain *Caproiciproducens galactitolivorans* (<91%) with the closest relative being [Clostridium] leptum strain DSM 753 (~93% similarity). *Anaerotignum*, *Lachnospiraceae* UCG-010 and *Sporoanaerobacter* related species were related with near-neutral pH conditions and formation of propionate and n-butyrate (Figure 6.5C-E). *Anaerotignum* spp. ASV4 and ASV15 were 98.5 and 98% similar to *Anaerotignum propionicum*, respectively. The closest relative to *Lachnospiraceae* UCG-010 ASVs 7 and 8 was *Anaerotignum aminivorans* (95% similarity for both). Less abundant ASV10 and ASV19 were both >99.5% similar to *Sporoanaerobacter acetigenes* DSM 13106. *Clostridium tyrobutyricum* spp. ASV3 and ASV6 (99.4% identity) were abundant throughout reactors operation and were both associated with MCC-producing microbiomes while *Clostridium luticellarii* spp. ASV9 and ASV11 were related with propionate/n-butyrate- and MCC-producing microbiomes, respectively (Figure 6.4, Figure 6.5D). Sequences of selected ASVs can be found in Table S4.

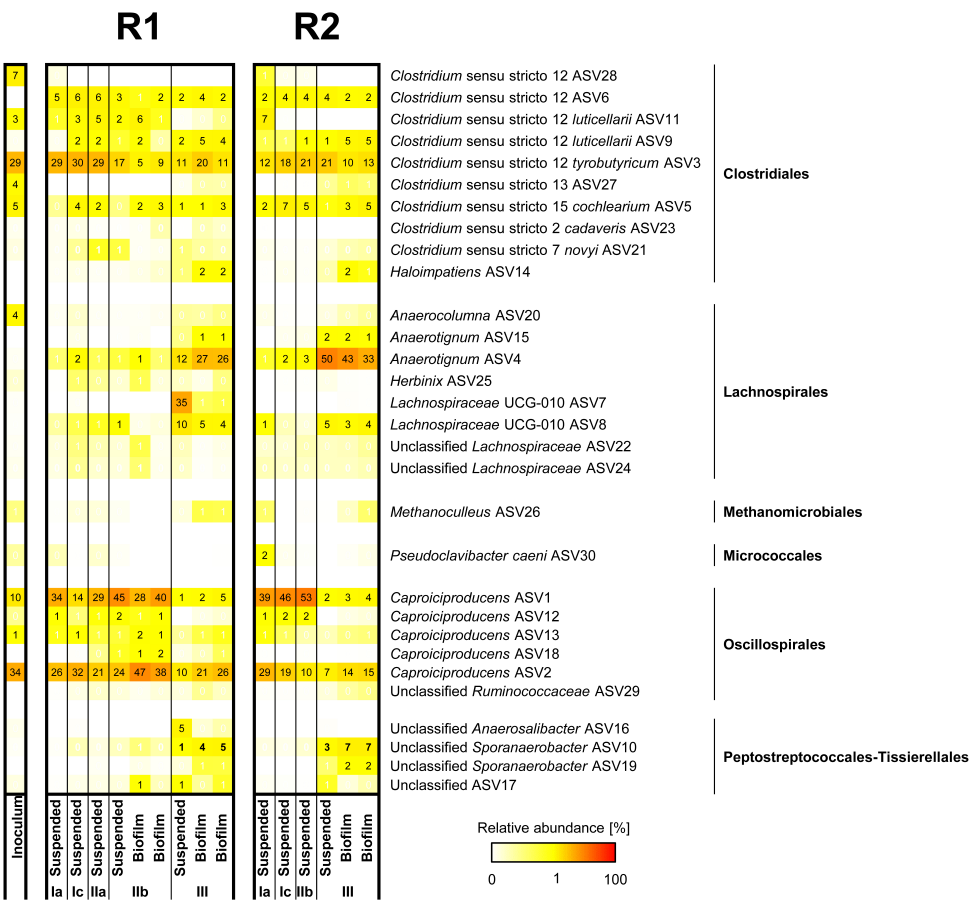

Figure 6.4 Reactor microbiomes composition at ASV level. Top 30 ASVs are displayed and relative abundance values ≥1% are shown. Independent biofilm samples were analyzed and shown as duplicates. Sampling days are shown in Figure S4. Taxonomy was assigned based on SILVA 138 SSU Ref NR 99 database.

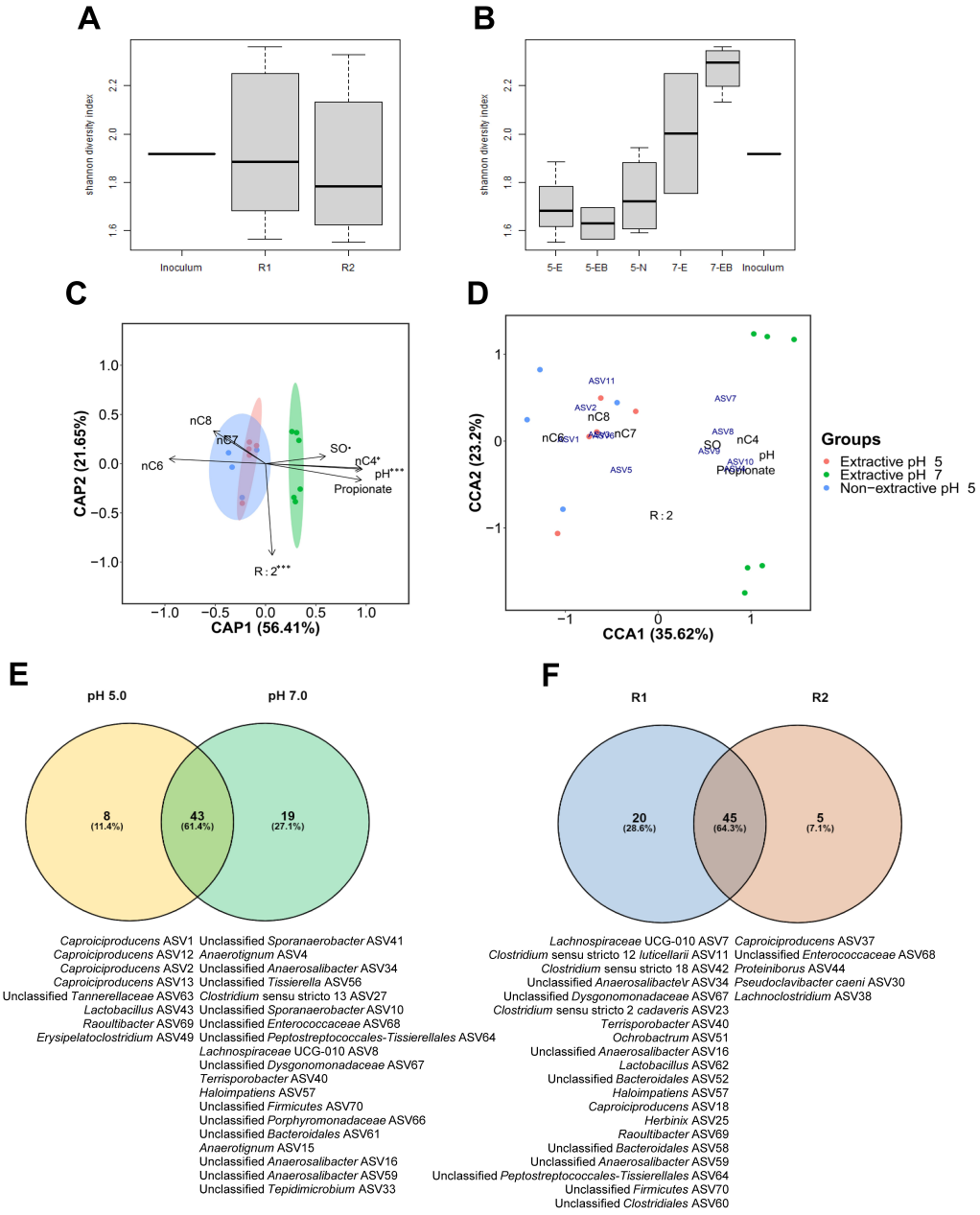

Figure 6.5 (**A**) Shannon diversity index of inoculum, R1 and R2 microbiomes. (**B**) Shannon diversity index of suspended microbiomes from non-extractive (5-N) and extractive chain elongation at pH 5.0 (5-E) and pH 7.0 (7-E); and biofilm microbiomes from extractive chain elongation at pH 5.0 (5-EB) and pH 7.0 (7-EB). Boxplots show the interquartile range (IQR) in boxes divided by median values (horizontal lines) with whiskers depicting ±1.5 IQR (**A**, **B**). (**C**) Distance-based Redundancy Analysis (dbRDA) using Bray-Curtis dissimilarity index; ASVs relative abundance as response variables; and environmental parameters as explanatory variables (constraints). Environmental parameters considered were: reactor (R1, R2), pH, sunflower oil (SO) (presence/absence) and steady-state electron selectivities (propionate, nC4, nC6, nC7, nC8, MCC and H2; Tables S2 and S3). Concentration ellipses depict confidence intervals with α = 0.05. Significance code: '***' associated with a variable at P <0.0005; '*' associated with a variable at P <0.01; and '.' associated with a variable at P

<0.05. (**D**) Canonical Correspondence Analysis (CCA) using Hellinger transformation and same constraints as in dbRDA. CCA triplot shows top 11 ASVs scaled proportionally to eigenvalues. Collinear (redundant) environmental parameters (MCC and H_2) were automatically dropped out in both dbRDA and CCA (**C**, **D**). (**E**-**F**) Differential abundance analyses at ASV level of microbiomes developed at different pH conditions (**E**) and between reactors (**F**). Differential abundance at different pH was analyzed using all samples from both reactors. IIa and IIb biofilms samples were left out when comparing microbiomes between reactors. (**E**, **F**). Analyses were done using CSS-normalized 16S rRNA gene sequencing data of ASVs with >0.01% of total counts.

About 65% of the ASVs were equally enriched in both reactors with 20 ASVs in R1 and 5 ASVs in R2 being differentially abundant (Figure 6.5F) which may help explain the more stable performance of R1. Of the differentially abundant taxa in R1, *Clostridium luticellarii* sp. ASV11 showed the highest betweenness centrality (BC) in the co-occurrence network constructed with samples from all operational periods (Figure 6.6A) suggesting its relevance in microbiomes composition dynamics throughout reactors operation. In MCC-producing microbiomes developed at pH 5.0, *Lactobacillus* sp. ASV43, *Clostridium tyrobutyricum* sp. ASV3 and *Clostridium luticellarii* sp. ASV11 showed the highest BC values (Figure 6.6B). Microbiomes from R1 showed highest BC for unclassified *Sporoanaerobacter* sp. ASV10, *C. luticellarii* sp. ASV9 and *C. cochlearum* sp. ASV5. R1 microbiomes show the co-occurrence of *Caproiciproducens* with *C. tyrobutyricum*, *C. luticellarii* sp. ASV11 and *Lactobacillus* organisms (Figure 6.6C).

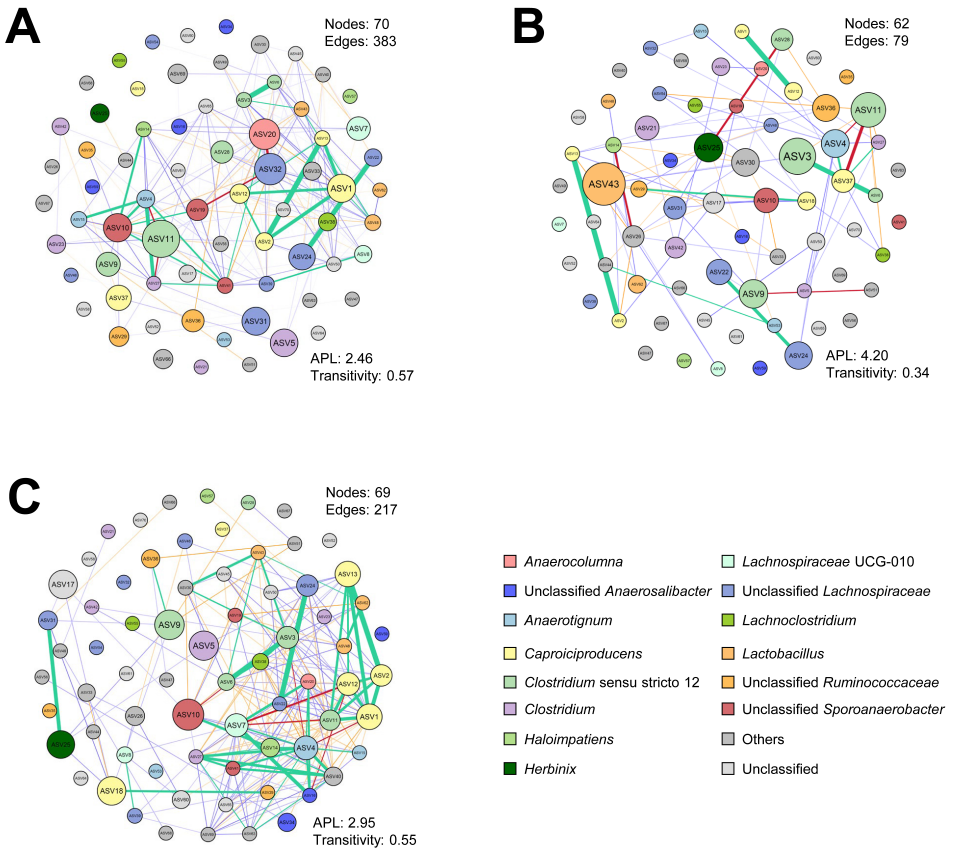

Figure 6.6 Co-occurrence networks of lactate-based chain elongation reactor microbiomes. (**A**) Reactor microbiomes developed throughout reactors operation (n=15); (**B**) at pH 5.0 (n=9); and (**C**) throughout R1 operation (n=9). Co-occurrence networks were build using significant correlations (P <0.05). Strong correlations are depicted with green (>0.8, positive correlation) and red (<-0.8, negative correlation) edges with boldness related to the strength of the correlation. Positive and negative correlations with absolute values >0.6 are shown with blue and orange edges, respectively, with increasing shading up to <0.8. Nodes are sized based on ASVs betweenness centrality scores and colored according to taxonomic classification at genus level.

6.4. Discussion

6.4.1. Lactate-based chain elongation microbiomes stand high undissociated n-caproic acid concentrations

Non-extractive continuous lactate-based chain elongation at pH 5.0 resulted in efficient production of MCC at an electron selectivity of ~75% (average R1 and R2). n-caproate was the main chain elongation product (98% of MCC) along with small but considerable amounts of n-heptylate and n-caprylate (~1% electron selectivity each). One study using continuously fed lactate reported n-caproate electron selectivities of 34% at pH 5.0 with n-heptylate but no n-caprylate formation (Candry et al., 2020a). Propionate production at high residual lactate concentrations has been reported to reduce chain elongation performance (Prabhu et al., 2012; Kucek et al., 2016a). In the present study, however, robust chain elongation to n-caproate (~6.5 g·L^{-1}) and n-caprylate (~0.08 g·L^{-1}) proceeded

with ~18 g·L^{-1} residual lactate. We hypothesize that the acidic conditions applied and the accumulation of MCC prevented the dominance of propionate-producing bacteria in the reactor microbiomes developed here. Propionate formation was observed in the first days of operation. However, as n-butyrate was elongated, n-caproate concentrations increased gradually and propionate formation dropped when undissociated n-caproic acid concentrations reached values of ~1 g·L^{-1} (8.8 mM). Stable n-caproate production and low propionate formation (~2% electron selectivity) were observed thereafter as these conditions led to reactor microbiomes with relatively low diversity specialized in MCC production. Uncultured *Caproiciproducens*-related microorganisms dominated MCC-producing microbiomes co-occurring with less abundant but highly connected (high betweenness centrality) hub microorganisms *Clostridium tyrobutyricum* sp. ASV3, *Clostridium cochlearium* sp. ASV5, *Lactobacillus* sp. ASV43 and *C. luticellarii* sp. ASV11. This suggests the relevance of low abundant organisms in the microbiomes structure and functioning where niche complementarity may have supported the conversion of a larger fraction of substrate into MCC. *Caproiciproducens* produce MCC from lactate (Contreras-Dávila et al., 2020, 2021). *C. tyrobutyricum*, *C. cochlearium* and *Lactobacillus* may convert part of the lactate into n-butyrate (Esquivel-Elizondo et al., 2017) which may be further elongated by *Caproiciproducens*. *C. luticellarii* sp. ASV11 seems to be a strain adapted to mild acidic pH conditions supporting MCC production while *C. luticellarii* sp. ASV9, identified to be strain FW431, was enriched in neutral pH conditions (Figure 6.5D) and is reported to produce propionate from lactate (Petrognani et al., 2020).

Undissociated n-caproic acid is believed to be toxic to chain elongation microbiomes (Roghair et al., 2018b) at concentrations of 7.5 mM (0.87 g·L^{-1}) for ethanol-based chain elongation microbiomes (Ge et al., 2015). However, *Caproiciproducens*-dominated microbiomes producing MCC from food waste with lactate as intermediary are reported to stand up to 20 mM undissociated n-caproic acid (Contreras-Dávila et al., 2020). In the present study, increased lactate conversion to n-caproate was observed when pH increased momentarily in non-extractive chain elongation and when MCC were removed during extractive chain elongation. These observations suggest that undissociated n-caproic acid concentrations ~26 mM (3 g·L^{-1}) were limiting further chain elongation and might represent threshold concentrations in efficient lactate-fed chain elongation systems. Moreover, complete inhibition of the microbiomes was observed when undissociated n-caproic acid concentrations reached 37 mM (4.3 g·L^{-1}) during manual pH readjustment (R1, day 46.8; R2, day 47.8). These threshold and inhibitory concentrations are 2 to 4 times higher than inhibitory concentrations proposed for ethanol-based chain elongation microbiomes (Ge et al., 2015). However, further adaptation may make reactor microbiomes more resilient to MCC toxicity as shown for the ethanol-based chain elongation process (Roghair et al., 2018b).

6.4.2. Extractive chain elongation improves bioprocess efficiency and rates

Removing part of the produced MCC *via* extractive chain elongation allowed the microbiomes to convert a larger fraction of the fed lactate which resulted in 50-60% higher n-caproate production rates. The highest n-caproate volumetric production rate achieved here (R1 period II-a; 5.16±0.41 g·L^{-1}·d^{-1}) is ~65% higher than those obtained in a reactor fed L-lactate and n-butyrate equipped with in-line extraction (Kucek et al., 2016a). Furthermore, extractive chain elongation increased n-caproate electron selectivity up to 83±6% (84±5% MCC; equivalent to 92% MCC *per* total carboxylates),

doubling previously achieved values in lactate-fed chain elongation reactors (34-41% n-C6) (Kucek et al., 2016a; Candry et al., 2020a) and being comparable to values obtained from ethanol and acetate chain elongation (80-94% MCC *per* total carboxylates) (Grootscholten et al., 2013d). It is worth noting that higher productivities can be achieved from complex waste streams with lactate as the assumed electron donor (Carvajal-Arroyo et al., 2019).

After 12 days of extractive fermentation at pH 5.0 (period II-b), however, carboxylate production was reduced by around half opposite to lactate consumption. The missing electrons between substrate conversion and carboxylates production (Figure 6.2) may indicate a low recovery of carboxylates by back-extraction during period II-b and III. Alternatively, toxic components derived from sunflower oil may have altered microbial activity and metabolism. The LCC oleic and linoleic acids, their triglycerides and LCC vesicles can cause cell membrane disruption (Yoon et al., 2018). Thus, their migration to the aqueous phase could have partially inhibited bacteria and increased energy demand for solvent tolerance adaptation and cell maintenance (Rühl et al., 2009). Additionally, some ruminant bacteria including chain-elongating bacteria *Megasphaera elsdenii* and *Eubacterium pyruvativorans* showed improved resistance to linoleic acid in the presence of lactate (Maia et al., 2007). Thus, resilience of *Caproiciproducens*-dominated microbiomes to sunflower oil presence during period II-a may be related to the use of lactate as electron donor. No known LCC degraders were observed in this study (Sousa et al., 2009). *Sporoanaerobacter*-related species detected at pH 7.0 (period III) have been observed in methane-inhibited reactors degrading monounsaturated LCC with no described role in such microbiomes (Cavaleiro et al., 2016).

Comparative stoichiometric analysis of non-extractive (periods I-a to I-c) and extractive (period II-a) chain elongation in R1 indicates that n-caproate selectivity was improved due to decreased propionate and n-butyrate yields (Table S5). Extractive chain elongation resulted in almost halved net acetate consumption compared to non-extractive conditions with molar ratios of lactate-to-acetate consumed being 6.4 and 11 during non-extractive and extractive chain elongation in R1, respectively, showing the metabolic flexibility of lactate-elongating microbiomes. n-caproate yields obtained in this study were 0.29-0.32 mol nC6·mol lactate^{-1}, similar to yields reported for pure cultures converting lactate and acetate (0.26 mol nC6·mol lactate^{-1}) (Zhu et al., 2017).

6.4.3. MCC extraction with sunflower oil

Sunflower oil showed to be biocompatible with chain-elongating microbiomes as similar amounts of carboxylates were produced compared to non-extractive and extractive fermentation with oleyl alcohol (section 6.3.1). Higher n-caproate production compared to oleyl alcohol was probably related with the high sunflower oil specificity for n-caproate extraction even when n-butyrate was the main fermentation product in batch extractive fermentation. Sunflower oil n-caproate extraction specificities attained here (55%) are similar to ionic liquids using synthetic chain elongation effluent (53%) (Chwialkowska et al., 2019) reaching a n-caproate recovery of 45% with only 6% n-butyrate extracted. To improve MCC recovery, sunflower oil could be modified with reactive extractants or mixed with more efficient solvents. A mixture of sunflower oil and 1-octanol showed n-caproate recoveries of ~95 and ~50% at pH 4.5 and 5.5, respectively, from equimolar C2-nC6 solutions (Kaur et al., 2020). However, other short-chain carboxylates (C3-nC5) were extracted together with n-

caproate. Thus, the modifiers should not reduce extraction selectivity substantially and must be compatible with the final application of the MCC-enriched solvent. Oleyl alcohol allowed higher n-caproate recovery with selectivities at pH 6.0-6.5 similar to sunflower oil but declining at lower pH conditions (pH ~5.0) (lactate vs food waste experiments).

Avoiding extraction of substrates and intermediates is important to sustain efficient extractive chain elongation processes. In continuous biotic and abiotic experiments at pH 5.0, sunflower oil exclusively extracted MCC and no SCC from the fermentation broth. The fact that lactate was not extracted in our experiments is in line with previous reports where non-reactive extraction of lactic acid showed very low efficiency (Tong et al., 1998). For ethanol-based chain elongation, use of vegetable oils could result in ethanol extraction (Offeman et al., 2006) and reduced bioprocess efficiency. n-caproate and n-caprylate were concentrated in MCC-enriched sunflower oil by a factor of ~11 (72 $g \cdot L^{-1}$) and ~38 (3 $g \cdot L^{-1}$), respectively, with respect to aqueous concentrations in non-extractive chain elongation (6.6 g $nC6 \cdot L^{-1}$, 0.08 g $nC8 \cdot L^{-1}$) to an equivalent of 8.3 wt% MCC (R1). In comparison, reactive mixtures of alamine 336 and oleyl alcohol accumulated ~30 g $nC6 \cdot L^{-1}$ (along with 2-3 $g \cdot L^{-1}$ of both acetate and n-butyrate) in batch extractive chain elongation with *C. galactitolivorans* (Jeon et al., 2013). At controlled pH 6.0, the same reactive mixture accumulated 50 g $nC6 \cdot L^{-1}$ from a 0.5 M n-caproate solution (Choi et al., 2013). Additionally, the achieved n-caproate content in MCC-enriched sunflower oil (8 wt%; R1, day114.7) is higher than reported n-caproate content in anion-exchange resins (≤6.2 wt%) (Yu et al., 2019).

Recovery of MCC was ~18% for n-caproate and 100% for n-caprylate during continuous extractive chain elongation at pH 5.0. Product recovery in continuous systems may be significantly enhanced by process operation/design in order to improve MCC flux to the organic phase. This could be accomplished, for instance, with higher aqueous-organic interface areas (e.g. membrane-supported pertraction) (Kucek et al., 2016a; Saboe et al., 2018) and solvent/broth recirculation (Weilnhammer and Blass, 1994). Conducting chain elongation at lower biocompatible pH values would increase the fraction of hydrophobic undissociated carboxylic acids and their extraction flux. However, this may reduce microbial productivity and MCC extraction specificity. SCC extraction rates may increase markedly compared to MCC (n-caproate) at $pH \leq pK_a$ as observed in membrane contactors (Saboe et al., 2018). MCC recovery could also be improved by refreshing the sunflower oil sooner, resulting in lower MCC content but higher extraction flux.

6.4.4. Potential of MCC-enriched vegetable oils as feed additives

Supplementation of vegetable oils to livestock diet has been intensively researched as a device for influencing their physiology and gut microbiomes. Oil addition can result in faster growth, improved feed efficiency and in modification of the derived food products (Hess et al., 2008; Li et al., 2019). On the other hand, MCC are metabolized differently than LCC (Hanczakowska, 2017) with beneficial effects in animal health and growth performance (Baltić et al., 2017; Jackman et al., 2020). Environmental benefits might also be achieved by using LCC and MCC due to their effectivity at reducing methane emissions in ruminant animals (Dohme et al., 2001; Poteko et al., 2020). Diet supplementation with 2-5 wt% of LCC (with respect to dry matter [DM] in the feed) might result in improved feed efficiency and growth in ruminants and swine (Hess et al., 2008; Li et al., 2019). Similar

positive effects such as weight gain, feed efficiency and gut health are observed with MCC addition to swine diet in the range of 0.2-1 wt% DM (Jackman et al., 2020). Additionally, adding MCC at 0.12-0.15 wt% DM shows therapeutic effects under stressful conditions (e.g. pathogen infections, weaning) by improving gut health, immune responses and survival rates in swine (Jackman et al., 2020). MCC can also be used against fish pathogens (Abdelhamed et al., 2019). Since the required MCC doses required to show significant effects are one order of magnitude lower than those of LCC, a product with 5-10 wt% MCC in vegetable oil could be suitable as feed additive. These values are comparable to the MCC-enriched sunflower oil produced in this study (6.3-8.3 wt% MCC; n-caproate + n-caprylate) which could potentially be used as biobased functionalized feed additive to improve livestock growth and well-being.

Another distinctive property of MCC is their capability to inhibit pathogens in livestock feed (Cochrane et al., 2019) when added at 1-2 wt% DM (Jackman et al., 2020). Similar MCC dietary proportions seem to be required to reduce methane mitigation (≤3 wt% DM), although lauric acid (C12:0) was the only effective MCC (Machmüller, 2006). LCC doses for methane mitigation are in the same order (2.6–3.6 wt% DM) (Poteko et al., 2020) which is in line with literature reports showing similar methane mitigation capabilities for lauric acid (MCC), myristic acid (LCC) and linoleic acid (main LCC in sunflower oil) (Dohme et al., 2001). Since similar MCC/LCC proportions in feed are required for feed pathogen inhibition and methane mitigation, the MCC-rich oil may need to be further enriched with MCC for these applications. However, synergistic antimicrobial activity is observed for different MCC or MCC-LCC mixtures. Antimicrobial activity is higher for MCC blends compared to individual MCC (Cochrane et al., 2019) and for MCC mixed with vegetable essential oils (Kim and Rhee, 2016) or LCC (Soliva et al., 2003). Using MCC-enriched oils would also avoid the negative impact of unpleasant MCC smell on feed intake (Zentek et al., 2011) and allow higher MCC dietary proportions. Properties of these enriched oils could be modulated by changing the MCC content and individual MCC ratios (n-caproate/n-caprylate). Although the MCC-LCC dietary requirements could be lowered by using MCC-enriched vegetable oils, their effectivity for the aforementioned applications requires further research.

6.4.5. Biotechnological outlook

Using microbially produced carboxylates from low-value organics is getting increasing attention as a way to valorize the growing amounts of waste (Agler et al., 2011). When carboxylates are used as feed additives, livestock-related concerns such as increasing antibiotic resistance (Li et al., 2019; Jackman et al., 2020) and greenhouse gases emissions (Machmüller, 2006) can also be addressed. MCC (in their salt form) produced *via* chain elongation from organic waste materials are now commercially available for animal nutrition (ChainCraft B.V.). Additionally, vegetable oils are also reported to positively influence livestock (Hess et al., 2008; Li et al., 2019) which can be used as application-compatible solvents for *in situ* MCC extraction in chain elongation processes. The use of solvents that are compatible with a specific application may reduce additional equipment, purification steps and salt waste generation. Some of these benefits have been proposed to be achieved in monoterpene-producing fermentations where product-enriched solvents are directly used in chemical hydrogenation for aviation fuel applications (Brennan et al., 2012). Or in sesquiterpene-enriched kerosene to reduce production costs and environmental impact of microbial

sesquiterpene production (Pedraza-de la Cuesta et al., 2019). MCC-enriched oils may also find application as biofuels and biochemicals precursors. For instance, MCC-enriched waste-derived oil may be converted into biodiesels with low unsaturation levels which show lower pollutant emissions compared to conventional unsaturated biodiesel (Cheng et al., 2018). LCC triglycerides in the enriched oil may be hydrolyzed to convert the resulting LCC and MCC salts into a variety of chemicals or aviation fuels through (Non-)Kolbe electrolysis (Holzhäuser et al., 2020). Sustainable aviation fuels (SAF) produced from waste oils and fats show high CO_2 savings (>85%) compared to conventional aviation fuels (SkyNRG, 2019) and ~7% of annual aviation fuel consumption could be replaced by SAF obtained from microbially produced MCC (Roghair et al., 2018c) in integrated (electro)biorefineries.

The potential benefits of application-compatible solvents for the process proposed here should be evaluated taking into account aspects related to vegetable oil production (Schmidt, 2015) and microbial chain elongation (Chen et al., 2017). Food waste-derived oil showed potential MCC extraction during fermentation (Contreras-Dávila et al., 2020) and may be used as an endogenous solvent to reduce the need of external solvents. Dangerous compounds possibly present in waste-derived oils may be removed (Maes et al., 2005) for feed applications. Additionally, microbial oils with high unsaturated LCC proportions can be obtained from agro-industrial waste streams using algae and/or yeast cultures (Liu et al., 2018). Unsaturated LCC can promote immune responses in cattle and accumulation of conjugated linoleic acids (CLA) in animal-derived food products (Hess et al., 2008). Feeding CLA to livestock increase CLA content in food products as well (Shinn et al., 2017). CLA are isomers of linoleic acid considered to have positive physiological effects on human health and are mostly sourced from dairy and meat products (Kim et al., 2016a). Thus, finding alternative ways to produce CLA could increase their dietary accessibility for human consumption. Microbial CLA production has been reported for different probiotic bacteria (Hosseini et al., 2015) and *M. elsdenii* (Kim et al., 2002), a chain-elongating microorganism. Although CLA were not detected in MCC-enriched sunflower oil, vegetable oils enriched with both CLA and MCC could be produced *via* chain elongation processes for feed or food purposes following pertinent regulations. MCC display differential effects on human health compared to unsaturated LCC (Marten et al., 2006) and CLA-rich food products are under development (Shinn et al., 2017). Alternatively, oleyl alcohol may be used in extractive chain elongation. Oleyl alcohol is approved as indirect food additive by the FDA and regulates LCC uptake in mammals (Murota et al., 2000). Biobased alkyl alcohols (e.g. oleyl alcohol) can be obtained from hydrogenation of plant-derived or microbially-produced LCC.

6.5. Conclusions

A reactor microbiome was developed for valorization of residual materials into potential functionalized feed additives. Sunflower oil displaying a high MCC extraction specificity was a biocompatible solvent in extractive lactate-based chain elongation similarly to oleyl alcohol. The use of oleyl alcohol could allow higher carboxylates recovery although with lower MCC extraction specificity. Lactate and intermediate carboxylates (acetate, propionate, n-butyrate) remained in the aqueous phase during continuous extractive chain elongation while transfer of n-caproate and n-caprylate to sunflower oil relieved the microbiomes from apparent undissociated MCC toxicity. Extractive chain elongation microbiomes showed improved substrate conversion, n-caproate

production rates and MCC specificities. Uncultured species belonging to the genus *Caproiciproducens* dominated the MCC-producing chain elongation microbiomes in coordination with hub *Clostridium* and *Lactobacillus* species. The genera *Anaerotignum* and *Lachnospiraceae* UCG-010 were dominant when n-butyrate and propionate were produced at pH 7.0. This shows the relevance of selection pressures (e.g. extractive fermentation, pH) and occurrence of hub organisms to develop effective chain elongation reactor microbiomes.

MCC-enriched solvents produced through extractive chain elongation are potential novel products obtained with simplified downstream processing. The MCC-enriched sunflower oil produced here contained up to 72 $g \cdot L^{-1}$ and 3 $g \cdot L^{-1}$ n-caproate and n-caprylate, respectively, corresponding to 8.3 wt% MCC. This concentration is high enough for several applications. MCC and LCC contained in the product could act synergistically aiding purposes such as feed pathogens inactivation or livestock gut microbiome regulation. Additionally, MCC-enriched solvents could be used in food and biofuels applications.

Chapter 7

General discussion

7.1. Research output

The development of innovative, effective resource recovery processes for materials cycling from residual streams will contribute to the transition to a more circular bioeconomy. This research develops chain elongation processes around lactate as the central intermediate in the upcycling of organic residual materials to a range of carboxylates, including branched, odd- and even-chain SCC and MCC (Chapters 2-5), demonstrating the versatility of lactate in the chain elongation platform. Alternative product separation methods with reduced complexity and with the potential to recover neat carboxylic acids or novel product formulations were explored in Chapters 5 and 6.

In Chapter 2, the proof-of-concept of a lactate-based chain elongation process that does not require external electron donor addition and demands low amounts of chemicals for pH control was developed. Acidification of complex food waste was steered toward lactate formation, which was subsequently used up as electron donor for chain elongation within the same bioreactor. This lactate cross-feeding, which is also observed in the human gut (Louis and Flint, 2017) and rumen (Counotte and Prins, 1981) microbiomes, enabled a balance between proton production/consumption and creates self-regulation of pH. Repeated batch operation lead to lactate and SCC elongation to n-caproate as the main MCC, with a maximum n-caproate selectivity (e^- eq *per* e^- eq carboxylates) of 38%. The hydroxide input values (0.47 mol OH^-·mol MCC^{-1}; 0.79 mol OH^-·kg $COD_{carboxylates}^{-1}$) obtained were 2- to 7-times lower compared to an effective chain elongation process using ethanol and acidified food waste (0.92 mol OH^-·mol MCC^{-1}; 5.5 mol OH^-·kg $COD_{carboxylates}^{-1}$) (Roghair et al., 2018c). This proof-of-concept avoids the use external electron donor (i.e. ethanol) and to reduce the input of pH-controlling chemicals, factors that impact the environmental footprint of the chain elongation technology (Chen et al., 2017). Food waste fermentation to lactate was also suggested as an attractive alternative to ethanol addition in previous research (Roghair et al., 2018c).

After showing that lactate is an important electron donor produced *in situ* from complex residues, further research focused on steering product formation from lactate. Operational conditions leading to the production of propionate, elongated SCC or MCC were identified. We showed that the type of lactate enantiomer does not determine the product spectrum of fermentation, due to the expected presence of lactate racemase in many microorganisms enriched in the developed reactor microbiomes (Chapter 3 and 4). This means that the applied operational conditions will select for the chain-elongation function in open cultures despite the type of lactate enantiomer fed. Lactate conversion was indeed predominantly directed to chain-elongating routes with limited propionate production (5-26% of products) due to the mildly acidic pH conditions applied (pH 5.0-5.5). Promising MCC selectivities (>66%) were obtained in continuous chain elongation where n-caprylate was also produced (Chapters 4-6). Apart from achieving sustained n-caprylate production (1-3% selectivity), relevant amounts of isobutyrate and n-heptylate (8-10% selectivity) were obtained by using conductive materials (Chapter 5) and supplying propionate (Chapter 4), respectively. Overall, these results contribute to broadening the spectrum of products derivable from lactate with reactor microbiomes, which was until now limited to n-caproate (Zhu et al., 2015; Kucek et al., 2016a), while isobutyrate was only obtained with pure cultures (Liu et al., 2020). The production of these new carboxylates may be further improved to achieve high selectivities and production rates.

For valorization, chain elongation products are typically separated from the fermentation broth and purified to carboxylate salts or neat carboxylic acids. MCC separation methods commonly used in chain elongation are liquid-liquid extraction coupled to back-extraction (Ge et al., 2015; Kucek et al., 2016a) and ion exchange (Yu et al., 2019), both of which produce carboxylate salts. To recover neat carboxylic acids, additional steps such as distillation and neutralization with inorganic acids may be needed (López-Garzón and Straathof, 2014). We explored alternative separation principles with the aim of concentrating neat MCC acids and simplifying DSP. In Chapter 5, a two-step DSP consisting of *in situ* adsorption with granular activated carbon (GAC) followed by thermal desorption was proposed for the recovery of neat medium-chain carboxylic acids. GAC showed high affinity for MCC adsorption (>6-times higher than C2-C4 SCC) which may allow selective MCC recovery from chain elongation reactors. Lastly, an alternative bioprocess to produce potential novel product formulations (e.g. MCC-rich feed additives) was studied in Chapter 6, where sunflower oil selectively accumulated MCC in continuous extractive lactate-based chain elongation. This proof-of-concept produced sunflower oil containing up to 8.3 wt% MCC and recovered ~18% of the produced MCC. The MCC-enriched sunflower oil was proposed as a potential functionalized feed additive for direct application with no further DSP. MCC-enriched solvents/adsorbents may be attractive alternatives for MCC valorization that have not been considered before.

7.2. Selected microbiome defines lactate enantiomers distribution

Lactate is a versatile electron donor that can be metabolized to different carboxylates under anaerobic conditions. Lactate exists in two optical isomers (enantiomers): D-lactate and L-lactate. Both lactate enantiomers are up taken by bacteria through lactate permease before being oxidized by stereospecific lactate dehydrogenases (Ldh). Prompt utilization of D-lactate is usually observed since D-Ldh is a constitutive enzyme in many microorganisms while L-Ldh is inducible by the presence of L-lactate (Kato et al., 2010). When only one of the two stereospecific Ldh is present, utilization of the other enantiomer may still proceed after isomerization with lactate racemase (Lar). For instance, Lar may isomerize L-lactate to supply the D-lactate needed for propionate formation in propionic acid bacteria (PAB) that use the acrylate pathway (Schweiger and Buckel, 1984; Hetzel et al., 2003).

Previous studies on lactate-based chain elongation were based on the metabolism of the type strain *Megasphaera elsdenii*, a DL-lactate-fermenting bacterium that converts D-lactate to acetate, n-butyrate and n-caproate and L-lactate to propionate and n-valerate (Hino and Kuroda, 1993; Weimer and Moen, 2013). In this species, the conversion of acrylate to lactate was found to be catalyzed by an external L-Ldh in activity assays and not by the D-Ldh purified from the strain (Baldwin et al., 1965). It was thus proposed that L-lactate was the substrate for propionate formation in chain elongation bioprocesses with isomerization to D-lactate being a rate-limiting step in n-caproate production (Kucek et al., 2016a). These assumptions may be true for pure cultures of or microbiomes dominated by *M. elsdenii*. However, feeding D-lactate to batch experiments in Chapter 3 did not result in higher conversion rates which were instead observed for the L-enantiomer, although after an adaptation phase. Our results show that lactate is racemized by batch and continuous chain-elongating microbiomes (Chapters 3 and 4) whereas L-lactate is isomerized to an excess of D-lactate when the acrylate pathway takes over (Chapters 3). Many known lactate-elongating bacteria have more than

one Ldh (Liu et al., 2020), suggesting that they are capable of metabolizing both lactate enantiomers. Further experiments could be performed to clarify the role of lactate racemization in chain elongation. The D-lactate excess was presumed to be driven by the selective reduction of this enantiomer in the acrylate pathway of known PAB (Akedo et al., 1983; Schweiger and Buckel, 1984; Kuchta and Abeles, 1985). Similar observations were drawn in rumen fermentation (Counotte and Prins, 1981) and an excess of D-lactate could be used to indicate the occurrence of the acrylate pathway. Although Lar may be excreted by lactate-racemizing bacteria rendering lactate optically inactive (Tatum et al., 1936).

7.3. Key selection pressures to steer MCC production with lactate-elongating reactor microbiomes

To obtain a desired function in reactor microbiomes, selection pressures are applied in adapted environments (bioreactors) to ecologically engineer open cultures and steer product formation (Lawson et al., 2019). Throughout this research, two key selection pressures were identified for achieving MCC production: I) mildly acidic conditions (pH 5.0-6.0) were applied to effectively steer food waste fermentation to lactate (Chapter 2) and lactate elongation to nC4-nC8 (Chapters 1-6); and II) continuous fermentation to steer to MCC production (Chapters 4-6).

7.3.1. Control of propionate formation allows efficient lactate use for chain elongation

In Chapter 2, we hypothesized that mildly acidic conditions would allow lactate production as well as lactate elongation while restricting propionate production. Previous research on lactate elongation was based on the metabolic features of *Megasphaera elsdenii*, which is a lactate-utilizing bacteria that grows at relatively low pH between 4.6-6.6 (Counotte and Prins, 1981; Weimer and Moen, 2013). On the other hand, propionate-producing bacteria (PAB) are known to show limited growth under these conditions (Hettinga and Reinbold, 1972; Tholozan et al., 1992). We successfully controlled propionate production from lactate at electron selectivities ≤26% in (repeated-)batch and below 5% in continuous chain elongation by applying mild acidic pH conditions (pH 5.0-5.5). This allowed the majority of lactate to be elongated to n-butyrate (57-100% selectivity) in batch and to MCC (>66% selectivity) in continuous processes. Propionate production took over chain elongation at near-neutral pH conditions when high doses of zero-valent iron nanoparticles (nZVI) were applied (Chapter 3) and when pH was controlled at 7.0 (Chapter 6). Recently, the beneficial effect of decreasing pH on lactate-based chain elongation was confirmed, with pH >6.0 supporting propionate production (Candry et al., 2020a). Propionate was also produced at low pH when gas mixing was applied at high superficial gas velocities in Chapter 4. Using low gas velocities allows the growth of chain-elongating bacteria over propionate/n-butyrate producers such as *Clostridium tyrobutyricum*. Propionate production can possibly be further limited by promoting DIET-based chain elongation (Chapter 5) which can be achieved by adding conductive materials to chain elongation reactors.

7.3.2. Batch lactate fermentation selects for SCC production while MCC formation requires high concentrations of electron acceptors

In batch reactors, n-butyrate was the main product of lactate fermentation (57-100% selectivity) at initial mildly acidic pH (5.0-5.5) with acetate as electron acceptor (Chapters 2, 3, 5 and 6). The selection of SCC producers in batch systems is related to the faster metabolism of n-butyrate

producers compared to MCC producers (Kim et al., 2018). With abundant substrate availability at the initial batch conditions, the growth of organisms displaying high-flux metabolism (q_s^{max}, μ^{max}) is favored, outcompeting organisms with high-yield metabolism ($Y_{X,ATP}$, K_S) (Andrews and Harris, 1986). This basic theory was likely observed in Chapter 3 where incubations inoculated with biomass from a continuous chain elongation reactor dominated by *Caproiciproducens* (Chapter 5) enriched for n-butyrate producers such as *Clostridium tyrobutyricum*. Similarly to MMC-producing bacteria, *C. tyrobutyricum* also uses the reverse β-oxidation (RBO) pathway to convert lactate and acetate to n-butyrate although the substrate affinity of the terminal enzyme acyl-CoA:acetate transferase (CoAT) differs. *C. tyrobutyricum* uses a butyryl-CoA:acetate transferase (BCoAT) specifically acting on butyryl-CoA(Yang et al., 2021), hampering further chain elongation to longer carboxylates. In consequence, the rapid regeneration of acetyl-CoA allows higher substrate uptake and growth rates for n-butyrate producers using the RBO pathway. One exception seems to be the recent isolate *Ruminococcaceae* bacterium CPB6 which dominates open-culture batch lactate fermentation at more neutral conditions (pH 6.0-7.0) (Zhu et al., 2015; Nzeteu et al., 2018; Wu et al., 2019). It was recently shown that this species possess a caproyl-CoA:acetate transferase (CCoAT) with high preference for caproyl-CoA over butyryl-CoA (~4:1) (Yang et al., 2021), explaining the high n-caproate production by this species (Zhu et al., 2015, 2017). n-Butyrate producers are less tolerant to n-caproate than chain-elongating bacteria (Kim et al., 2018), which likely supports the dominance of *Ruminococcaceae* bacterium CPB6.

Nevertheless, MCC are produced when high concentrations of electron acceptors are present (~100 mM). In Chapter 2, SCC accumulated during repeated-batch fermentation and were elongated with lactate to increasing n-caproate selectivities, enriching overtime MCC-producing microbiomes dominated by *Caproiciproducens* species. A similar outcome was obtained when adding nZVI to batch experiments, where lactate, resulting from the hydrolysis of lactate oligomers, was used to elongate n-butyrate late in the incubations (Chapter 3). Addition of electron acceptors and external hydrogen also promotes MCC production in batch pure cultures of *Ruminococcaceae* bacterium CPB6 or microbiomes dominated by related species (Nzeteu et al., 2018; Wang et al., 2018; Wu et al., 2019). Additional hydrogen did not promote MCC formation in our batch experiments where *C. tyrobutyricum* species were dominant (Chapter 3), likely due to the inability of this species to produce MCC.

7.3.3. Continuous chain elongation at mildly acidic conditions yields high MCC selectivities similar to ethanol-based processes

MCC selectivities attainable in continuous lactate-based chain elongation were substantially improved to comparable values as ethanol-based chain elongation, showing that MCC production from lactate can be as effective as from ethanol. The obtained MCC selectivities (67-85% [e^- eq MCC *per* e^- eq products]) are higher than values reported in recent studies (<42%) converting lactate (Candry et al., 2020a) or lactate and n-butyrate with in-line extraction (Kucek et al., 2016a). The improved MCC selectivities are similar to those reported for ethanol-based chain elongation bioprocesses converting ethanol and acidified food waste (82%) (Roghair et al., 2018c) and ethanol and acetate (80-94% MCC *per* total carboxylates) (Grootscholten et al., 2013d) (up to 92% MCC *per* total carboxylates in Chapter 6).

Open-culture chain elongation of lactate was previously limited to n-caproate (Zhu et al., 2015; Kucek et al., 2016a), with *Ruminococcaceae* strain CPB6 producing n-heptylate but not n-caprylate when supplied with different electron acceptors (Wang et al., 2018). Here we obtained n-heptylate and n-caprylate at pH 5.0-5.5. Although they were produced at relatively low selectivities. Both pH and acetate supply likely influenced MCC formation. MCC selectivities were slightly lower from lactate at pH 5.5 (67-72%) compared to when acetate was supplied at pH 5.0 (76-80%). In contrast, significant n-heptylate selectivities (5-7%) were observed with lactate at pH 5.5 whereas acetate supplementation at pH 5.0 limited its formation (≤1%). Likely, low pH decreased propionate formation and the supplied acetate was elongated to even-chains, both limiting the formation of odd-chain MCC. Adding propionate promoted n-heptylate (9%) at the expense of n-caprylate formation (Chapter 4). Similar n-heptylate selectivities have been achieved in ethanol and propionate elongation (9-23%) (Grootscholten et al., 2013c; Roghair et al., 2018a). Similarly to ethanol-based chain elongation, selectivity of odd-chains could possibly be improved by tuning the electron donor-to-acceptor ratio (Candry et al., 2020b) where a trade-off between propionate and n-valerate elongation to n-heptylate, and elongation of even-chains may be found. n-Caprylate electron selectivities were 1-3% regardless of acetate supplementation.

7.3.4. Uncultured lactate-elongating *Caproiciproducens* species – effective, acid-tolerant bacteria of the future

The reactor microbiomes developed during the course of this research show that dominant uncultured species belonging to the genus *Caproiciproducens* produce MCC from lactate. In Chapter 2 we observed that chain elongation relied on metabolic cross-feeding between homofermentative *Lactobacillus* and *Caproiciproducens* with lactate as an important intermediate. The following research in Chapters 4-6 established that *Caproiciproducens* species enriched in continuous reactor microbiomes were responsible for lactate conversion to MCC at pH 5.0-5.5. The *Caproiciproducens*-enriched microbiomes (roughly 50-70% relative abundance) produced n-caproate at 5.0-7.5 $g \cdot L^{-1}$ and tolerated high concentrations of its undissociated form (up to 26 mM; 3 $g \cdot L^{-1}$), which are two-times higher than the inhibitory concentrations reported for ethanol-based chain elongation (7.5 mM) (Ge et al., 2015). This tolerance to high n-caproate concentrations is also extended to pH 6.0 at which *Caproiciproducens*-dominated microbiomes (related to *Ruminococcaceae* bacterium CPB6) produced 20-34 $g \cdot L^{-1}$ n-caproate (12-20 mM undissociated) (Zhu et al., 2021), setting a new record over ethanol-based chain elongation (25.7 $g \cdot L^{-1}$) (Roghair et al., 2018c). Thus, species from this genus seem to be efficient chain-elongating organisms that may become more relevant in future chain elongation processes involving lactate. The enriched species in our research were relatively distant from the type strain *Caproiciproducens galactitolivorans* (90-95% similarity; based on partial 16S rRNA gene). Although the type strain and other recently isolated *Caproiciproducens* species are described to grow on carbohydrates (Kim et al., 2015; Flaiz et al., 2020; Esquivel-Elizondo et al., 2021), a recent metanalysis highlighted the ubiquity of *Caproiciproducens*, and other members of the family *Oscillospiraceae*, in lactate-based chain elongation processes using synthetic media and complex residual streams (Candry and Ganigué, 2021). Thus, their isolation and study may help to further improve MCC production from lactate.

7.4. *In situ* product separation with biocompatible materials further improves MCC production rates and selectivities

MCC productivities were enhanced by ~50% when including *in situ* product separation either through extractive fermentation or *in situ* adsorption with GAC (Chapters 6 and 7), probably as a result of alleviated product inhibition. At the acidic pH conditions applied (pH 5.0), about half of the n-caproate is in its undissociated form which is thought to be toxic to bacteria (Roghair et al., 2018b). Removing part of the MCC produced (composed of mainly n-caproate) allowed higher substrate conversions and productivities. Similarly, in-line extraction improves chain elongation rates from ethanol (Ge et al., 2015). The highest combined MCC production rates and selectivities were obtained in Chapter 6 from extractive chain elongation at pH 5.0 (11.5 g $COD \cdot L^{-1} \cdot d^{-1}$; 84% e^- eq MCC *per* e^- eq products). These values are similar to ethanol-based chain elongation from ethanol-rich or ethanol-supplemented organic residues (10-12 g $COD \cdot L^{-1} \cdot d^{-1}$) (Ge et al., 2015; Roghair et al., 2018c) and are close to methane productivities achieved from lactate-rich acidified vegetable waste in UASB anaerobic digesters (~17 g $COD \cdot L^{-1} \cdot d^{-1}$) (Wu et al., 2016). Thus showing that the efficiency of MCC production from lactate can be further improved. With ethanol as electron donor, in-line extraction has been shown to increase the production of the longer carboxylate n-caprylate (Kucek et al., 2016b). Since n-caprylate production from lactate was shown to be feasible in continuous experiments, optimizing fermentation and in-line extraction could possibly increase n-caprylate selectivities by using higher substrate concentrations and extraction rates as is already more optimized for ethanol-based chain elongation (Kucek et al., 2016b).

7.5. Challenges and opportunities in MCC production from food waste and lactate

7.5.1. Enhanced hydrolysis for efficient conversion of high-solids feedstocks

Chain elongation from food waste was limited by low hydrolysis of particulate substrates with n-caproate production reaching only 12% of the total chemical oxygen demand (COD) (Chapter 2). Slightly higher conversion efficiencies have been obtained using fresh food waste in leach-bed reactors (19% COD conversion) (Nzeteu et al., 2018) but so far COD conversion to MCC has been limited to <20% when using high-solids organic residues without ethanol supply (Stamatopoulou et al., 2020). This highlights the relevance of developing efficient processes that allow to utilize larger fractions of these substrates. To achieve higher substrate conversions, existing hydrolytic pretreatments could be applied (e.g. chemical and enzymatic). Novel bioprocesses may also be developed such as consolidated fungi-bacteria microbiomes (Shahab et al., 2020).

7.5.2. Biomass retention may enhance lactate conversion efficiency but granulation drivers in biochemical-producing reactors need to be elucidated

Despite competitive MCC production rates were obtained in continuous reactors, a major fraction of lactate was left unconverted during MCC production without product separation (>45%). Substrate conversion and MCC production rates from lactate were improved to some extent by adding propionate as electron acceptor (Chapter 4) and implementing *in situ* product separation methods (Chapter 6 and 7). However, further improvements can be achieved by increasing biomass

concentrations through the addition of carrier materials or obtaining granular sludge. Several theories exist around the granulation phenomenon (Hulshoff Pol et al., 2004), with selection pressures reported to promote biomass aggregation and eventual granulation in anaerobic reactors including applying shear force through gas supply (Wu et al., 2009), providing complex nutrients (Gagliano et al., 2020), shortening hydraulic retention times (Carvajal-Arroyo et al., 2019) or applying intermittent regimes of substrate supply and settling times in sequencing batch reactors (Tamis et al., 2015). In Chapter 4, granulation was not observed in an upflow reactor with added proteins (yeast extract and tryptone) and nitrogen gas supply at different gas velocities. Literature shows, nonetheless, that MCC-producing granules can be obtained in ethanol-fed reactors showing excessive ethanol oxidation and slight methanogenic activity (Roghair et al., 2016), or in reactors converting complex organic feedstock (thin stillage) (Carvajal-Arroyo et al., 2019; Wu et al., 2020), both achieving high MCC production rates (27-31 g $COD \cdot L^{-1} \cdot d^{-1}$) (Roghair et al., 2016; Carvajal-Arroyo et al., 2019; Wu et al., 2020). However, it is not known what the effects of syntrophic processes or individual substrates and nutrients present in complex residues are on granulation. Finding conditions triggering granulation in lactate-fed reactors will require further research (Hulshoff Pol et al., 2004) with defined substrates using self-assembled or synthetic microbiomes. Granular sludge could also increase carbon recovery through syntrophic processes (see following section).

7.5.3. Increasing carbon efficiency through carbon dioxide recapture

For every lactate used for chain elongation, one molecule of CO_2 is produced during pyruvate oxidative decarboxylation to acetyl-CoA (Figure 7.1). This limits the carbon efficiency of pure-culture lactate-based chain elongation given that known lactate-elongating bacteria do not seem to be capable of reducing CO_2 to carboxylates (Tao et al., 2017; Liu et al., 2020). More complex reactor microbiomes, on the other hand, could achieve higher carbon efficiencies if CO_2 reduction to carboxylates with H_2 or electrons by homoacetogenesis occurs along with chain elongation. Several potential homoacetogenic species were enriched in both batch (Chapter 3) and continuous (Chapter 4 and 7) reactors. However, carbon lost to CO_2 was still significant and MCC carbon selectivities in efficient continuous chain elongation ranged between 50-65%. Homoacetogenic activity and carbon recapture seemed low in continuous reactors (0.7-1.4 mol CO_2·mol $lactate^-$) while extensive H_2 and CO_2 consumption was typically observed late in the batch incubations when pH increased close to neutrality. Since homoacetogenic bacteria require four H_2 molecules to reduce two CO_2 to acetate (H_2/CO_2 ratio = 2) and the theoretical stoichiometric H_2/CO_2 ratio produced from lactate is either 1 or 2/3 when n-butyrate or n-caproate are produced, CO_2 recapture would be limited to 33-50% (Chapter 3). The additional electrons required for full CO_2 reduction may be provided with external H_2 or through a cathode (Isipato et al., 2020). Increased MCC carbon selectivities (up to 72%) were recently reported in H_2-supplemented batch reactors at neutral pH conditions where homoacetogens and alcohol-elongating species were enriched (Wu et al., 2019). How mildly acidic pH and high concentrations of undissociated MCC affect the growth of homoacetogens may be studied to evaluate their potential co-occurrence within chain-elongating microbiomes.

7.6. The lactate platform: homogenized complex substrates and diversity of products

Lactate typically accumulates during storage of complex organic residual materials e.g. food waste (Chapter 2) and storage conditions could be optimized to maximize lactate production (Zhang et al., 2021). In this way, different organic feedstocks could be pooled together and the initial mixtures of carbohydrates and proteins homogenized to mainly lactate to be further converted into a variety of carboxylates simultaneously or after storage. This may be achieved due to the metabolic capabilities of lactic acid bacteria (LAB) to ferment C5-C6 oligo and monosaccharides (Hofvendahl and Hahn-Hägerdal, 2000; Gänzle and Follador, 2012) and their tolerance to oxidative stress and acidic pH conditions (Gänzle, 2015). These physiological properties of LAB have inspired the development of synthetic cross-kingdom consortia to convert lignocellulose through the lactate platform (Shahab et al., 2020).

7.6.1. High-strength, nutrient-rich residues are suitable feedstock supporting lactate formation

The fermentation route used in open-culture processes may depend on the type of substrate and the selective pressures applied. LAB are known for requiring complex nutrient demands and displaying high-flux metabolism (Rombouts et al., 2020; Regueira et al., 2021). Thus, they thrive in complex substrates where fermentable carbohydrates and complex nutrients are abundant. Conditions like high organic loading rates and acidic pH promote lactate production from food waste (Kim et al., 2016b). Apart from food waste, also garden waste, residues from breweries, municipal solid waste, enzymatically-pretreated lignocellulose and food-processing wastewater are feedstocks potentially supporting lactate accumulation (Pejin et al., 2018; Xu et al., 2018; López-Gómez et al., 2020). These substrates could in principle be easily integrated in existing two-stage processes such as the currently used by the company ChainCraft (EFSA (European Food Safety Authority), 2018), where the acidification step could be complemented with or directed toward lactate production to supply SCC and/or lactate to a following chain elongation reactor. Ethanol supply may be reduced or fully avoided in this way. During the course of this research, many bioprocesses aimed at MCC production relied on lactate accumulation to achieve chain elongation from organic residues such as thin stillage (Carvajal-Arroyo et al., 2019), food waste (Nzeteu et al., 2018) and acid whey (Duber et al., 2018; Xu et al., 2018). One challenge in using lactate as intermediate may be the selection of homolactic *vs* heterolactic fermentation to reduce carbon and energy losses to by-products other than lactate.

7.6.2. Expanding the product spectrum of lactate-based chain elongation to isobutyrate, isocaproate and n-heptanoate

7.6.2.1. Potential isobutyrate formation through direct interspecies electron transfer

The production of isobutyrate with lactate as electron donor was obtained for the first time with reactor microbiomes (Chapter 6). Isobutyrate is a branched SCC that has been obtained in pure cultures from lactate (Liu et al., 2020) or one-carbon compounds such as methanol and H_2/CO_2 fermentation (Petrognani et al., 2020) and from methanol with reactor microbiomes (Chen et al., 2016a; de Leeuw et al., 2020). Although the formation mechanism remains unproven, conductive materials i.e. granular activated carbon (GAC) and nickel foam (NF) presumably promoted direct

interspecies electron transfer (DIET) between lactate-oxidizing bacteria and electron-accepting, chain-elongating bacteria. Based on literature reports, it was hypothesized that electron-accepting bacteria could use a combination of electrons and/or H_2 to reduce acetate and/or CO_2 to isobutyrate. The potential uptake of extracellular electrons is supported by research done with bioelectrochemical systems were isobutyrate has been produced from cathode-assisted fermentation of substrates such as CO_2 (Vassilev et al., 2018) and a mixture of glucose, ethanol and acetate (Villano et al., 2017). This DIET-based chain elongation may display increased overall conversion rates compared to single-species fermentative pathways, resulting from division of labor between two organisms (Tsoi et al., 2018) and the smoothed electron transfer by conductive materials (Viggi et al., 2014). Further research using GAC, NF or bioelectrochemical systems could enrich such organisms to improve isobutyrate production and study its formation mechanisms with either H_2 or electrons.

7.6.2.2. Two-stage lactate conversion to odd-chain and branched MCC

Currently, n-caproate is the main MCC produced in lactate-based chain elongation in the present research (Chapter 4-6) and literature reports (Kucek et al., 2016a; Candry et al., 2020a). To broaden the product spectrum of the process, lactate can be used as electron donor in two-stage chain elongation systems. In Chapter 4, we showed that propionate can be elongated with lactate to n-heptylate. A two-stage system for odd-chain MCC production was proposed, where lactate is converted to propionate in a first reactor (e.g. under high gas velocities or neutral pH) and then propionate is elongated with additional lactate to n-valerate and n-heptylate in a second reactor. With propionate as electron acceptor, similar n-heptylate selectivities (9%) to ethanol and propionate elongation (9-23%) (Grootscholten et al., 2013c; Roghair et al., 2018a) were achieved (Chapter 4). In a similar fashion, lactate fermentation could be steered toward isobutyrate in a first stage (e.g. batch fermentation with conductive materials [Chapter 6]) for further chain elongation with lactate to isocaproate. n-Heptylate has previously been produced from propionate in ethanol-elongating microbiomes (Grootscholten et al., 2013c) where propionate was proposed to be sourced from biomass fermentation. Isocaproate production has been obtained with ethanol-elongating microbiomes as well with the proposed process requiring methanol in a first step (to produce iC4) (Chen et al., 2016b; de Leeuw et al., 2020) and ethanol in the second step (to elongate iC4 to iC6) (de Leeuw et al., 2019). Producing odd-chain and branched MCC from lactate would increase the availability of these chemical building blocks and reduce the dependency on different feedstock for their production. The enzyme systems used in chain elongation may have lower affinities for propionate and isobutyrate elongation compared to acetate (formed *in situ* from lactate), which may require tuning lactate use and lactate-to-electron acceptor ratio for selective elongation to branched and odd-chain MCC, This could be done following similar approaches to ethanol-based chain elongation processes (de Leeuw et al., 2019; Candry et al., 2020b).

7.7. Implications of the proposed product separation processes

7.7.1. Trade-off between process complexity, product specificities and energy efficiency

The fact that chain elongation with lactate is best favored at pH values close to the pK_a of MCC (pK_a nC6-nC8 ~ 4.9) enables the application of *in situ* or in-line product separation techniques that take advantage of MCC hydrophobicity, such as liquid-liquid extraction (LL-Ext) or adsorption. Common MCC separation approaches in chain elongation involve membrane-based LL-Ext (pertraction) at

mildly acidic conditions (Ge et al., 2015; Kucek et al., 2016b), which was previously applied in lactate-based chain elongation (Kucek et al., 2016a), and ion exchange at near-neutral pH (Yu et al., 2019). Recent developments aim at obtaining neat carboxylic acids and decreasing energy input (Figure 7.1). Neat medium-chain carboxylic acids with low energy input have been obtained in three-step DSP trains by coupling liquid-liquid extraction, back-extraction and either water electrolysis or electrodialysis (Xu et al., 2015, 2021). A modelled two-step process involving LL-Ext and distillation was also projected to have a low energy demand (Scarborough et al., 2018b). In Chapter 6, a two-step DSP consisting of MCC adsorption on GAC followed by thermal desorption was proposed as an alternative to obtain neat medium-chain carboxylic acids after spontaneous phase separation. Although the actual energy demand and MCC desorption efficiency was not evaluated, the estimated minimum energy input for thermal desorption is within the range of technologies under development (Figure 7.1). Further improvements in adsorbent material and process design may make *in situ* adsorption an attractive separation process with potential trade-off between DSP complexity and energy demand. For instance, thermal desorption under vacuum conditions may decrease the energy input due to lowered boiling points (Saboe et al., 2018). Decreased production costs may come with reduced complexity since DSP usually represents between 30 to 40% of biochemicals production costs (Straathof, 2011). The choice of energy source used is also relevant since DSP contributes considerably to the carbon and environmental footprints (Chen et al., 2017; Saboe et al., 2018). While electricity may be easily obtained from renewable sources for electrodialysis processes, MCC thermal desorption may require temperatures >205°C (boiling point of n-caproate) which would demand burning hydrocarbons or biogas.

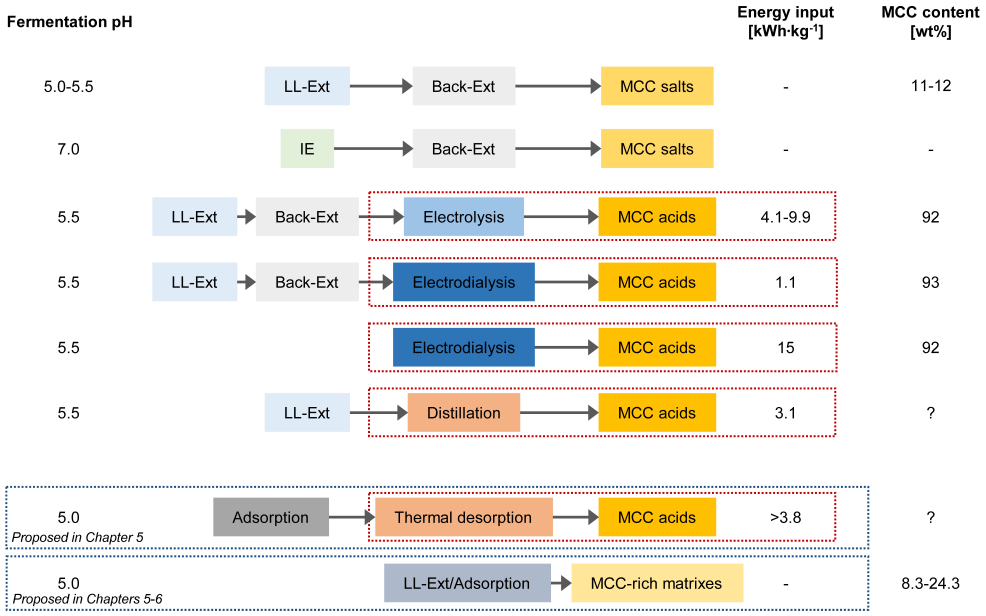

Figure 7.1 Product separation approaches developed in lab-scale chain elongation processes. Liquid-liquid extraction (LL-Ext) followed by back-extraction (Back-Ext) to produce MCC salts has been used for ethanol- (Ge et al., 2015; Kucek et al., 2016b) and lactate-based (Kucek et al., 2016a) chain elongation with MCC contents estimated from Urban et al. (2017). Ion exchange (IE) and back-extraction has been used in ethanol-based chain elongation (Yu et al., 2019) as well as DSP

using water electrolysis (Xu et al., 2015, 2021) and electrodialysis (Xu et al., 2021) to obtain neat acids. LL-Ext coupled to distillation was modelled for a process converting lignocellulose stillage (Scarborough et al., 2018b).

Further simplified DSP schemes were proposed by using application-compatible solvents/adsorbing materials (Chapter 5-6). MCC-loaded organic solvents such as vegetable oils and porous materials like GAC or biochar could be harvested as potential novel products for direct application without further purification steps e.g. direct use for animal nutrition applications or soil amendments. This implies that the MCC-accumulating matrixes are the main co-products and their use must be justified by the potential techno-economic and environmental footprint advantages.

7.7.2. Technical challenges in proposed separation processes -- Improving extraction flux and adsorption selectivity

Although extractive chain elongation with sunflower oil increased the productivity of fermentation and accumulated high concentrations of MCC in sunflower oil (Chapter 6), most of the produced MCC remained in the effluent due to limited extraction fluxes. This can be further improved by applying lower pH conditions, using solvents with higher partition coefficients (e.g. oleyl alcohol) and increasing the interface contact area between the organic and aqueous phases (e.g. membrane-based liquid-liquid extraction). When implementing *in situ* adsorption, improved mass transfer or several packed columns may be needed to keep low MCC effluent concentrations whilst reaching high MCC loadings on GAC. Additionally, most of the energy required for MCC recovery is used for evaporation of the adsorbed water (Chapter 5). Thus, reducing water adsorption or content before thermal regeneration would significantly decrease the energy demand. Finding alternative desorption methods using renewable energy may improve the sustainability of the proposed DSP. Achieving higher MCC-loads in both solvents and adsorbing materials would also decrease the need of these co-products when intended for direct applications.

7.7.3. Potential drivers and limitations of novel product formulations with simplified DSP

The use of application-compatible solvents and adsorbents in chain elongation has the potential to generate products with novel features. In Chapter 6, biocompatible organic solvents such as vegetable oils, food waste-derived oil and oleyl alcohol were proposed to be enriched with MCC for feed, food and fuel applications. Vegetable oils are already used as feed additives (Hess et al., 2008; Li et al., 2019) which may facilitate the introduction of MCC-rich vegetable oils to the existing market. Unsaturated long-chain carboxylates, present in vegetable oils, and MCC may show synergistic effects and lead to novel applications in food and feed applications (Jackson and Jewell, 2020). Porous carbons are also being investigated as feed additives (Schmidt et al., 2019) and, when loaded with MCC, could potentially deliver slowly-released MCC for nutritional or methane mitigation purposes in ruminal species. There is evidence that n-caproate has the potential to inhibit hydrogenotrophic methanogens (Roghair et al., 2018b) which are the main source of methane in rumen (Patra et al., 2017). The methane inhibitory effects of medium- and long-chain carboxylates persists for a longer period of time than other inhibitors (Patra et al., 2017) and may be further extended depending on the residence time of porous carbons in the rumen. The feasibility of these applications will likely be influenced by the production costs, applicable regulations and their competitiveness compared with other available additives such as alternative hydrogen sinks (e.g. nitrate) or antimicrobials (e.g. 3-nitrooxypropanol) (Patra et al., 2017). The resulting manure rich with

carbons may also show improved properties for soil amendment when cascading approaches are applied (Schmidt et al., 2019).

The choice of fermentation substrate for chain elongation, co-product (solvent or adsorbent) and process design may determine what is a suitable application. For instance, fermenting unspoiled sidestreams from the food industry using food-grade vegetable oils as solvent could more easily meet safety regulations for food or feed applications than fermenting food waste and using residual oils. On the other hand, the oil contained in food waste can itself be used as solvent and reduce the demand of external vegetable oil. These types of MCC-enriched residual oils may be used for low-grade applications like biodiesels with low pollutant emissions (Kannengiesser et al., 2016; Cheng et al., 2018). Although carefully selected and processed streams could still be used to valorize the nutritional value of unsaturated long-chain carboxylic acids present in food waste components (Canakci, 2007).

7.7.3.1. Solvent demand for MCC-rich products

To illustrate the effect of using different solvents, the potential demand of vegetable and waste-derived oils is estimated. Considering that vegetable oils like sunflower oil can be enriched with 8.3 wt% MCC (Chapter 6), 25-30·10^6 ton·y^{-1} of vegetable oil would be needed to accumulate the MCC potentially obtained from the yearly food waste production in EU through lactate-based chain elongation (see Figure 7.2). This equals to 16-19% of the global vegetable oils production (~160·10^6 ton·y^{-1} in 2012) (Schmidt, 2015), thus posing a relatively high stress on their availability for current applications. When using food waste-derived oil as endogenous solvent, the available oil (assuming an oil content of 26 wt% in food waste (Carmona-Cabello et al., 2018)) could accumulate 77-91% of the MCC potentially produced from lactate-based chain elongation.

7.8. Potential of aviation fuels production from food waste through lactate-based chain elongation

An attractive application of MCC is the production of biodiesels and sustainable aviation fuels. While electric and hydrogen-powered aircrafts are under development, alternative drop-in biofuels may be obtained in integrated (electro)biorefineries upcycling MCC (Urban et al., 2017) and residual organic oils (SkyNRG, 2019). Previous estimations for the bioconversion of food waste and ethanol reported the potential to produce high quantities of MCC and aviation fuels (Roghair et al., 2018c). However, ethanol is the main source of MCC (~75% in COD basis) (Roghair et al., 2018c) which seems to limit the potential of ethanol-based chain elongation for fuels applications since the current global ethanol production (0.84·10^9 barrels·y^{-1}) (Roghair et al., 2018c) is not enough for converting the food waste produced worldwide (Figure 7.2). Although the development of ethanol-producing fermentation processes from residual materials may increase its future availability. The alternative of using lactate as endogenous electron donor yields about 10-times less MCC and fuels, with the advantages of not needing external ethanol and reducing the chemicals input, both of which may impact the environmental footprint of the process (Chen et al., 2017). Single-stage and two-stage lactate-based chain elongation processes have the potential to produce roughly 10% (0.2-0.3·10^9 barrels·y^{-1}) of the aviation fuel demand (~2.7·10^9 barrels·y^{-1}) (Roghair et al., 2018c) from the worldwide food waste generation (Figure 7.2). Currently, single-stage chain elongation have reached MCC yields of 23.8 g

MCC·kg FW^{-1} (n-caproate) (Nzeteu et al., 2018). An hypothetical two-stage process converting food waste to lactate in a thermophilic reactor (64 g lactate·kg FW^{-1}) (Kim et al., 2016b) followed by extractive lactate-based chain elongation (43.8 g MCC·kg lactate^{-1} [Chapter 6]) would reach a 20% higher MCC production (28.1 g MCC·kg FW^{-1} [nC6]). However, more chemicals are probably needed for pH control in the acidification (alkali) and chain elongation (acid) stages in the two-stage process. On the other hand, pH is to some extent self-regulated in single-stage chain elongation since n-caproate production from lactate neutralizes 2/3 of the protons produced during acidification (Chapter 2). The chemical input for pH control during lactate production is not reported but an acid input of 0.75 g HCl·g MCC^{-1} was required to control pH at 5.0 during lactate-based chain elongation with synthetic medium. The chemical input needed is determined by the systems buffer capacity (alkalinity and acidity) of the substrate, as discussed in Chapter 2. Hence, HCl input will be lower when using organic residues with a higher acidity than the synthetic medium. The future production of alkali (OH^-) and acid (H^+) through on-site water electrolysis may be a more sustainably source of these chemicals.

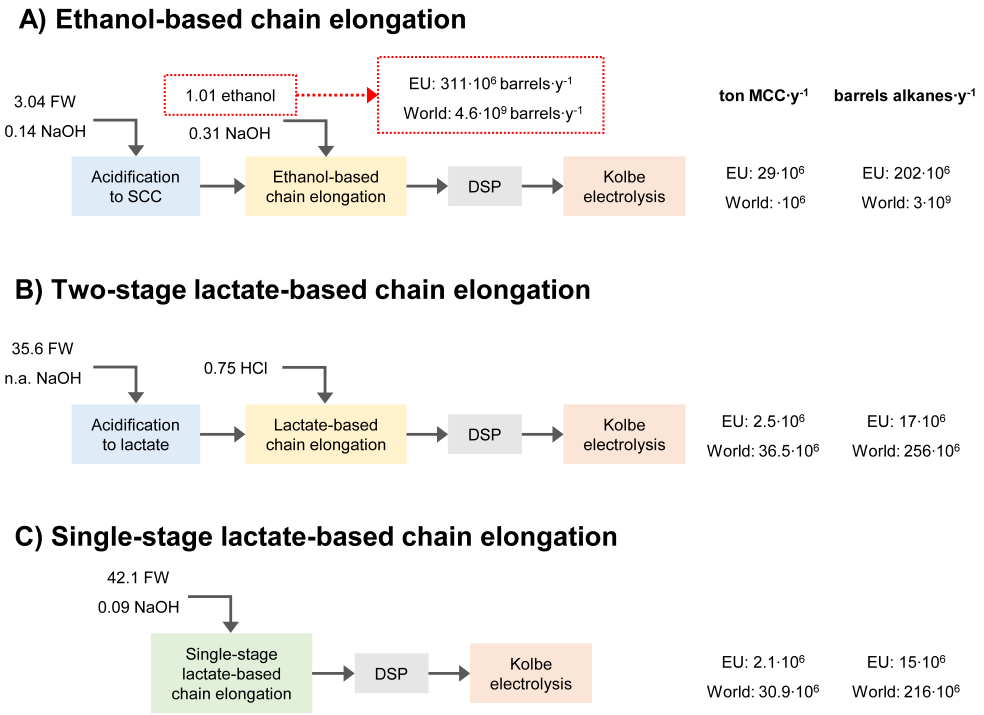

Figure 7.2 Mass balance of chain elongation bioprocesses (ton of materials *per* ton MCC produced) converting food waste (FW) and the potential of medium-chain carboxylates and aviation fuel production based on food waste generated in the European Union (88·10^6 ton·y^{-1}) (Stenmarck et al., 2016) and worldwide (1.3·10^9 ton·y^{-1}) (FAO, 2011). (**A**) Chain elongation from ethanol and acidified food waste (Roghair et al., 2018c). Red lines depict the ethanol demand. (**B**) Hypothetical two-stage lactate-based chain elongation coupling thermophilic lactate production (Kim et al., 2016b) and extractive lactate-based chain elongation (Chapter 6). NaOH input during acidification to lactate is not available. MCC yield and acid input of extractive chain elongation were obtained from experiments with synthetic medium (Chapter 6; R1, period II-a). (**C**) Single-stage food waste fermentation to MCC with lactate as intermediate assuming a yield of 23.8 g MCC·kg FW^{-1} (Nzeteu et al., 2018) and alkali input of 87.1 g NaOH·kg MCC^{-1} (Chapter 2, cycle 3 of 1L-RBF). Assumptions include no losses in the downstream processing (DSP) and a Kolbe electrolysis efficiency of 0.61 g alkane·g MCC^{-1} (Roghair et al., 2018c) (**A**-**C**).

7.9. Concluding remarks

Open cultures were engineered to produce medium-chain carboxylates from food waste and lactate. It is clear that lactate is a versatile intermediate in the bioprocessing of complex organic residues, avoiding the need of supplying external electron donors and allowing the production of a range of elongated carboxylates. Developing alternative processes such as DIET-based and electrode-assisted chain elongation with integrated *in situ* product separation may be essential to obtain novel products and further expand the applicability of chain elongation. Attaining robust bioprocesses that offer a flexible product spectrum will eventually facilitate the transition to a biobased circular economy.

Supplementary Material

Supplementary material – Chapter 2

Consecutive lactate formation and chain elongation from food waste

Carlos A. Contreras-Dávila, Víctor J. Carrión, Vincent R. Vonk, Cees J.N. Buisman and David P.B.T.B. Strik

Microbiome composition analysis

Samples were taken from CSTR and RBF experiments on days depicted in Figure S1. DNA sequences were processed with the DADA2 pipeline and the entire ASV table was used and normalized using the function cumNorm from the R package metagenomeSeq (v.1.12) (Paulson et al., 2016). We used a cumulative-sum scaling (CSS) method, which calculates the scaling factors equal to the sum of counts up to a determined quantile to normalize the read counts, in order to avoid biases generated with current sequencing technologies due to uneven sequencing depth (Paulson et al., 2013). A Bray–Curtis dissimilarity matrix was calculated and used to build Principal Coordinate Analyses and Constrained Principal Coordinate Analysis using the function capscale retrieved from Vegan package (v.2.3-2) (Oksanen et al., 2019) and implemented in the Phyloseq package (v.1.10) (McMurdie and Holmes, 2013), both in R. The nonparametric adonis test was used to assess the percentage of variation explained by the status grouping along with its statistical significance. Permutational multivariate analyses of variance were performed to evaluate the significance of the constrained principal coordinate analyses, both retrieved from Phyloseq and Vegan packages. To compare the differences in taxonomic composition and to assess whether some bacterial taxa were differentially abundant, we conducted a statistical analysis in which we assessed separately the read counts at ASV level. The function calculateEffectiveSamples from the metagenomeSeq R package was applied to the filtered ASV table and features with less than the average number of effective samples in all features were removed. We used normalized tables applying the CSS normalization as described above. Then, a Zero-Inflated Gaussian Distribution Mixture Model was applied using the fitZig function from metagenomeSeq. With the coefficients from the model, we applied moderated t-tests between accessions using the makeContrasts and eBayes commands retrieved from the R package Limma (v.3.22.7) (Ritchie et al., 2015). Obtained P-values were adjusted using the Benjamini–Hochberg correction method. Differences in the abundance of taxa between accessions were considered significant when adjusted P-values were lower than 0.05. Volcano plots were built to graphically represent the results of the moderated t-tests using the R package ggplot2 (v.2.0.0) (Wickham, 2008).

Phylogenetic analysis and identity network

A multiple alignment sequences of approximately 400 bp was performed using Muscle v3.7 (Edgar, 2004) with the default parameters. This multiple alignment was used to create an approximate maximum- likelihood tree using FastTree v2.1.8 (Price et al., 2010) with default parameters. The tree was visualized with iTOL (Letunic and Bork, 2016). For the identity network, using the multiple sequence alignment created for the phylogenetic tree, a pairwise distance was calculated using Clustal Omega - 1.2.3 (Sievers et al., 2011) for all detected 16S rDNA sequences and thresholds were settled at 0.9 and 0.95 for the clustering. Network visualizations were constructed using Cytoscape (v. 3.7.1) (Shannon et al., 2003).

Co-occurrence networks

Non-random co-occurrence analyses were performed using SparCC. For this, we calculated SparCC correlations between microbial taxa at ASV level based on the 16S rDNA extracted from the metagenomics reads. For each network analysis, P-values were obtained by 99 permutations of random selections of the data table, subjected to the same analytical pipeline. SparCC correlations with a magnitude > 0.8 or < -0.8 and statistical significance ($P < 0.01$) were included into the network analyses. The nodes in the reconstructed networks represent the ASVs, whereas the edges (that is, connections) correspond to the correlation between nodes. The topology of the network was calculated based on a set of measures, including number of nodes and edges, modularity, number of communities, average path length, network diameter, averaged degree and clustering coefficient (Newman, 2003, 2006). Co-occurrence analyses were carried out using the Python module 'SparCC' and network visualizations were constructed using Cytoscape (v. 3.7.1) (Shannon et al., 2003).

Table S1. Acidity and alkalinity measurements.

	Concentrated food waste	**Concentrated food waste pH 6.0**	**Mixture 10% v/v food waste pH 6.0 + mineral medium***
Acidity[1] (mg CaCO3/L)	15036±152	4109±70	2094±44
Alkalinity[2] (mg CaCO3/L)	-	6664±443	810±53

1: total acidity to pH 8.3. 2: total alkalinity to pH 4.3. *Acidity was measured to pH 7.0

Table S2. Carbon selectivity, conversion efficiency, n-caproate production rates and hydroxide input in food waste repeated-batch fermentation.

		Cycle 1	Cycle 2	Cycle 3
	1L-RBF			
Carbon specificity (%)	***ethanol***	2.3±0.5	3.7±0.1	6.8±0.1
	acetate	31.3±0.5	21.8±0.1	15.8±0
	propionate	5.3±0.4	4.1±0.1	4.7±0
	isobutyrate	2.8±0.1	3.6±0	2.4±0
	n-butyrate	48.5±1	46.7±0.2	31.2±0.2
	b-valerate	2.1±0	3.3±0.1	2.7±0.1
	n-valerate	0.7±0.7	2.1±0	3.8±0
	isocaproate	0±0	0±0	0±0
	n-caproate	9.4±0.5	18.4±0.4	38.2±0
	n-heptanoate	0±0	0±0	0.4±0
	n-octanoate	0±0	0±0	0.7±0.1
COD_T conversion efficiency (%)	***n-butyrate***	14.9±0	11.1±0	9.5±0.1
	n-caproate	3.1±0.1	4.7±0.1	12.4±0
n-C6 production rate during lactate consumption (g COD/L-d)		0.55	1.48	1.93
Overall n-C6 production rate (g COD/L-d)		NA	NA	1.35
Hydroxide input	***mol OH^- /mol MCFA***	4.35	2.96	0.77
	mol OH^- /kg COD-FA	1.35	1.54	0.99
	0.3L-RBF			
Carbon specificity (%)	***ethanol***	4.4±2.7	5.4±2.9	6±2.3
	acetate	24±5.4	14.2±5.1	10.4±1.2
	propionate	8.5±0.5	6.4±0.3	4.2±1.2
	isobutyrate	3±0.3	2±0	1.6±0.3
	n-butyrate	37.6±0.4	42±4.6	40.6±0.8
	b-valerate	2.3±0.2	2±0.1	2.2±0.1
	n-valerate	2.9±0.2	7±1.8	9±2.4
	isocaproate	0.1±0.2	0.1±0	0.1±0.4
	n-caproate	10.3±0.2	17.3±7.6	22.4±6.2
	n-heptanoate	0.2±0.1	0.2±0.1	0.2±0
	n-octanoate	0.1±0	0±0	0±0.2
COD_T conversion efficiency (%)	***n-butyrate***	15.7±0.1	17.6±0.3	14.5±0
	n-caproate	4.6±0.03	7.7±0.6	8.5±0.3
n-C6 production rate during chain elongation phase (g COD/L-d)		0.2±0.1	0.6±0.1	0.5±0.1
Overall n-C6 production rate (g COD/L-d)		0.1±0	0.3±0	0.3±0
Hydroxide input	***mol OH^- /mol MCFA***	1.47	0.51	0.47
	mol OH^- /kg COD-FA	2.24	0.99	0.79

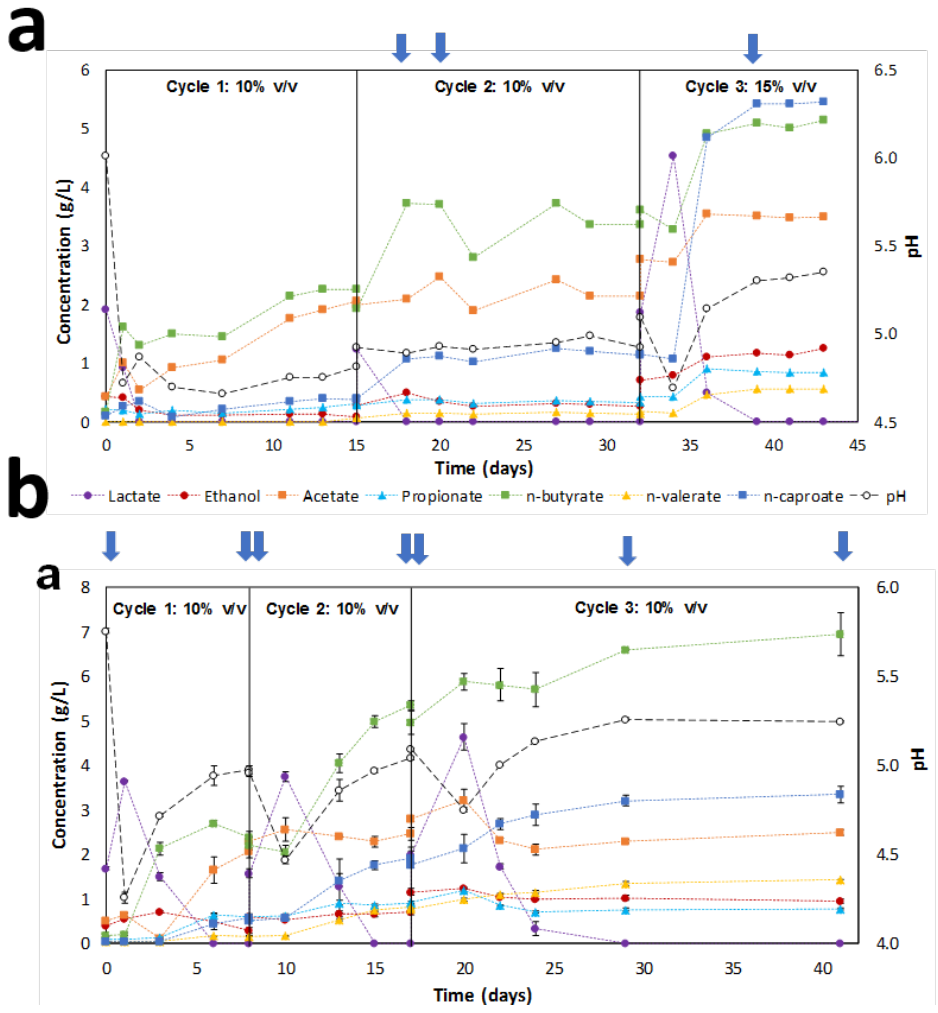

Figure S1. Sampling points for DNA extraction. Arrows indicate days when samples were taken. (**a**) Samples from day 18 and 20 of 1L-RBF were pooled together and regarded as 1L-RBF cycle 2 (inoculum for 0.3L-RBF was taken on day 19). (**b**) Samples from 0.3L-RBF were taken at the beginning and end of each cyle (before and after food waste addition).

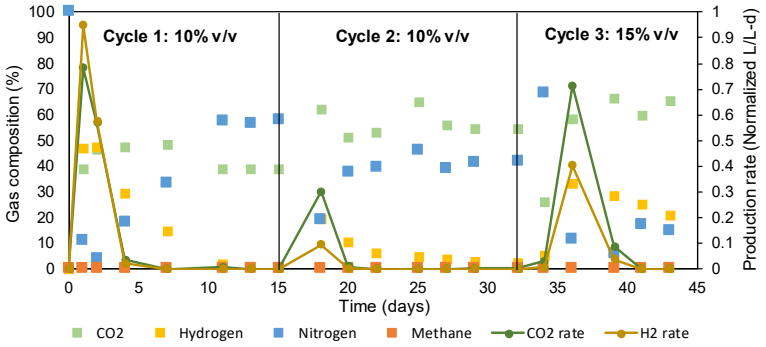

Figure S2. Headspace composition and gas production rates in 1L-RBF.

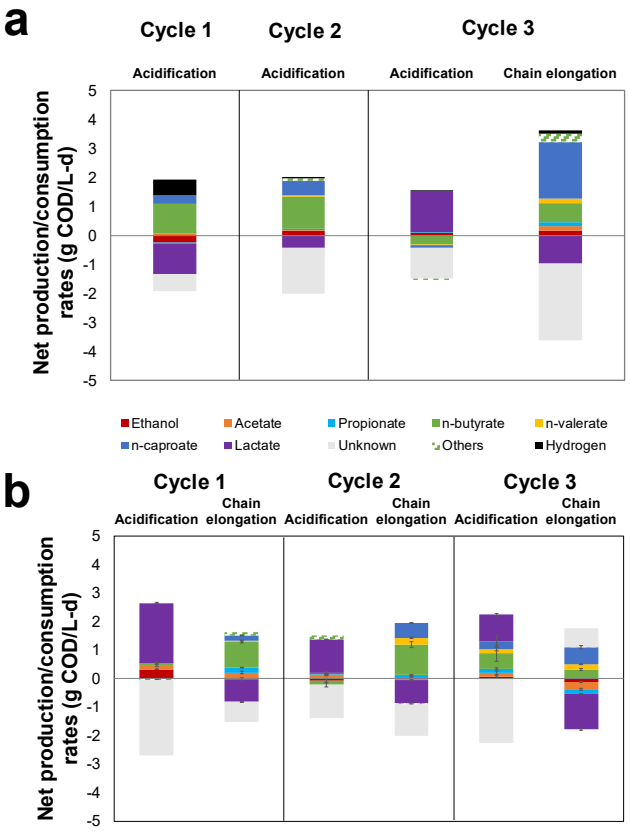

Figure S3. Metabolites production and consumption rates during acidification (Ac) and chain elongation (CE) phases for 1L-RBF (**a**) and 0.3L-RBF (**b**). Acidification rate in 1L-RBF was calculated from days 32 to 34 (cycle 3); and chain elongation rates from days 0 to 2 (cycle 1), 15 to 18 (cycle 2) and 34 to 39 (cycle 3). For 0.3L-RBF, acidification rates were calculated from days 0 to 1 (cycle 1), 8 to 10 (cycle 2) and 17 to 20 (cycle 3); and chain elongation rates from days 1 to 6 (cycle 1), 10 to 15 (cycle 2) and 20 to 24 (cycle 3). Values for 0.3L-RBF are average of duplicates and error bars depict actual values with respect to the mean.

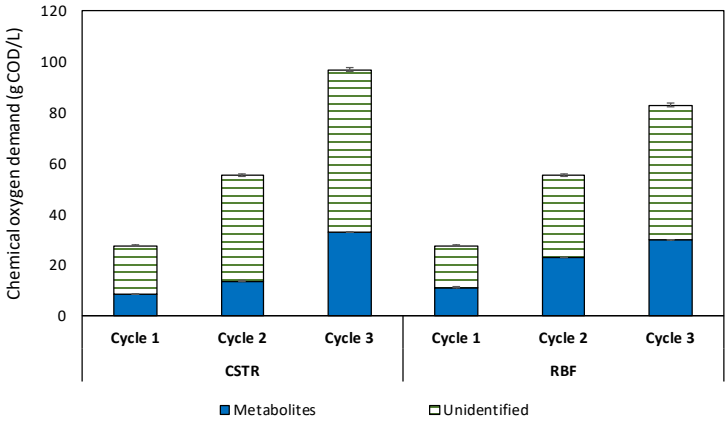

Figure S4. COD_T distribution in 1L-RBF and 0.3L-RBF experiments. Bars depict actual values with respect to the mean.

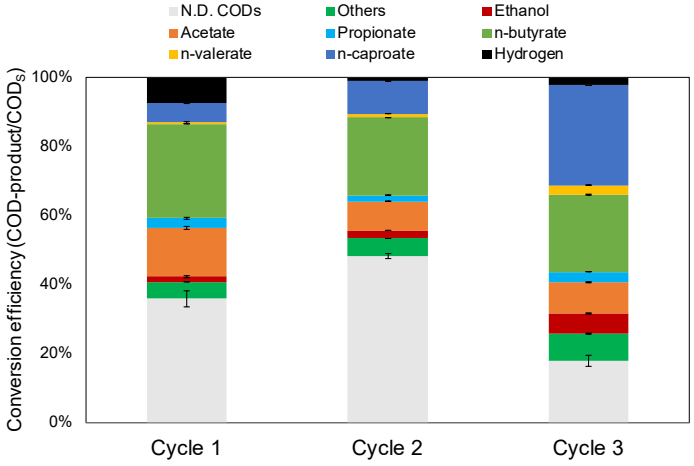

Figure S5. COD_S conversion efficiency in 1L-RBF. Values for cycle 1 (days 13 and 15), cycle 2 (days 29 and 32) and cycle 3 (days 39 and 41) were averaged and error bars depict actual values with respect to the mean.

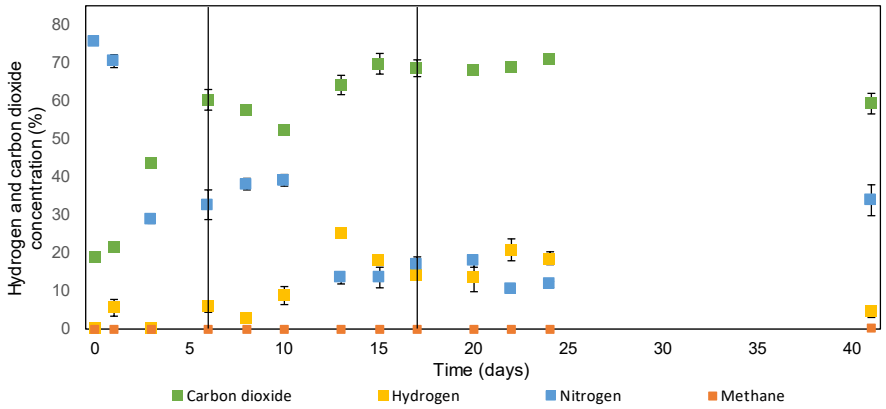

Figure S6. Headspace composition and gas production rates in 0.3L-RBF.

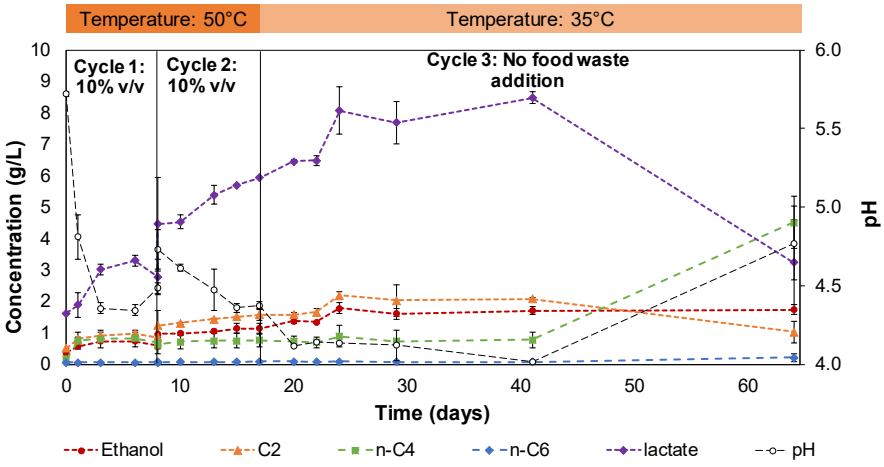

Figure S7. Metabolites and pH profiles for repeated-batch fermentation at 50°C and subsequent chain elongation at 35°C. Duplicates values were averaged and error bars depict actual values with respect to the mean.

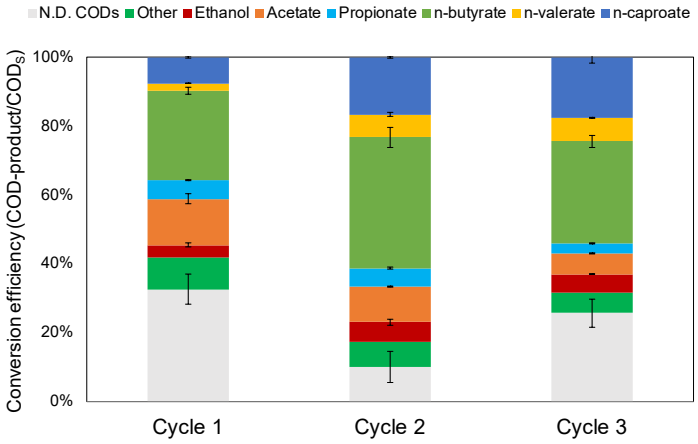

Figure S8. COD_S conversion efficiency in 0.3L-RBF. Duplicates values were averaged and error bars depict actual values with respect to the mean.

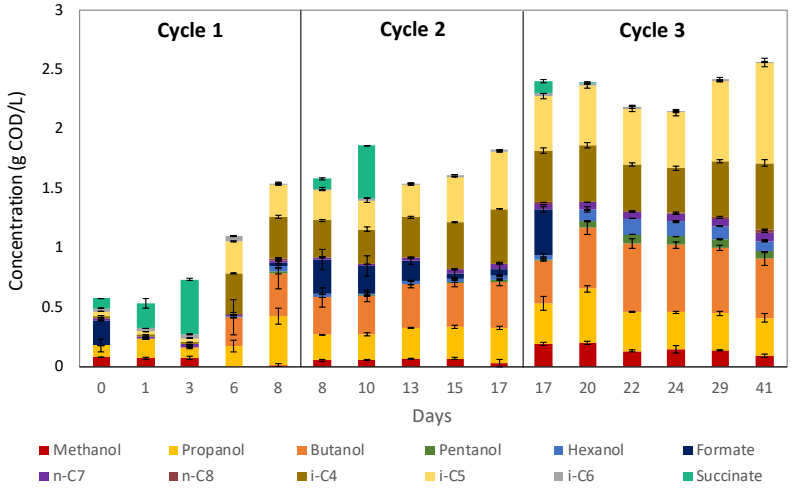

Figure S9. Trace metabolites in 0.3L-RBF. Duplicates values were averaged and error bars depict actual values with respect to the mean.

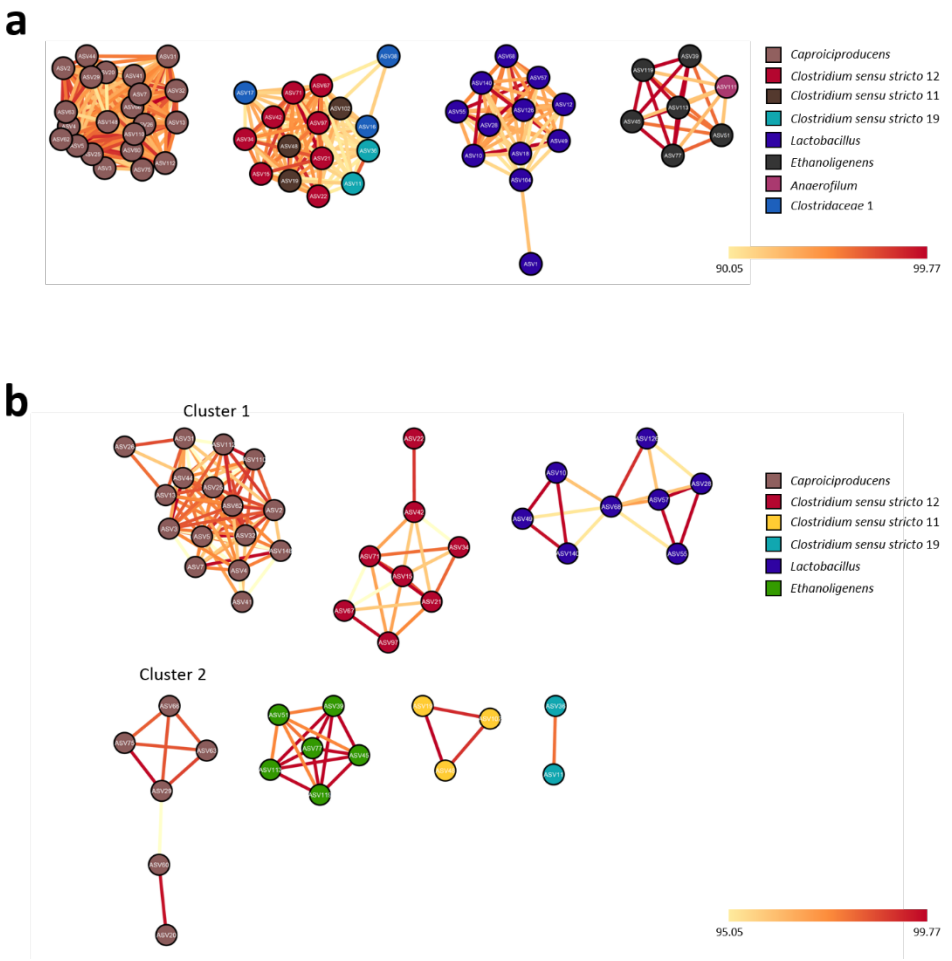

Figure S10. Identity networks for ASVs with similarities of 90% (**a**) and 95% (**b**). 22 ASVs annotated as *Caproiciproducens* were detected in the microbial community of both reactors. Clustering at 90% similarity showed a unique cluster, however clustering at 95% this big group was divided into two clusters.

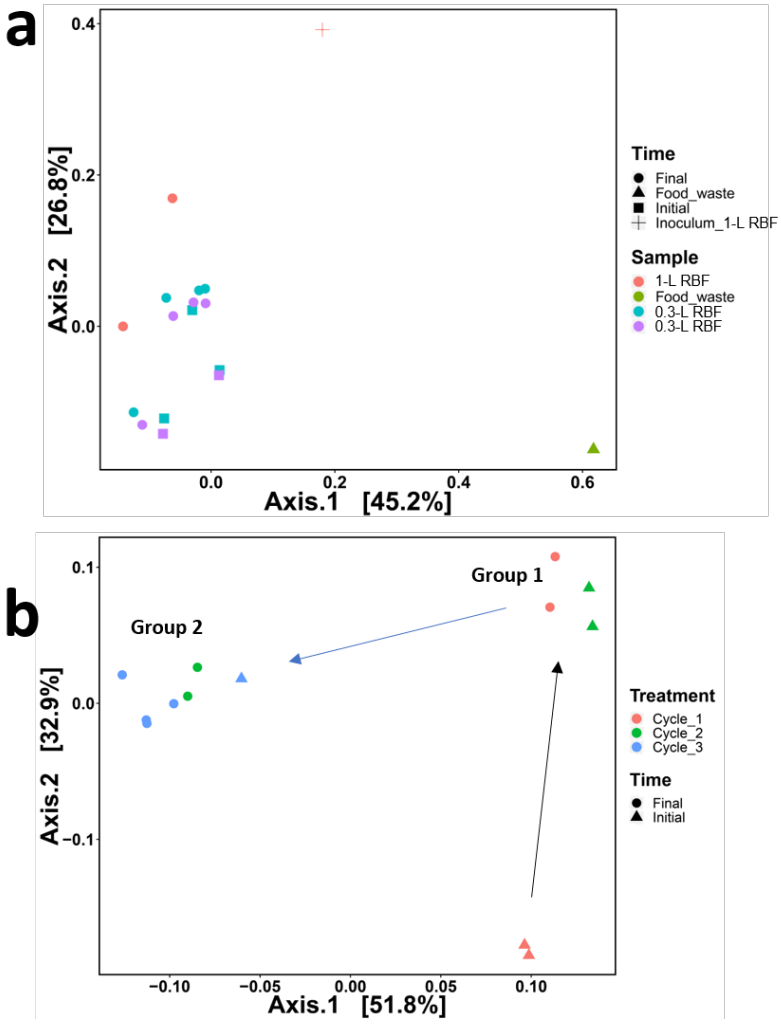

Figure S11. Principal Coordinate Analysis (PCoA) of Bray-Curtis dissimilarities of 16S rRNA data for (**a**) 1L-RBF, 0.3L-RBF and concentrated food waste microbiomes and (**b**) 0.3L-RBF microbiomes at the beginning (Initial) and end (Final) of each cycle. CSS (cumulative-sum scaling) transformed reads were used to calculate Bray-Curtis distances. The treatment category was the main explaining variable as assessed by PERMANOVA (85%; P<0.001). Food waste was used as the sole substrate in the fermentation experiments and its microbiome composition is showed as reference. Arrows in (b) show remarkable differences in the microbiome between the beginning of the experiment and the end of cycle 1 (black arrow) and between cycle 1 and the rest of the experiment (cycles 2 and 3) (blue arrow).

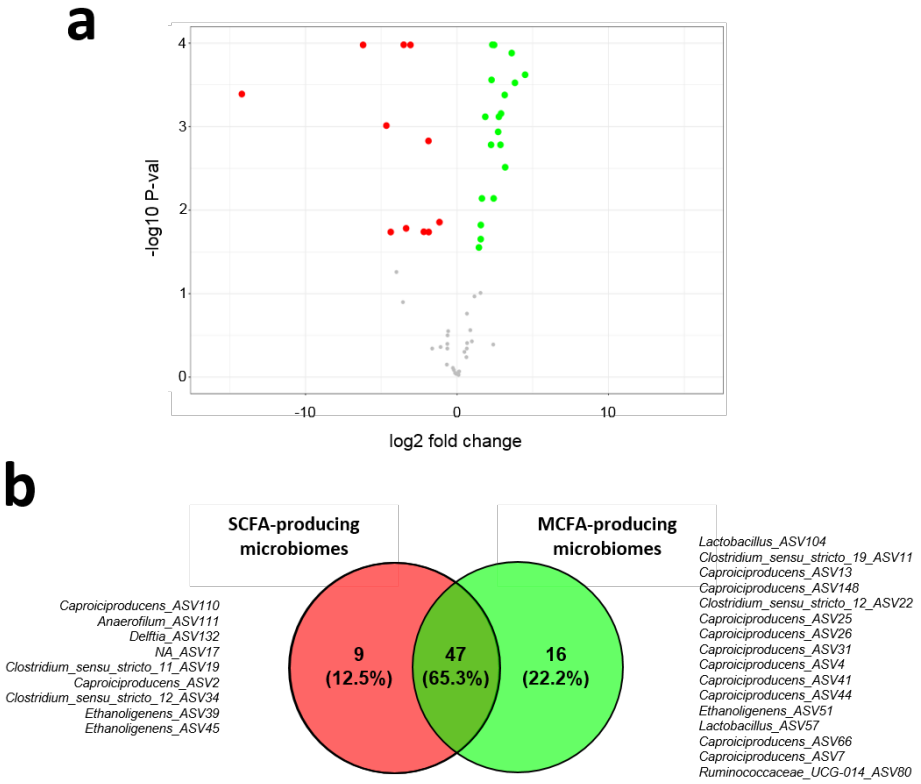

Figure S12. Differential abundance of ASVs between group 1 and group 2. (**a**) Volcano plot showing the differentially abundant ASVs enriched between group 2 (green) and group 3 (red). The plot was constructed using the significance and the log fold change of the comparison of the ASV abundances using a zero-inflated Gaussian distribution mixture model followed by an empirical Bayesian model. The y-axis represents the -log10P.val, which shows the significance of the differential abundance; the x-axis represents the log2 of the fold change for each ASV. Colourful dots are differentially abundant ASVs with an adjusted P-value (BH)<0.05. (**b**) Venn diagram showing ASVs enriched in samples from group 1 (left circle) and group 2 (right circle).

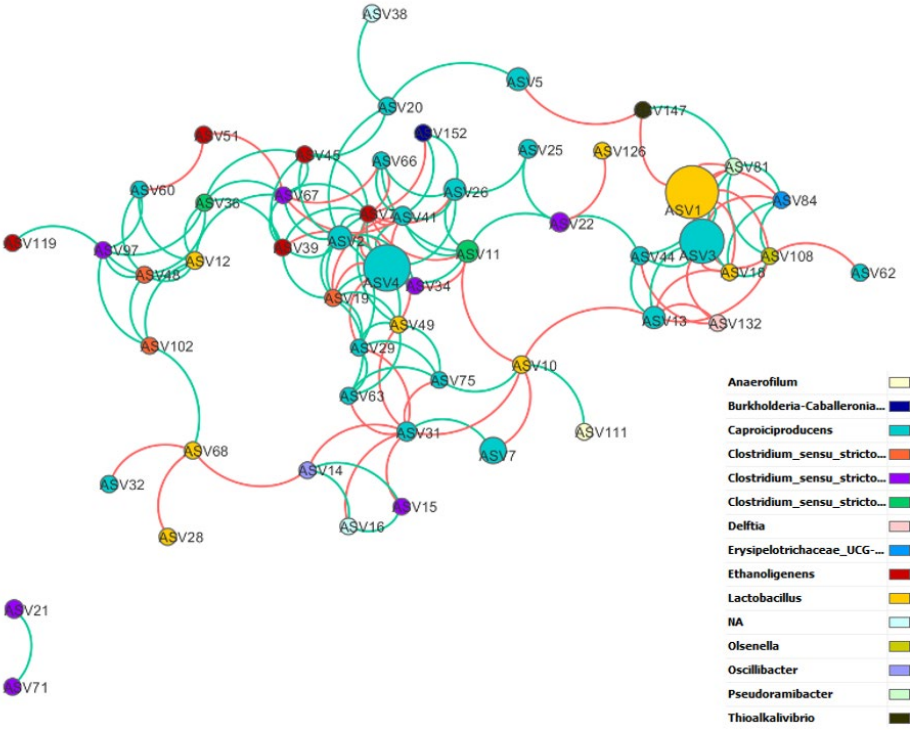

Figure S13. Co-occurrence network based on 0.3L-RBF experiments. Non-random correlations between ASVs were calculated using data from all cycles. Statistically significant (P<0.01) negative <-0.8 (red edges) and positive >0.8 (green edges) correlations are displayed. Node size depicts relative abundance at the end of the experiment.

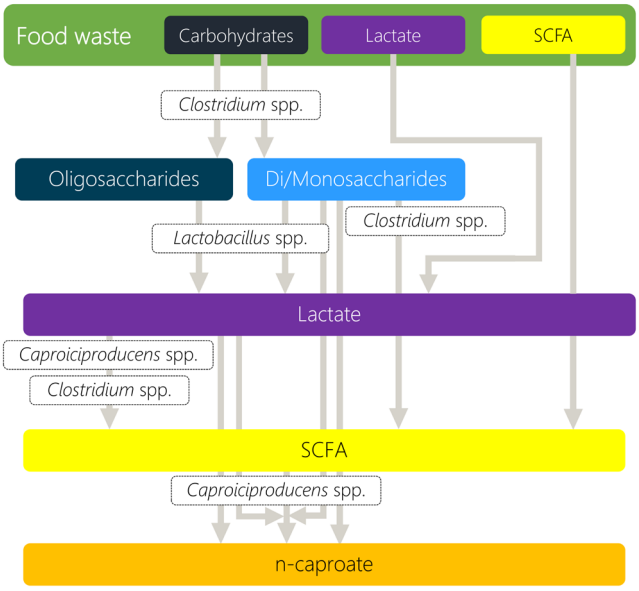

Figure S14. Possible microbial pathways in repeated-batch food waste fermentation microbiome.

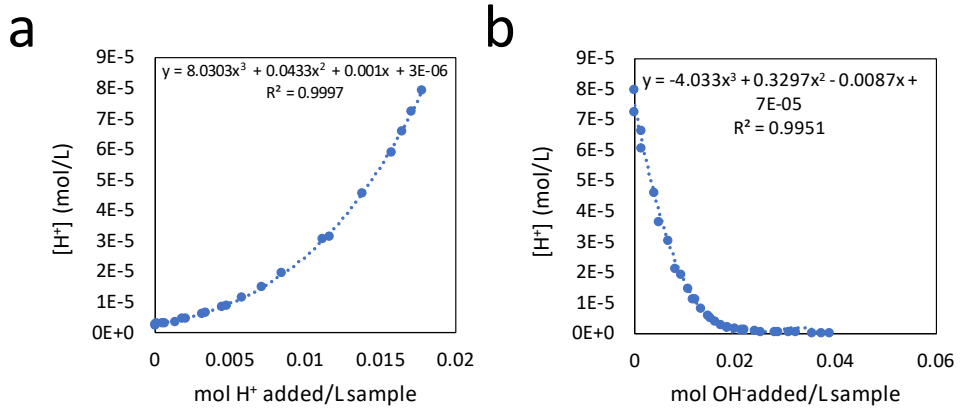

Figure S15. Titration curves for (**a**) alkalinity and (**b**) acidity of the mixture of 10% v/v food waste previously adjusted to pH 6 + mineral medium and nutrients (Table S1).

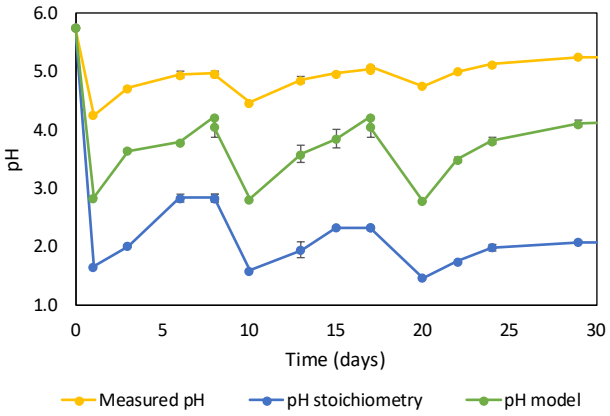

Figure S16. pH dynamics for the 0.3L-RBF experiments according to actual measurements (yellow line), expected protons dynamics based on stoichiometry during lactate production (eq. 1) and lactate-based chain elongation to n-butyrate (eq. 2) in the absence of buffer capacity (blue line), and modelled proton behaviour (green light). For the modelled proton behaviour the initial buffer capacity of the 10% food waste pH 6, mineral medium and nutrients mixture (Figure S15), HCO_3^- in equilibrium with CO_2 and dissociated fatty acids were considered. The empirical titration curves determined for alkalinity (Figure S15a) and acidity (Figure S15b) were used for the acidification and the chain elongation phases, respectively.

Supplementary material – Chapter 3

Effects of nZVI and lactate enantiomers on batch fermentation of lactate and acetate

Carlos A. Contreras-Dávila, Johan Esveld, Cees J.N. Buisman and David P.B.T.B. Strik

Analytical methods

Lactate (both D- and L-lactate monomers together), succinate and formate were measured by HPLC (Contreras-Dávila et al., 2020). Lactate enantiomers (D-lactate and L-lactate) were separated and quantified with a chiral column Astec CLC-L (15 cm × 4.6 mm, 5 µm) (Supelco) using isocratic HPLC (Thermo Scientific Dionex UltiMate 3000 RS, Thermo Fischer) with UV-detection at 254 nm (Dionex UltiMate VWD-3400). The mobile phase was 5 mM cupric sulfate at 1 mL/min and injection volume of 30 µL. Temperature in the column oven was 25°C. Chromatography data were analyzed with Chromeleon software (v6.8).

Fatty acids and alcohols, i.e. straight-chain fatty acids (C2-C8), isobutyrate, isovalerate (both 2- and 3-methylbutanoic acids together), isocaproate (4- methyl-pentanoic acid) and straight-chain alcohols (C1-C6) were quantified by gas chromatography (Agilent 7890B) using FID-detection at 240°C and a HP-FFAP column (25m x 0.32mm x 0.50µm). The carrier gas was helium at 1.25 $mL \cdot min^{-1}$ for the first 3 min and 2 $mL \cdot min^{-1}$ for the rest of the run. Injection volume was 1 µL (split injection 1:25) and injection valve temperature kept constant at 250°C. Oven temperature ramp was: 60°C for the first 3 min; 21°C·min^{-1} up to 140°C; 8°C·min^{-1} up to 150°C and constant for 1.5 min; 120°C·min^{-1} up to 200°C and constant for 1.25 min; 120°C·min^{-1} up to 240°C and constant for 3 minutes.

Nitrogen, oxygen, methane and carbon dioxide were measured using GC (Shimadzu GC-2010, Japan) equipped with TCD detector and parallel column setup (gas split 1:1) of Agilent PoraBOND Q (50 m x 0.53 mm x 10 µm) and Molsieve 5A (25 m x 0.53 mm x 50 µm). Carrier gas was helium at 22.5 $mL \cdot min^{-1}$. The oven temperature was 80 °C and TCD 150 °C. Hydrogen was measured with an HP 5890 gas chromatograph by injecting 100 µl of gas-sample on a Molsieve 5A column (30 m × 0.53 mm × 25 µm) with thermal conductivity detection (TCD). The oven temperature was 40 °C and µ-TCD 150 °C. The carrier gas was argon with a flow rate of 20 $mL \cdot min^{-1}$.

Calculations

Substrate conversion was calculated based on electron equivalents (e^- eq) in final products divided by substrate added (total lactate + acetate) (eq. S1): propionate (14 e^- eq/mol), n-butyrate (20 e^- eq/mol), n-valerate (26 e^- eq/mol), n-caproate (32 e^- eq/mol) and hydrogen (2 e^- eq/mol) related to lactate (12 e- eq/mol) and acetate (8 e^- eq/mol). Electron selectivity for product *i* is related to the total products measured (eq. S2). Carbon selectivity is regarded as the fraction of carbon in product *i* relative to carboxylates and total carbon dioxide produced (eq. S3). Total carbon dioxide (CO_2) includes gaseous CO_2 and aqueous inorganic carbon (IC_{aq}) species (H_2CO_3, HCO_3^- and CO_3^{2-}) according to eq. S4 where γ_{CO2} = CO_2 headspace fraction; P_{tot} = total pressure in batch bottle; and V_{liq} = liquid volume. IC_{aq} was calculated after de Leeuw et al. (2020) (eq. S5 and S6) where: $[H^+] = 10^{-pH}$; $K_{a1} = 10^{-6.35}$; $K_{a2} = 10^{-10.33}$; and K_H = 29.41 atm/M^2. Lastly, the proportions of L- or D-lactate were expressed as enantiomeric excess with respect to L-lactate according to eq. S7. Enantiomeric excess is a measurement of purity used for chiral substances where enantiopure solutions have an excess of 100%. An enantiomeric excess of 90% for L-lactate denotes that the other 10% is a racemic mixture (1:1) of both enantiomers. To calculate D-lactate enantiomeric excess, the difference between D-lactate and L-lactate concentrations replaces the numerator in eq. S7. Enantiomeric excess is expressed with respect to L-lactate unless stated otherwise.

$$\text{Substrate conversion} = 100 \times \frac{e^- eq_{products}}{e^- eq_{substrate}} \quad \text{(S1)}$$

$$\text{Electron selectivity} = 100 \times \frac{e^- eq_i}{e^- eq_{products}} \quad \text{(S2)}$$

$$\text{Carbon selectivity} = 100 \times \frac{\text{mol } C_i}{\text{mol } C_{products}} \quad \text{(S3)}$$

$$\text{Total } CO_2 = \frac{\gamma_{CO_2}\,(-) \times P_{tot}\,(atm) \times V_{gas}}{V_{liq} \times R \times T} + IC_{aq} \quad \text{(S4)}$$

$$IC_{aq} = \frac{[H_2CO_3] \times ([H^+]^2 + K_{a1} \times [H^+] + K_{a2} \times K_{a1})}{[H^+]^2} \quad \text{(S5)}$$

$$[H_2CO_3] = \frac{\gamma_{CO_2}\,(-) \times P_{tot}\,(atm)}{K_H} \quad \text{(S6)}$$

$$\text{Enantiomeric excess} = 100 \times \frac{\text{(L-lactate-D-lactate)}}{\text{(L-lactate+D-lactate)}} \quad \text{(S7)}$$

Table S1. Gibbs energy of formation values used for thermodynamics calculations.

Compound	$G^o f$ (kJ·mol^{-1})	$S_{298.1}$ (cal·mol^{-1}·K^{-1})	Reference
L-lactate		34.3	(Huffman et al., 1940)
D-lactate		34	
lactate	-517.1		(Kleerebezem and van Loosdrecht, 2010)
acetate	-369.4		
propionate	-361.1		
n-butyrate	-352.7		
n-valerate	-344.3		
n-caproate	-336		
carbon dioxide	-394.4		
lactyl lactic acid	-727.8		(De Clercq et al., 2018)
water	-237.2		(Kleerebezem and van Loosdrecht, 2010)
OH^-	-237.2		$G^o f_{OH-} = G^o f_{H2O}$ from water equilibrium
Fe^{2+}	-90.53		(Rickard and Iii, 2007)

Table S2. Experiment II - Substrate conversion and oligomers hydrolysis at different nZVI concentrations.

Experiment	Electrons in nZVI[a] [%]	Substrate conversion[b,d] [%]	Oligomers hydrolysis[c,d] [%]
Control	NA	75±4	17±12
0.5 g nZVI·L^{-1}	0.3	87±1	54±2
1 g nZVI·L^{-1}	0.6	88±4	57±16
2 g nZVI·L^{-1}	1.2	87±6	55±20
3.5 g nZVI·L^{-1}	2.4	89±1	63±4
5 g nZVI·L^{-1}	3	72±3	5±9

[a]With respect to initial acetate and total lactate assuming full Fe^0 anaerobic corrosion to Fe^{2+}.

[b]Electrons in products related to initial acetate, lactate monomers, oligomers and Fe^0 (full corrosion to Fe^{2+}).

[c]Estimated as the difference between unconverted substrate and initial lactate oligomers.

[d]Lactate oligomers were estimated as a fraction (0.56) of initial lactate monomers.

Table S3. Substrate conversion and lactate oligomers hydrolysis in experiment III.

Experiment	Substrate conversion[b,d] [%]	Oligomers hydrolysis[c,d] [%]
Control	72±3	7±9
Hydrogen 0.45 atm	76±4	24±12
Hydrogen 1.2 atm	81±5	38±16

[a]With respect to initial acetate and total lactate assuming full Fe^0 anaerobic corrosion to Fe^{2+}.

[b]Electrons in products related to initial acetate, lactate monomers, oligomers and Fe^0 (full corrosion to Fe^{2+}).

[c]Estimated as the difference between unconverted substrate and initial lactate oligomers.

[d]Lactate oligomers were estimated as a fraction (0.56) of lactate monomers.

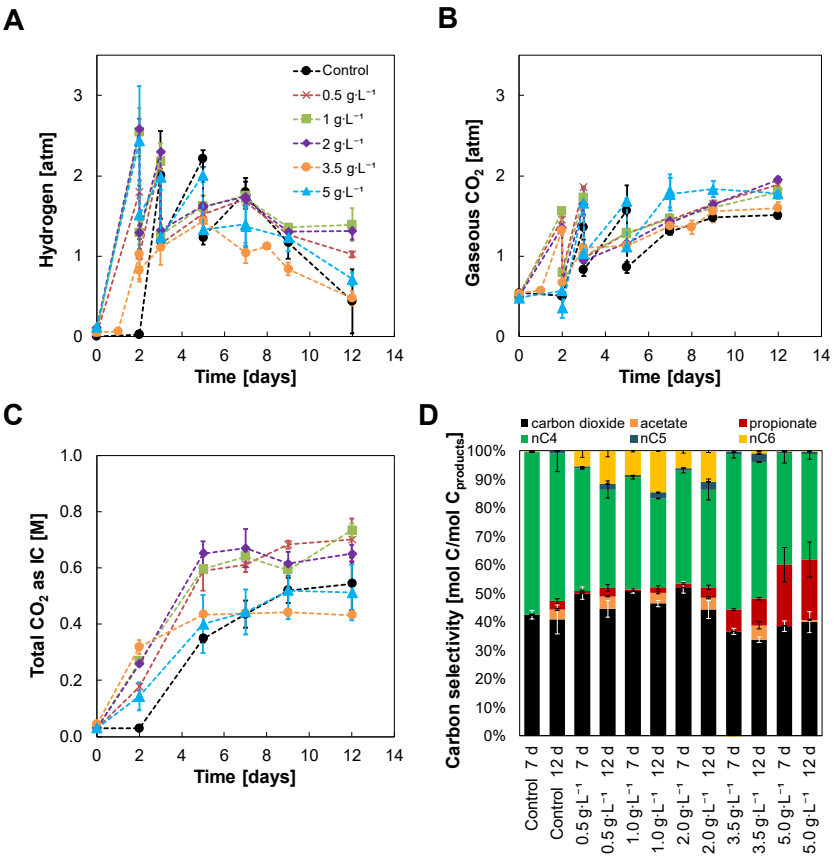

Figure S1. Experiment II – Hydrogen (**A**) and carbon dioxide (**B**) gasses partial pressures; total carbon dioxide (**C**) and carbon selectivity (**D**) in lactate-based chain elongation incubations with different nZVI doses. Total carbon dioxide as inorganic carbon (IC) refers to IC_{aq} + CO_2 gas (normalized for liquid volume) as in eq. S4-S5 (**C**). Carbon selectivity by the end of the chain elongation phase (days 0 to 7) and by the end of the experiment (days 0 to 12) (**D**). Error bars show duplicates absolute deviation from the average.

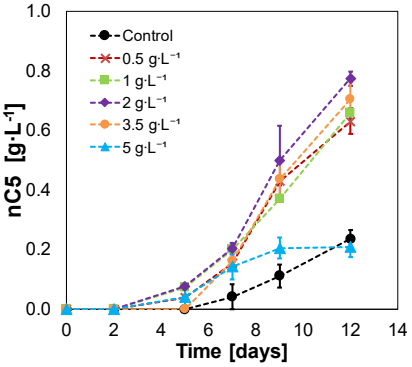

Figure S2. Experiment II - n-valerate (nC5) concentration profiles at different nZVI doses. Error bars show duplicates absolute deviation from the average.

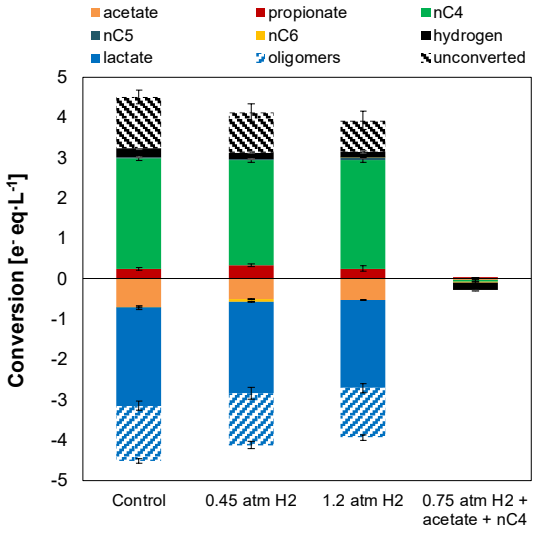

Figure S3. Experiment III - Lactate-based chain elongation without (control) and with additional hydrogen (0.45 and 1.2 atm). Hydrogen (0.75 atm) was also tested as sole electron donor with acetate and n-butyrate as electron acceptors with no chain elongation activity observed. CO_2 was added at 0.3 atm in all cases and incubations lasted for 15 days. Error bars show duplicates absolute deviation from the average.

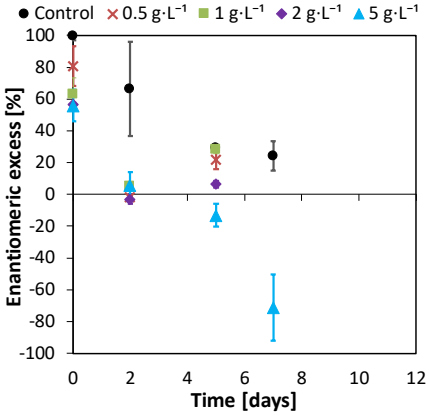

Figure S4. Experiment II - Enantiomeric excess during lactate conversion at different nZVI doses showing that L-lactate was racemized close to equimolar concentrations (excess 0%) during chain elongation at 0-2 g nZVI·L^{-1}. In contrast, D-lactate was in excess on days 5-7 coinciding with an increased propionate formation at 5 g nZVI·L^{-1}. Negative values indicate an excess of the D-lactate enantiomer. Error bars show duplicates absolute deviation from the average.

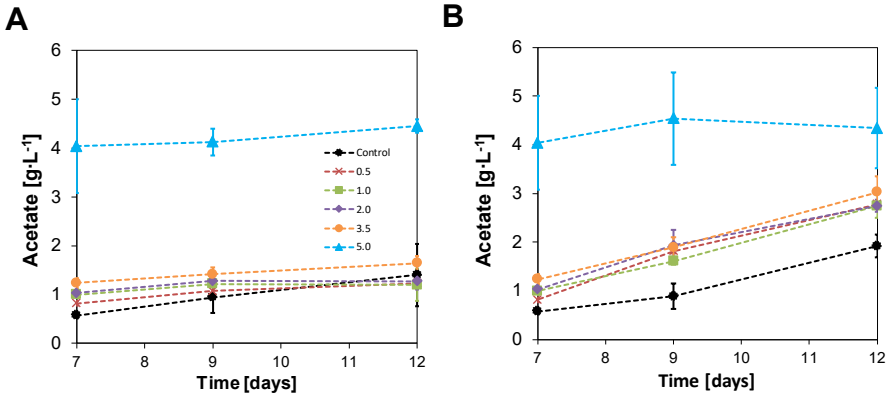

Figure S5. Experiment II - Calculated (**A**) and measured (**B**) acetate concentrations increase during the hydrogen consumption phase. Calculated acetate formation was based on hydrogen consumption assuming stoichiometry 4 H_2 + 2 CO_2 → acetate. Error bars show duplicates absolute deviation from the average.

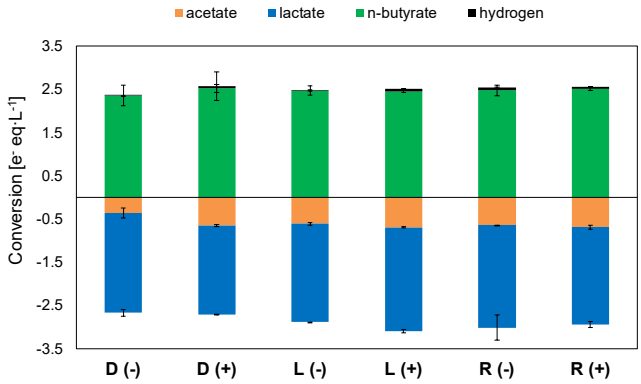

Figure S6. Experiment IV - Net conversion of lactate enantiomers and acetate by the end of the experiments with enantiopure or racemic lactate. D-lactate (D), L-lactate (L) or racemic lactate (R) with (+) and without (-) nZVI (1 g·L^{-1}). Error bars indicate ±one standard deviation.

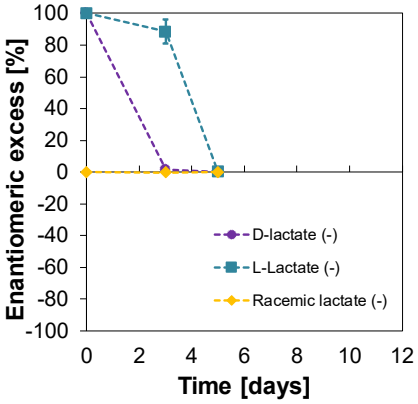

Figure S7. Experiment IV - Enantiomeric excess during lactate enantiomers conversion to n-butyrate. Enantiomeric excess was calculated with respect to D-lactate for the D- and racemic lactate experiments. The figure shows that L-lactate was to a limited extent isomerized to D-lactate during the 3-days lag phase. Enantiopure lactate was racemized to equilibrium during conversion. Lactate concentration were below the quantification limit (10 mg·L^{-1}) on day 5 but enantiomeric excess was close to the racemic equilibrium based on the chromatograms areas. Error bars indicate ±one standard deviation.

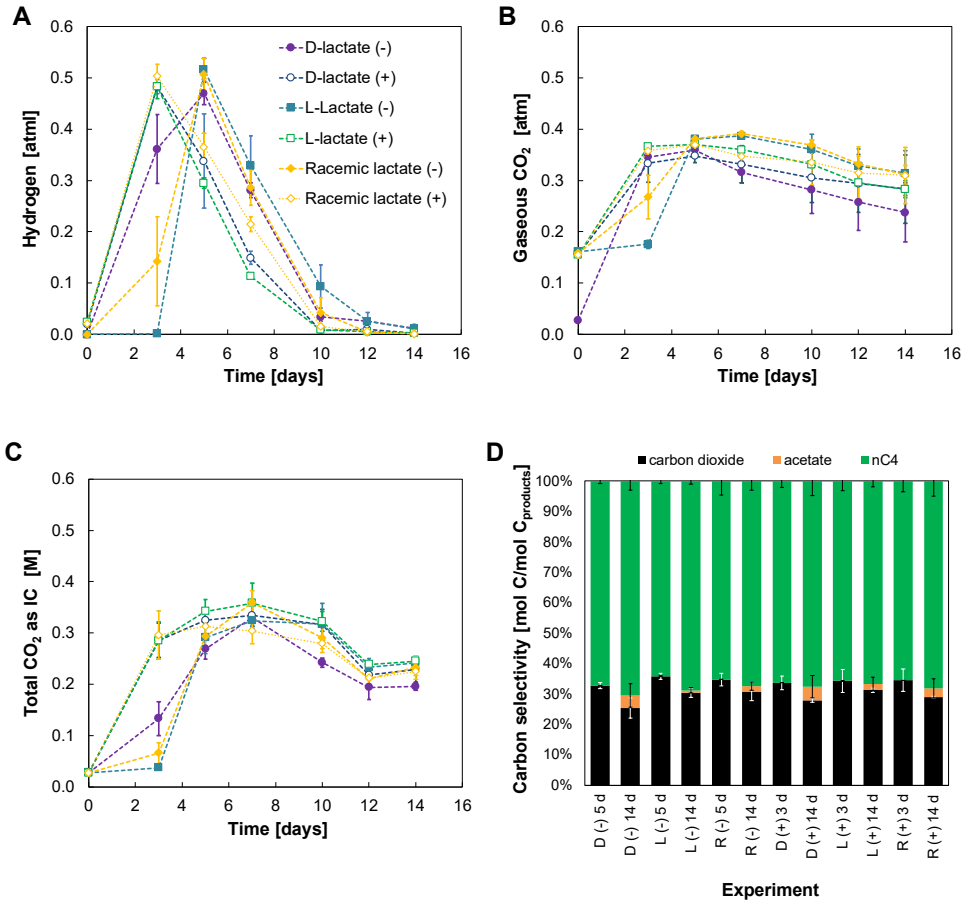

Figure S8. Experiment IV - Hydrogen (**A**) and carbon dioxide (**B**) partial pressures; total inorganic carbon (**C**) and carbon selectivity (**D**) in lactate-based chain elongation incubations fed enantiopure or racemic lactate. D-lactate (D), L-lactate (L) or racemic lactate (R) in the absence (-) or presence (+) of nZVI (1 g·L-1). Total carbon dioxide as inorganic (IC) refers to ICaq + CO_2 gas (normalized for liquid volume) as in eq. 4-5 (**D**). Carbon selectivity by the end of the chain elongation phase (day 0 to day 5 and day 3 without and with nZVI, respectively) and by the end of the experiment (days 0 to 14). Error bars show ±one standard deviation.

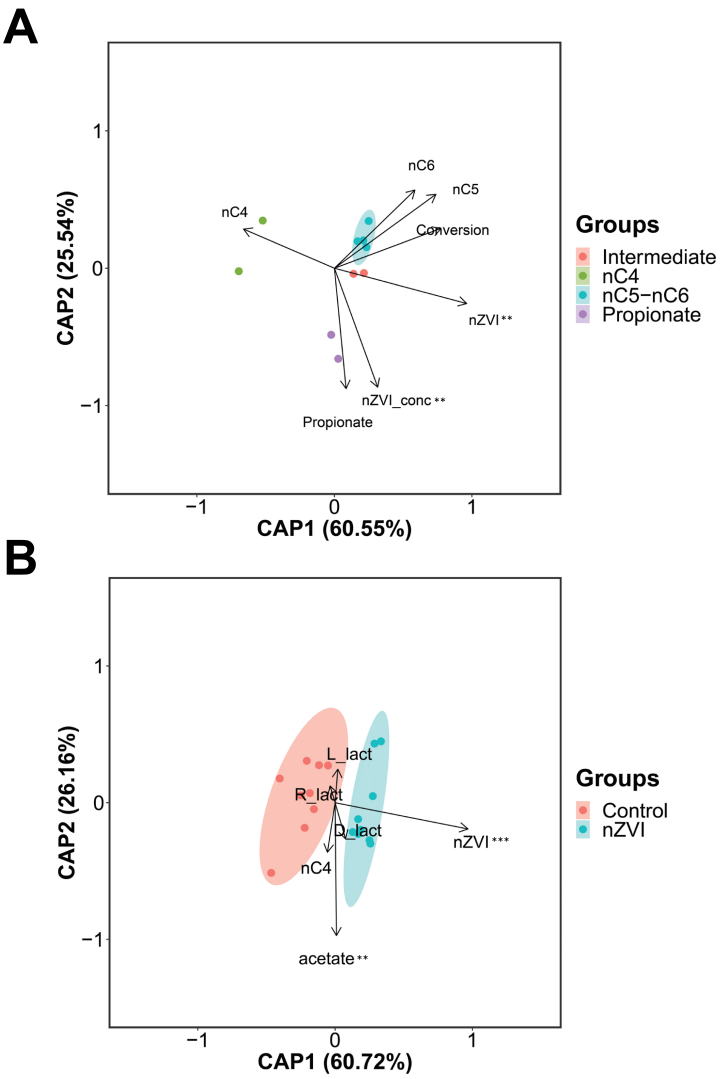

Figure S9. Distance-based redundancy analysis (dbRDA) for microbiomes from experiment II (**A**) and experiment IV (**B**). The analyses used Bray-Curtis dissimilarity index; ASVs relative abundance as response variables; and environmental parameters as explanatory variables. Environmental parameters considered were: nZVI presence, nZVI concentration, substrate conversion and final concentrations of propionate, nC4, nC5 and nC6 for (**A**); nZVI presence, initial D- and L-lactate concentrations, final nC4 concentrations and acetate production during the hydrogen consumption phase for (**B**). Concentration ellipses depict confidence intervals with α = 0.05. Significance code: '***' associated with a variable at P <0.0005; '**' associated with a variable at P <0.001; and '*' associated with a variable at P <0.01.

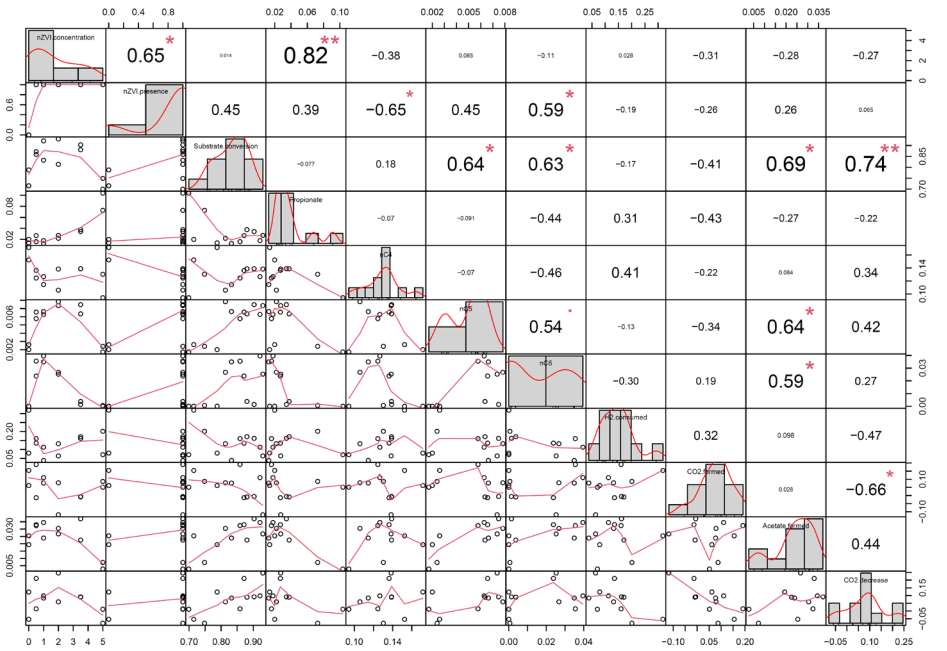

Figure S10. Experiment II – Correlation matrix for physicochemical parameters based on Spearman's rank correlation. The distribution of each variable is shown on the diagonal; the bivariate scatter plots with a fitted line below the diagonal; and Spearman's correlation coefficients above the diagonal. Correlations significance level is depicted with stars ('***' indicates p-values <0.0005; '**' indicates p-values <0.001; '*' indicates p-values <0.01 and '▪' indicates p-values <0.05). Molar concentrations for all metabolites was used. H_2 consumed, CO_2 and acetate formed refer to their change in molar concentrations during the hydrogen consumption phase (days 7 to 12). CO_2 decrease refers to the decrease in CO_2 carbon selectivity during the hydrogen consumption phase (1 – CO_2-selectivity$_{day12}$/CO_2-selectivity$_{day7}$).

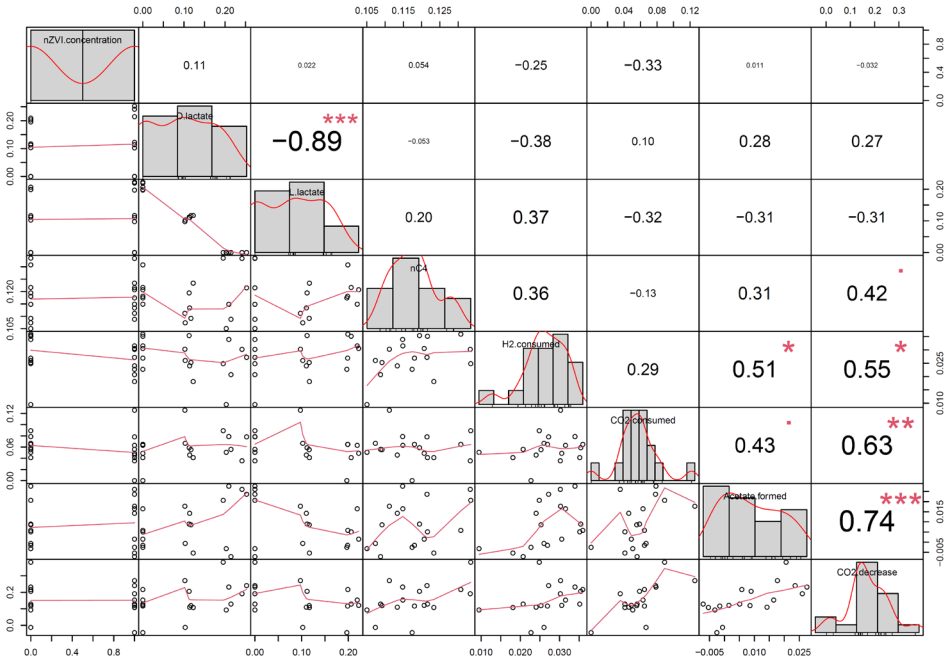

Figure S11. Experiment IV – Correlation matrix for physicochemical parameters based on Spearman's rank correlation. The distribution of each variable is shown on the diagonal; the bivariate scatter plots with a fitted line below the diagonal; and Spearman's correlation coefficients above the diagonal. Correlations significance level is depicted with stars ('***' indicates p-values <0.0005; '**' indicates p-values <0.001; '*' indicates p-values <0.01 and '▪' indicates p-values <0.05). Molar concentrations were used for all metabolites. H_2 and CO_2 consumed as well as acetate formed refer to their change in concentrations during the hydrogen consumption phase (days 3 to 14 and days 5 to 14 with and without nZVI, respectively). CO_2 decrease refers to the decrease in CO_2 carbon selectivity during the hydrogen consumption phase (1 – CO_2-selectivity$_{day12}$/CO_2-selectivity$_{day7}$).

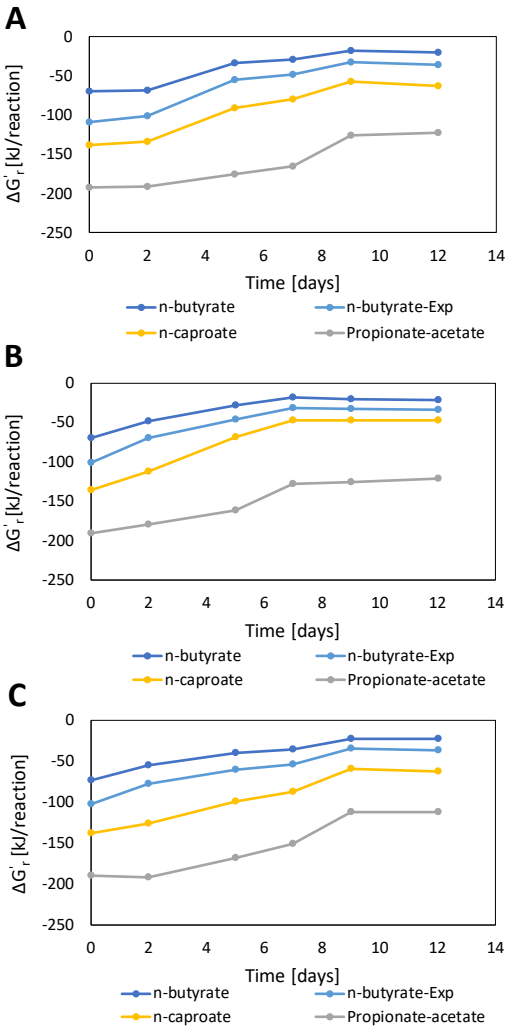

Figure S12. Actual Gibbs free energy of reaction ($\Delta G'_r$) adjusted for variations in metabolites and proton concentrations over time for experiments with (**A**) 0, (**B**) 1 and (**C**) 5 g nZVI·L^{-1} (section 3.3.2). Water concentrations was assumed 55 M. Reactions stoichiometry are described in Table 3.1 equations 4, 5, 8 and 9 for n-butyrate, n-butyrate-Exp, n-caproate and Propionate-acetate, respectively. Gibbs free energy values were calculated according to $\Delta G'_r = \Delta G°'_r + R \cdot T \cdot \ln Q$ using values given in Table S1.

Supplementary Material – Chapter 4

Continuous lactate-based chain elongation with nitrogen gas supply to n-caproate and n-heptylate

Carlos A. Contreras-Dávila, Arielle Ali, Cees J.N. Buisman and David P.B.T.B. Strik

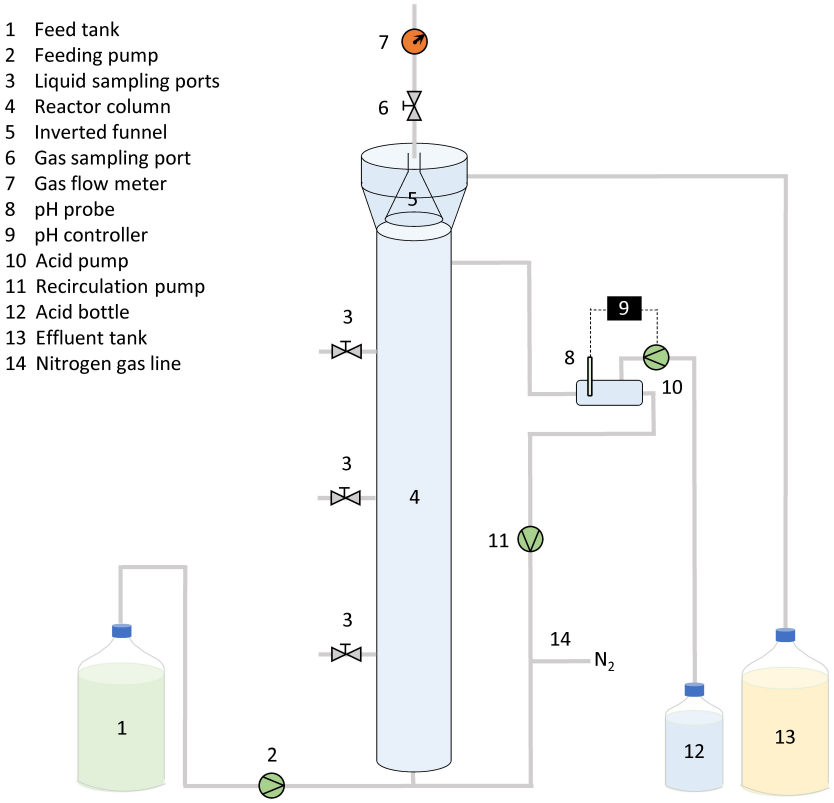

Figure S1. Schematic of upflow anaerobic reactor set-up.

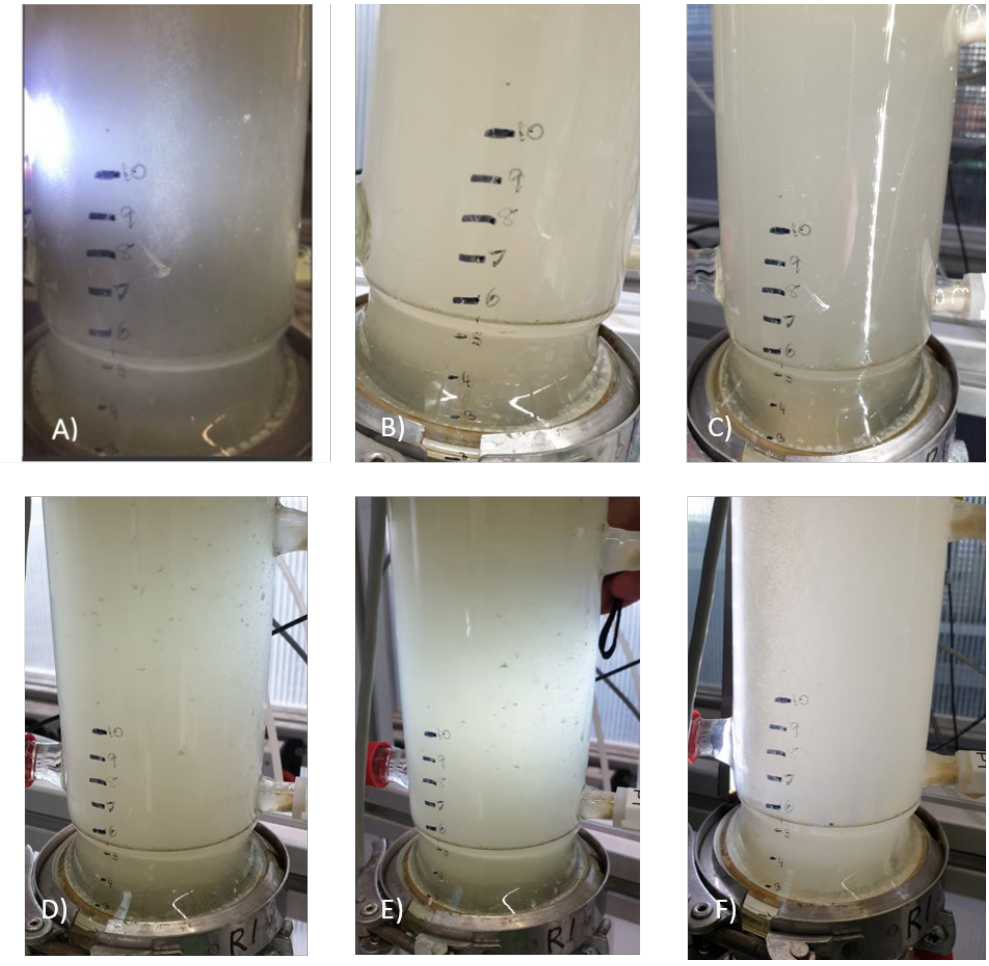

Figure S2. Biomass appearance (**A**) before continuous gas supply (day 57.7); (**B**) during continuous gas supply at 12 mL·min^{-1} (day 84.7); (**C**) during continuous gas supply at 120 mL·min^{-1}; (**D**) intermittent gas supply at HRT 2 days (day 140.8); (**E**) intermittent gas supply at HRT 1 day (day 171.7); and (**F**) without gas supply (day 219).

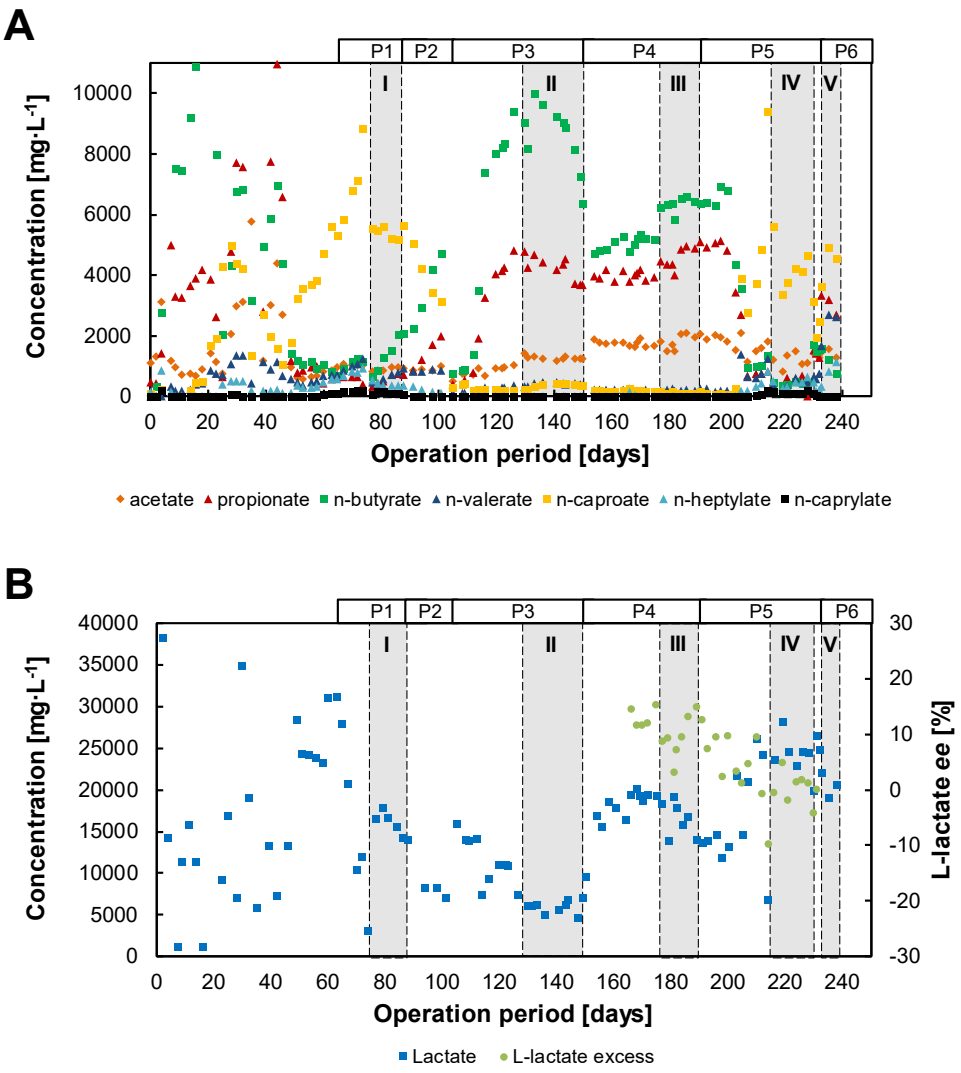

Figure S3. Carboxylates concentrations over operation time. (**A**) Metabolites concentrations, (**B**) residual lactate concentrations and L-lactate enantiomeric excess (*ee*). Shaded areas I-V indicate stabilized operation time periods.

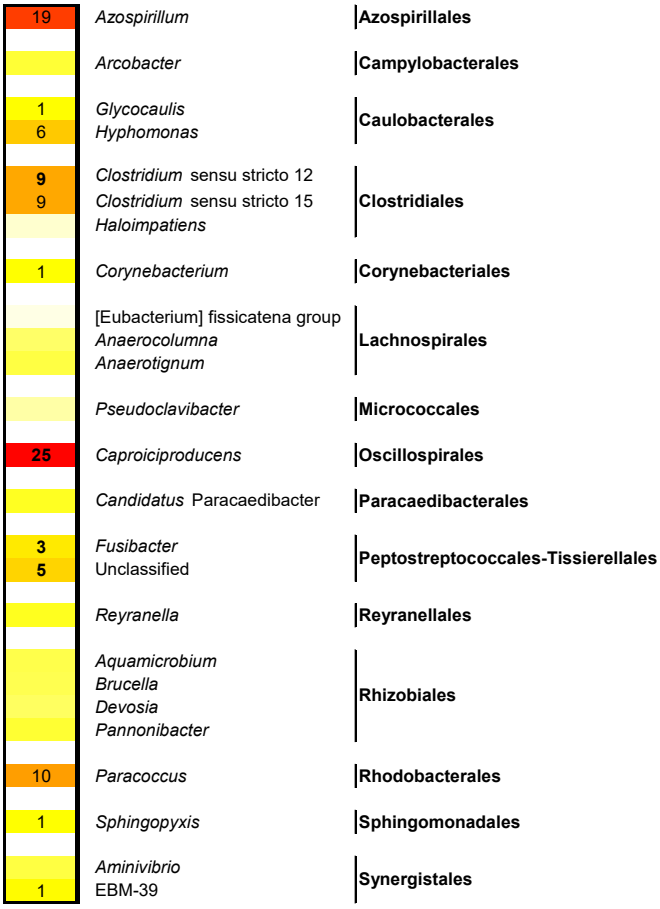

Figure S4. Inoculum composition at genus level. Taxonomy was assigned based on SILVA 138 SSU Ref NR 99 database.

Supplementary Material – Chapter 5

n-Caproate adsorption-recovery with granular activated carbon and isobutyrate formation with conductive materials

Carlos A. Contreras-Dávila, Natalia Nadal Alemany, Cris Garcia-Saravia Ortiz-de-Montellano, Zhipeng Bao, Cees J.N. Buisman and David P.B.T.B. Strik

Calculations

Batch chain elongation with conductive materials

Substrate conversion was calculated based on electron equivalents (e^- eq) in final products divided by substrate added (total lactate + acetate) (eq. S1): lactate (12 e^- eq·mol^{-1}), acetate (8 e^- eq·mol^{-1}), propionate (14 e^- eq·mol^{-1}), isobutyrate (20 e^- eq·mol^{-1}), n-butyrate (20 e^- eq·mol^{-1}), n-valerate (26 e^- eq·mol^{-1}), n-caproate (32 e^- eq·mol^{-1}) and n-caprylate (44 e^- eq·mol^{-1}). Electron selectivity for product *i* is related to the total products measured (eq. S2).

$$\text{Substrate conversion} = 100 \cdot \frac{e^-eq_{products}}{e^-eq_{substrate}} \quad \text{(S1)}$$

$$\text{Electron selectivity} = 100 \cdot \frac{e^-eq_{i}}{e^-eq_{products}} \quad \text{(S2)}$$

Continuous chain elongation

Chain elongation performance in the continuous reactor was evaluated based on conversion rates (e^- eq·L^{-1}·d^{-1}; eq. S3) and selectivity (eq. S4).

$$\text{Conversion rate} = \frac{n_{e,i}}{V_r}(Q_{out} \cdot C_{out,i} - Q_{in} \cdot C_{in,i}) \quad \text{(S3)}$$

$$\text{Selectivity} = 100 \cdot \frac{rate_i}{\sum_i^j rate_{liq} + \sum_i^j rate_{gas}} \quad \text{(S4)}$$

where $n_{e,i}$ refers to the number of electrons in compound i (liquid and gas metabolites quantified); V_r the reactor working volume (L); Q_{in} the influent and Q_{out} the effluent flow rates (L·d^{-1}); $C_{in,i}$ the concentration in the influent and $C_{out,i}$ the concentration in the effluent for compound i (mmol·L^{-1}). $rate_i$ is calculated as in eq. S3 for product i; $rate_{liq}$ is the production rate of liquid metabolites (propionate, isobutyrate, n-butyrate, n-valerate, n-caproate, n-heptylate and n-caprylate) and $rate_{gas}$ is the production rate of gaseous metabolites (hydrogen and methane).

Adsorption-desorption experiments

The amount of each carboxylate adsorbed ($q_{ads,}$ mmol·g GAC^{-1}) was calculated from mass balances (eq. S5-S6)

$$q_{ads} = \frac{V \cdot (C_0 - C_{t1})}{m_A} \quad (S5)$$

$$\text{Adsorption [\%]} = 100 \cdot \frac{C_0 - C_{ads1}}{C_0} \quad (S6)$$

Where V is the liquid volume (L); C_0 and C_{ads1} are the initial concentrations and concentrations after adsorption, respectively (mmol·L^{-1}); and m_A is the mass of GAC (g). Desorption was evaluated based on the desorbed fractions relative to the amount adsorbed (eq. S7), where C_{des1} and C_{des2} are the concentrations at the beginning and after desorption, respectively. The fraction of each carboxylate recovered after one adsorption-desorption cycle was calculated with respect to the initial concentrations (eq. S8).

$$\text{Desorption [\%]} = 100 \cdot \frac{C_{des2} - C_{des1}}{C_0 - C_{ads1}} \quad (S7)$$

$$\text{Recovery [\%]} = 100 \cdot \frac{C_{des2} - C_{des1}}{C_0} \quad (S8)$$

Adsorption isotherms

The equilibrium load of n-caproate on GAC (q_e, mg·g GAC^{-1}) was calculated from mass balances according to eq. S9:

$$q_e = \frac{V \cdot (C_0 - C_e)}{m_A} \quad (S9)$$

Where V is the liquid volume (L); C_0 and C_e are respectively the initial and equilibrium n-caproate concentrations (mg·L^{-1}); and m_A is the mass of GAC (g). The experimental data was fitted to the Freundlich model (eq. S10) using the nonlinear optimization method (Tran et al., 2017). K_F is the Freundlich constant (mg·g^{-1}) and n the Freundlich intensity parameter (dimensionless).

$$q_e = K_F \cdot C_e^{1/n} \quad (S10)$$

Thermodynamic calculations

The feasibility of a set of biological reactions possibly occurring in the incubations with conductive materials was estimated based on their Gibbs free energy change (ΔG'). The Gibbs free energy change was calculated using Gibbs free energy of formation values from Kleerebezem and van Loosdrecht (2010). Values for fermentative reactions were corrected for temperature (30℃), reactants and products concentrations, and pH according to equation S11.

$$\Delta G' = \Delta G° + R \cdot T \cdot \ln Q \quad (S11)$$

The reduction potential (E') of reactions involved in direct interspecies electron transfer (DIET) was calculated by expressing them in the reduction direction and using equation S12, where *n* is the

number of electrons involved in the reaction and F is the Faraday constant in kilocoulombs *per* mole (96.485 kC·mol^{-1}).

$$E' = -\frac{\Delta G'}{nF} \quad \text{(S12)}$$

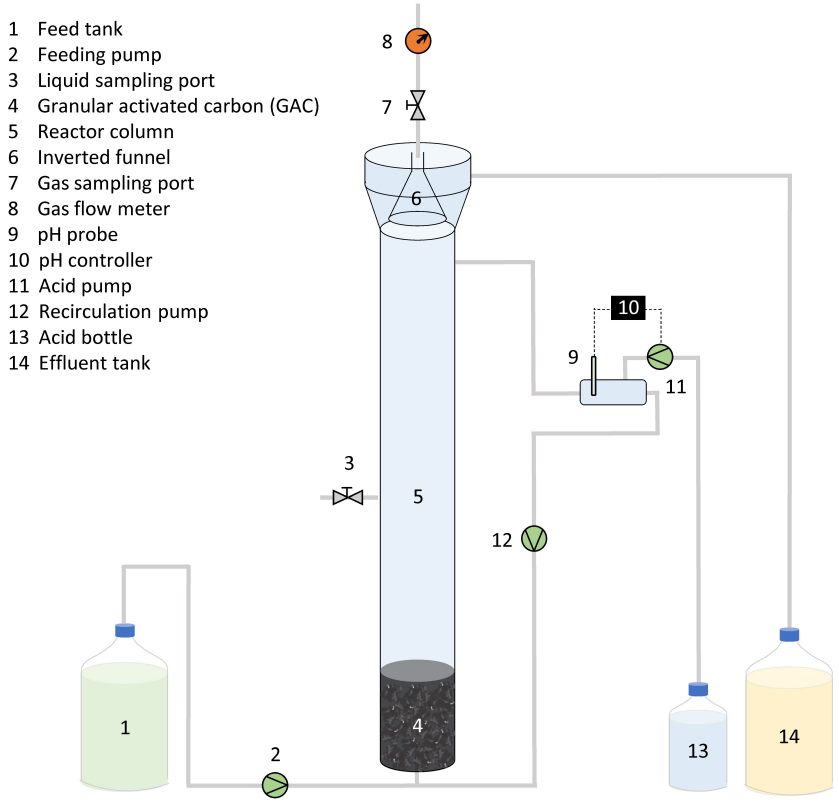

Figure S1. Schematic of the upflow anaerobic reactor set-up.

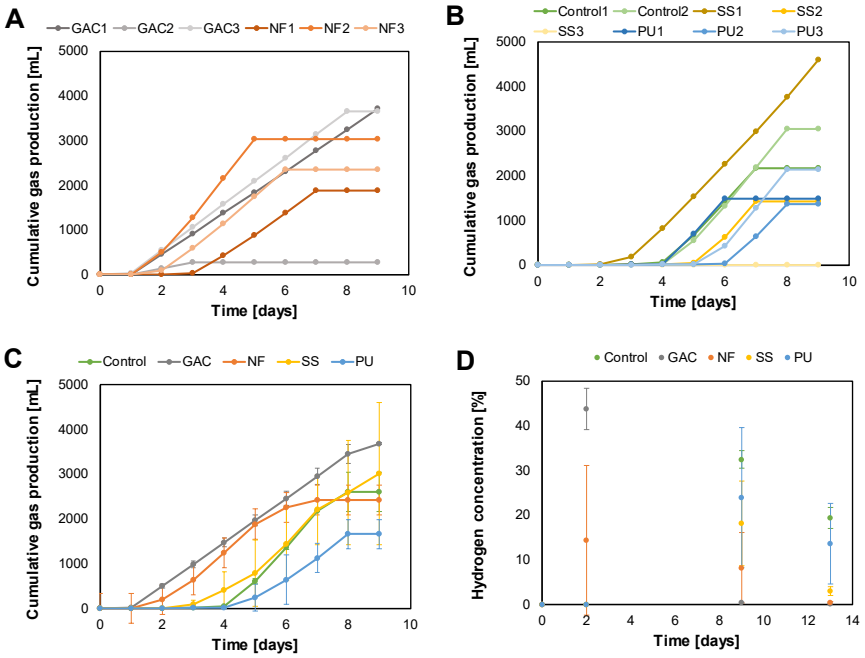

Figure S2. Gas production in incubations with conductive materials. Cumulative gas production in replicates with (**A**) granular activated carbon [GAC] and nickel foam [NF]; and (**B**) stainless steel mesh [SS], polyurethane foam [PU] and control without materials. (**C**) Average gas production for each material. GAC2 and SS3 were left out since low or no gas production was measured. (**D**) Average hydrogen headspace concentrations.

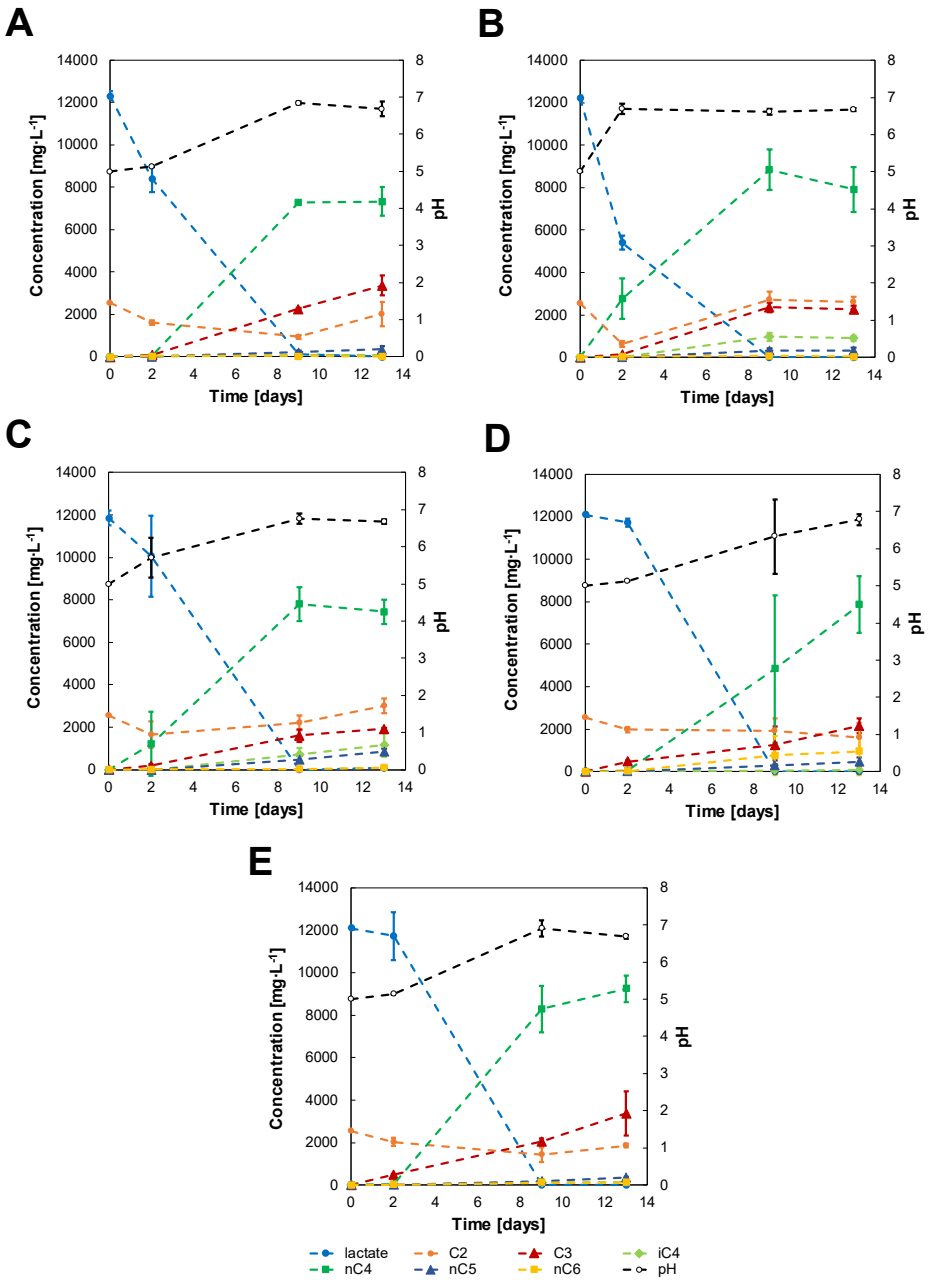

Figure S3. Metabolites profile in incubations with conductive materials. (**A**) Control; (**B**) granular activated carbon [GAC]; (**C**) nickel foam [NF]; (**D**) stainless steel mesh [SS]; and (**E**) polyurethane foam [PU].

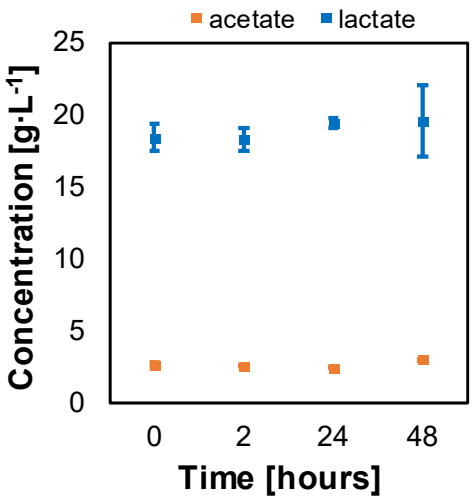

Figure S4. Adsorption test with GAC and feeding medium of the continuous reactor. The figure shows that lactate and acetate were not further adsorbed onto "pre-treated" GAC.

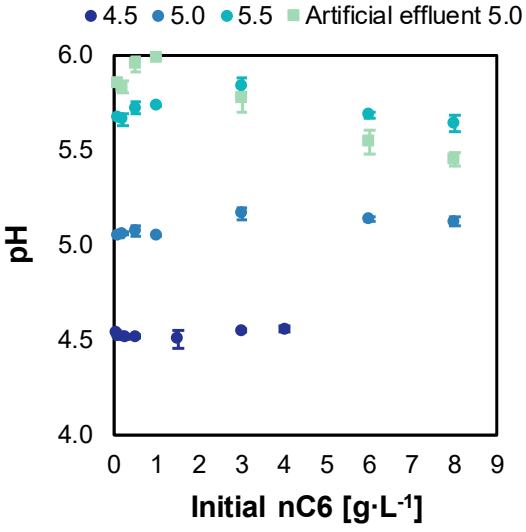

Figure S5. Measured pH at equilibrium in adsorption isotherms. Adsorption isotherms were carried out using acetate buffers to keep pH values of 4.5, 5 and 5.5 and artificial effluent (AE) at initial pH 5.

Table S1. Continuous reactor performance without (period I) and with (period II) GAC.

Compound	Productivity [e^- eq·L^{-1}·d^{-1}]		Selectivity [%]		Concentrations [g·L^{-1}][a]	
	Period I	Period II	Period I	Period II	Period I	Period II
lactate	-0.76±0.14	-1.05±0.07	-	-	3.12±1.57	0±0
acetate	-0.03±0.01	-0.03±0.03	-	-	0.77±0.14	0.91±0.4
propionate	0.01±0.01	0.01±0	2±1	2±0	0.17±0.08	0.16±0.02
n-butyrate	0.06±0.02	0.09±0.01	8±2	11±2	0.73±0.4	0.81±0.16
n-caproate	0.59±0.06	0.66±0.12 (0.91)[b]	81±2	80±2 (85)[b]	4.9±0.58	5.14±0.83
n-caprylate	0.02±0.01	0±0	3±1	0±0	0.16±0.03	0±0
hydrogen	0.04±0.01	0.05±0.02	6±2	7±3	0.29±0.12	0.27±0.06
Electron recovery [%][c]	96±15	79±11	-	-	-	-

[a] Partial pressure for hydrogen.

[b] Brackets show estimated values assuming that missing electrons end up in n-caproate.

[c] Assuming lactate monomers and acetate are metabolized.

Table S2. Freundlich parameters obtained from n-caproate adsorption isotherms.

pH	Maximum q_e measured	Freundlich coefficients		Model fit	
		K_F	n	R^2	χ^2
	[mg·g GAC^{-1}]	[mg·g GAC^{-1}]	[-]	[-]	[-]
4.5	243	24.5	3.41	0.999	9.8
5.0	239	19.7	3.46	0.998	17.3
5.5	184	17.6	3.72	0.997	16
5.0 (Artificial effluent)	205	19.4	3.65	0.998	16.4

Table S3. Estimated minimum energy input for n-caproate desorption.

Compound	Mass[a]	Boiling point	C_p	$\Delta H°_{vap}$	Sensible heat[b]	Total energy	Minimum heat for desorption
	[g]	[ºC]	[J·g^{-1}·K^{-1}]	[J·g^{-1}]	[J·g^{-1}]	[J·g^{-1}]	[J·g $nC6^{-1}$]
n-caproate	1	205	1.94	630	339.5	969.5	969.5
Water	4.8	100	4.18	2258	292.6	2550.6	12242.9
GAC	4.11	-	0.84	-	147	147	604.2
Total energy for thermal desorption							13816.6
							13.8 kJ·g $nC6^{-1}$ / 3.84 kWh·kg $nC6^{-1}$

[a] Sensible heat to heat water from 30ºC to 100ºC; and nC6 and GAC from 30ºC to 205ºC.

[b] Based on an adsorption capacity of 0.243 g nC6·g GAC^{-1} and assuming a water adsorption of 1.2 g·g GAC^{-1}.

Supplementary Material – Chapter 6

Reactor microbiome enriches vegetable oil with n-caproate and n-caprylate *via* extractive chain elongation

Carlos A. Contreras-Dávila, Norwin Zuidema, Cees N.J. Buisman and David P.B.T.B. Strik

Analytical methods

Lactate (both D- and L-lactate monomers together), succinate and formate were measured by HPLC (Contreras-Dávila et al., 2020). Fatty acids and alcohols, i.e. straight-chain fatty acids (C2-C8), isobutyrate, isovalerate (both 2- and 3-methylbutanoic acids together), isocaproate (4- methyl-pentanoic acid) and straight-chain alcohols (C1-C6) were quantified by gas chromatography (Agilent 7890B) using FID-detection at 240°C and a HP-FFAP column (25m x 0.32mm x 0.50µm). The carrier gas was helium at 1.25 mL·min^{-1} for the first 3 min and 2 mL·min^{-1} for the rest of the run. Injection volume was 1 µL (split injection 1:25) and injection valve temperature kept constant at 250°C. Oven temperature ramp was: 60°C for the first 3 min; 21°C·min^{-1} up to 140°C; 8°C·min^{-1} up to 150°C and constant for 1.5 min; 120°C·min^{-1} up to 200°C and constant for 1.25 min; 120°C·min^{-1} up to 240°C and constant for 3 minutes.

Nitrogen, oxygen, methane and carbon dioxide were measured using GC (Shimadzu GC-2010, Japan) equipped with TCD detector and parallel column setup (gas split 1:1) of Agilent PoraBOND Q (50 m x 0.53 mm x 10 µm) and Molsieve 5A (25 m x 0.53 mm x 50 µm). Carrier gas was helium at 22.5 mL·min^{-1}. The oven temperature was 80 °C and TCD 150 °C. Hydrogen was measured with an HP 5890 gas chromatograph by injecting 100 µl of gas-sample on a Molsieve 5A column (30 m × 0.53 mm × 25 µm) with thermal conductivity detection (TCD). The oven temperature was 40 °C and µ-TCD 150 °C. The carrier gas was argon with a flow rate of 20 mL·min^{-1}.

Calculations

Solvents extraction efficiency was evaluated by looking at the distribution ratio (K_D) of the extracted carboxylates (eq. S1); partition coefficient (eq. S2); the recovery of each individual carboxylate (*i*) compared to its total mass production (mg) (eq. S3); and the solvent specificity towards each carboxylate with respect to all extracted carboxylates (eq. S3). Where HA and A^- stand for undissociated and dissociated carboxylic acid, respectively, assuming that only HA species are extracted into the solvents. Concentrations are in mg·L^{-1}.

$$\text{Distribution ratio } (K_D) = \frac{[HA_i]_{org}}{[HA_i + A_i]_{aq}} \quad \text{(S1)}$$

$$\text{Partition coefficient } (P) = \frac{[HA_i]_{org}}{[HA_i]_{aq}} \quad \text{(S2)}$$

$$\text{Recovery} = 100 \times \frac{HA_{i,\ org}}{HA_{i,org} + HA_{i,aq} + A^-_{i,\ aq}} \quad \text{(S3)}$$

$$\text{Extraction specificity} = 100 \times \frac{[HA_i]_{org}}{\sum_i^j [HA]_{org}} \quad \text{(S4)}$$

Chain elongation performance was evaluated based on conversion rates (eq. S5); selectivity (eq. S6) and conversion efficiency (eq. S7).

Conversion rate (e^- meq·L^{-1}·d^{-1}) is based on mass balance:

$\text{Conversion rate}_{i,t} = \text{accumulation}_{i,t} + \text{out}_{i,t} - \text{in}_{i,t}$

$$\text{Conversion rate}_{i,t} = \frac{n_{e,i}}{V_r}\left[\frac{V_{org}}{\Delta t}\left(C_{i,org,t} - C_{i,org,t-1}\right) + Q_{out}C_{out,i} - Q_{in}C_{in,i}\right] \quad \text{(S5)}$$

where $n_{e,i}$ refers to the number of electrons in compound *i* (liquid and gas metabolites quantified as described in the analytical methods section); V_r the reactor working volume (1.2 L); V_{org} the organic phase volume (0.24 L); Δt the time between sampling time t and t-1 (d); $C_{i.org}$ the concentration of compound *i* in the organic phase (mmol·L^{-1}); Q_{in} the influent and Q_{out} the effluent flow rates (L·d^{-1}); $C_{in,i}$ the concentration of compound *i* in the influent and $C_{out,i}$ in the effluent (mmol·L^{-1}). The number of carbon atoms *per* mole of product ($n_{c,i}$) is used instead of $n_{e,i}$ to express conversion rates in mmol C·L^{-1}·d^{-1}.

Electron and carbon selectivity was calculated with respect to liquid and gas metabolites production rates (eq. S6):

$$\text{Selectivity}_{i,t} = 100 \times \frac{\text{rate}_i}{\sum_i^j \text{rate}_{liq} + \sum_i^j \text{rate}_{gas}} \quad \text{(S6)}$$

where rate_i is calculated as in eq. S5 for product *i*; rate_{liq} is the production rate of liquid metabolites (propionate, isobutyrate, n-butyrate, isovalerate, n-valerate, isocaproate, n-caproate, n-heptanoate and n-caprylate) and rate_{gas} is the production rate of gaseous metabolites (hydrogen for electron selectivity; carbon dioxide for carbon selectivity). Carbon dioxide (CO_2) includes gaseous CO_2 off gas and aqueous inorganic carbon (IC_{aq}) species (H_2CO_3, HCO_3^- and CO_3^{2-}). IC_{aq} was calculated after de Leeuw et al. (2020) (de Leeuw et al., 2020) (eq. S8-S9) where: $[H^+] = 10^{-pH}$; $K_i = 10^{-6.35}$; $K_{a2} = 10^{-10.33}$; and $K_H = 29.41$ atm/M^2. Methane was sporadically produced at <5 mmol·L^{-1}·d^{-1} only during CSTRs recovery from biomass wash out.

Conversion efficiency (mol $C_{product}$·mol $C_{consumed}^{-1}$) was calculated based on lactate and acetate consumed (eq. S7):

$$\text{Conversion efficiency}_{i,t} = 100 \times \frac{\text{rate}_i}{\text{rate}_{lactate} + \text{rate}_{acetate}} \quad \text{(S7)}$$

where $rate_i$, $rate_{lactate}$ and $rate_{acetate}$ are calculated for product *i*, lactate and acetate, respectively, in mmol C·L^{-1}·d^{-1} according to eq. S5.

$$IC_{aq} = \frac{[H_2CO_3] \times ([H^+]^2 + K_{a1} \times [H^+] + K_{a2} \times K_{a1})}{[H^+]^2} \quad \text{(S8)}$$

$$[H_2CO_3] = \frac{Y_{CO_2}\ (-) \times P_{tot}\ (atm)}{K_H} \quad \text{(S9)}$$

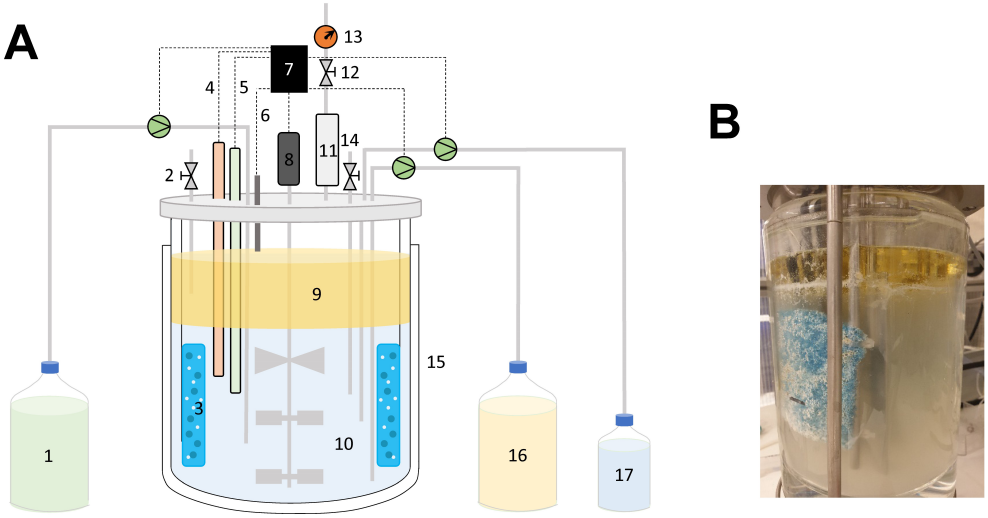

Figure S1. (**A**) CSTR schematic and (**B**) picture. 1 – feed tank; 2 – oil sampling port; 3 – polyurethane foam; 4 – redox sensor; 5 – pH sensor; 6 – liquid level sensor; 7 – controller (Biocontroller ADI 1010, Applikon); 8 – stirring engine; 9 – solvent; 10 – fermentation broth; 11 – gas condenser (4°C); 12 – gas sampling port; 13 – gas meter (μFlow, Bioprocess Control); 14 – liquid sampling port; 15 – water jacket; 16 – effluent tank; 17 – acid tank (**A**).

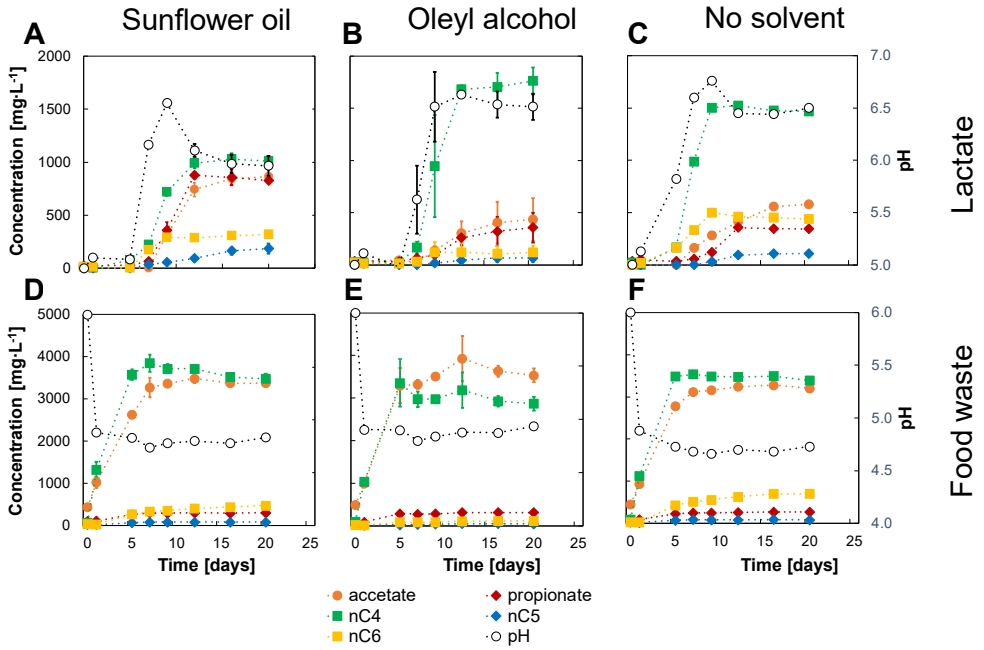

Figure S2. Metabolites concentration in the aqueous phase during extractive batch fermentation with: (**A**, **D**) sunflower oil and (**B**, **E**) oleyl alcohol. (**C**, **F**) Non-extractive fermentation singletons. Substrates were lactate (**A**-**C**) and food waste (**D**-**F**). Error bars depict duplicates absolute deviation from the average.

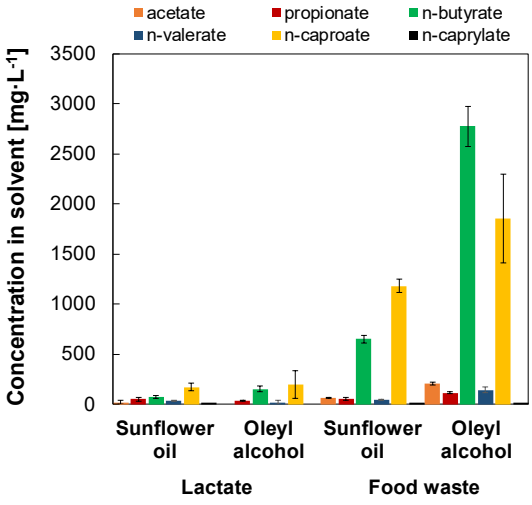

Figure S3. Carboxylates concentration in solvents during batch extractive fermentation. Error bars depict duplicates absolute deviation from the average.

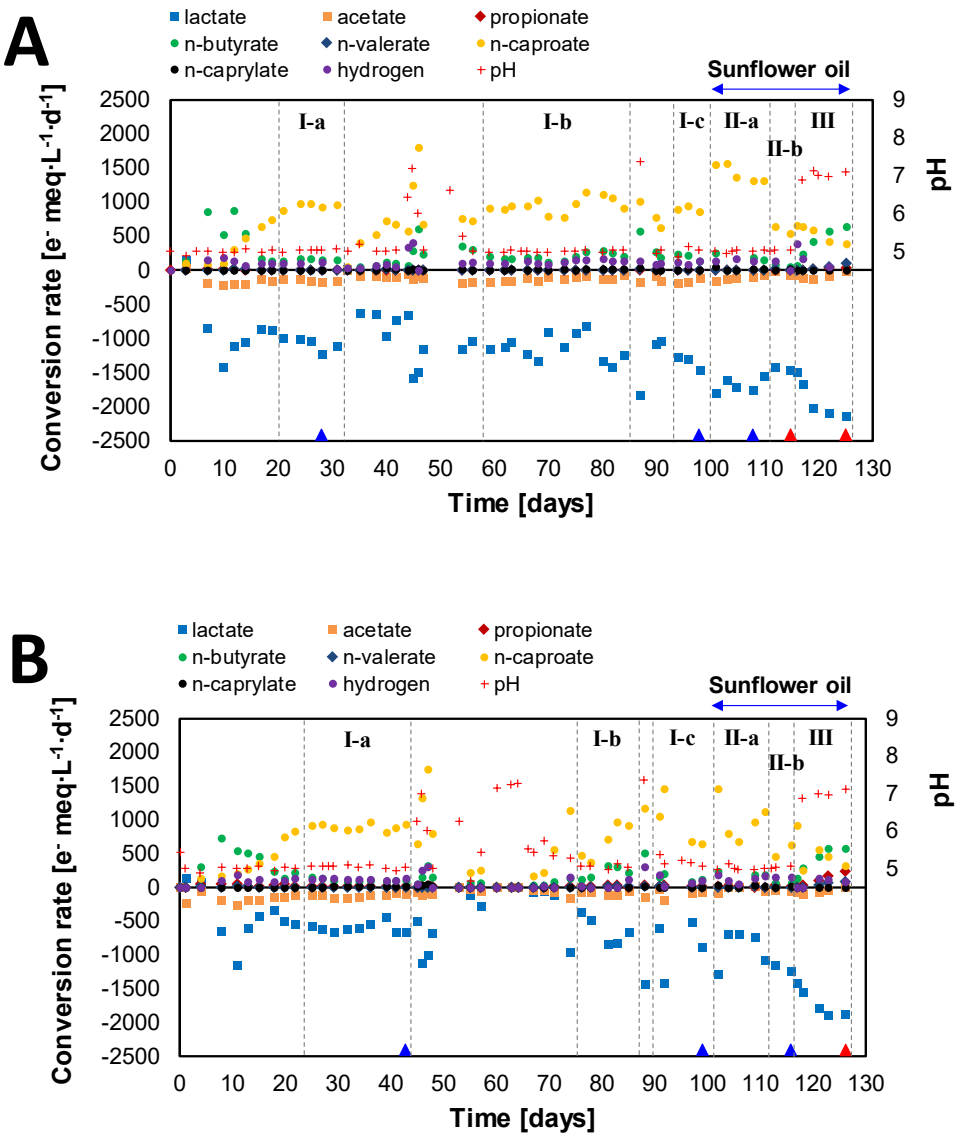

Figure S4. Conversion rates for lactate-based chain elongation as measured over time in: (**A**) R1 and (**B**) R2. Batch periods correspond to days 46.8-54 in R1; days 47.8-55 and 57-64 in R2. Triangles show DNA sampling days (blue – suspended biomass samples, red – both suspended biomass and biofilm samples). DNA sample from period II-a was taken only for R1.

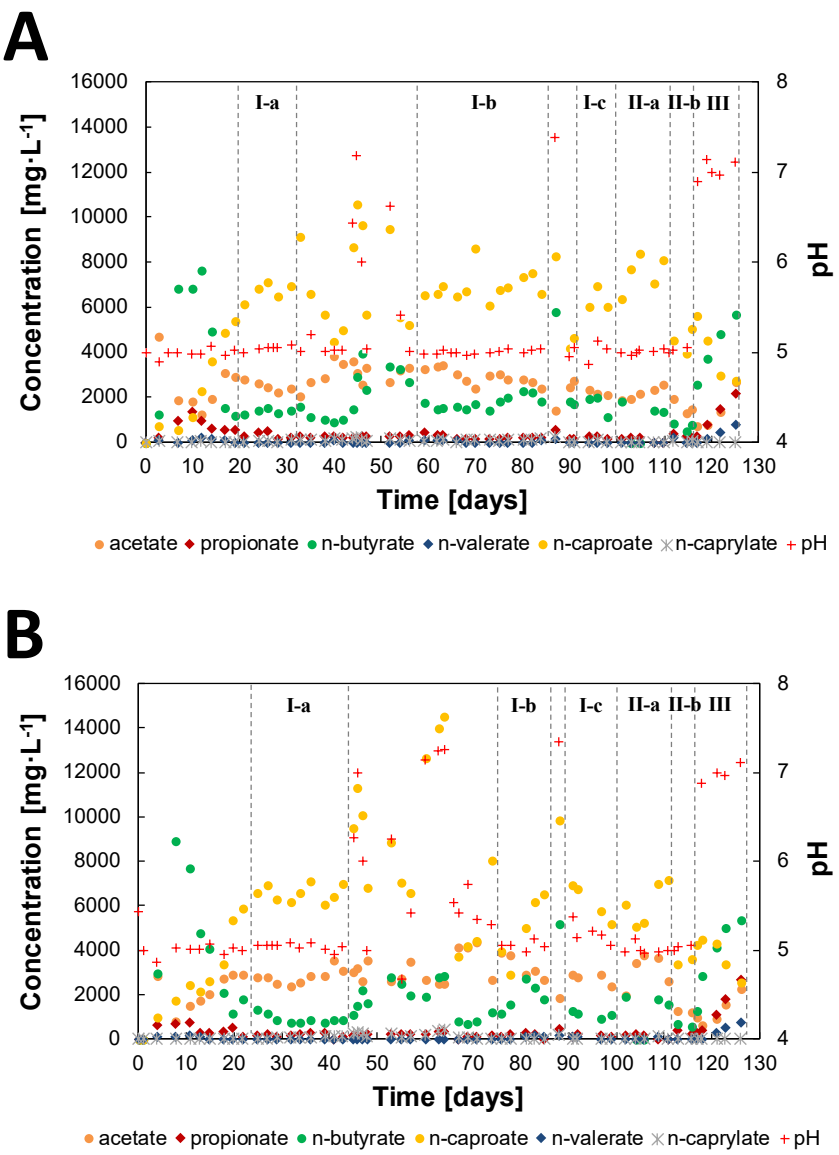

Figure S5. Aqueous phase metabolites concentrations and pH over time in: (**A**) R1 and (**B**) R2.

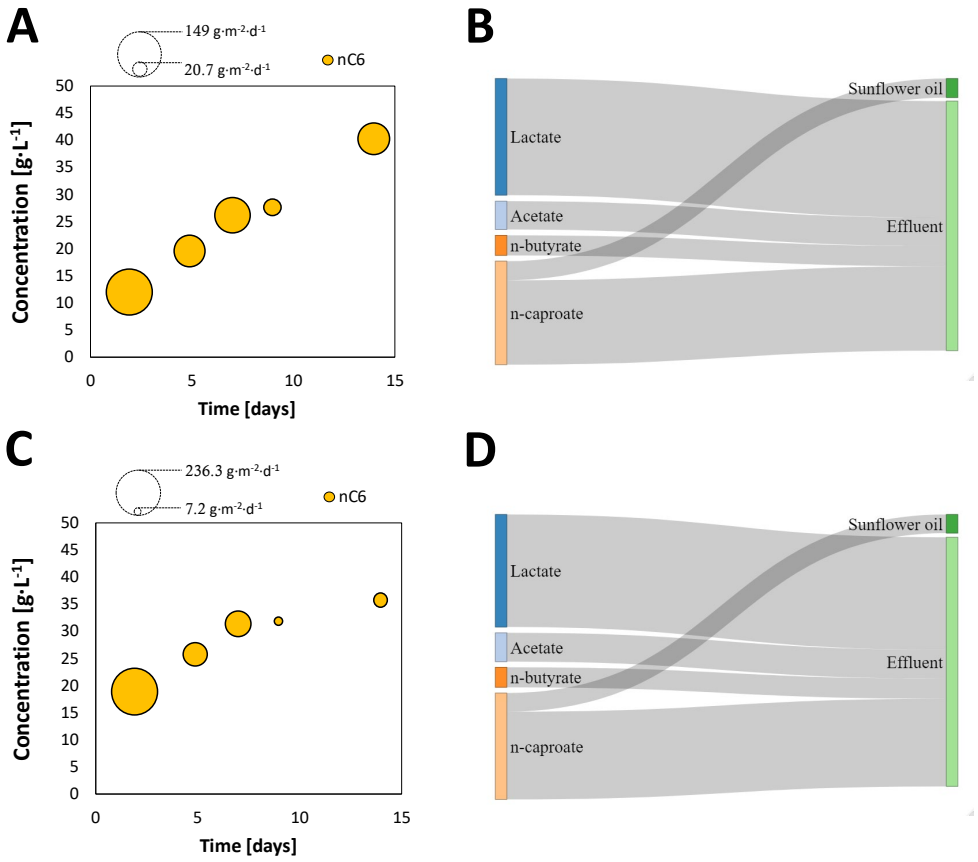

Figure S6. Selective extraction of n-caproate with sunflower oil from continuously fed synthetic medium. n-caproate concentrations in sunflower oil as measured from back-extracted samples in: (**A**) R3 and (**C**) R4. Bubble size extraction flux into the solvent based on cumulative carboxylates concentrations between two contiguous sampling points. Sankey diagrams show the carbon flux (mmol C·d^{-1}) for (**B**) R3 and (**D**) R4. The synthetic effluent contained lactate, acetate, propionate, n-butyrate and n-caproate fed to an HRT of 2 days and aqueous phase pH was controlled at 5.0. Nitrogen sources were left out to avoid microbial growth.

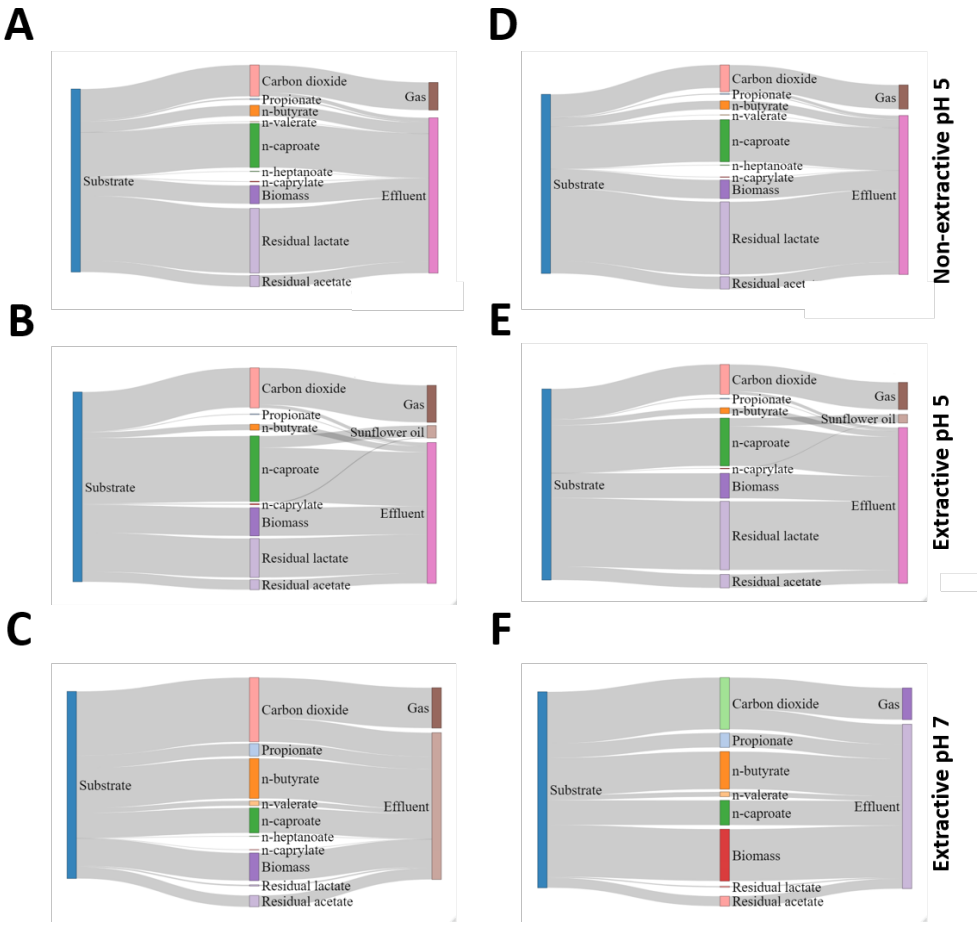

Figure S7. Carbon flux (mmol C·d^{-1}) during non-extractive and extractive lactate-based chain elongation in (**A**-**C**) R1 and (**D**-**F**) R2. Sankey diagrams were built using data of periods I-a to I-b (non-extractive pH 5), period II-a (extractive pH 5.0) and period III (extractive pH 7.0). The unidentified missing carbon was assumed to be assimilated into biomass.

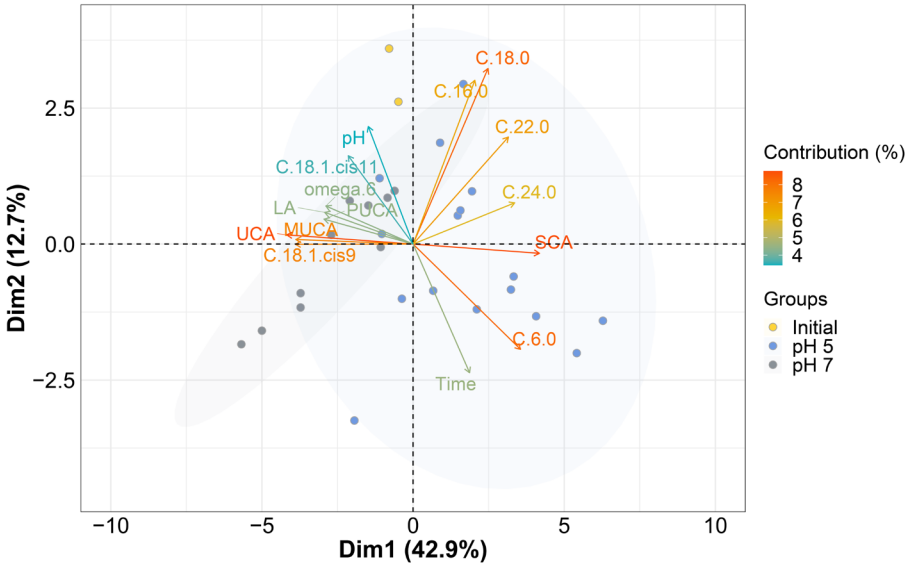

Figure S8. Principal Components Analysis (PCA) plot of carboxylic acids composition of initial sunflower oil and MCC-enriched sunflower oil at different pH conditions. MCC-enriched sunflower oil samples were taken from both reactors at different times during extractive fermentation with sampling points same as in Figure 3. Carboxylic acids compositions was measured according to the ISO 15885 standard. Variables were scaled and centered for analysis. Top 15 variables are shown with vectors colored according to their contribution to variance in the PCA plot. Concentration ellipses depict confidence intervals with α = 0.05 for groups with n>3. Principal Components Analysis (PCA) was done in R Studio using the prcomp function and visualized using the factoextra package (Kassambara and Mundt, 2020).

Table S1. Overview of continuous chain elongation operational parameters.

		Non-extractive chain elongation			Extractive chain elongation		
	Operational period	**I-a**	**I-b**	**I-c**	**II-a**	**II-b**	**III**
	pH	5.0±0.0	5.0±0.0	5.0±0.1	5.0±0.0	5.0±0.0	7.0±0.1
R1	HRT [days]	1.9±0.0	2.0±0.3	1.9±0.1	1.8±0.1	2.0±0.1	1.9±0.0
	Days	21-31	59-84	94-98	99-111	112-115	116-125
	pH	5.0±0.0	5.1±0.0	5.2±0.1	5.0±0.1	5.0±0.0	7.0±0.1
R2	HRT [days]	2.0±0.0	2.0±0.2	1.9±0.4	2.1±0.2	2.1±0.1	2.1±0.1
	Days	25-43	76-85	91-99	100-111	112-116	117-126

Error represents ±one standard deviation.

Table S2. Overview of chain elongation reactor R1 performance under non-extractive (I-a to I-c) and extractive (II-a to III) conditions.

		R1					
		I-a	**I-b**	**I-c**	**II-a**	**II-b**	**III**
Operational parameters	**days / (n)**	21-31 / (5)	59-84 / (12)	94-98 / (3)	99-111 / (5)	112-115 / (2)	122-125 / (2)
	HRT [days]	1.9±0.0	2.0±0.3	1.9±0.1	1.8±0.1	2.0±0.1	1.9±0.0
	pH	5.0±0.0	5.0±0.0	5.0±0.1	5.0±0.0	5.0±0.0	7.0±0.1
	Redox [mV]	-496±1	-493±6	-475±8	-479±8	-474±1	-567±12
Conversion rates [e^- meq·L^{-1}·d^{-1}]	**lactate**	-1067±87	-1131±176	-1332±81	-1679±92	-1430±25	-2105±30
	acetate	-140±10	-118±30	-150±29	-107±24	-39±22	-44±0
	propionate	31±12	22±8	23±4	12±10	31±7	179±40
	iso-butyrate	0	0	0	0	8±8	10±31
	n-butyrate	161±9	203±47	198±44	119±102	73±20	612±10
	iso-valerate	0	0	0	0	8±8	12±41
	n-valerate	0	5±6	0	0	13±13	78±1
	iso-caproate	0	1±3	0	0	13±13	0
	n-caproate	943±36	960±109	897±35	1421±114	593±46	397±0
	n-heptanoate	18±35	9±20	0	0	47±33	6±30
	n-caprylate	8±7	16±7	5±7	19±19	22±8	2±6
	hydrogen	116±7	129±26	111±13	157±14	150±3	107±2
Substrate conversion [%]	**lactate**	47±4	53±9	62±4	73±2	85±1	99±1
	acetate	45±4	37±6	49±5	39±7	27±15	24±22
Selectivity [%] (electrons/carbon)	**propionate**	2±1 / 2±1	2±1 / 1±1	2±1 / 2±0	<1/<1	3±1 / 2±0	13±2 / 9±1
	iso-butyrate	0/0	0/0	0/0	0/0	<1/<1	<1/<1
	n-butyrate	13±0 / 9±0	15±2 / 11±1	16±3 / 12±2	7±5 / 5±4	8±1 / 5±1	44±2 / 27±1
	iso-valerate	0/0	0/0	0/0	0/0	<1/<1	<1/<1
	n-valerate	0/0	<1/0	0/0	0/0	1±1 / 1±1	6±1 / 3±1
	iso-caproate	0/0	<1/0	0/0	0/0	1±1 / 1±1	0/0
	n-caproate	74±2 / 52±1	72±3 / 50±3	73±3 / 52±3	83±6 / 58±3	63±4 / 38±0	28±3 / 17±1
	n-heptanoate	1±3 / 1±2	<1/<1	0/0	0/0	5±3 / 3±2	<1/<1
	n-caprylate	<1/<1	1±0 / 1±0	<1/<1	1±1 / 1±1	3±1 / 1±1	<1/<1
	hydrogen / carbon dioxide	9±1 / 35±2	10±1 / 36±2	9±0 / 34±1	9±1 / 35±3	16±2 / 48±5	8±4 / 44±3
Conversion efficiency [%] (carbon)	**propionate**	2±1	1±0	1±0	0	1±0	7±1
	iso-butyrate	0	0	0	0	0	0
	n-butyrate	8±1	9±1	8±2	4±3	3±1	22±2
	iso-valerate	0	0	0	0	0	0
	n-valerate	0	0	0	0	1±1	3±1
	iso-caproate	0	0	0	0	1±1	0
	n-caproate	43±3	42±3	35±2	45±3	24±2	13±1
	n-heptanoate	1±2	0	0	0	2±1	0
	n-caprylate	0	1±0	0	1±1	1±0	0
	carbon dioxide	29±1	30±3	23±3	27±1	29±0	35±1
	biomass[a]	17±5	17±6	33±7	23±3	38±7	19±4
Acid addition for pH control	**mmol HCl·L^{-1}·d^{-1}**	76±4	82±32	54±38	106±8	46±46	17±13
	mol H^+·mol MCC^{-1}	2.5±0.1	2.6±0.8	1.9±1.3	2.4±0.1	2±2	1.3±0.9

±one standard deviation is shown for periods with n≥3. Absolute deviation is shown for periods with n=2.

[a]Unidentified carbon was assumed to be assimilated into biomass.

Table S3. Overview of chain elongation reactor R2 performance under non-extractive (I-a to I-c) and extractive (II-a to III) conditions.

		R2					
		I-a	**I-b**	**I-c**	**II-a**	**II-b**	**III**
Operational parameters	**days / (n)**	25-43 / (9)	76-85 / (5)	91-99 / (4)	100-111 / (5)	112-116 / (2)	123-126 / (2)
	HRT [days]	2.0±0.0	2.0±0.2	1.9±0.4	2.1±0.2	2.1±0.1	2.1±0.1
	pH	5.0±0.0	5.1±0.0	5.2±0.1	5.0±0.1	5.0±0.0	7.0±0.1
	Redox [mV]	-405±8	-367±19	-400±45	-358±22	-349±12	-503±5
Conversion rates [e^- meq·L^{-1}·d^{-1}]	**lactate**	-595±67	-627±186	-844±353	-897±238	-1191±42	-1868±9
	acetate	-122±20	-82±25	-90±57	-25±40	-41±4	-21±20
	propionate	15±7	16±10	16±9	10±8	27±6	205±34
	iso-butyrate	0	0	0	0	6±6	5±5
	n-butyrate	102±23	221±79	140±44	118±98	66±3	570±0
	iso-valerate	0	0	0	0	0	13±2
	n-valerate	0	9±8	10±10	2±5	0	76±10
	iso-caproate	0	0	0	3±6	0	0
	n-caproate	894±46	689±236	957±325	1002±273	542±87	381±72
	n-heptanoate	16±26	0	0	10±19	8±8	0
	n-caprylate	12±7	0	0	15±14	7±7	0
	hydrogen	118±9	28±49	93±58	130±49	158±1	102±21
Substrate conversion [%]	**lactate**	32±4	35±9	44±7	48±12	81±0	99±1
	acetate	40±7	27±6	29±11	11±18	34±2	15±14
Selectivity [%] (electrons/carbon)	**propionate**	1±1 / 1±1	2±2 / 2±1	1±1 / 1±1	1±1 / 1±1	3±1 / 2±1	15±3 / 11±2
	iso-butyrate	0/0	0/0	0/0	0/0	<1/<1	<1/<1
	n-butyrate	9±2 / 7±1	23±5 / 22±7	12±1 / 9±1	7±6 / 6±5	8±1 / 5±0	42±1 / 29±0
	iso-valerate	0/0	0/0	0/0	0/0	0/0	1±0 / <1
	n-valerate	0/0	<1/<1	<1/<1	<1/<1	0/0	6±1 / 4±1
	iso-caproate	0/0	0/0	0/0	<1/<1	0/0	0±0 / 0±0
	n-caproate	77±2 / 54±2	72±4 / 62±8	78±4 / 59±11	80±8 / 58±8	66±5 / 36±4	28±4 / 18±3
	n-heptanoate	1±2 / 1±2	0/0	0/0	<1/<1	1±1 / <1	0/0
	n-caprylate	1±1 / <1	0/0	0/0	1±1 / <1	1±1 / <1	0/0
	hydrogen / carbon dioxide	10±1 / 37±2	2±4 / 13±13	8±5 / 30±13	10±2 / 35±4	20±2 / 55±3	8±1 / 38±0
Carbon conversion efficiency [%]	**propionate**	1±1	2±1	1±1	1±1	2±1	8±2
	iso-butyrate	0	0	0	0	1±1	1±1
	n-butyrate	6±2	13±2	7±2	5±5	3±1	20±1
	iso-valerate	0	0	0	0	0	1±1
	n-valerate	0	1±1	1±1	1±1	0	3±1
	iso-caproate	0	0	0	1±1	0	0
	n-caproate	46±3	38±9	45±9	43±5	21±3	13±2
	n-heptanoate	1±2	0	0	1±1	1±1	0
	n-caprylate	1±1	0	0	1±1	1±1	0
	carbon dioxide	32±2	11±15	25±13	27±7	32±1	26±1
	biomass[a]	16±5	39±21	24±18	25±16	44±1	33±2
Acid addition for pH control	**mmol HCl·L^{-1}·d^{-1}**	67±5	55±24	63±35	78±22	90±1	19±10
	mol H^+·mol MCC^{-1}	2.4±0.2	2.5±0.5	2.3±1.1	2.5±0.5	5.3±0.9	1.5±0.6

±one standard deviation is shown for periods with n≥3. Absolute deviation is shown for periods with n=2.

[a]Unidentified carbon was assumed to be assimilated into biomass.

Table S4. Selected 16S rRNA gene amplicon sequence variants (ASV).

ASV	Sequence	SILVA	NCBI		
		Genus	Strain	Coverage [%]	Identity [%]
1	GCAGCAACGCCGCGTGAAGGAAGACGGTCTTCGGATTGTAAACTTTTGTACTCAGGGA CGATAATGACGGTACCTGAGCAGCAAGCTCCGGCTAACTACGTGCCAGCAGCCGCGGT AATACGTAGGGAGCGAGCGTTGTCCGGATTTACTGGGTGTAAAGGGTGCGTAGGCGGC AGGACAAGTCAGCTGTGAAAACTATGGGCTTAACCCATAGCCTGCAGTTGAAACTGTTC TGCTTGAGTGAAGTAGAGGTAGGTGGAATTCCCGGTGTAGCGGTGAAATGCGTAGAGA TCGGGAGGAACACCAGTGGCGAAGGCGGCCTACTGGGCTTTAAC	*Caproiciproducens*	[Clostridium] *leptum* strain DSM 753	100	92.86
2	GCAGCAACGCCGCGTGAAGGAAGACGGTCTTCGGATTGTAAACTTTTGTACCTAGGGA CGATAATGACGGTACCTAGGCAGCAAGCTCCGGCTAACTACGTGCCAGCAGCCGCGGT AATACGTAGGGAGCGAGCGTTGTCCGGATTTACTGGGTGTAAAGGGTGCGTAGGCGGC CAAGCAAGTCAGCTGTGAAAACTATGGGCTTAACCCATAGCCTGCAATTGAAACTGTTT GGCTTGAGTGAAGTAGAGGTAGGTGGAATTCCCGGTGTAGCGGTGAAATGCGTAGAGA TCGGGAGGAACACCAGTGGCGAAGGCGACCTACTGGGCTTTAAC	*Caproiciproducens*	[Clostridium] *leptum* strain DSM 753	100	92.54
4	GCAGCAACGCCGCGTGAAGGAAGAAGGGTTTCGGCTCGTAAACTTCTATCAACAGGGA CGAAAAAAATGACGGTACCTGAATAAGAAGCCCCGGCTAACTACGTGCCAGCAGCCGC GGTAATACGTAGGGGGCAAGCGTTATCCGGAATTACTGGGTGTAAAGGGTGAGTAGGC GGCATGGTAAGTTAGATGTGAAAGCCCGAGGCTTAACCTCGGGATTGCATTTAAAACTA TCAAGCTAGAGTACAGGAGAGGAAAGCGGAATTCCTAGTGTAGCGGTGAAATGCGTAG ATATTAGGAAGAACACCAGTGGCGAAGGCGGCTTTCTGGACTGAAAC	*Anaerotignum*	*Anaerotignum propionicum* strain JCM 1430	100	98.52
7	GCAGCAACGCCGCGTGAAGGAAGACGGTTTTCGGATTGTAAACTTCTATCAATAGGGAC GAAATAAATGACGGTACCTAAATAAGAAGCCCCGGCTAACTACGTGCCAGCAGCCGCG GTAATACGTAGGGGGCAAGCGTTATCCGGAATTACTGGGTGTAAAGGGTGAGTAGGCG GCATGATAAGTAAGATGTGAAAGCCCGCGGCTTAACTGCGGGATTGCATTTTAAACTAT TGAGCTAGAGTACAGGAGAGGAAAGCGGAATTCCCAGTGTAGCGGTGAAATGCGTAGA TATTGGGAAGAACACCAGTGGCGAAGGCGGCTTTCTGGACTGAAAC	*Lachnospiraceae* UCG-010	*Anaerotignum aminivorans* strain SH021	100	94.97
8	GCAGCAACGCCGCGTGAAGGAAGACGGTTTTCGGATTGTAAACTTCTATCAATAGGGAA GAAAGAAATGACGGTACCTAAATAAGAAGCCCCGGCTAACTACGTGCCAGCAGCCGCG GTAATACGTAGGGGGCAAGCGTTATCCGGAATTACTGGGTGTAAAGGGTGAGTAGGCG GCATGACAAGTAAGATGTGAAAGCCCGCGGCTTAACTGCGGGATTGCATTTTAAACTGT TGAGCTAGAGTACAGGAGAGGAAAGCGGAATTCCCAGTGTAGCGGTGAAATGCGTAGA TATTGGGAAGAACACCAGTGGCGAAGGCGGCTTTCTGGACTGAAAC	*Lachnospiraceae* UCG-010	*Anaerotignum aminivorans* strain SH021	100	94.97

Table S4. Selected 16S rRNA gene amplicon sequence variants (ASV) (continued).

ASV	Sequence	SILVA	NCBI		
		Genus	Strain	Coverage [%]	Identity [%]
9	GCAGCAACGCCGCGTGAGTGAAGAAGGTTTTCGGATTGTAAAGCTCTGTCATCTGGGA CGATAATGACGGTACCAGATGAGGAAGCCACGGCTAACTACGTGCCAGCAGCCGCGGT AATACGTAGGTGGCAAGCGTTGTCCGGAATTACTGGGCGTAAAGGGTGCGCAGGCGGA CATTTAAGTGAGATGTGAAAGACCCGGGCTTAACTTGGGCAGTGCATTTCAAACTGGAT GTCTGGAGTGCAGGAGAGGAGAACGGAATTCCTAGTGTAGCGGTGAAATGCGTAGAGA TTAGGAAGAACACCAGTGGCGAAGGCGGTTCTCTGGACTGTAAC	*Clostridium luticellarii*	*Clostridium luticellarii* strain FW431	100	100
10	GCAGCGACGCCGCGTGAGCGATGAAGGTTTTCGGATCGTAAAGCTCTGTCCTAAGGGA CGATAATGACGGTACCTTAGGAGGAAGCCCCGGCTAACTACGTGCCAGCAGCCGCGGT AATACGTAGGGGGCGAGCGTTGTCCGGATTTATTGGGCGTAAAGGGTGCGTAGGCGG CCTTGTAAGTCAGATGTGAAATCTCACGGCTTAACCGTGGTAAGCATTTGAAACTGTGA GGCTTGAGTACAGGAGAGGAGAGTGGAATTCCTAGTGTAGCGGTGAAATGCGTAGATA TTAGGAGGAATACCAGTGGCGAAGGCGACTCTCTGGACTGTAAC	Unclassified *Sporanaerobacter*	*Sporoanaerobacter acetigenes* strain DSM13106	100	100
11	GCAGCAACGCCGCGTGAGTGAAGAAGGTTTTCGGATTGTAAAGCTCTGTCATCTGGGA CGATAATGACGGTACCAGATGAGGAAGCCACGGCTAACTACGTGCCAGCAGCCGCGGT AATACGTAGGTGGCAAGCGTTGTCCGGAATTACTGGGCGTAAAGGGTGCGCAGGCGGA CATTTAAGTGAGATGTGAAATACCCGGGCTTAACCCGGGCAGTGCATTTCAAACTGGGT GTCTGGAGTGCAGGAGAGGAGAACGGAATTCCTAGTGTAGCGGTGAAATGCGTAGAGA TTAGGAAGAACACCAGTGGCGAAGGCGGTTCTCTGGACTGTAAC	*Clostridium luticellarii*	*Clostridium luticellarii* strain FW431	100	98.8

Table S5. Stoichiometry of lactate-based chain elongation in R1 at pH 5.0 with(out) extraction with sunflower oil.

	mol·mol n-caproate^{-1}		
	Non-extractive[a]	**Extractive[b]**	**Ruminococcaceae CPB6[c]**
lactate	-3.39 (0.54)	-3.17 (0.27)	-3.83
acetate	-0.56 (0.14)	-0.3 (0.05)	-0.43
propionate	0.06 (0.02)	0.02 (0.02)	N.A.
n-butyrate	0.37 (0.05)	0.14 (0.11)	0.17
n-caproate	1	1	1
n-caprylate	0.01 (0.01)	0.01 (0.01)	N.A.
hydrogen	2.13 (0.24)	1.79 (0.27)	2.36
carbon dioxide	4.28 (0.42)	3.64 (0.37)	N.A.

[a]Periods I-a to I-c, n=20; [b]Period II-a, n=5; [c]As reported for lactate and acetate as substrates in Zhu et al. (2017).

Standard deviation is shown in braces.

References

References

Abdelhamed, H., Ozdemir, O., Ibrahim, I., Lawrence, M., and Karsi, A. (2019). Antibacterial activities of trans-cinnamaldehyde, caprylic acid, and β-resorcylic acid against catfish pathogens. *Aquaculture* 504, 334–344. doi:10.1016/j.aquaculture.2019.02.017.

Agler, M. T., Wrenn, B. A., Zinder, S. H., and Angenent, L. T. (2011). Waste to bioproduct conversion with undefined mixed cultures : the carboxylate platform. *Trends Biotechnol.* 29, 70–78. doi:10.1016/j.tibtech.2010.11.006.

Akedo, M., Cooney, C. L., and Sinskey, A. J. (1983). Direct demonstration of lactate-acrylate interconversion in Clostridium propionicum. *Nat. Biotechnol.*, 28–31.

Andrews, J. H., and Harris, R. F. (1986). "r- and K-Selection and Microbial Ecology," in *Advances in Microbial Ecology*, ed. K. C. Marshall (Boston, MA: Springer), 99–147. doi:doi.org/10.1007/978-1-4757-0611-6_3.

Angenent, L. T., and Agler, M. T. (2014). Production of carboxylates and methane from biomass waste. Available at: https://patents.google.com/patent/US20140331942A1/en.

Angenent, L. T., Richter, H., Buckel, W., Spirito, C. M., Steinbusch, K. J. J., Plugge, C. M., et al. (2016). Chain Elongation with Reactor Microbiomes: Open-Culture Biotechnology To Produce Biochemicals. *Environ. Sci. Technol.* 50, 2796–2810. doi:10.1021/acs.est.5b04847.

Balcome, S., and Carlson, M. (2020). interactiveDisplay: Package for enabling powerful shiny web displays of Bioconductor objects.

Baldwin, R. L., Wood, W. A., and Emery, R. S. (1965). Lactate metabolism by peptostreptococcus elsdenii: Evidence for lactyl coenzyme a dehydrase. *BBA - Gen. Subj.* 97, 202–213. doi:10.1016/0304-4165(65)90084-X.

Baltić, B., Starčević, M., Dordević, J., Mrdović, B., and Marković, R. (2017). Importance of medium chain fatty acids in animal nutrition. *IOP Conf. Ser. Earth Environ. Sci.* 85. doi:10.1088/1755-1315/85/1/012048.

Barker, H. A. (1947). Clostridium Kluyveri. *Antonie Van Leeuwenhoek* 12, 167–176. doi:10.1007/BF02272663.

Barker, H. A., Kamen, M. D., and Bornstein, B. T. (1945). The synthesis of butyric and caproic acids from ethanol and acetic acid by Clostridium kluyveri. *Proc. Natl. Acad. Sci.* 31, 373–381. doi:10.1073/pnas.31.12.373.

Barker, H. A., and Taha, M. (1941). Clostridium Kluyverii, an organism concerned in the formation of caproic acid from ethyl alcohol. *J. Bacteriol.* 43, 347–363.

Beck, M. W., and Mikryukov, V. (2020). ggord: Ordination Plots with ggplot2. doi:10.5281/zenodo.842225.

Bengelsdorf, F. R., Poehlein, A., and Dürre, P. (2019). Genome Sequence of the Caproic Acid-Producing Bacterium Caproiciproducens galactitolivorans BS-1T (JCM 30532). *Microbiol. Resour. Announc.* 8. doi:10.1128/MRA.00346-19.

Blanchet, E., Vahlas, Z., Etcheverry, L., Rafra, Y., Erable, B., Délia, M., et al. (2018). Coupled iron-microbial catalysis for CO2 hydrogenation with multispecies microbial communities. *Chem. Eng. J.* 346, 307–316. doi:10.1016/j.cej.2018.03.191.

Bolaji, I. O., and Dionisi, D. (2017). Acidogenic fermentation of vegetable and salad waste for chemicals production: Effect of pH buffer and retention time. *J. Environ. Chem. Eng.* 5, 5933–5943. doi:10.1016/j.jece.2017.11.001.

Breitenstein, A., Wiegel, J., Haertig, C., Weiss, N., Andreesen, J. R., and Lechner, U. (2002). Reclassification of Clostridium hydroxybenzoicum as Sedimentibacter hydroxybenzoicus gen. nov., comb. nov., and description of Sedimentibacter saalensis sp. nov. *Int. J. Syst. Evol. Microbiol.* 52, 801–807. doi:10.1099/ijs.0.01998-0.

Brennan, T. C. R., Turner, C. D., Krömer, J. O., and Nielsen, L. K. (2012). Alleviating monoterpene toxicity using a two-phase extractive fermentation for the bioproduction of jet fuel mixtures in Saccharomyces cerevisiae. *Biotechnol. Bioeng.* 109, 2513–2522. doi:10.1002/bit.24536.

Buckel, W., and Thauer, R. K. (2013). Energy conservation via electron bifurcating ferredoxin reduction and proton/Na+ translocating ferredoxin oxidation. *Biochim. Biophys. Acta - Bioenerg.* 1827, 94–113. doi:10.1016/j.bbabio.2012.07.002.

Buckel, W., and Thauer, R. K. (2018). Flavin-Based Electron Bifurcation, A New Mechanism of Biological Energy Coupling. *Chem. Rev.* 118, 3862–3886. doi:10.1021/acs.chemrev.7b00707.

Burkhardt, E. M., Bischoff, S., Akob, D. M., Büchel, G., and Küsel, K. (2011). Heavy metal tolerance of Fe(III)-reducing microbial communities in contaminated creek bank soils. *Appl. Environ. Microbiol.* 77, 3132–3136. doi:10.1128/AEM.02085-10.

Callahan, B. J., Mcmurdie, P. J., and Holmes, S. P. (2017). Exact sequence variants should replace operational taxonomic units in marker-gene data analysis. *ISME J.* 11, 2639–2643. doi:10.1038/ismej.2017.119.

Callahan, B. J., Mcmurdie, P. J., Rosen, M. J., Han, A. W., Johnson, A. J. A., and Holmes, S. P. (2016). DADA2: High-resolution sample inference from Illumina amplicon data. *Nat. Methods* 13, 581–583. doi:10.1038/nmeth.3869.

Canakci, M. (2007). The potential of restaurant waste lipids as biodiesel feedstocks. *Bioresour. Technol.* 98, 183–190. doi:10.1016/j.biortech.2005.11.022.

Candry, P., and Ganigué, R. (2021). Chain elongators, friends, and foes. *Curr. Opin. Biotechnol.* 67, 99–110. doi:10.1016/j.copbio.2021.01.005.

Candry, P., Radić, L., Favere, J., Carvajal-Arroyo, J. M., Rabaey, K., and Ganigué, R. (2020a). Mildly acidic pH selects for chain elongation to caproic acid over alternative pathways during lactic acid fermentation. *Water Res.* 186. doi:10.1016/j.watres.2020.116396.

Candry, P., Ulcar, B., Petrognani, C., Rabaey, K., and Ganigué, R. (2020b). Ethanol:propionate ratio drives product selectivity in odd-chain elongation with Clostridium kluyveri and mixed communities. *Bioresour. Technol.* 313, 1–5.

doi:10.1016/j.biortech.2020.123651.
Carmona-Cabello, M., Leiva-Candia, D., Castro-Cantarero, J. L., Pinzi, S., and Dorado, M. P. (2018). Valorization of food waste from restaurants by transesterification of the lipid fraction. *Fuel* 215, 492–498. doi:10.1016/j.fuel.2017.11.096.
Carvajal-Arroyo, J. M., Candry, P., Andersen, S. J., Props, R., Seviour, T., Ganigué, R., et al. (2019). Granular fermentation enables high rate caproic acid production from solid-free thin stillage. *Green Chem.* 21, 1330–1339. doi:10.1039/c8gc03648a.
Cavaleiro, A. J., Pereira, M. A., Guedes, A. P., Stams, A. J. M., Alves, M. M., and Sousa, D. Z. (2016). Conversion of Cn-Unsaturated into Cn-2-Saturated LCFA Can Occur Uncoupled from Methanogenesis in Anaerobic Bioreactors. *Environ. Sci. Technol.* 50, 3082–3090. doi:10.1021/acs.est.5b03204.
Cazzolla Gatti, R., and Velichevskaya, A. (2020). Certified "sustainable" palm oil took the place of endangered Bornean and Sumatran large mammals habitat and tropical forests in the last 30 years. *Sci. Total Environ.* 742, 1–6. doi:10.1016/j.scitotenv.2020.140712.
ChainCraft B.V. Available at: www.chaincraft.nl [Accessed January 12, 2021].
Chen, W., Huang, S., Strik, D. P., and Buisman, C. N. J. (2016a). Isobutyrate biosynthesis via methanol chain elongation : converting organic wastes to platform chemicals. *J. Chem. Technol. Biotechnol.* doi:10.1002/jctb.5132.
Chen, W. S., Strik, D. P. B. T. B., Buisman, C. J. N., and Kroeze, C. (2017). Production of Caproic Acid from Mixed Organic Waste: An Environmental Life Cycle Perspective. *Environ. Sci. Technol.* 51, 7159–7168. doi:10.1021/acs.est.6b06220.
Chen, W. S., Ye, Y., Steinbusch, K. J. J., Strik, D. P. B. T. B., and Buisman, C. J. N. (2016b). Methanol as an alternative electron donor in chain elongation for butyrate and caproate formation. *Biomass and Bioenergy* 93, 201–208. doi:10.1016/j.biombioe.2016.07.008.
Cheng, Q., and Call, D. F. (2016). Hardwiring microbes via direct interspecies electron transfer: mechanisms and applications. *Environ. Sci. Process. Impacts* 18, 968–980. doi:10.1039/c6em00219f.
Cheng, X., Ng, H. K., Gan, S., Ho, J. H., and Pang, K. M. (2018). Numerical Analysis of the Effects of Biodiesel Unsaturation Levels on Combustion and Emission Characteristics under Conventional and Diluted Air Conditions. *Energy and Fuels* 32, 8392–8410. doi:10.1021/acs.energyfuels.8b00650.
Cherubini, F. (2010). The biorefinery concept: using biomass instead of oil for producing energy and chemicals. *Energy Convers. Manag.* 51, 1412–1421. doi:10.1016/j.enconman.2010.01.015.
Choi, K., Jeon, B. S., Kim, B. C., Oh, M. K., Um, Y., and Sang, B. I. (2013). In situ biphasic extractive fermentation for hexanoic acid production from sucrose by megasphaera elsdenii NCIMB 702410. *Appl. Biochem. Biotechnol.* 171, 1094–1107. doi:10.1007/s12010-013-0310-3.
Christensen, W. B., Johnson, M. J., and Peterson, W. H. (1939). Properties of the lactic acid-racemizing enzyme of Clostridium butylicum. *J. Biol. Chem.* 127, 421–430.
Chwialkowska, J., Duber, A., Zagrodnik, R., Walkiewicz, F., Łężyk, M., and Oleskowicz-Popiel, P. (2019). Caproic acid production from acid whey via open culture fermentation – Evaluation of the role of electron donors and downstream processing. *Bioresour. Technol.* 279, 74–83. doi:10.1016/j.biortech.2019.01.086.
Cochrane, R. A., Dritz, S. S., Woodworth, J. C., Stark, C. R., Saensukjaroenphon, M., Gebhardt, J. T., et al. (2019). Assessing the effects of medium-chain fatty acids and fat sources on PEDV infectivity. *Transl. Anim. Sci.* 4, 1051–1059. doi:10.1093/tas/txz179.
Contarini, G., Povolo, M., Pelizzola, V., Monti, L., and Lercker, G. (2013). Interlaboratory evaluation of milk fatty acid composition by using different GC operating conditions. *J. Food Compos. Anal.* 32, 131–140. doi:10.1016/j.jfca.2013.08.008.
Contreras-Dávila, C. A., Ali, A., Buisman, C. J. N., and Strik, D. P. B. T. B. (2021). Lactate Metabolism and Microbiome Composition Are Affected by Nitrogen Gas Supply in Continuous Lactate-Based Chain Elongation. *Fermentation* 7, 1–16. doi:10.3390/fermentation7010041.
Contreras-Dávila, C. A., Carrión, V. J., Vonk, V. R., Buisman, C. N. J., and Strik, D. P. B. T. B. (2020). Consecutive lactate formation and chain elongation to reduce exogenous chemicals input in repeated-batch food waste fermentation. *Water Res.* 169, 1–10. doi:10.1016/j.watres.2019.115215.
Costa, S., Summa, D., Semeraro, B., Zappaterra, F., Rugiero, I., and Tamburini, E. (2021). Fermentation as a Strategy for Bio-Transforming Waste into Resources: Lactic Acid Production from Agri-Food Residues. *Fermentation* 7, 2–12. doi:10.3390/fermentation7010003.
Counotte, G. H. M., and Prins, R. A. (1981). Regulation of lactate metabolism in the rumen. *Vet. Res. Commun.* 5, 101–115. doi:10.1007/BF02214975.
Crow, V. L. (1986). Utilization of lactate isomers by Propionibacterium freudenreichii subsp. shermanii: Regulatory role for intracellular pyruvate. *Appl. Environ. Microbiol.* 52, 352–358. doi:10.1128/aem.52.2.352-358.1986.
De Clercq, R., Dusselier, M., Makshina, E., and Sels, B. F. (2018). Catalytic Gas-Phase Production of Lactide from Renewable Alkyl Lactates. *Angew. Chemie - Int. Ed.* 57, 3074–3078. doi:10.1002/anie.201711446.
de Leeuw, K. D., Buisman, C. J. N., and Strik, D. P. B. T. B. (2019). Branched Medium Chain Fatty Acids: Iso-Caproate Formation from Iso-Butyrate Broadens the Product Spectrum for Microbial Chain Elongation. *Environ. Sci. Technol.* 53, 7704–7713. doi:10.1021/acs.est.8b07256.
de Leeuw, K. D., de Smit, S. M., van Oossanen, S., Moerland, M. J., Buisman, C. J. N., and Strik, D. P. B. T. B. (2020). Methanol-Based Chain Elongation with Acetate to n-Butyrate and Isobutyrate at Varying Selectivities Dependent on pH. *ACS Sustain. Chem. Eng.* 8, 8184–8194. doi:10.1021/acssuschemeng.0c00907.
Dennis, D., and Kaplan, N. O. (1965). Lactic acid racemization. *Ann. N. Y. Acad. Sci.* 119, 868–876. doi:10.1111/j.1749-6632.1965.tb47448.x.
Desguin, B., Goffin, P., Viaene, E., Kleerebezem, M., Martin-Diaconescu, V., Maroney, M. J., et al. (2014). Lactate racemase

is a nickel-dependent enzyme activated by a widespread maturation system. *Nat. Commun.* 5. doi:10.1038/ncomms4615.

Desguin, B., Soumillion, P., Hausinger, R. P., and Hols, P. (2017). Unexpected complexity in the lactate racemization system of lactic acid bacteria. *FEMS Microbiol. Rev.* 41, S71–S83. doi:10.1093/femsre/fux021.

Dessì, P., Sánchez, C., Mills, S., Cocco, F. G., Isipato, M., Ijaz, U. Z., et al. (2021). Carboxylic acids production and electrosynthetic microbial community evolution under different CO2 feeding regimens. *Bioelectrochemistry* 137. doi:10.1016/j.bioelechem.2020.107686.

Diao, M., and Yao, M. (2009). Use of zero-valent iron nanoparticles in inactivating microbes. *Water Res.* 43, 5243–5251. doi:10.1016/j.watres.2009.08.051.

Dickey, A., Grenié, M., Thompson, R., Selzer, L., and Strbenac, D. (2019). Igraph manual-Network Analysis and Visualization: Package. 426. Available at: http://igraph.org.

Diez-Gonzalez, F., Russell, J. B., and Hunter, J. B. (1995). The role of an NAD-independent lactate dehydrogenase and acetate in the utilization of lactate by Clostridium acetobutylicum strain P262. *Arch. Microbiol.* 164, 36–42. doi:10.1007/BF02568732.

Ding, H.-B., Tan, G.-Y. A., and Wang, J.-Y. (2010). Caproate formation in mixed-culture fermentative hydrogen production. *Bioresour. Technol.* 101, 9550–9559. doi:10.1016/j.biortech.2010.07.056.

Dohme, F., Machmüller, A., Wasserfallen, A., and Kreuzer, M. (2001). Ruminal methanogenesis as influenced by individual fatty acids supplemented to complete ruminant diets. *Lett. Appl. Microbiol.* 32, 47–51. doi:10.1046/j.1472-765X.2001.00863.x.

Duber, A., Jaroszynski, L., Zagrodnik, R., Chwialkowska, J., Juzwa, W., Ciesielski, S., et al. (2018). Exploiting the real wastewater potential for resource recovery - n-caproate production from acid whey. *Green Chem.* 20, 3790–3803. doi:10.1039/c8gc01759j.

Edgar, R. C. (2004). MUSCLE : multiple sequence alignment with high accuracy and high throughput. *Nucleic Acids Res.* 32, 1792–1797. doi:10.1093/nar/gkh340.

EFSA (European Food Safety Authority) (2018). Evaluation of the application for a new alternative processing method for animal by-products of Category 3 material (ChainCraft B.V.). *EFSA J.* 16. doi:10.2903/j.efsa.2018.5281.

El-Gebali, S., Mistry, J., Bateman, A., Eddy, S. R., Luciani, A., Potter, S. C., et al. (2019). The Pfam protein families database in 2019. *Nucleic Acids Res.* 47, D427–D432. doi:10.1093/nar/gky995.

Elsden, S. R., Volcani, B. E., Gilchrist, F. M. C., and Lewis, D. (1956). Properties of a fatty acid forming organism isolated from the rumen of sheep. *J. Bacteriol.*, 681–689.

Epskamp, S., Cramer, A. O. J., Waldorp, L. J., Schmittmann, V. D., and Borsboom, D. (2012). Qgraph: Network visualizations of relationships in psychometric data. *J. Stat. Softw.* 48. doi:10.18637/jss.v048.i04.

Esquivel-Elizondo, S., Bağcı, C., Temovska, M., Jeon, B. S., Bessarab, I., Williams, R. B. H., et al. (2021). The Isolate Caproiciproducens sp. 7D4C2 Produces n-Caproate at Mildly Acidic Conditions From Hexoses: Genome and rBOX Comparison With Related Strains and Chain-Elongating Bacteria. *Front. Microbiol.* 11, 1–18. doi:10.3389/fmicb.2020.594524.

Esquivel-Elizondo, S., Ilhan, Z. E., Garcia-Peña, I., and Krajmalnik-Brown, R. (2017). Insights into Butyrate Production in a Controlled Fermentation System via Gene Predictions. *mSystems* 2. doi:10.1128/mSystems.00051-17.

European Commision (2019). Report on the implementation of the circular economy action plan. Brussels Available at: https://eur-lex.europa.eu/legal-content/EN/TXT/?qid=1551871195772&uri=CELEX:52019DC0190 [Accessed April 22, 2021].

Fan, D., O'Brien Johnson, G., Tratnyek, P. G., and Johnson, R. L. (2016). Sulfidation of nano zerovalent iron (nZVI) for improved selectivity during in-situ chemical reduction (ISCR). *Environ. Sci. Technol.* 50, 9558–9565. doi:10.1021/acs.est.6b02170.

FAO (2011). Global food losses and food waste – Extent, causes and prevention. doi:10.4337/9781788975391.

Flaiz, M., Baur, T., Brahner, S., Poehlein, A., Daniel, R., and Bengelsdorf, F. R. (2020). Caproicibacter fermentans gen. nov., sp. nov., a new caproate-producing bacterium and emended description of the genus Caproiciproducens. *Int. J. Syst. Evol. Microbiol.* doi:10.1099/ijsem.0.004283.

Friedman, J., and Alm, E. J. (2012). Inferring Correlation Networks from Genomic Survey Data. *PLoS Comput. Biol.* 8. doi:10.1371/journal.pcbi.1002687.

Fu, X., Ye, R., Jin, X., and Lu, W. (2020). Effect of nano zero-valent iron addition on caproate fermentation in carboxylate chain elongation system. *Sci. Total Environ.* 743. doi:10.1016/j.scitotenv.2020.140664.

Gagliano, M. C., Sudmalis, D., Pei, R., Temmink, H., and Plugge, C. M. (2020). Microbial Community Drivers in Anaerobic Granulation at High Salinity. *Front. Microbiol.* 11, 1–15. doi:10.3389/fmicb.2020.00235.

Gänzle, M. G. (2015). Lactic metabolism revisited: metabolism of lactic acid bacteria in food fermentations and food spoilage. *Curr. Opin. Food Sci.* 2, 106–117. doi:10.1016/j.cofs.2015.03.001.

Gänzle, M. G., and Follador, R. (2012). Metabolism of oligosaccharides and starch in lactobacilli: a review. *Front. Microbiol.* 3, 1–15. doi:10.3389/fmicb.2012.00340.

Ge, S., Usack, J. G., Spirito, C. M., and Angenent, L. T. (2015). Long-Term n-Caproic Acid Production from Yeast-Fermentation Beer in an Anaerobic Bioreactor with Continuous Product Extraction. *Environ. Sci. Technol.* 49, 8012–8021. doi:10.1021/acs.est.5b00238.

Ghysels, S., Buffel, S., Rabaey, K., Ronsse, F., and Ganigu, R. (2021). Biochar and activated carbon enhance ethanol conversion and selectivity to caproic acid by Clostridium kluyveri. *Bioresour. Technol.* 319. doi:10.1016/j.biortech.2020.124236.

Giusti, D. M., Conway, R. A., and Lawson, C. T. (1974). Activated carbon adsorption of petrochemicals. *J. Water Pollut. Control Fed.* 46, 947–965.

Godwin, S., Kang, A., Gulino, L.-M., Manefield, M., Gutierrez-Zamora, M.-L., Kienzle, M., et al. (2014). Investigation of the

microbial metabolism of carbon dioxide and hydrogen in the kangaroo foregut by stable isotope probing. *ISME Jorunal* 8, 1855–1865. doi:10.1038/ismej.2014.25.

Goffin, P., Deghorain, M., Mainardi, J. L., Tytgat, I., Champomier-Vergès, M. C., Kleerebezem, M., et al. (2005). Lactate racemization as a rescue pathway for supplying D-lactate to the cell wall biosynthesis machinery in Lactobacillus plantarum. *J. Bacteriol.* 187, 6750–6761. doi:10.1128/JB.187.19.6750-6761.2005.

Gong, Z., Yu, H., Zhang, J., Li, F., and Song, H. (2020). Microbial electro-fermentation for synthesis of chemicals and biofuels driven by bi-directional extracellular electron transfer. *Synth. Syst. Biotechnol.* 5, 304–313. doi:10.1016/j.synbio.2020.08.004.

Gonzalez-Garcia, R. A., McCubbin, T., Navone, L., Stowers, C., Nielsen, L. K., and Marcellin, E. (2017). Microbial propionic acid production. *Fermentation* 3, 1–20. doi:10.3390/fermentation3020021.

Grootscholten, T. I. M., Borgo, F. K., Hamelers, H. V. M., and Buisman, C. J. N. (2013a). Promoting chain elongation in mixed culture acidification reactors by addition of ethanol. *Biomass and Bioenergy* 48, 10–16. doi:10.1016/j.biombioe.2012.11.019.

Grootscholten, T. I. M., Steinbusch, K. J. J., Hamelers, H. V. M., and Buisman, C. J. N. (2013b). Chain elongation of acetate and ethanol in an upflow anaerobic filter for high rate MCFA production. *Bioresour. Technol.* 135, 440–445. doi:10.1016/j.biortech.2012.10.165.

Grootscholten, T. I. M., Steinbusch, K. J. J., Hamelers, H. V. M., and Buisman, C. J. N. (2013c). High rate heptanoate production from propionate and ethanol using chain elongation. *Bioresour. Technol.* 136, 715–718. doi:10.1016/j.biortech.2013.02.085.

Grootscholten, T. I. M., Steinbusch, K. J. J., Hamelers, H. V. M., and Buisman, C. J. N. (2013d). Improving medium chain fatty acid productivity using chain elongation by reducing the hydraulic retention time in an upflow anaerobic filter. *Bioresour. Technol.* 136, 735–738. doi:10.1016/j.biortech.2013.02.114.

Guo, X., Sun, C., Lin, R., Xia, A., Huang, Y., and Zhu, X. (2020). Effects of foam nickel supplementation on anaerobic digestion: Direct interspecies electron transfer. *J. Hazard. Mater.* 399. doi:10.1016/j.jhazmat.2020.122830.

Hanczakowska, E. (2017). The Use of Medium-Chain Fatty Acids in Piglet Feeding – A Review. *Ann. Anim. Sci.* 17, 967–977. doi:10.1515/aoas-2016-0099.

Hedderich, R., and Forzi, L. (2005). Energy-Converting [NiFe] Hydrogenases: More than Just H2 Activation. *J. Mol. Microbiol. Biotechnol.* 10, 92–104. doi:10.1159/000091557.

Hess, B. W., Moss, G. E., and Rule, D. C. (2008). A decade of developments in the area of fat supplementation research with beef cattle and sheep. *J. Anim. Sci.* 86, 188–204. doi:10.2527/jas.2007-0546.

Hettinga, D. H., and Reinbold, G. W. (1972). The propionic-acid bacteria-A review. 1. Growth. *J. Milk Food Technol.* 35, 295–301. doi:10.4315/0022-2747-35.5.295.

Hetzel, M., Brock, M., Selmer, T., Pierik, A. J., Golding, B. T., and Buckel, W. (2003). Acryloyl-CoA reductase from Clostridium propionicum: An enzyme complex of propionyl-CoA dehydrogenase and electron-transferring flavoprotein. *Eur. J. Biochem.* 270, 902–910. doi:10.1046/j.1432-1033.2003.03450.x.

Hino, T., and Kuroda, S. (1993). Presence of lactate dehydrogenase and lactate racemase in Megasphaera elsdenii grown on glucose or lactate. *Appl. Environ. Microbiol.* 59, 255–259. doi:10.1128/aem.59.1.255-259.1993.

Hoelzle, R. D., Virdis, B., and Batstone, D. J. (2014). Regulation Mechanisms in Mixed and Pure Culture Microbial Fermentation. *Biotechnol. Bioeng.* 111, 2139–2154. doi:10.1002/bit.25321.

Hofvendahl, K., and Hahn-Hägerdal, B. (2000). Factors affecting the fermentative lactic acid production from renewable resources. *Enzyme Microb. Technol.* 26, 87–107. doi:10.1016/S0141-0229(99)00155-6.

Holtzapple, M. T., and Granda, C. B. (2009). Carboxylate platform: The MixAlco process part 1: Comparison of three biomass conversion platforms. *Appl. Biochem. Biotechnol.* 156, 525–536. doi:10.1007/s12010-008-8466-y.

Holzhäuser, F. J., Mensah, J. B., and Palkovits, R. (2020). (Non-)Kolbe electrolysis in biomass valorization-a discussion of potential applications. *Green Chem.* 22, 286–301. doi:10.1039/c9gc03264a.

Hosseini, E. S., Kermanshahi, R. K., Hosseinkhani, S., Shojaosadati, S. A., and Nazari, M. (2015). Conjugated linoleic acid production from various substrates by probiotic Lactobacillus plantarum. *Ann. Microbiol.* 65, 27–32. doi:10.1007/s13213-014-0832-0.

Huffman, H. M., Ellis, E. L., and Borsook, H. (1940). Thermal Data XI. The Heat Capacities and Entropies of Guanidine Carbonate, Glutamic Acid Hydrochloride, Ornithine Dihydrochloride, D-Lactic Acid and L-Lactic Acid. *J. Am. Chem. Soc.* 62, 297–299. doi:10.1021/ja01859a016.

Hulshoff Pol, L. W., De Castro Lopes, S. I., Lettinga, G., and Lens, P. N. L. (2004). Anaerobic sludge granulation. *Water Res.* 38, 1376–1389. doi:10.1016/j.watres.2003.12.002.

Imachi, H., Sakai, S., Kubota, T., Miyazaki, M., Saito, Y., and Takai, K. (2016). Sedimentibacter acidaminivorans sp. nov., an anaerobic, amino-acid-utilizing bacterium isolated from marine subsurface sediment. *Int. J. Syst. Evol. Microbiol.* 66, 1293–1300. doi:10.1099/ijsem.0.000878.

Ingham, S. C., Hassler, J. R., Tsai, Y., and Ingham, B. H. (1998). Differentiation of lactate-fermenting, gas-producing Clostridium spp. isolated from milk. *Int. J. Food Microbiol.* 43, 173–183. doi:https://doi.org/10.1016/S0168-1605(98)00108-1.

Isipato, M., Dessì, P., Sánchez, C., Mills, S., Ijaz, U. Z., Asunis, F., et al. (2020). Propionate Production by Bioelectrochemically-Assisted Lactate Fermentation and Simultaneous CO2 Recycling. *Front. Microbiol.* 11, 1–16. doi:10.3389/fmicb.2020.599438.

Ivanova, T., Panaiotov, I., Boury, F., Saulnier, P., Proust, J. E., and Verger, R. (2000). Role of the electrostatic interactions on the basic or acidic hydrolysis kinetics of poly-(D,L-lactide) monolayers. *Colloids Surfaces B Biointerfaces* 17, 241–254. doi:10.1016/S0927-7765(99)00043-0.

Jackman, J. A., Boyd, R. D., and Elrod, C. C. (2020). Medium-chain fatty acids and monoglycerides as feed additives for pig production: Towards gut health improvement and feed pathogen mitigation. *J. Anim. Sci. Biotechnol.* 11, 1–15.

doi:10.1186/s40104-020-00446-1.
Jackson, M. I., and Jewell, D. E. (2020). Docosahexaenoate-enriched fish oil and medium chain triglycerides shape the feline plasma lipidome and synergistically decrease circulating gut microbiome-derived putrefactive postbiotics. *PLoS One* 15, 1–26. doi:10.1371/journal.pone.0229868.
Janssen, P. H. (1991). Isolation of Clostridium propionicum strain 19acry3 and further characteristics of the species. *Arch. Microbiol.* 155, 566–571. doi:10.1007/BF00245351.
Jeon, B. S., Moon, C., Kim, B. C., Kim, H., Um, Y., and Sang, B. I. (2013). In situ extractive fermentation for the production of hexanoic acid from galactitol by Clostridium sp. BS-1. *Enzyme Microb. Technol.* 53, 143–151. doi:10.1016/j.enzmictec.2013.02.008.
Jourdin, L., Raes, S. M. T., Buisman, C. J. N., and Strik, D. P. B. T. B. (2018). Critical Biofilm Growth throughout Unmodified Carbon Felts Allows Continuous Bioelectrochemical Chain Elongation from CO2 up to Caproate at High Current Density. *Front. Energy Res.* 6, 1–15. doi:10.3389/fenrg.2018.00007.
Kahyarian, A., Achour, M., and Nesic, S. (2017). "CO2 corrosion of mild steel," in *Trends in Oil and Gas Corrosion Research and Technologies*, ed. A. M. El-Sherik (Woodhead Publishing), 149–190. doi:10.1016/B978-0-08-101105-8.00007-3.
Kammann, C. I., Schmidt, H. P., Messerschmidt, N., Linsel, S., Steffens, D., Müller, C., et al. (2015). Plant growth improvement mediated by nitrate capture in co-composted biochar. *Sci. Rep.* 5, 1–13. doi:10.1038/srep11080.
Kannengiesser, J., Sakaguchi-Söder, K., Mrukwia, T., Jager, J., and Schebek, L. (2016). Extraction of medium chain fatty acids from organic municipal waste and subsequent production of bio-based fuels. *Waste Manag.* 47, 78–83. doi:10.1016/j.wasman.2015.05.030.
Kardung, M., Cingiz, K., Costenoble, O., Delahaye, R., Heijman, W., Lovrić, M., et al. (2021). Development of the circular bioeconomy: Drivers and indicators. *Sustain.* 13, 1–24. doi:10.3390/su13010413.
Kashket, E. R. (1987). Bioenergetics of lactic acid bacteria: cytoplasmic pH and osmotolerance. *FEMS Microbiol. Rev.* 46, 233–244. doi:10.1016/0378-1097(87)90110-8.
Kassambara, A., and Mundt, F. (2020). Package "factoextra." doi:http://www.sthda.com/english/rpkgs/factoextra BugReports.
Katagiri, H., Sugimori, T., Imai, K., Komaki, S., Okuzumi, M., and Anyoji, H. (1961). On the Metabolism of Organic Acids by Clostridium acetobutylicum. *Agric. Biol. Chem.* 25, 281–313. doi:10.1080/00021369.1961.10857808.
Kato, O., Youn, J., Stansen, K. C., Matsui, D., Oikawa, T., and Wendisch, V. F. (2010). Quinone-dependent D-lactate dehydrogenase Dld (Cg1027) is essential for growth of Corynebacterium glutamicum on D-lactate. *BMC Microbiol.* 10, 1–11.
Kaur, G., Garcia-Gonzalez, L., Elst, K., Truzzi, F., Bertin, L., Kaushik, A., et al. (2020). Reactive extraction for in-situ carboxylate recovery from mixed culture fermentation. *Biochem. Eng. J.* 160, 107641. doi:10.1016/j.bej.2020.107641.
Kim, B. C., Jeon, B. S., Kim, S., Kim, H., Um, Y., and Sang, B. I. (2015). Caproiciproducens galactitolivorans gen. Nov., sp. nov., a bacterium capable of producing caproic acid from galactitol, isolated from a wastewater treatment plant. *Int. J. Syst. Evol. Microbiol.* 65, 4902–4908. doi:10.1099/ijsem.0.000665.
Kim, H., Seung, B., Pandey, A., and Sang, B. (2018). New coculture system of Clostridium spp. and Megasphaera hexanoica using submerged hollow-fiber membrane bioreactors for caproic acid production. *Bioresour. Technol.* 270, 498–503. doi:10.1016/j.biortech.2018.09.033.
Kim, J. H., Kim, Y., Kim, Y. J., and Park, Y. (2016a). Conjugated Linoleic Acid: Potential Health Benefits as a Functional Food Ingredient. *Annu. Rev. Food Sci. Technol.* 7, 221–244. doi:10.1146/annurev-food-041715-033028.
Kim, M., Na, J., Lee, M., Ryu, H., Chang, Y., Triolo, J. M., et al. (2016b). More value from food waste: Lactic acid and biogas recovery. *Water Res.* 96, 208–216. doi:10.1016/j.watres.2016.03.064.
Kim, S. A., and Rhee, M. S. (2016). Highly enhanced bactericidal effects of medium chain fatty acids (caprylic, capric, and lauric acid) combined with edible plant essential oils (carvacrol, eugenol, β-resorcylic acid, trans-cinnamaldehyde, thymol, and vanillin) against Escherichia coli O15. *Food Control* 60, 447–454. doi:10.1016/j.foodcont.2015.08.022.
Kim, Y. J., Liu, R. H., Rychlik, J. L., and Russell, J. B. (2002). The enrichment of a ruminal bacterium (Megasphaera elsdenii YJ-4) that produces the trans-10, cis-12 isomer of conjugated linoleic acid. *J. Appl. Microbiol.* 92, 976–982. doi:10.1046/j.1365-2672.2002.01610.x.
Kittl, S., Brodard, I., Rychener, L., Jores, J., Roosje, P., and Gobeli Brawand, S. (2018). Otitis in a cat associated with Corynebacterium provencense. *BMC Vet. Res.* 14, 4–9. doi:10.1186/s12917-018-1526-9.
Kleerebezem, R., Joosse, B., Rozendal, R., and Van Loosdrecht, M. C. M. (2015). Anaerobic digestion without biogas? *Rev. Environ. Sci. Biotechnol.* 14, 787–801. doi:10.1007/s11157-015-9374-6.
Kleerebezem, R., and van Loosdrecht, M. C. M. (2010). A generalized method for thermodynamic state analysis of environmental systems. *Crit. Rev. Environ. Sci. Technol.* 40, 1–54. doi:10.1080/10643380802000974.
Klindworth, A., Pruesse, E., Schweer, T., Peplies, J., Quast, C., Horn, M., et al. (2013). Evaluation of general 16S ribosomal RNA gene PCR primers for classical and next-generation sequencing-based diversity studies. *Nucleic Acids Res.* 41, 1–11. doi:10.1093/nar/gks808.
Kracke, F., Vassilev, I., and Krömer, J. O. (2015). Microbial electron transport and energy conservation - The foundation for optimizing bioelectrochemical systems. *Front. Microbiol.* 6, 1–18. doi:10.3389/fmicb.2015.00575.
Kucek, L. A., Nguyen, M., and Angenent, L. T. (2016a). Conversion of L-lactate into n-caproate by a continuously fed reactor microbiome. *Water Res.* 93, 163–171. doi:10.1016/j.watres.2016.02.018.
Kucek, L. A., Spirito, C. M., and Angenent, L. T. (2016b). High n-caprylate productivities and specificities from dilute ethanol and acetate: chain elongation with microbiomes to upgrade products from syngas fermentation. *Energy Environ. Sci.* doi:10.1039/c0ee00729c.
Kucek, L. A., Xu, J., Nguyen, M., and Angenent, L. T. (2016c). Waste conversion into n-caprylate and n-caproate: Resource recovery from wine lees using anaerobic reactor microbiomes and in-line extraction. *Front. Microbiol.* 7, 1–14.

doi:10.3389/fmicb.2016.01892.
Kuchta, R. D., and Abeles, R. H. (1985). Lactate reduction in Clostridium propionicum. Purification and properties of lactyl-CoA dehydratase. *J. Biol. Chem.* 260, 13181–13189.
Lawson, C. E., Harcombe, W. R., Hatzenpichler, R., Lindemann, S. R., Löffler, F. E., O'Malley, M. A., et al. (2019). Common principles and best practices for engineering microbiomes. *Nat. Rev. Microbiol.* 17, 725–741. doi:10.1038/s41579-019-0255-9.
Lee, J., Jang, Y., Han, M., Kim, Y., and Lee, Y. (2016). Deciphering Clostridium tyrobutyricum Metabolism Based on the Whole-Genome Sequence and Proteome Analyses. *MBio* 7, 1–12. doi:10.1128/mBio.00743-16.
Leng, L., Yang, P., Mao, Y., Wu, Z., Zhang, T., and Lee, P. (2017). Thermodynamic and physiological study of caproate and 1 , 3-propanediol co-production through glycerol fermentation and fatty acids chain elongation. *Water Res.* 114, 200–209. doi:10.1016/j.watres.2017.02.023.
Letunic, I., and Bork, P. (2016). Interactive tree of life (iTOL) v3: an online tool for the display and annotation of phylogenetic and other trees. *Nucleic Acids Res.* 44, 242–245. doi:10.1093/nar/gkw290.
Li, B., and Elliott, S. J. (2016). The Catalytic Bias of 2-Oxoacid:ferredoxin Oxidoreductase in CO2: Evolution and reduction through a ferredoxin-mediated electrocatalytic assay. *Electrochim. Acta* 199, 349–356. doi:10.1016/j.electacta.2016.02.119.
Li, X., Zhang, W., Xue, S., Lai, S., Li, J., Chen, H., et al. (2017). Enrichment of D-lactic acid from organic wastes catalyzed by zero-valent iron: An approach for sustainable lactate isomerization. *Green Chem.* 19, 928–936. doi:10.1039/c6gc02402e.
Li, Z., Xu, B., Lu, Z., and Wang, Y. (2019). Effects of long-chain fatty acid supplementation on the growth performance of grower and finisher pigs: A meta-analysis. *J. Anim. Sci. Biotechnol.* 10, 1–12. doi:10.1186/s40104-019-0374-1.
Lin, R., Deng, C., Cheng, J., Xia, A., Lens, P. N. L., Jackson, S. A., et al. (2018). Graphene Facilitates Biomethane Production from Protein-Derived Glycine in Anaerobic Digestion. *iScience* 10, 158–170. doi:10.1016/j.isci.2018.11.030.
Liu, B., Popp, D., Müller, N., Sträuber, H., Harms, H., and Kleinsteuber, S. (2020). Three Novel Clostridia Isolates Produce n-Caproate and iso-Butyrate from Lactate: Comparative Genomics of Chain-Elongating Bacteria. *Microorganisms* 8. doi:10.3390/microorganisms8121970.
Liu, F., Rotaru, A., Shrestha, P. M., Malvankar, N. S., Nevin, K. P., and Lovley, D. R. (2012). Promoting direct interspecies electron transfer with activated carbon. *Energy Environ. Sci.* 5, 8982–8989. doi:10.1039/c2ee22459c.
Liu, L., Chen, J., Lim, P. E., and Wei, D. (2018). Dual-species cultivation of microalgae and yeast for enhanced biomass and microbial lipid production. *J. Appl. Phycol.* 30, 2997–3007. doi:10.1007/s10811-018-1526-y.
Liu, Y., He, P., Shao, L., Zhang, H., and Lü, F. (2017). Significant enhancement by biochar of caproate production via chain elongation. *Water Res.* 119, 150–159. doi:10.1016/j.watres.2017.04.050.
López-Garzón, C. S., and Straathof, A. J. J. (2014). Recovery of carboxylic acids produced by fermentation. *Biotechnol. Adv.* 32, 873–904. doi:10.1016/j.biotechadv.2014.04.002.
López-Gómez, J. P., Pérez-Rivero, C., and Venus, J. (2020). Valorisation of solid biowastes: The lactic acid alternative. *Process Biochem.* 99, 222–235. doi:10.1016/j.procbio.2020.08.029.
Louis, P., and Flint, H. J. (2017). Formation of propionate and butyrate by the human colonic microbiota. *Environ. Microbiol.* 19, 29–41. doi:10.1111/1462-2920.13589.
Lux, S., Baldauf-Sommerbauer, G., Ottitsch, B., Loder, A., and Siebenhofer, M. (2019). Iron Carbonate Beneficiation Through Reductive Calcination – Parameter Optimization to Maximize Methane Formation. *Eur. J. Inorg. Chem.*, 1748–1758. doi:10.1002/ejic.201801394.
Machmüller, A. (2006). Medium-chain fatty acids and their potential to reduce methanogenesis in domestic ruminants. *Agric. Ecosyst. Environ.* 112, 107–114. doi:10.1016/j.agee.2005.08.010.
Maes, J., De Meulenaer, B., Van Heerswynghels, P., De Greyt, W., Eppe, G., De Pauw, E., et al. (2005). Removal of dioxins and PCB from fish oil by activated carbon and its influence on the nutritional quality of the oil. *JAOCS, J. Am. Oil Chem. Soc.* 82, 593–597. doi:10.1007/s11746-005-1114-1.
Maia, M. R. G., Chaudhary, L. C., Figueres, L., and Wallace, R. J. (2007). Metabolism of polyunsaturated fatty acids and their toxicity to the microflora of the rumen. *Antonie Van Leeuwenhoek* 91, 303–314. doi:10.1007/s10482-006-9118-2.
Marshall, C. W., Ross, D. E., Handley, K. M., Weisenhorn, P. B., Edirisinghe, J. N., Henry, C. S., et al. (2017). Metabolic reconstruction and modeling microbial electrosynthesis. *Sci. Rep.* 7, 1–12. doi:10.1038/s41598-017-08877-z.
Marten, B., Pfeuffer, M., and Schrezenmeir, J. (2006). Medium-chain triglycerides. *Int. Dairy J.* 16, 1374–1382. doi:10.1016/j.idairyj.2006.06.015.
Maus, I., Bremges, A., Stolze, Y., Hahnke, S., Cibis, K. G., Koeck, D. E., et al. (2017). Genomics and prevalence of bacterial and archaeal isolates from biogas-producing microbiomes. *Biotechnol. Biofuels* 10, 1–22. doi:10.1186/s13068-017-0947-1.
McMurdie, P. J., and Holmes, S. (2013). phyloseq: An R Package for Reproducible Interactive Analysis and Graphics of Microbiome Census Data. *PLoS One* 8. doi:10.1371/journal.pone.0061217.
Meng, X., Zhang, Y., Li, Q., and Quan, X. (2013). Adding Fe0 powder to enhance the anaerobic conversion of propionate to acetate. *Biochem. Eng. J.* 73, 80–85. doi:10.1016/j.bej.2013.02.004.
Moscoviz, R., Toledo-Alarcón, J., Trably, E., and Bernet, N. (2016). Electro-Fermentation: How To Drive Fermentation Using Electrochemical Systems. *Trends Biotechnol.* 34, 856–865. doi:10.1016/j.tibtech.2016.04.009.
Murota, K., Kawada, T., Matsui, N., Sakakibara, M., Takahashi, N., and Fushiki, T. (2000). Oleyl alcohol inhibits intestinal long-chain fatty acid absorption in rats. *J. Nutr. Sci. Vitaminol. (Tokyo).* 46, 302–308. doi:10.3177/jnsv.46.302.
Nagarajan, H., Embree, M., Rotaru, A., Shrestha, P. M., Feist, A. M., Palsson, B. Ø., et al. (2013). Characterization and modelling of interspecies electron transfer mechanisms and microbial community dynamics of a syntrophic association. *Nat. Commun.* 4, 1–10. doi:10.1038/ncomms3809.
Newman, M. E. J. (2003). The Structure and Function of Complex Networks ∗. *SIAM Rev.* 45, 167–256.

Newman, M. E. J. (2006). Modularity and community structure in networks. *Proc. Natl. Acad. Sci.* 103, 8577–8582.
Nguyen, V. K., and Ahn, Y. (2018). Electrochemical removal and recovery of iron from groundwater using non-corrosive electrodes. *J. Environ. Manage.* 211, 36–41. doi:10.1016/j.jenvman.2018.01.046.
Noorman, H. J., Van Winden, W., Heijnen, J. J., and Van Der Lans, R. G. J. M. (2018). "Intensified Fermentation Processes and Equipment," in *Intensification of Biobased Processes*, eds. A. Górak and A. Stankiewicz (The Royal Society of Chemistry), 1–41. doi:10.1039/9781788010320-00001.
Nouaille, C., and Pessiot, J. (2017). Process for extracting carboxylic acids produced by anaerobic fermentation from fermentable biomass.
Nzeteu, C. O., Trego, A. C., Abram, F., and Flaherty, V. O. (2018). Reproducible, high-yielding, biological caproate production from food waste using a single-phase anaerobic reactor system. *Biotechnol. Biofuels*, 1–14. doi:10.1186/s13068-018-1101-4.
Nzeteu, C. O., Trego, A. C., Abram, F., and O'Flaherty, V. Reproducible, high-yielding, biological caproate production from food waste using a single-phase anaerobic reactor system. *SI*.
Offeman, R. D., Stephenson, S. K., Robertson, G. H., and Orts, W. J. (2006). Solvent extraction of ethanol from aqueous solutions using biobased oils, alcohols, and esters. *JAOCS, J. Am. Oil Chem. Soc.* 83, 153–157. doi:10.1007/s11746-006-1188-9.
Ohkouchi, Y., and Inoue, Y. (2006). Direct production of L (+)-lactic acid from starch and food wastes using Lactobacillus manihotivorans LMG18011. *Bioresour. Technol.* 97, 1554–1562. doi:10.1016/j.biortech.2005.06.004.
Oksanen, J., Blanchet, F. G., Friendly, M., Kindt, R., Legendre, P., Mcglinn, D., et al. (2019). vegan: Community Ecology Package. *CRAN*, https://cran.r-project.org/web/packages/vegan/vega. Available at: https://cran.r-project.org/web/packages/vegan/vegan.pdf [Accessed March 19, 2021].
Oleskowicz-Popiel, P. (2018). Designing Reactor Microbiomes for Chemical Production from Organic Waste. *Trends Biotechnol.* 36, 747–750. doi:10.1016/j.tibtech.2018.01.002.
Patra, A., Park, T., Kim, M., and Yu, Z. (2017). Rumen methanogens and mitigation of methane emission by anti-methanogenic compounds and substances. *J. Anim. Sci. Biotechnol.* 8, 1–18. doi:10.1186/s40104-017-0145-9.
Paulson, J. N., Stine, O. C., Bravo, H. C., and Pop, M. (2013). Differential abundance analysis for microbial marker-gene surveys. *Nat. Methods* 10, 1200–1202. doi:10.1038/nmeth.2658.
Paulson, J. N., Talukder, H., Pop, M., and Corrada Bravo, H. (2016). metagenomeSeq: Statistical analysis for sparse high-throughput sequencing. *Bioconductor Packag. http//cbcb.umd.edu/software/metagenomeSeq*.
Pedraza-de la Cuesta, S., Knopper, L., van der Wielen, L. A. M., and Cuellar, M. C. (2019). Techno-economic assessment of the use of solvents in the scale-up of microbial sesquiterpene production for fuels and fine chemicals. *Biofuels, Bioprod. Biorefining* 13, 140–152. doi:10.1002/bbb.1949.
Pejin, J., Mladenovi, D., Djuki, A., and Mojovi, L. (2018). Brewers' spent grain and thin stillage as raw materials in L-(+)-lactic acid fermentation. *J. Inst. Brew.* 124, 23–30. doi:10.1002/jib.462.
Peterson, B. G., Carl, P., Boudt, K., Bennett, R., Ulrich, J., Zivot, E., et al. (2020). Package "PerformanceAnalytics." doi:https://github.com/braverock/PerformanceAnalytics.
Petrognani, C., Boon, N., and Ganigué, R. (2020). Production of isobutyric acid from methanol by Clostridium luticellarii. *Green Chem.* 22, 8389–8402. doi:10.1039/d0gc02700f.
Piai, L., Wal, A. Van Der, Boelee, N., and Langenhoff, A. (2021). Melamine degradation to bioregenerate granular activated carbon. *J. Hazard. Mater.* 414. doi:10.1016/j.jhazmat.2021.125503.
Poehlein, A., Bremekamp, R., Lutz, V. T., Schulz, L. M., and Daniel, R. (2018). Draft Genome Sequence of the Butanoic Acid-Producing Bacterium Clostridium luticellarii DSM 29923, Used for Strong Aromatic Chinese Liquor Production. *Genome Announc.* 6. doi:10.1128/genomeA.00377-18.
Poteko, J., Schrade, S., Zeyer, K., Mohn, J., Zaehner, M., Zeitz, J. O., et al. (2020). Methane emissions and milk fatty acid profiles in dairy cows fed linseed, measured at the group level in a naturally ventilated housing and individually in respiration chambers. *Animals* 10, 1–18. doi:10.3390/ani10061091.
Prabhu, R., Altman, E., and Eitemana, M. A. (2012). Lactate and acrylate metabolism by Megasphaera elsdenii under batch and steady-state conditions. *Appl. Environ. Microbiol.* 78, 8564–8570. doi:10.1128/AEM.02443-12.
Pradhan, N., Rene, E. R., Lens, P. N. L., Dipasquale, L., D'Ippolito, G., Fontana, A., et al. (2017). Adsorption behaviour of lactic acid on granular activated carbon and anionic resins: Thermodynamics, isotherms and kinetic studies. *Energies* 10, 1–16. doi:10.3390/en10050665.
Price, M. N., Dehal, P. S., and Arkin, A. P. (2010). FastTree 2 – Approximately Maximum-Likelihood Trees for Large Alignments. *PLoS One* 5. doi:10.1371/journal.pone.0009490.
Qin, H., Guan, X., Bandstra, J. Z., Johnson, R. L., and Tratnyek, P. G. (2018). Modeling the Kinetics of Hydrogen Formation by Zerovalent Iron: Effects of Sulfidation on Micro- and Nano-Scale Particles. *Environ. Sci. Technol.* 52, 13887–13896. doi:10.1021/acs.est.8b04436.
Quast, C., Pruesse, E., Yilmaz, P., Gerken, J., Schweer, T., Glo, F. O., et al. (2013). The SILVA ribosomal RNA gene database project: improved data processing and web-based tools. *Nucleic Acids Res.* 41, 590–596. doi:10.1093/nar/gks1219.
Raes, S. M. T., Jourdin, L., Buisman, C. J. N., and Strik, D. P. B. T. B. (2020). Bioelectrochemical Chain Elongation of Short-Chain Fatty Acids Creates Steering Opportunities for Selective Formation of n-Butyrate , n-Valerate or n-Caproate. *ChemistrySelect* 5, 9127–9133. doi:10.1002/slct.202002001.
Raes, S. M. T., Jourdin, L., Carlucci, L., van den Bruinhorst, A., Strik, D. P. B. T. B., and Buisman, C. J. N. (2018). Water-Based Synthesis of Hydrophobic Ionic Liquids [N8888][oleate] and [P666,14][oleate] and their Bioprocess Compatibility. *ChemistryOpen* 7, 878–884. doi:10.1002/open.201800187.
Reddy, M. V., Hayashi, S., Choi, D., Cho, H., and Chang, Y. C. (2018). Short chain and medium chain fatty acids production using food waste under non-augmented and bio-augmented conditions. *J. Clean. Prod.* 176, 645–653.

doi:10.1016/j.jclepro.2017.12.166.
Regueira, A., Rombouts, J. L., Iglesias, M. M., Lema, J. M., and Kleerebezem, R. (2021). Resource allocation explains lactic acid production in mixed - culture anaerobic fermentations. *Biotechnol. Bioeng.* 118, 745–758. doi:10.1002/bit.27605.
Reichardt, N., Duncan, S. H., Young, P., Belenguer, A., McWilliam Leitch, C., Scott, K. P., et al. (2014). Phylogenetic distribution of three pathways for propionate production within the human gut microbiota. *ISME J.* 8, 1323–1335. doi:10.1038/ismej.2014.14.
Rickard, D., and Iii, G. W. L. (2007). Chemistry of Iron Sulfides. *Chem. Rev.* 107, 514–562. doi:10.1021/cr0503658.
Ritchie, M. E., Phipson, B., Wu, D., Hu, Y., Law, C. W., Shi, W., et al. (2015). Limma powers differential expression analyses for RNA-sequencing and microarray studies. *Nucleic Acids Res.* 43, e47. doi:10.1093/nar/gkv007.
Robles, A. (2019). Reductive dechlorination sustained by microbial chain elongation.
Roghair, M., Hoogstad, T., Strik, D. P. B. T. B., Plugge, C. M., Timmers, P. H. A., Weusthuis, R. A., et al. (2018a). Controlling Ethanol Use in Chain Elongation by CO2 Loading Rate. *Environ. Sci. Technol.* 52, 1496–1505. doi:10.1021/acs.est.7b04904.
Roghair, M., Liu, Y., Adiatma, J. C., Weusthuis, R. A., Bruins, M. E., Buisman, C. J. N., et al. (2018b). Effect of n-Caproate Concentration on Chain Elongation and Competing Processes. *ACS Sustain. Chem. Eng.* 6, 7499–7506. doi:10.1021/acssuschemeng.8b00200.
Roghair, M., Liu, Y., Strik, D. P. B. T. B., Weusthuis, R. A., Bruins, M. E., and Buisman, C. J. N. (2018c). Development of an Effective Chain Elongation Process From Acidified Food Waste and Ethanol Into n-Caproate. *Front. Bioeng. Biotechnol.* 6, 1–11. doi:10.3389/fbioe.2018.00050.
Roghair, M., Strik, D. P. B. T. B., Steinbusch, K. J. J., Weusthuis, R. A., Bruins, M. E., and Buisman, C. J. N. (2016). Granular sludge formation and characterization in a chain elongation process. *Process Biochem.* 51, 1594–1598. doi:10.1016/j.procbio.2016.06.012.
Rombouts, J. L., Madeleine, E., Kranendonk, M., Regueira, A., Weissbrodt, D. G., Kleerebezem, R., et al. (2020). Selecting for lactic acid producing and utilising bacteria in anaerobic enrichment cultures. *Biotechnol. Bioeng.* 117, 1281–1293. doi:10.1002/bit.27301.
Rühl, J., Schmid, A., and Blank, L. M. (2009). Selected Pseudomonas putida strains able to grow in the presence of high butanol concentrations. *Appl. Environ. Microbiol.* 75, 4653–4656. doi:10.1128/AEM.00225-09.
Ryan, P., Forbes, C., and Colleran, E. (2008). Investigation of the diversity of homoacetogenic bacteria in mesophilic and thermophilic anaerobic sludges using the formyltetrahydrofolate synthetase gene. *Water Sci. Technol.* 57, 675–680. doi:10.2166/wst.2008.059.
Saboe, P. O., Manker, L. P., Michener, W. E., Peterson, D. J., Brandner, D. G., Deutch, S. P., et al. (2018). In situ recovery of bio-based carboxylic acids. *Green Chem.* 20, 1791–1804. doi:10.1039/c7gc03747c.
Salvador, A. F., Martins, G., Melle-franco, M., Serpa, R., Stams, A. J. M., Cavaleiro, A. J., et al. (2017). Carbon nanotubes accelerate methane production in pure cultures of methanogens and in a syntrophic coculture. *Environ. Microbiol.* 19, 2727–2739. doi:10.1111/1462-2920.13774.
Scalschi, L., Vicedo, B., Camañes, G., Fernandez-Crespo, E., Lapeña, L., González-Bosch, C., et al. (2013). Hexanoic acid is a resistance inducer that protects tomato plants against Pseudomonas syringae by priming the jasmonic acid and salicylic acid pathways. *Mol. Plant Pathol.* 14, 342–355. doi:10.1111/mpp.12010.
Scarborough, M. J., Lawson, C. E., Hamilton, J. J., Donohue, T. J., and Noguera, D. R. (2018a). Metatranscriptomic and Thermodynamic Insights into Medium-Chain Fatty Acid Production Using an Anaerobic Microbiome. *mSystems* 3, 1–21. doi:doi.org/10.1128/msystems.00221-18.
Scarborough, M. J., Lynch, G., Dickson, M., McGee, M., Donohue, T. J., and Noguera, D. R. (2018b). Increasing the economic value of lignocellulosic stillage through medium-chain fatty acid production. *Biotechnol. Biofuels* 11, 1–17. doi:10.1186/s13068-018-1193-x.
Schink, B. (1997). Energetics of syntrophic cooperation in methanogenic degradation. *Microbiol. Mol. Biol. Rev.* 61, 262–280. doi:10.1128/.61.2.262-280.1997.
Schmidt, H. P., Hagemann, N., Draper, K., and Kammann, C. (2019). The use of biochar in animal feeding. *PeerJ*, 1–54. doi:10.7717/peerj.7373.
Schmidt, J. H. (2015). Life cycle assessment of five vegetable oils. *J. Clean. Prod.* 87, 130–138. doi:10.1016/j.jclepro.2014.10.011.
Schouten, N., van der Ham, L. G. J., Euverink, G.-J. W., and de Haan, A. B. (2007). Selection and evaluation of adsorbents for the removal of anionic surfactants from laundry rinsing water. *Water Res.* 41, 4233–4241. doi:10.1016/j.watres.2007.05.044.
Schweiger, G., and Buckel, W. (1984). On the dehydration of (R)-lactate in the fermentation of alanine to propionate by Clostridium propionicum. *FEBS Lett.* 171, 79–84. doi:10.1016/0014-5793(84)80463-9.
Seedorf, H., Fricke, W. F., Veith, B., Bruggemann, H., Liesegang, H., Strittmatter, A., et al. (2008). The genome of Clostridium kluyveri, a strict anaerobe with unique metabolic features. *Proc. Natl. Acad. Sci.* 105, 2128–2133. doi:10.1073/pnas.0711093105.
Seeliger, S., Janssen, P. H., and Schink, B. (2002). Energetics and kinetics of lactate fermentation to acetate and propionate via methylmalonyl-CoA or acrylyl-CoA. *FEMS Microbiol. Lett.* 211, 65–70. doi:10.1016/S0378-1097(02)00651-1.
Shahab, R. L., Brethauer, S., Davey, M. P., Smith, A. G., Vignolini, S., Luterbacher, J. S., et al. (2020). A heterogeneous microbial consortium producing short-chain fatty acids from lignocellulose. *Science (80-.).* 369. doi:10.1126/science.abb1214.
Shannon, P., Markiel, A., Ozier, O., Baliga, N. S., Wang, J. T., Ramage, D., et al. (2003). Cytoscape: A Software Environment for Integrated Models of Biomolecular Interaction Networks. *Genome Res.*, 2498–2504. doi:10.1101/gr.1239303.metabolite.

Shinn, S. E., Ruan, C. M., and Proctor, A. (2017). Strategies for Producing and Incorporating Conjugated Linoleic Acid-Rich Oils in Foods. *Annu. Rev. Food Sci. Technol.* 8, 181–204. doi:10.1146/annurev-food-030216-025703.

Sievers, F., Wilm, A., Dineen, D., Gibson, T. J., Karplus, K., Li, W., et al. (2011). Fast, scalable generation of high-quality protein multiple sequence alignments using Clustal Omega. *Mol. Syst. Biol.* 7. doi:10.1038/msb.2011.75.

Singh, A., Müller, B., Fuxelius, H. H., and Schnürer, A. (2019). AcetoBase: a functional gene repository and database for formyltetrahydrofolate synthetase sequences. *Database* 2019, 1–14. doi:10.1093/database/baz142.

SkyNRG (2019). SkyNRG, KLM and SHV Energy announce project first European plant for sustainable aviation fuel. Available at: https://skynrg.com/press-releases/klm-skynrg-and-shv-energy-announce-project-first-european-plant-for-sustainable-aviation-fuel/ [Accessed January 11, 2021].

Soliva, C. R., Hindrichsen, I. K., Meile, L., Kreuzer, M., and Machmüller, A. (2003). Effects of mixtures of lauric and myristic acid on rumen methanogens and methanogenesis in vitro. *Lett. Appl. Microbiol.* 37, 35–39. doi:10.1046/j.1472-765X.2003.01343.x.

Sousa, D. Z., Smidt, H., Alves, M. M., and Stams, A. J. M. (2009). Ecophysiology of syntrophic communities that degrade saturated and unsaturated long-chain fatty acids. *FEMS Microbiol. Ecol.* 68, 257–272. doi:10.1111/j.1574-6941.2009.00680.x.

Spirito, C. M., Marzilli, A. M., and Angenent, L. T. (2018). Higher Substrate Ratios of Ethanol to Acetate Steered Chain Elongation toward n-Caprylate in a Bioreactor with Product Extraction. *Environ. Sci. Technol.* 52, 13438–13447. doi:10.1021/acs.est.8b03856.

Spirito, C. M., Richter, H., Rabaey, K., Stams, A. J. M., and Angenent, L. T. (2014). Chain elongation in anaerobic reactor microbiomes to recover resources from waste. *Curr. Opin. Biotechnol.* 27, 115–122. doi:10.1016/j.copbio.2014.01.003.

Stamatopoulou, P., Malkowski, J., Conrado, L., Brown, K., and Scarborough, M. (2020). Fermentation of organic residues to beneficial chemicals: A review of medium-chain fatty acid production. *Processes* 8, 1–25. doi:10.3390/pr8121571.

Steffen, W., Richardson, K., Rockström, J., Cornell, S. E., Fetzer, I., Bennett, E. M., et al. (2015). Planetary boundaries: Guiding human development on a changing planet. *Science (80-.).* 347, 1259855. doi:10.1126/science.1259855.

Steinbusch, K. J. J., Hamelers, H. V. M., Plugge, M., and Buisman, C. J. N. (2011). Biological formation of caproate and caprylate from acetate: fuel and chemical production from low grade biomass. *Energy Environ. Sci.* 4, 216–224. doi:10.1039/c0ee00282h.

Stenmarck, Å., Jensen, C., Quested, T., Moates, G., Cseh, B., Juul, S., et al. (2016). Estimates of European food waste levels. 1–80.

Stinson, E. E., and Naftulin, K. A. (1991). Effect of pH on organic acid production by Clostridium propionicum in test tube and fermentor cultures. *J. Ind. Microbiol.* 8, 59–63. doi:10.1007/BF01575592.

Straathof, A. J. J. (2011). "The Proportion of Downstream Costs in Fermentative Production Processes," in *Comprehensive Biotechnology*, ed. M. Moo-Young (Elsevier), 811–814. doi:10.1016/B978-0-08-088504-9.00492-X.

Sträuber, H., Bühligen, F., Kleinsteuber, S., and Dittrich-Zechendorf, M. (2018). Carboxylic acid production from ensiled crops in anaerobic solid-state fermentation - trace elements as pH controlling agents support microbial chain elongation with lactic acid. *Eng. Life Sci.* 18, 447–458. doi:10.1002/elsc.201700186.

Sudirjo, E., Constantino Diaz, P. Y., Cociancich, M., Lisman, R., Snik, C., Buisman, C. J. N., et al. (2020). A thin layer of activated carbon deposited on polyurethane cube leads to new conductive bioanode for (plant) microbial fuel cell. *Energies* 13, 1–21. doi:10.3390/en13030574.

Sudmalis, D., Gagliano, M. C., Pei, R., Grolle, K., Plugge, C. M., Rijnaarts, H. H. M., et al. (2018). Fast anaerobic sludge granulation at elevated salinity. *Water Res.* 128, 293–303. doi:10.1016/j.watres.2017.10.038.

Sun, Z., Ramsay, J. A., Guay, M., and Ramsay, B. A. (2007). Carbon-limited fed-batch production of medium-chain-length polyhydroxyalkanoates from nonanoic acid by Pseudomonas putida KT2440. *Appl. Microbiol. Biotechnol.* 74, 69–77. doi:10.1007/s00253-006-0655-4.

Takahashi, S., Tomita, J., Nishioka, K., Hisada, T., and Nishijima, M. (2014). Development of a Prokaryotic Universal Primer for Simultaneous Analysis of Bacteria and Archea Using Next-Generation Sequencing. *PLoS One* 9. doi:10.1371/journal.pone.0105592.

Takeno, S., Takasaki, M., Urabayashi, A., Mimura, A., Muramatsu, T., Mitsuhashi, S., et al. (2013). Development of fatty acid-producing Corynebacterium glutamicum strains. *Appl. Environ. Microbiol.* 79, 6775–6783. doi:10.1128/AEM.02003-13.

Tamis, J., Joosse, B. M., van Loosdrecht, M. C. M., and Kleerebezem, R. (2015). High-rate volatile fatty acid (VFA) production by a granular sludge process at low pH. *Biotechnol. Bioeng.* 112, 2248–2255. doi:10.1002/bit.25640.

Tang, H., Holmes, D. E., Ueki, T., Palacios, P. A., and Lovley, D. R. (2019). Iron Corrosion via Direct Metal-Microbe Electron Transfer. *MBio*, 1–10.

Tao, Y., Zhu, X., Wang, H., Wang, Y., Li, X., Jin, H., et al. (2017). Complete genome sequence of Ruminococcaceae bacterium CPB6: A newly isolated culture for efficient n-caproic acid production from lactate. *J. Biotechnol.* 259, 91–94. doi:10.1016/j.jbiotec.2017.07.036.

Tatum, E. L., Peterson, W. H., and Fred, E. B. (1936). Enzymic racemization of optically active lactic acid. *Biochem. J.* 30, 1892–1897. doi:10.1042/bj0301892.

Tay, H., and Liu, S. (2001). The effects of shear force on the formation, structure and metabolism of aerobic granules. *Appl. Microbiol. Biotechnol.* 57, 227–233. doi:10.1007/s002530100766.

Thauer, R. K., Jungermann, K., Decker, K., and Pi, P. P. H.-- (1977). Energy Conservation in Chemotrophic Anaerobic Bacteria. 41, 100–180.

The Circularity gap report (2021). *Circ. Econ.*, 1–71. Available at: www.circle-economy.com [Accessed May 3, 2021].

Tholozan, J. L., Touzel, J. P., Samain, E., Grivet, J. P., Prensier, G., and Albagnac, G. (1992). Clostridium neopropionicum sp. nov., a strict anaerobic bacterium fermenting ethanol to propionate through acrylate pathway. *Arch. Microbiol.* 157,

249–257.
Tomlinson, N., and Barker, H. A. (1954). Carbon dioxide and acetate utilization by clostridium kluyveri. I. Influence of nutritional conditions on utilization patterns. *J. Biol. Chem.* 209, 585–595. doi:10.1016/S0021-9258(18)65485-7.
Tong, Y., Hirata, M., Takanashi, H., Hano, T., Matsumoto, M., and Miura, S. (1998). Solvent screening for production of lactic acid by extractive fermentation. *Sep. Sci. Technol.* 33, 1439–1453. doi:10.1080/01496399808545059.
Tran, H. N., You, S. J., Hosseini-Bandegharaei, A., and Chao, H. P. (2017). Mistakes and inconsistencies regarding adsorption of contaminants from aqueous solutions: A critical review. *Water Res.* 120, 88–116. doi:10.1016/j.watres.2017.04.014.
Tratnyek, P. G., Scherer, M. M., Johnson, T. ., and Matheson, L. J. (2003). "Permeable Reactive Barriers of Iron and Other Zero-Valent Metals," in *Chemical Degradation Methods for Wastes and Pollutants: Environmental and Industrial Applications*, ed. M. A. Tarr (New York-Basel: Marcel Dekker, Inc.), 371–421. doi:10.1201/9780203912553.ch9.
Tsoi, R., Wu, F., Zhang, C., Bewick, S., Karig, D., and You, L. (2018). Metabolic division of labor in microbial systems. *Proc. Natl. Acad. Sci.* 115, 2526–2531. doi:10.1073/pnas.1716888115.
Turpeinen, A., and Merimaa, P. (2011). "Functional fats and spreads," in *Functional Foods* (Woodhead Publishing), 383–400. doi:10.1533/9780857092557.3.383.
Urban, C., Xu, J., Sträuber, H., Dos Santos Dantas, T. R., Mühlenberg, J., Härtig, C., et al. (2017). Production of drop-in fuels from biomass at high selectivity by combined microbial and electrochemical conversion. *Energy Environ. Sci.* 10, 2231–2244. doi:10.1039/c7ee01303e.
Vandamme, P., Pot, B., Gillis, M., Vos, P. D. E., and Kersters, K. (1996). Polyphasic Taxonomy, a Consensus Approach to Bacterial Systematics. *Microbiol. Rev.* 60, 407–438.
Vassilev, I., Hernandez, P. A., Batlle-Vilanova, P., Freguia, S., Krömer, J. O., Keller, J., et al. (2018). Microbial Electrosynthesis of Isobutyric, Butyric, Caproic Acids, and Corresponding Alcohols from Carbon Dioxide. *ACS Sustain. Chem. Eng.* 6, 8485–8493. doi:10.1021/acssuschemeng.8b00739.
Velenturf, A. P. M., and Purnell, P. (2017). Resource recovery from waste: Restoring the balance between resource scarcity and waste overload. *Sustainability* 9, 1–17. doi:10.3390/su9091603.
Viggi, C. C., Rossetti, S., Fazi, S., Paiano, P., Majone, M., and Aulenta, F. (2014). Magnetite Particles Triggering a Faster and More Robust Syntrophic Pathway of Methanogenic Propionate Degradation. *Environ. Sci. Technol.* 48, 7536–7543. doi:10.1021/es5016789.
Vilajeliu-Pons, A., Bañeras, L., Puig, S., Molognoni, D., Vilà-Rovira, A., Amo, E. H. Del, et al. (2016). External resistances applied to MFC affect core microbiome and swine manure treatment efficiencies. *PLoS One* 11, 1–19. doi:10.1371/journal.pone.0164044.
Villano, M., Paiano, P., Palma, E., Miccheli, A., and Majone, M. (2017). Electrochemically Driven Fermentation of Organic Substrates with Undefined Mixed Microbial Cultures. *ChemSusChem* 10, 3091–3097. doi:10.1002/cssc.201700360.
Vu, D. T., Kolah, A. K., Asthana, N. S., Peereboom, L., Lira, C. T., and Miller, D. J. (2005). Oligomer distribution in concentrated lactic acid solutions. *Fluid Phase Equilib.* 236, 125–135. doi:10.1016/j.fluid.2005.06.021.
Wang, H., Li, X., Wang, Y., Tao, Y., Lu, S., Zhu, X., et al. (2018). Improvement of n-caproic acid production with Ruminococcaceae bacterium CPB6: selection of electron acceptors and carbon sources and optimization of the culture medium. *Microb. Cell Fact.* 17, 1–9. doi:10.1186/s12934-018-0946-3.
Wang, Y., Wei, W., Wu, S. L., and Ni, B. J. (2020). Zerovalent Iron Effectively Enhances Medium-Chain Fatty Acids Production from Waste Activated Sludge through Improving Sludge Biodegradability and Electron Transfer Efficiency. *Environ. Sci. Technol.* 54, 10904–10915. doi:10.1021/acs.est.0c03029.
WBA (2019). Global potential of biogas. Available at: worldbiogasassociation.org.
Weghoff, M. C., Bertsch, J., and Müller, V. (2015). A novel mode of lactate metabolism in strictly anaerobic bacteria. *Environ. Microbiol.* 17, 670–677. doi:10.1111/1462-2920.12493.
Weilnhammer, C., and Blass, E. (1994). Continuous fermentation with product recovery by in-situ extraction. *Chem. Eng. Technol.* 17, 365–373. doi:10.1002/ceat.270170602.
Weimer, P. J., and Moen, G. N. (2013). Quantitative analysis of growth and volatile fatty acid production by the anaerobic ruminal bacterium Megasphaera elsdenii T81. *Appl. Microbiol. Biotechnol.* 97, 4075–4081. doi:10.1007/s00253-012-4645-4.
Wickham, H. (2008). *ggplot2: Elegant Graphics for Data Analysis*. Springer.
Woolf, D., Amonette, J. E., Street-Perrott, F. A., Lehmann, J., and Joseph, S. (2010). Sustainable biochar to mitigate global climate change. *Nat. Commun.* 1, 1–9. doi:10.1038/ncomms1053.
Wu, J., Zhou, H., Li, H., Zhang, P., and Jiang, J. (2009). Impacts of hydrodynamic shear force on nucleation of flocculent sludge in anaerobic reactor. *Water Res.* 43, 3029–3036. doi:10.1016/j.watres.2009.04.026.
Wu, Q., Feng, X., Guo, W., Bao, X., and Ren, N. (2020). Long-term medium chain carboxylic acids production from liquor-making wastewater: Parameters optimization and toxicity mitigation. *Chem. Eng. J.* 388, 124218. doi:10.1016/j.cej.2020.124218.
Wu, Q., Guo, W., You, S., Bao, X., Luo, H., Wang, H., et al. (2019). Concentrating lactate-carbon flow on medium chain carboxylic acids production by hydrogen supply. *Bioresour. Technol.* 291. doi:10.1016/j.biortech.2019.121573.
Wu, Q., Liu, T., Zhu, L., Huang, H., and Jiang, L. (2017). Insights from the complete genome sequence of Clostridium tyrobutyricum provide a platform for biotechnological and industrial applications. *J. Ind. Microbiol. Biotechnol.* 44, 1245–1260. doi:10.1007/s10295-017-1956-6.
Wu, S., Xu, S., Chen, X., Sun, H., Hu, M., Bai, Z., et al. (2018). Bacterial communities changes during food waste spoilage. *Sci. Rep.* 8, 1–9. doi:10.1038/s41598-018-26494-2.
Wu, Y., Wang, C., Liu, X., Ma, H., Wu, J., Zuo, J., et al. (2016). A new method of two-phase anaerobic digestion for fruit and vegetable waste treatment. *Bioresour. Technol.* 211, 16–23. doi:10.1016/j.biortech.2016.03.050.

Xu, J., Guzman, J. J. L., Andersen, S. J., Rabaey, K., and Angenent, L. T. (2015). In-line and selective phase separation of medium-chain carboxylic acids using membrane electrolysis. *Chem. Commun.* 51, 6847–6850. doi:10.1039/c5cc01897h.

Xu, J., Guzman, J. J. L., and Angenent, L. T. (2021). Direct Medium-Chain Carboxylic Acid Oil Separation from a Bioreactor by an Electrodialysis/Phase Separation Cell. *Environ. Sci. Technol.* 55, 634–644. doi:10.1021/acs.est.0c04939.

Xu, J., Hao, J., Guzman, J. J. L., Spirito, C. M., Harroff, L. A., and Angenent, L. T. (2018). Temperature-Phased Conversion of Acid Whey Waste Into Medium-Chain Carboxylic Acids via Lactic Acid: No External e-Donor. *Joule* 2, 280–295. doi:10.1016/j.joule.2017.11.008.

Xue, C., Liu, F., Xu, M., Tang, I. C., Zhao, J., Bai, F., et al. (2016). Butanol production in acetone-butanol-ethanol fermentation with in situ product recovery by adsorption. *Bioresour. Technol.* 219, 158–168. doi:10.1016/j.biortech.2016.07.111.

Yang, Q., Guo, S., Lu, Q., Tao, Y., Zheng, D., Zhou, Q., et al. (2021). Butyryl/Caproyl-CoA:Acetate CoA-Transferase: Cloning, Expression and Characterization of the Key Enzyme Involved in Medium-Chain Fatty Acid Biosynthesis. *bioRxiv*, 1–32.

Yang, Q., Wei, C., Guo, S., Liu, J., and Tao, Y. (2020). Cloning and characterization of a L-lactate dehydrogenase gene from Ruminococcaceae bacterium CPB6. *World J. Microbiol. Biotechnol.* 36. doi:10.1007/s11274-020-02958-4.

Yoon, B. K., Jackman, J. A., Valle-González, E. R., and Cho, N. J. (2018). Antibacterial free fatty acids and monoglycerides: Biological activities, experimental testing, and therapeutic applications. *Int. J. Mol. Sci.* 19. doi:10.3390/ijms19041114.

Yousuf, A., Bonk, F., and Schmidt, J. E. (2016). Recovery of carboxylic acids produced during dark fermentation of food waste by adsorption on Amberlite IRA-67 and activated carbon. *Bioresour. Technol.* 217, 137–140. doi:10.1016/j.biortech.2016.02.035.

Yu, J., Liao, J., Huang, Z., Wu, P., Zhao, M., Liu, C., et al. (2019). Enhanced anaerobic mixed culture fermentation with anion-exchange resin for caproate production. *Processes* 7, 1–12. doi:10.3390/pr7070404.

Zagrodnik, R., Duber, A., Łężyk, M., and Oleskowicz-Popiel, P. (2020). Enrichment Versus Bioaugmentation - Microbiological Production of Caproate from Mixed Carbon Sources by Mixed Bacterial Culture and Clostridium kluyveri. *Environ. Sci. Technol.* 54, 5864–5873. doi:10.1021/acs.est.9b07651.

Zellner, G., Messner, P., Winter, J., and Stackebrandt, E. (1998). Methanoculleus palmolei sp. nov., an irregularly coccoid methanogen from an anaerobic digester treating wastewater of a palm oil plant in North- Sumatra, Indonesia. *Int. J. Syst. Bacteriol.* 48, 1111–1117. doi:10.1099/00207713-48-4-1111.

Zentek, J., Buchheit-Renko, S., Ferrara, F., Vahjen, W., Van Kessel, A. G., and Pieper, R. (2011). Nutritional and physiological role of medium-chain triglycerides and medium-chain fatty acids in piglets. *Anim. Health Res. Rev.* 12, 83–93. doi:10.1017/S1466252311000089.

Zhang, F., Ding, J., Zhang, Y., Chen, M., Ding, Z.-W., van Loosdrecht, M. C. M., et al. (2013). Fatty acids production from hydrogen and carbon dioxide by mixed culture in the membrane biofilm reactor. *Water Res.* 47, 6122–6129. doi:10.1016/j.watres.2013.07.033.

Zhang, K., Zhang, L., and Yang, S. T. (2014). Fumaric acid recovery and purification from fermentation broth by activated carbon adsorption followed with desorption by acetone. *Ind. Eng. Chem. Res.* 53, 12802–12808. doi:10.1021/ie501559f.

Zhang, X., Mandelco, L., and Wiegel, J. (1994). Clostridium hydroxybenzoicum sp. nov., an amino acid-utilizing, hydroxybenzoate-decarboxylating bacterium isolated from methanogenic freshwater pond sediment. *Int. J. Syst. Bacteriol.* 44, 214–222. doi:10.1099/00207713-44-2-214.

Zhang, Z., Tsapekos, P., Alvarado-morales, M., and Angelidaki, I. (2021). Impact of storage duration and micro-aerobic conditions on lactic acid production from food waste. *Bioresour. Technol.* 323, 1–9.

Zhu, X., Feng, X., Liang, C., Li, J., Jia, J., Feng, L., et al. (2021). Microbial ecological mechanism for long-term production of high concentrations of n-caproate via lactate-driven chain elongation. *Appl. Environ. Microbiol.* doi:10.1128/aem.03075-20.

Zhu, X., Tao, Y., Liang, C., Li, X., Wei, N., Zhang, W., et al. (2015). The synthesis of n-caproate from lactate: A new efficient process for medium-chain carboxylates production. *Sci. Rep.* 5, 1–9. doi:10.1038/srep14360.

Zhu, X., Zhou, Y., Wang, Y., Wu, T., Li, X., Li, D., et al. (2017). Production of high-concentration n-caproic acid from lactate through fermentation using a newly isolated Ruminococcaceae bacterium CPB6. *Biotechnol. Biofuels* 10, 1–12. doi:10.1186/s13068-017-0788-y.

Summary

Summary

The transition to a circular economy needs development on alternative sources of energy and materials to decrease our dependency on fossil resources. Renewable and residual resources may provide alternative, more sustainable products through efficient bioprocessing and upcycling into useful biobased products. Resource recovery bioprocesses, like anaerobic digestion, rely on reactor microbiomes for effective bioconversion of non-sterile complex feedstock. Through microbial chain elongation, reactor microbiomes convert complex feedstocks into medium-chain carboxylates (MCC), valuable platform chemicals with diverse applications in the energy, agri-food and chemical industries. The addition of external chemicals like ethanol (electron donor) and alkali (for pH control) negatively impact the environmental footprint of chain elongation. However, lactate is an alternative electron donor that may be obtained from complex residues to replace ethanol and may also reduce the use of alkali for pH control.

This thesis presents open-culture microbial chain elongation processes for the production of different (even-chain and odd-chain) MCC from food waste and lactate. Since MCC need to be separated and purified for commercial application, alternative product separation approaches are explored. Chapter 1 briefly describes the state-of-the-art of chain elongation and carboxylates separation.

In Chapter 2, acidification of complex food waste was steered toward lactate formation, which was subsequently used up as electron donor for chain elongation within the same bioreactor. The consecutive lactate production and consumption reduced the input of chemicals needed for pH control due to partial pH self-regulation and promoted MCC production without exogenous electron donor.

At this point, lactate produced from complex organic residues was shown to be an important electron donor for chain elongation. Therefore, further research focused on steering product formation from lactate. Operational conditions leading to the production of propionate, n-butyrate, n-valerate or MCC were identified.

In Chapter 3, zero-valent iron nanoparticles (nZVI) were added to batch fermentation experiments to evaluate its potential to promote odd-chain MCC formation. nZVI affected n-caproate and propionate formation in a dose-dependent manner, mainly through abiotic reactions (e.g. hydrolysis of lactate oligomers and increased pH). During chain elongation, enantiopure lactate was racemized and converted to even-chain carboxylates independently of the lactate enantiomer fed. This results from the apparent presence of lactate racemase in many microorganisms enriched in chain-elongating microbiomes.

Continuous lactate-based chain elongation was studied in Chapter 4, where nitrogen gas was supplied at different regimes to evaluate its effect on L-lactate conversion and biomass growth at mildly acidic conditions (pH 5.5). High MCC selectivities at low gas mixing were sustained. However, high superficial gas velocities washed out chain-elongating bacteria, changing lactate metabolism

lactate conversion rates toward odd-chain carboxylates (n-valerate and n-heptylate), which may be used to produce odd-chain MCC from lactate as the sole electron donor in two-stage bioprocesses.

In Chapter 5, the addition of the conductive materials granular activated carbon (GAC) and nickel foam (NF) steered batch chain elongation toward significant amounts of isobutyrate, a new product of open-culture lactate fermentation. GAC, NF and stainless steel (SS) all decreased propionate production, which is a competing process from lactate. When added to continuous chain elongation, GAC adsorbed the microbially produced MCC. Since this adsorptive behavior may allow MCC separation and recovery, GAC adsorption properties were characterized. Given its high MCC affinity and adsorption capacity, *in situ* MCC adsorption with GAC followed by thermal desorption is proposed as an attractive approach to recover neat medium-chain carboxylic acids.

An alternative bioprocess to produce potential novel product formulations (e.g. MCC-rich feed additives) from chain elongation using application-compatible solvents was studied in Chapter 6. Sunflower oil, which had a similar biocompatibility with chain-elongating microbiomes as oleyl alcohol, selectively extracted MCC in continuous extractive chain elongation and the obtained MCC-enriched oil was proposed as a potential functionalized feed additive for direct application with no further DSP.

Chapter 7 collects the insights obtained through this research in the context of resource recovery from complex organic residues. Potential feedstocks and processing schemes supporting the production of even-chain, odd-chain and branched MCC with lactate as the key electron donor are proposed. Additionally, an outlook is given on the potential and implications of producing MCC-rich products (e.g. feed additives, soil amendments) and sustainable aviation fuels from food waste. Overall, lactate-based chain elongation is envisioned as a promising, versatile platform to upcycle nutrient-rich, complex organic residues into a variety of valuable products supporting the development of the circular economy.

Resumen

Resumen

La transición hacia una economía circular incluye la búsqueda de fuentes renovables de energía y materiales para disminuir la dependencia de recursos fósiles. Los residuos orgánicos y otros recursos renovables tienen el potencial de utilizarse como materias primas sostenibles que a través de bioprocesos eficientes y el suprarreciclaje pueden sustituir materias primas no renovables para la obtención de combustibles y compuestos valorizables. Los bioprocesos de recuperación de recursos, tales como la digestión anaerobia, dependen de consorcios microbianos para la conversión eficaz de materias primas complejas no estériles. En el bioproceso conocido como elongación de cadena, los consorcios microbianos tienen la facultad de convertir la materia orgánica en carboxilatos de cadena media (MCC), los cuales son productos de valor agregado con diversos usos en las industrias energética, agroalimentaria y química. La adición de productos químicos externos como etanol (donador de electrones) y álcali (para el control del pH) reduce los beneficios ambientales de la recuperación de recursos a través del proceso de elongación de la cadena. Sin embargo, el lactato es un donador de electrones alternativo que se puede obtener fácilmente a partir de residuos complejos y puede además reducir el uso de álcali para la regulación del pH en el proceso.

Esta tesis presenta procesos microbianos de elongación de cadena basados en cultivos abiertos para la producción de diferentes MCC (de cadena par y de cadena impar) a partir de residuos de alimentos y lactato. Dado que los MCC debe separarse y purificarse para su aplicación comercial, se exploran enfoques alternativos de separación de productos. El Capítulo 1 describe brevemente los avances en las áreas de elongación de cadena y separación de carboxilatos.

En el Capítulo 2, se presentan los resultados de dirigir la fermentación de residuos de alimentos hacia la formación de lactato, el cual fungió como donador de electrones, dentro del mismo biorreactor, en el proceso de elongación de cadena. Se describe además cómo la producción y el consumo sucesivo de lactato redujeron la adición de sustancias químicas para el control del pH, debido a la autorregulación parcial del pH y promovieron la producción de MCC sin la necesidad de agregar un donador de electrones exógeno.

Una vez demostrado que el lactato producido a partir de residuos orgánicos complejos es un donador de electrones importante para el proceso de elongación de cadena, la investigación se centró en controlar la formación de metabolitos generados a partir de lactato, donde se identificaron las condiciones de operación que conducen a la producción de propionato, n-butirato, n-valerato o de MCC tales como n-caproato, n-heptylato y n-caprilato.

En el Capítulo 3, se presentan los resultados de experimentos donde se agregaron nanopartículas de hierro cero valente (nZVI) a experimentos de fermentación en lote para evaluar su potencial para promover la formación de MCC de cadena impar. Se concluyó que diferentes dosis de nZVI afectaron la formación de n-caproato y propionato, principalmente a través de reacciones abióticas (e.g. hidrólisis de oligómeros de lactato y aumento del pH). Se concluyó que durante la elongación de cadena el lactato enantiopuro fue racemizado y convertido en carboxilatos de cadena par,

independientemente del enantiómero de lactato añadido, probablemente debido a la presencia de la enzima lactato racemasa en muchos de los microorganismos enriquecidos.

En el Capítulo 4 se estudió la producción continua de MCC a partir de lactato por medio de elongación de cadena, evaluando el efecto de la adición de nitrógeno gas bajo diferentes regímenes para evaluar su efecto en la conversión de L-lactato y el crecimiento de biomasa en condiciones ligeramente ácidas (pH 5.5). La producción de MCC se mantuvo con altas proporciones a velocidades superficiales de gas bajas. Sin embargo, las bacterias productoras de MCC fueron lavadas fuera del reactor a altas velocidades superficiales de gas, cambiando el metabolismo del lactato hacia la coproducción de propionato y n-butirato. La adición de propionato aumentó las tasas de conversión de lactato hacia carboxilatos de cadena impar (n-valerato y n-heptilato), hecho que puede aprovecharse para producir MCC de cadena impar a partir de lactato como el único donador de electrones en bioprocesos de dos etapas.

En el Capítulo 5, se estudió la adición de materiales conductores como carbón activado granular (GAC) y espuma de níquel (NF) en la elongación de cadena en lote, los cuales dirigieron el proceso hacia la producción de cantidades significativas de isobutirato, un nuevo producto de la fermentación de lactato en cultivos abiertos. La adición de GAC, NF y acero inoxidable (SS) disminuyó la producción de propionato, el cual es un proceso antagónico. El GAC adsorbió los MCC producidos por las bacterias cuando fue agregado a reactores continuos. Dicho comportamiento de adsorción, el cual puede permitir la separación y recuperación de MCC, se caracterizó mediante pruebas experimentales. Dada su alta afinidad y capacidad de adsorción de MCC, se propone un proceso que incluye la adsorción *in situ* de MCC usando GAC seguido por una desorción térmica como un proceso atractivo para recuperar ácidos carboxílicos de cadena media con una alta pureza.

En el Capítulo 6 se estudió un bioproceso alternativo para producir productos novedosos (por ejemplo, aditivos alimenticios ricos en MCC) utilizando solventes que sean compatibles con la aplicación final. El aceite de girasol, que mostró una biocompatibilidad similar al alcohol oleico, extrajo MCC de manera selectiva durante la fermentación extractiva en reactores continuos, y el aceite vegetal enriquecido con MCC se propuso como un posible aditivo alimenticio funcionalizado que puede ser empleado directamente sin aplicar procesos de separación o purificación adicionales.

El Capítulo 7 recopila los conocimientos obtenidos a través de esta investigación los cuales se discuten en el contexto de la recuperación de recursos a partir de residuos orgánicos complejos. Se proponen posibles materias primas y esquemas de procesamiento que permiten la producción de MCC de cadena par, impar y ramificados utilizando lactato como el donador de electrones principal. Además, se ofrece una perspectiva sobre el potencial y las implicaciones de la producción de productos enriquecidos con MCC (por ejemplo, aditivos alimenticios para ganado, mejoradores de suelo) así como de combustibles de aviación sustentables a partir de residuos de alimentos. En general, el proceso de elongación de cadena a partir de lactato se concibe como una plataforma versátil y prometedora para el suprarreciclaje de residuos orgánicos complejos y ricos en nutrientes, dirigido hacia la producción de una amplia variedad de productos valiosos, y así contribuir al desarrollo de la economía circular.

Acknowledgements

Doing my PhD at ETE was a very inspiring and fun pursuit. I thank all the people from ETE, Wageningen and beyond for the nice memories. I want to thank my promotor Cees and supervisor David for following on that random email and accepting to start this journey, for their guidance and their contribution to this research. David, thank you for your patience and for encouraging me to grow my creative thinking during regular meetings, bouldering attempts or occasional ETE drinks. Cees, thank you for accepting me in your group; for your bold comments and experience shared, which were much valuable for this research and for my personal development.

Many people contributed to this research. I want to thank Víctor for the great collaboration that contributed to the first article of this thesis. The work presented in this thesis was partially done as part of MSc studies by Vincent, Norwin, Cris, Zhipeng, Johan, Natalia and Arielle. Thank you for your contributions. I enjoyed your enthusiasm and the energizing discussions. My gratitude to the support staff, Vinnie, Livio, Jean, Bert, Hans, Pieter, Julián, Katja, Jill and Zoe, as well as to Liesbeth, Marjolein and Wies. Without you performing this research would have proven extremely challenging and less enjoyable.

Togetherness is one of the strengths of ETE, and this would not have been such a pleasant experience without many nice people around. Thanks to my colleagues for the nice talks during breaks; Miriam, Annemerel, Sanne, Koen vG, Baptiste, Bingnan, Dilan, Darja, Ivonne, Joeri, Arnoud, Kasper, Kamonashish; Pradip, Shiyang, Elackiya and more office mates. The Chile trip also contributed to the togetherness, thanks for the pleasant moments Alette, Rosanne, Farzaneh, Pim. I also appreciate the good times doing sports, in the surf trips with Dainis and Koen, as well as during football with Ilse, Thomas, Nora, Ludo and Daniel completing the lineup. I would also like to thank the party people for the fun gatherings before and after the lockdown: Livio, Selin, Emilius, Fatma, Laura, Debora, Silvi, Victor. My especial thanks to my paranymphs Andrea and Jort for your friendship and all the good times. My acknowledgements to my good friends from Mexico as well who in some way also contributed to the successful completion of this journey.

My infinite gratitude and love to my family, for their immeasurable support. Mamá y papá, muchas gracias por su apoyo inmenso en todo momento, especialmente durante mis aventuras en tierras lejanas. A mi hermano Luis y tu bonita familia. A mi tío Gus. Y a toda mi familia. Gracias.

About the author

Carlos Alberto Contreras Dávila was born in May 11th 1990 in Colima, Mexico. He received his BSc diploma in Environmental Engineering from Instituto Tecnológico de Colima in 2013 where he received an award for graduating top of his class. Afterwards, he did his MSc in Environmental Sciences at IPICYT, Mexico. During his MSc studies, he researched the biological production of hydrogen from residual biomass of the agri-food industry using mixed cultures and majored in Environmental Biotechnology in 2015. He worked as research assistant at IPICYT for a brief period after graduating and published a scientific article.

Afterwards, he received a grant to do his PhD research at Environmental Technology in Wageningen University. The project focused on the production of valuable chemicals such as medium-chain carboxylates from organic residual materials through mixed-culture fermentation and the simultaneous separation of these chemicals.

Publications list

Carlos A. Contreras-Dávila, Johan Esveld, Cees J.N. Buisman and David P.B.T.B. Strik (2021). nZVI impacts substrate conversion and microbiome composition in chain elongation from D- and L-lactate substrates. *Front Bioeng Biotechnol*. 9, 666582.

Carlos A. Contreras-Dávila, Arielle Ali, Cees N.J. Buisman and David P.B.T.B. Strik (2021). Lactate metabolism and microbiome composition are affected by nitrogen gas supply in continuous lactate-based chain elongation. *Fermentation*. 7,41, 7010041.

Carlos A. Contreras-Dávila, Víctor J. Carrión, Vincent R. Vonk, Cees J.N. Buisman and David P.B.T.B. Strik (2020). Consecutive lactate formation and chain elongation to reduce exogenous chemicals input in repeated-batch food waste fermentation. *Water Res*. 169, 115215.

Carlos A. Contreras-Dávila, Hugo O. Méndez-Acosta, Luis Arellano-García, Felipe Alatriste-Mondragón, Elías Razo-Flores (2017). Continuous hydrogen production from enzymatic hydrolysate of Agave tequilana bagasse: Effect of the organic loading rate and reactor configuration. *Chem Eng J*. 313, 671-679.

Netherlands Research School for the
Socio-Economic and Natural Sciences of the Environment

D I P L O M A

for specialised PhD training

The Netherlands research school for the
Socio-Economic and Natural Sciences of the Environment
(SENSE) declares that

Carlos Alberto Contreras Davila

born on 11th May 1990 in Colima, Mexico

has successfully fulfilled all requirements of the
educational PhD programme of SENSE.

Wageningen, 3rd September 2021

Chair of the SENSE board

Prof. dr. Martin Wassen

The SENSE Director

Prof. Philipp Pattberg

The SENSE Research School has been accredited by the Royal Netherlands Academy of Arts and Sciences (KNAW)

KONINKLIJKE NEDERLANDSE
AKADEMIE VAN WETENSCHAPPEN

The SENSE Research School declares that **Carlos Alberto Contreras Davila** has successfully fulfilled all requirements of the educational PhD programme of SENSE with a work load of 47.9 EC, including the following activities:

SENSE PhD Courses

- Environmental research in context (2017)
- Research in context activity: 'Initiating, organizing and coordinating successful study trip to Chile for PhD candidates from the Dept. of Environmental Technology (2-16 March 2019)'

Other PhD and Advanced MSc Courses

- Sustainable Production Systems: Shaping cross-company innovation, Climate-KIC (2017)
- Project and time management, Wageningen Graduate Schools (2018)
- Speaking Skills, Wageningen Graduate Schools (2018)
- Scientific Writing and Presenting, Wageningen Graduate Schools (2019)
- Reviewing a scientific paper, Wageningen Graduate Schools (2021)

Management and Didactic Skills Training

- Co-organizing the 1st International Chain Elongation Conference (2020)
- Supervising six MSc students with thesis (2018-2020)
- Supervising BSc student with thesis (2018)
- Assisting practicals of the MSc course 'Renewable energy (2018-2019)
- Assisting practicals of the BSc course 'Biorefinery' (2019-2020)

Oral Presentations

- *N-caproate production from food waste without pH control: lactate formation and chain elongation*. IWA Resource Recovery Conference, 8-12 September 2019, Venice, Italy
- *Catalytic effects of zero-valent iron nanoparticles in microbial lactate-based chain elongation*. Environmental Technology for Impact, 3-5 June 2020, Wageningen (virtual), The Netherlands
- *Effects of zero-valent iron nanoparticles on lactate-based chain elongation*. 1st International Chain Elongation Conference, 26 -27 October 2020, Wageningen (virtual), The Netherlands

SENSE coordinator PhD education

Dr. ir. Peter Vermeulen

The research described in this thesis was financially supported by the joint trust-fund CONACYT-SENER Sustentabilidad Energética, Mexico, with grant number 297027.

Financial support from Wageningen University for printing this thesis is gratefully acknowledged.

Cover designed by nopal design, Mexico (www.nopal.design).